Synthèse de nanoparticules d'or fonctionnalisées par l'acide dihydrolipoïque : caractérisation, étude de stabilité et impact sur l'homéostasie redox cellulaire

Juliana Tournebize-Pego Lima

UNIVERSITÉ DE LORRAINE

Ecole Doctorale BioSE (Biologie-Santé-Environnement)

Thèse

Présentée et soutenue publiquement pour l'obtention du titre de

DOCTEUR DE L'UNIVERSITE DE LORRAINE

Mention : « Sciences de la Vie et de la Santé »

par **Juliana TOURNEBIZE née PEGO LIMA**

Synthèse de nanoparticules d'or fonctionnalisées par l'acide dihydrolipoïque : caractérisation, étude de stabilité et impact sur l'homéostasie redox cellulaire

Le 6 juillet 2012

Membres du jury :

Rapporteurs :	M Stéphane ROUX	PRU, Université de Franche-Comté, Besançon
	Mme Sylvie BEGU	MCU-HDR, Université Montpellier 1, Montpellier
Examinateurs :	Mme Anne SAPIN-MINET	MCU, EA 3452, Université de Lorraine, co-Directeur de thèse
	M Pierre LEROY	PRU, EA 3452, Université de Lorraine, Directeur de thèse
Membres invités :	M Raphaël SCHNEIDER	PRU, UPR 3349, Université de Lorraine, Nancy
	M Grzegorz BARTOSZ	PRU, University of Lodz, Lodz, Poland

EA 3452 CITHEFOR ; Cibles Thérapeutiques, Formulation et Expertise Préclinique du Médicament – 5, rue Albert Lebrun, BP 80403, 54001 Nancy Cedex, France

Ce travail a été réalisé dans l'EA 3452 CITHEFOR, sous la direction du Pr Pierre Leroy et du Dr Anne Sapin-Minet.

Remerciements

Je n'aurais jamais pu réaliser cette thèse sans l'aide et l'encouragement d'un grand nombre de personnes qui je tiens à exprimer mes vifs remerciements.

Je tiens tout d'abord à remercier Monsieur le Professeur ***Pierre Leroy****, pour m'avoir toujours soutenue et encouragée tout au long de ce travail, pour toutes ses suggestions, son soutien et sa disponibilité tout au long de cette thèse. Je le remercie aussi pour son organisation qui m'a évité le maximum de soucis administratifs. Cette thèse n'aurait jamais été ce qu'elle est sans lui. Qu'il trouve ici toute ma reconnaissance pour ces années de travail sous sa direction.*

Je remercie également Madame le Docteur ***Anne Sapin-Minet****, ma co-directrice de thèse, pour ses conseils et pour sa bonne humeur de tous les jours. Le côté humain qu'elle a apporté à ces années de thèse à travers sa gentillesse, sa disponibilité et sa rigueur dans le travail est un des éléments majeurs du bon déroulement de cette thèse.*

Je remercie sincèrement Monsieur le Professeur ***Philippe Maincent*** *de m'avoir accueillie au sein de son équipe de recherche mais aussi pour ses conseils et ses encouragements.*

Je remercie Monsieur le Professeur ***Raphaël Schneider*** *de m'avoir fait découvrir la synthèse de nanoparticules d'or, pour ses conseils et ses suggestions très utiles dans ce domaine, ce qui a grandement contribué à l'avancement de cette thèse.*

Je remercie également Madame le Docteur ***Ariane Boudier*** *pour son soutien, son intérêt enthousiaste pour le sujet de ce manuscrit, ainsi que pour les nombreuses discussions tout au long de cette thèse.*

Je remercie les membres du jury, Monsieur le Professeur ***Stéphane Roux*** *et Madame le Docteur* ***Sylvie Bégu*** *d'avoir accepté de juger ce travail.*

Je remercie sincèrement Monsieur le Professeur ***Grzegorz Bartosz*** *pour ses conseils indispensables au sujet de l'homéostasie redox cellulaire.*

*Je remercie Monsieur le Professeur **Jean-François Collet** et Monsieur le Professeur **Vincent Haufroid** pour leur contribution dans les analyses par ICP-MS.*

*Je remercie Madame le Docteur **Lavinia Balan** d'avoir réalisé les images des NP d'or par TEM.*

*Je remercie également Monsieur le Professeur **Bernard Foliguet** et Madame **Chanel** pour la réalisation des images des cellules par TEM.*

*Je remercie Madame le Docteur **Caroline Gaucher** pour sa bonne humeur, sa gentillesse et ses conseils scientifiques ont contribué à mener à bien cette thèse.*

*Je tiens à remercier le Docteur **Olivier Joubert**, pour son aide et ses précieux conseils de culture cellulaire.*

*Je remercie à tous les membres de l'équipe CITHEFOR, et particulièrement les anciens thésards (**Houssan, Javier, Julien, Lucie, Myriem**) et thésards (**Cristina, Fatima, Marianne**) qui j'ai rencontrés au cours de ces années pour leur amitié, leur gentillesse et pour l'ambiance amicale qu'ils ont su créer.*

*Je remercie les anciens stagiaires (**Magdalena, Rima, Ana, Débora**) qui ont beaucoup contribué à ce présent travail.*

*Merci à **mes parents** pour leur soutien inconditionnel dans toutes les étapes de ma vie, merci de m'avoir toujours laissé faire mes choix et les assumer.*

*Merci à **mes beaux-parents** pour leur soutien. Un grand merci aussi pour leur précieuse aide dans la dernière ligne droite.*

Merci à mes amis français qui m'ont entourée lors de ce travail.

*Enfin, mes plus vifs remerciements vont à mon fils (**Félicien**) et à mon mari (**Ferréol**), pour leur patience ; je leur dédie cette thèse*

.

Table des Matières

Travaux scientifiques (2009-2012)

Publications internationales

Acceptées

1. Boudier A., Tournebize J., Bartosz G., El Hani S., Bengueddour R., Sapin-Minet A., and Leroy P. High-performance liquid chromatographic method to evaluate the hydrogen atom transfer during reaction between 1,1-diphenyl-2-picryl-hydrazyl radical and antioxidants. *Anal. Chim. Acta*. **711: 97-106** (2012).

2. Eidi H., Joubert O., Némos C., Grandemange S., Mograbi B., Foliguet B., Tournebize J., Maincent P., LeFaou A., Aboukhamis I., and Rihn B.H. Drug delivery by polymeric nanoparticles induces autophagy in macrophages. *Int. J. Pharmaceut.* **422: 495-503** (2012).

3. Tournebize J., Sapin-Minet A., Schneider R., Boudier A., Maincent P., and Leroy P. Simple spectrophotocolorimetric method for quantitative determination of gold in nanoparticles, *Talanta*. **83: 1780-1783** (2011).

4. Leroy P., Sapin-Minet A., Pitarch-Sierra A., Boudier A., Tournebize J., and Schneider R. Interactions between gold nanoparticles and macrophages : activation or inhibition ? Letter to the Editor. *Nitric Oxide-Biol. Chem.* **25: 54 –56** (2011).

*Soumises et en preparation**

5. Tournebize J., Boudier A., Joubert O., Eidi H., Bartosz G., Leroy P., and Sapin-Minet A. Impact of gold nanoparticle coating on redox homeostasis. Soumise le 04 mai 2012 à *International Journal of Pharmaceutics*.

6. * Tournebize J., Boudier A., Sapin-Minet A., Maincent P., Leroy P., and Schneider R. Role of gold nanoparticles capping density on stability and surface reactivity to design a drug delivery platform. En préparation pour soumettre à *Macromolecules*.

7. * Tournebize J., Sapin-Minet A., Boudier A., Bartosz G. and Leroy P. Pitfalls of assays devoted to evaluation of oxidative stress induced by inorganic nanoparticles. En préparation pour soumettre à Talanta.

Communications orales* et affichées

1. Tournebize J., Sapin-Minet A., Boudier A., Schneider R., Pitarch-Sierra A., Maincent P., and Leroy P. Synthesis, characterization and in vitro biocompatibility evaluation of gold nanoparticles for biomedical applications. Journée Scientifique BioSE, Nancy, 26 janvier 2011.

2. Tournebize J., Sapin-Minet A., and Leroy P. L'or : intérêt en nanotechnologie pharmaceutique? Doctoriales de Lorraine, Ventron, 16 – 21 mai 2010.

3.*(présentation « flash »). Tournebize J., Leroy P., Sapin-Minet A., Boudier A., Maincent P., Balan L. et Schneider R. Synthèse de nanoparticules d'or fonctionnalisées par l'acide dihydrolipoïque. Caractérisation et étude de stabilité. First Cross Border Conference on NanoSciences and Materials for Health (NanoSMH), Pont-à-Mousson, 21 – 25 june 2010.

4.* Tournebize J., Leroy P., Sapin-Minet A., Boudier A., Maincent P., Balan L. et Schneider R. Synthèse de nanoparticules d'or fonctionnalisées par l'acide dihydrolipoïque. Caractérisation et étude de stabilité. XVIIème Journée Jeunes Chercheurs de la Société de Chimie Thérapeutique, Université Paris Descartes, Paris, 5 février 2010.

5.*(présentation "flash") Tournebize J., Leroy P., Sapin-Minet A., Maincent P., Balan L., and Schneider R. Gold Nanoparticles Functionalized with Glutathione: New Platforms for Delivery and Imaging Applications. Journées de Printemps 2009 du GFP2P, ENSIC, Nancy, 13 – 15 mai 2009

Prix

1. **Prix BIOMAT du meilleur poster** au First Cross Border Conference on NanoSciences and Materials for Health (NanoSMH).

2. **Prix du 2ème meilleur poster** aux Doctoriales de Lorraine 2010.

Liste des tableaux

De la partie écrite en français

Article 2

Article 3

Article 4

Article 5

Article 6

Article 7

Liste des figures

De la partie écrite en français

Article 1

Article 2

Article 5

Article 6

Article 7

Liste des abréviations

De la partie écrite en français

$ABTS^{\bullet+}$	2',2'-azinobis(3-éthylbenzothiazoline)-6-sulfonique
AFM	Microscope à force atomique (*atomic force microscopy*)
BSA	Albumine de sérum bovin (*bovine serum albumin*)°
CTAB	Bromure de cétyltriméthylammonium (*cetyltrimethylammonium bromide*)
CFL-SM	Microscope confocal à balayage laser (*confocal-laser scanning microscopy*)
DLS	Diffusion dynamique de la lumière (*dynamic light scattering)*
DHLA	Acide dihydrolipoïque
DMAP	Diméthylaminopyridine
$DPPH^{\bullet}$	1,1-diphényl-2-picrylhydrazyle
DTT	Dithiothréitol
GSH	Glutathion réduit
GSNO	*S*-nitrosoglutathion
ICP-MS	Spectrométrie de masse à source plasma à couplage inductif (*inductively coupled plasma mass spectrometry*)
ICP-OES	Spectrométrie d'émission optique à source plasma à couplage inductif (*inductively coupled plasma optical emission spectrometry)*
MSA	Acide mercaptosuccinique
$^{\bullet}NO$	Monoxyde d'azote
ND	Non déterminé
NP	Nanoparticules
NP Au@DHLA	Nanoparticules d'or fonctionnalisées par le DHLA
ROS	Espèces réactives de l'oxygène (*reactive oxygen species*)
RNS	Espèces réactives de l'azote (*reactive nitrogen species*)
PBS	Tampon phosphate salin *(phosphate-buffered saline)*
PEG	Polyéthylène glycol
r	Barre (*rod*)
sph	Sphérique
SPM	Système des phagocytes mononucléés
SPR	Résonnance plasmonique de surface (*surface plasmon resonance*)
TEM	Microscope électronique à transmission (*transmission electron microscopy*)
TOAB	Bromure de tétraoctylammonium (*tetraoctylammonium bromide*)

Introduction générale

Depuis le début des années 1980 l'emploi des nanotechnologies dans une approche thérapeutique a pris un essor important et les domaines d'application sont aujourd'hui multiples, allant de l'imagerie médicale au transport de médicaments et à leur ciblage. Selon la norme ISO TS/27687 de 2008, les nanoparticules (NP) sont définies comme étant des particules ayant au moins une dimension inférieure à 100 nm. Néanmoins, cette définition est encore discutée et de nombreux auteurs décrivent des NP comme étant des particules colloïdales ayant une taille comprise entre 10 et 1000 nm (Prabha *et al.*, 2002, Gargouri *et al.*, 2009, Muthu *et al.*, 2009, Eidi *et al.*, 2010).

Il existe une grande variété de NP de composition organique (polymères, dendrimères,...) ou inorganique (métaux, oxydes métalliques, silicium, carbone,...) (Teow *et al.*, 2011). Parmi ces dernières, les NP d'or sont les plus anciennes, elles sont utilisées depuis longtemps avant même la définition du terme nanotechnologie. Un exemple célèbre est la coupe de Lycurgue d'époque romaine, qui possède des propriétés optiques particulières (éclairée de l'intérieur, elle apparaît verte ; éclairée de l'extérieur, elle apparaît rouge) dues à la présence de NP d'or dans le verre. Les NP d'or offrent un intérêt très important aujourd'hui et elles représentent une grande partie des travaux rapportés dans la littérature, notamment dans le domaine biomédical (Daniel et Astruc, 2004, Huang *et al.*, 2008, Boisselier et Astruc, 2009, Dreaden *et al.*, 2012, Jans et Huo, 2012, Llevot et Astruc, 2012). Dans ce domaine, les NP d'or représentent en effet des outils parfaitement adaptés non seulement par leur synthèse aisée mais aussi par leurs grandes capacités de fonctionnalisation (voire de multifonctionnalisation) en surface, par greffage soit de molécules soufrées, soit de molécules biologiques qui s'adsorbent spontanément sur les NP d'or (Lubitz et Kotlyar, 2011, Xu *et al.*, 2011).

L'utilisation des NP dans le domaine biomédical exige notamment une solubilité élevée en solution aqueuse et une excellente stabilité en conditions physiologiques. Cependant les NP d'or en solution ont tendance à s'agréger et à précipiter, du fait des interactions de type Van der Waals qui existent entre elles. Différentes stratégies ont été employées ces dernières années afin d'améliorer leur stabilité en solution aqueuse. Parmi celles-ci, figure la formation de liaisons covalentes entre les atomes d'or et des composés porteurs d'une ou plusieurs fonctions sulfhydryles ou thiols (citons par exemple le glutathion comme monothiol (Zhang *et al.*, 2010), l'acide dihydrolipoïque (DHLA) comme dithiol (Roux *et al.*, 2005), des espèces trithiols (Li *et al.*, 2002), et des cyclodextrines présentant plusieurs fonctions thiols (Liu *et al.*, 2000)). L'utilisation de multithiols semble accroître la stabilité des NP d'or par rapport à l'emploi d'un monothiol.

Dans ce contexte, nous avons cherché à travers nos travaux de thèse, à mieux comprendre l'origine de la meilleure stabilisation des NP d'or par l'emploi d'un dithiol, plus précisément le DHLA. Pour ce faire, nous avons tout d'abord synthétisé les NP d'or en milieu aqueux par la méthode de Turkevich *et al.*, (1951), en employant un excès de DHLA (4 concentrations différentes) par rapport à la concentration en Au présent en surface des NP (*i.e.* $DHLA/Au_{surface}$ = × 28, × 56, × 140, × 222). Les NP obtenues différemment recouvertes en DHLA nous ont permis d'évaluer l'impact de la densité de couverture sur leur stabilité.

Les NP d'or, du fait de leur nombre fini d'atomes, présentent des propriétés physiques, chimiques et optiques différentes de celles de l'or massif et leurs propriétés dépendent fortement de la taille de la particule, de sa forme, de la distance inter-particulaire et de la nature du métal (Daniel et Astruc, 2004, Duncan *et al.*, 2010). En outre, l'or devient extrêmement réactif à l'échelle nanométrique et il est susceptible d'engendrer une certaine toxicité. Actuellement, les connaissances sur la toxicité des NP d'or demeurent assez limitées du fait du faible nombre d'études toxicologiques et des résultats souvent contradictoires qu'elles exposent. Récemment, il a été démontré que la cytotoxicité des NP d'or peut être liée à l'induction d'un stress oxydant (Jia *et al.*, 2009, Gao *et al.*, 2011, Jia *et al.*, 2011, Zhao *et al.*, 2011). C'est pourquoi il est indispensable d'étudier, en parallèle à l'aspect fondamental et appliqué des NP d'or, l'impact de ces nouveaux objets sur le statut redox des organismes.

Nos travaux de thèse ont nécessité une approche multidisciplinaire associant la physico-chimie et la biologie cellulaire. Après l'optimisation de la synthèse de NP d'or présentant une forte stabilité, celles-ci ont été évaluées *in vitro* dans une lignée cellulaire de type macrophage, en axant l'étude sur des paramètres reliés au statut redox de ces cellules en culture.

Notre manuscrit est organisé en quatre chapitres.

Le premier chapitre présente une synthèse bibliographique des propriétés générales de l'or massif et de ses nouvelles propriétés à l'échelle nanométrique ainsi que des méthodes pour évaluer l'impact des NP d'or sur la régulation redox. Ce dernier aspect fait l'objet d'une revue générale en préparation pour soumettre à *Talanta* (**article 1**).

Le second chapitre est consacré à la synthèse de NP d'or fonctionnalisées soit par les ions citrate, soit par un composé dithiol, le DHLA, ainsi qu'à leur caractérisation physico-chimique approfondie.

Dans un premier temps, nous avons étudié l'impact de la densité de couverture sur la stabilité des NP d'or, en variant le rapport [DHLA]/[Au] lors de la synthèse. De plus, l'effet du rapport [DHLA]/[Au] sur la réactivité des NP vis-à-vis de biomolécules a été évalué. Ces études ont permis de parfaitement définir une plateforme fonctionnalisée en surface et stable en fonction du temps qui fait l'objet d'un manuscrit en préparation pour soumettre à *Macromolecules* (**article 2)**. Enfin, nous avons développé une méthode de dosage spectrophotocolorimétrique de l'or contenu dans les NP, ce qui permet de calculer le rendement de synthèse, la concentration et l'absorbance molaires des NP (**article 3**, Tournebize *et al.*, *Talanta*, 2011 (83); 1780-1783).

Dans un second temps, nous avons optimisé une méthode chromatographique sensible et sélective pour évaluer le pouvoir antiradicalaire de matrices complexes d'origine végétale ainsi que de NP (diamant, or). Cette étude correspond à un manuscrit accepté le 30 octobre 2011 dans *Analytica Chimica Acta* (**article 4**, Boudier A., Tournebize J. *et al.*, *Anal. Chim. Acta*, 2012 (711); 97-106).

Le troisième chapitre est consacré à l'effet de la fonctionnalisation de la surface des NP d'or sur l'homéostasie redox. Des résultats récents de la littérature suggèrent que les NP d'or sont capables d'éliminer les espèces réactives de l'azote (*reactive nitrogen species*, RNS) produites par les macrophages (Ma *et al.*, 2010). Néanmoins, ces résultats nous ont paru incomplets, en raison d'un manque d'informations sur les caractéristiques des NP d'or, ce qui nous a conduit à écrire une lettre à l'éditeur (**article 5,** Leroy *et al.*, *Letter to the Editor, Nitric Oxide-Biol Chim.*, 2011 (25); 54-56). Nous avons évalué le rôle de la fonctionnalisation de surface des NP d'or sur l'interaction avec des composés constituant des biomarqueurs de la régulation de l'homéostasie redox cellulaire. Pour ce faire, nous avons développé des méthodes en absence de cellules pour étudier l'interaction des NP d'or avec des protéines, le glutathion réduit (GSH) et un donneur de monoxyde d'azote ($^{\bullet}NO$).

Du fait de la quasi inexistence de données de la littérature concernant la réponse précoce des macrophages à une exposition à de faibles concentrations en NP d'or, nous nous sommes également intéressés à l'exposition des macrophages à des doses non toxiques de NP d'or sur des temps courts, en examinant certaines modifications du statut redox. Ces résultats font l'objet d'un manuscrit soumis le 04 Mai dans *International Journal of Pharmaceutics* (**article 6**). Des NP polymériques (Eudragit® RS) ont été utilisées comme contrôle positif lors de la mesure des concentrations intracellulaires en GSH et en espèces réactives de l'oxygène (*reactive oxygen species*, ROS) selon les conditions décrites dans un article dont nous sommes co-auteur (**article 7**, Eidi *et al.*, *Int. J. Pharmaceut.*, 2012 (422); 495-503).

Ce mémoire se termine par une discussion et une conclusion générale (4ème chapitre) résumant les faits marquants de nos travaux et développant les perspectives de nos recherches.

Chapitre I.
Etude bibliographique

I.1 L'or : du métal aux nanoparticules

L'or est le deuxième élément métallique que l'homme a découvert après le cuivre, et il a suivi l'évolution des civilisations, depuis l'Antiquité jusqu'à nos jours (Jansen, 2008). Son intérêt du Moyen Âge à aujourd'hui se traduit par de nombreuses applications (figure 1) : il a été beaucoup utilisé comme monnaie, dans la bijouterie, dans la décoration et dans l'art (broderie sur soie, reliure, céramique ; comme colorant pour le verre (coupe de Lycurgus, IV^{ème} siècle après J.C.)) ainsi qu'en médecine et en thérapeutique (élixir de jeunesse, traitement contre la syphilis, etc...). Plus récemment, l'or est conservé en lingots pour la spéculation ; il est également utilisé en microélectronique mais aussi dans le traitement de différentes formes d'arthrite sous forme de complexes organométalliques (Ridauran®, Myochrysine®, etc...). Enfin, l'intérêt grandissant des recherches sur les nanotechnologies de ces dernières années a révélé l'emploi de l'or, à une échelle nanométrique, dans des applications très diverses allant de l'ingénierie à la médicine (Paciotti *et al.*, 2004, Loo *et al.*, 2005, Joshi *et al.*, 2006, Pissuwan *et al.*, 2006, Rosi *et al.*, 2006, Baptista *et al.*, 2008, Ghosh *et al.*, 2008, Sperling *et al.*, 2008, Boisselier et Astruc, 2009, Libutti *et al.*, 2010, Alan, 2011, Pissuwan *et al.*, 2011).

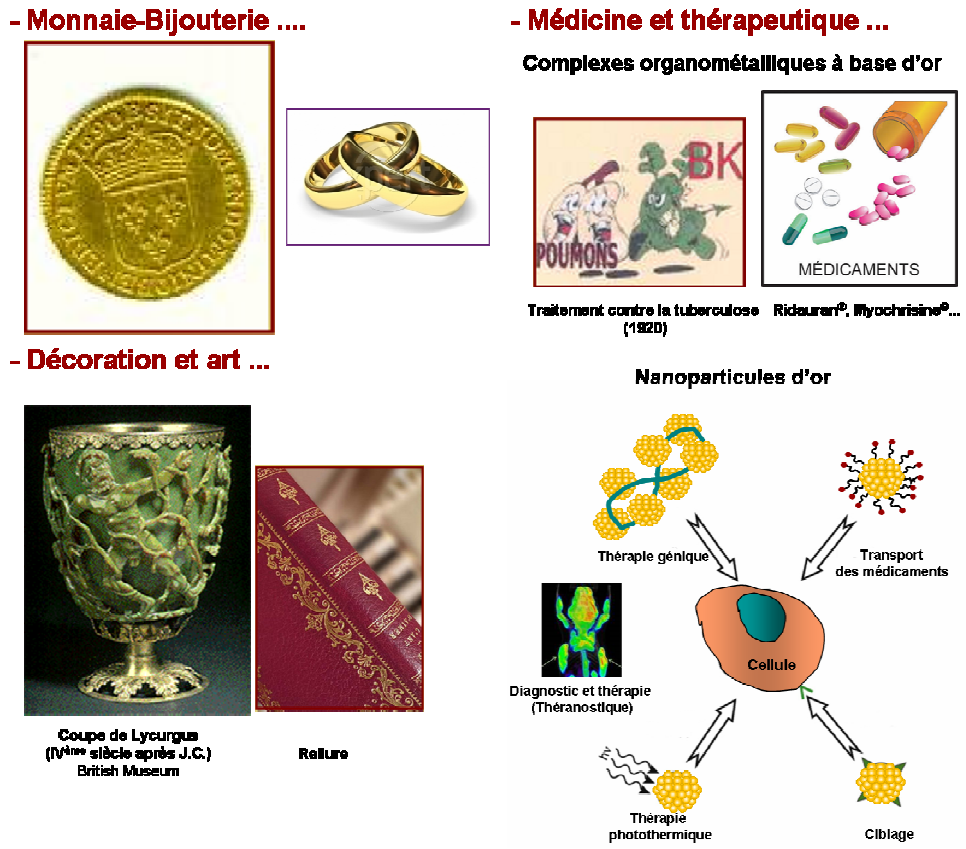

Figure 1. Différentes utilisations de l'or du Moyen Age à nos jours.

Dans les prochaines sections, nous décrirons les propriétés générales de l'or métallique ainsi que leurs nouvelles propriétés liées à une échelle nanométrique.

I.1.1 Propriétés atomiques et chimiques de l'or

L'élément or (symbole : Au) appartient à la colonne 11 et à la période 6 du tableau de la classification périodique. La masse atomique de l'or est de 196,96 $g.mol^{-1}$ et sa masse volumique est de 19,3 $g.cm^{-3}$ à 20°C. Le numéro atomique de l'or est 79, ce qui signifie qu'il possède 79 protons dans son noyau. L'or possède donc 79 électrons répartis autour du noyau et sa configuration électronique se décline ainsi : [Xe] $4f^{14}$ $5d^{10}$ $6s^1$. De plus, l'atome Au est le premier élément du tableau à posséder 5 couches électroniques saturées.

Du point de vue chimique, l'or présente des propriétés exceptionnelles. L'or est un métal de transition qui est susceptible de former plusieurs composés dans lesquels son nombre d'oxydation peut varier de (-I) à (+VII); Au (+I) et Au (+III) sont majoritaires et Au (-I), Au (+II), Au (+V) et Au (+VII) sont les états d'oxydation moins communs (tableau 1).

Tableau 1. Différents nombres d'oxydation de l'élément or (Au)

Au^{-1} (d^{10} s^2)	$[Au(NH_3)_n]^-$
Au° (d^{10} s^1)	Nanoparticules d'or
Au^I (d^{10})	Au_2S, $[Au(CN)_2]^-$ et d'autres complexes
Au^{II} (d^9)	Rare, quelques complexes sont connus
Au^{III} (d^8)	Au_2O_3, $Au(OH)_4^-$ (aq), $AuCl_4^-$ (aq), $AuCl_3(OH)^-$ (aq), Au_2S_3 , AuF_3, Au_2Cl_6, $AuBr_3$, complexes
Au^V (d^6)	AuF_5
Au^{VII} (d^4)	AuF_7

De plus, l'or est le métal le plus électronégatif ; il offre donc une grande résistance à l'oxydation. Par contre, il est sensible à l'attaque des halogènes ou à des solutions aqueuses les produisant comme l'eau régale (HNO_3-HCl) ; dans ce dernier cas, le produit obtenu est l'acide chloroaurique. L'ion Au (+I) présente la particularité d'interagir avec lui-même pour former des complexes comme $[Au(CN)_2]^-$, par l'intermédiaire d'interactions d^{10} – d^{10}, appelées interactions

aurophiliques (Schmidbaur et Schier, 2012). De plus, les composés d'Au (+II) sont généralement diamagnétiques et peuvent former un complexe remarquable avec le gaz noble xénon, ce qui correspond à une propriété inattendue et spectaculaire de l'or (Jansen, 2008). Cette propriété est mise à profit dans le domaine de la microélectronique pour la préparation de supraconducteurs.

I.1.2 Propriétés physiques de l'or

L'or est très ductile et malléable, et il possède un grand pouvoir réflecteur. Les atomes d'or cristallisent dans un système cubique à faces centrées (CFC), ce qui permet sa déformation mécanique (figure 2).

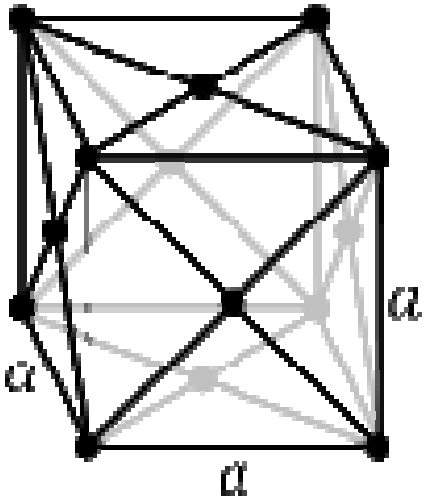

Figure 2. Les atomes d'or sont empilés selon une structure cubique à faces centrées.
a (paramètre de maille théorique) = 0,408 nm

L'or est très malléable. En effet, il est possible d'obtenir une feuille de 8 m^2 (épaisseur réduite à ~ 0,2 µm) avec environ 28 g de ce métal. L'or métallique se déforme facilement à froid, par martelage ou par étirement (tréfilage, laminage) et il se cisèle facilement.

I.1.3 L'or métallique *versus* les nanoparticules d'or : nouvelles propriétés

Les NP d'or sont produites artificiellement par l'Homme à partir de l'association de plusieurs dizaines et milliers d'atomes d'or.

Ces dernières années, le développement de NP d'or a permis de potentialiser les propriétés de l'or métallique mais surtout d'en révéler de nouvelles, telles que des propriétés catalytiques induites par des effets de surface et des propriétés optiques uniques, élargissant les domaines d'application.

La première suspension colloïdale d'or scientifiquement documentée a été préparée en 1857 par Michaël Faraday par réduction du chlorure d'or au moyen de phosphore blanc (Faraday, 1857).

Les méthodes de synthèse des nanoparticules d'or les plus couramment utilisées aujourd'hui sont décrites par la suite.

I.1.3.1 Méthodes de synthèse des nanoparticules d'or

De nouvelles méthodes de synthèse des NP d'or ont été récemment introduites (Jana *et al.*, 2001, Guo et Wang, 2007, Grzelczak *et al.*, 2008, Alkilany et Murphy, 2009, Sakamoto *et al.*, 2009, Ackerson *et al.*, 2010, Nguyen *et al.*, 2011). Selon la méthode de synthèse utilisée, nous pouvons obtenir des NP d'or avec des tailles variant du nanomètre à quelques dizaines de nanomètres. De plus, les NP d'or peuvent être sous forme de sphères (Goodman *et al.*, 2004, Connor *et al.*, 2005, Shukla *et al.*, 2005), de nano-tiges (Perez-Juste *et al.*, 2005), de nano-cages (Skrabalak *et al.*, 2008), ou de nano-bâtonnets (Murphy *et al.*, 2005, Alkilany et Murphy, 2009).

Les méthodes de synthèse peuvent être divisées en deux approches principales : la synthèse par voie physique ou chimique (Nguyen *et al.*, 2011).

La voie physique de préparation dite « top-down » consiste à fragmenter l'or massif à l'aide de techniques mécaniques. Citons par exemple, l'ablation laser (Dadras *et al.*, 2009) et l'irradiation ionique (Belloni *et al.*, 1998) qui permettent d'élaborer une large gamme de NP. Néanmoins, l'approche « top-down » présente quelques inconvénients : 1°) la distribution de la taille est relativement large, et 2°) l'absence de contrôle de la composition chimique des clusters (Dreaden *et al.*, 2012). Dans la suite, nous n'aborderons pas ces méthodes.

La voie chimique d'association dénommée « bottom-up » est la fabrication de NP d'or *via* l'assemblage d'atomes. Cette méthode consiste à la réduction d'un précurseur d'or par des

techniques de chimie douce comme la réduction chimique, sonochimique et électrochimique. Parmi ces dernières, la réduction chimique est de loin la méthode la plus utilisée pour la synthèse de NP d'or. Elle permet un meilleur contrôle des caractéristiques des NP, telles que leur taille, leur morphologie et leur distribution de taille (Nguyen *et al.*, 2011).

Le principe général de la voie chimique consiste en la réduction d'un sel d'or de degré d'oxydation +III en or métallique (degré d'oxydation 0) dans un milieu aqueux ou biphasique en présence d'un agent stabilisant. De plus, cette synthèse subit deux étapes successives de nucléation et de croissance. La nucléation est la collision en solution avec des ions, atomes ou clusters afin de former un noyau tandis que la croissance correspond à l'ajout progressif d'atomes ou de groupes d'atomes sur le noyau déjà existant, donnant ainsi naissance à des agrégats de quelques nanomètres avec des formes sphériques (croissance isotrope) ou non sphériques (croissance anisotrope) (figure 3).

De nombreuses méthodes ont été développées et se différencient par la nature du réducteur et/ou de l'agent stabilisant. Par la suite, seules les méthodes par réduction chimique les plus couramment utilisées seront abordées et divisées en deux groupes : la synthèse de NP d'or en milieu aqueux et la synthèse de NP d'or dans un solvant organique.

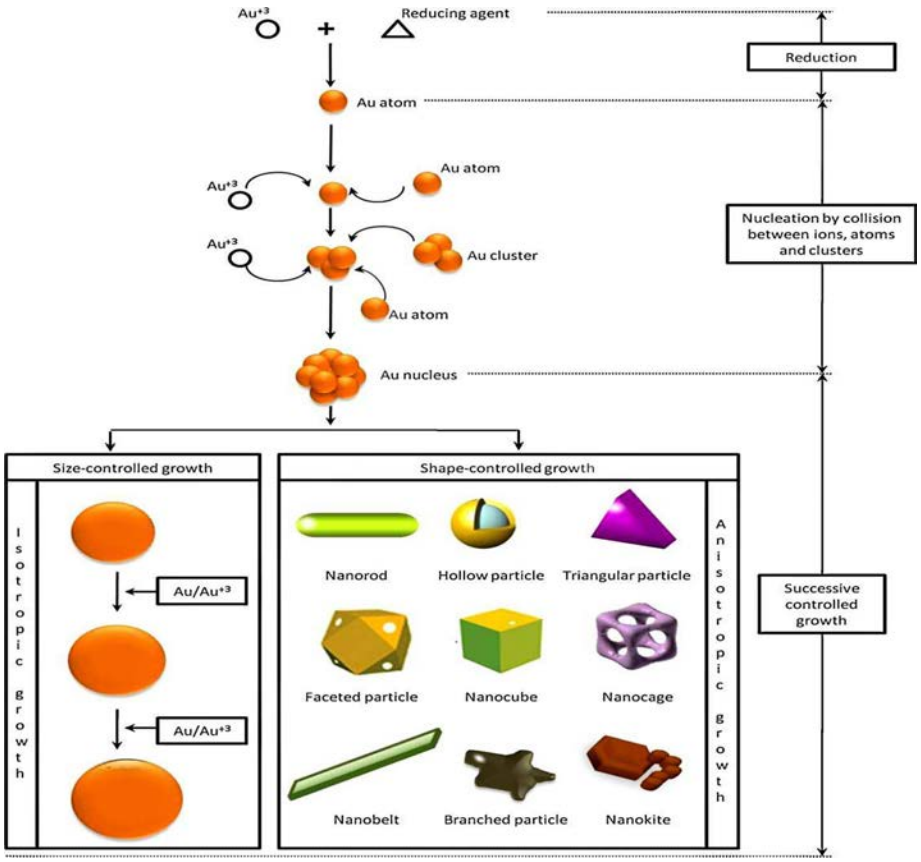

Figure 3. Préparation par réduction chimique de nanoparticules d'or avec obtention de différentes tailles et formes (Nguyen *et al.*, 2011).

Synthèse de nanoparticules d'or en solution aqueuse

La méthode de Faraday (1857) est encore couramment utilisée aujourd'hui, améliorée par les travaux de Turkevich *et al.* (1951) et de Frens (1973). Ces travaux consistent en la réduction par les ions citrate d'un sel d'or pour former des NP d'or de taille comprise entre 10 et 20 nm. L'ion citrate agit à la fois comme réducteur et agent stabilisant des particules formées, en s'adsorbant à la surface des NP pour créer une couche chargée négativement. Ceci va introduire une répulsion électrostatique entre les particules empêchant leur agrégation et donc permettant leur stabilisation ; cette méthode ne demande recours à aucun autre stabilisant. L'ion citrate a donc une grande importance dans la formation de NP d'or, sa concentration et sa vitesse d'addition étant les paramètres clés de la synthèse (Turkevich *et al.*, 1951, Kimling *et al.*, 2006).

De nos jours, plusieurs compagnies (SPI, Sigma-Aldrich, Meliorum Technologies, BB International, Ted Pella, etc...) commercialisent des NP d'or stabilisées par les ions citrate et présentant différentes tailles.

Plus récemment, une évolution de cette méthode proposée par Brown *et al.* (1999) a permis d'obtenir des NP d'or plus petites, de l'ordre de 5 nm ; la réduction d'$HAuCl_4$ se fait par l'intermédiaire de tétraborohydrure de sodium ($NaBH_4$), en présence de citrate de sodium.

Les NP d'or peuvent également être synthétisées dans un milieu aqueux par la réduction d'un sel d'or en présence d'autres molécules telles que la diméthylaminopyridine (Griffin et Fitzmaurice, 2007), l'acide mercaptosuccinique (MSA) (Chen et Kimura, 1999), des méthoxy-polyéthylène glycols (PEG) porteurs de groupements fonctionnels thiol (Sakura *et al.*, 2005), des peptides (Slocik *et al.*, 2005), des dendrimères (Zheng *et al.*, 2002), pour ne citer que quelques uns. Toutes ces molécules présentent un groupement chimique qui est capable de se lier à la surface métallique des NP ainsi que de ralentir et de contrôler leur croissance. Contrairement aux NP d'or stabilisées par des ions citrate, les NP d'or stabilisées par ces molécules ont une gamme de taille très étroite et leur taille dépend directement de la molécule utilisée.

Synthèse de nanoparticules d'or en milieu organique

En 1994, Brust et Schiffrin ont mis au point une méthode de synthèse des NP d'or non plus en solution aqueuse mais en milieu organique à base de toluène (Brust *et al.*, 1994). La méthode consiste à nouveau à réduire un sel d'or mais de très vite empêcher l'agrégation des nanocristaux par des ligands formant une liaison covalente avec l'or. Cette méthode repose sur le transfert d'un sel d'or (dissous dans une solution aqueuse) vers une solution organique au moyen d'un agent de transfert de phase tel que le bromure de tétraoctylammonium (TOAB). Puis, un agent réducteur puissant doit alors être ajouté, comme le $NaBH_4$, pour provoquer la formation du cœur métallique d'or. Le TOAB sert d'agent stabilisant et de catalyseur entre les deux phases lors de la réaction. Du fait de la faible interaction entre le TOAB et les NP, ces dernières peuvent être stabilisées en greffant à leur surface, par liaisons covalentes, de longues chaînes alkyles portant au moins un groupement thiol. Il est possible d'obtenir des NP d'or de taille comprise entre 1,5 et 5,2 nm. De plus, la quantité de thiol en excès, la température et la vitesse à laquelle la réaction se produit, sont des paramètres clés de cette synthèse.

La stabilisation des NP d'or peut également être assurée par l'utilisation d'amines à longue chaîne alkyle (Chen *et al.*, 2000, Jana et Peng, 2003) qui se lient néanmoins moins fortement à la surface des NP que les thiols (Leff *et al.*, 1996). D'autres molécules telles que le bromure de

cétyltriméthylammonium (CTAB) (Fan et Jiang, 1997), les micelles de copolymère à blocs (Youk *et al.*, 2002, Zheng *et al.*, 2006b), les thioéthers (Li *et al.*, 2001, Peterle *et al.*, 2008), les polyéthylènes glycols (PEG) (Wuelfing *et al.*, 1998) et d'autres polymères (Hussain *et al.*, 2005a) ont également été utilisés.

Contrairement à la synthèse en milieu aqueux, la synthèse en milieu organique n'est pas limitée par la concentration d'or en solution et elle permet la synthèse de NP à l'échelle du gramme (Jana et Peng, 2003, Hiramatsu et Osterloh, 2004). Par contre, cette technique est beaucoup moins adaptée aux applications biomédicales. En effet, la bioconjugaison n'est pas possible en milieu organique et elle requiert donc le transfert de phase de NP du milieu organique vers le milieu aqueux. Le transfert de phase est notamment discuté dans la référence suivante : Rao *et al.* (2004).

Une description plus détaillée des méthodes de synthèse, des techniques de caractérisation physico-chimique et des applications des NP d'or peut être trouvée dans un grand nombre de revues (Daniel et Astruc, 2004, Ghosh *et al.*, 2008, Murphy *et al.*, 2008, Nguyen *et al.*, 2011, Dreaden *et al.*, 2012).

I.1.3.2. Nouvelles propriétés : catalytiques et optiques

L'or a longtemps été considéré comme catalytiquement inactif par les chimistes du fait de son caractère inerte. Cependant, cet élément devient extrêmement réactif à l'échelle nanométrique de par la très grande surface des NP d'or et aussi les différentes configurations que peuvent adopter les atomes de surface d'une NP.

En 1973, Bond *et al.* ont montré que sous forme nanométrique, l'or semblait avoir des propriétés catalytiques pour des réactions d'hydrogénation (Bond *et al.*, 1973). Néanmoins, c'est seulement en 1987 que les remarquables propriétés catalytiques de l'or ont été découvertes : Haruta *et al.* ont révélé la capacité de NP d'or déposées sur un substrat poreux d'oxyde de titane à catalyser la réaction d'oxydation du monoxyde de carbone en dioxyde de carbone et ce, même à température ambiante ainsi qu'à très basses températures (entre 25°C et -70°C), réaction qu'aucun autre métal n'était capable de catalyser à de telles températures (Haruta *et al.*, 1987). Depuis, les NP d'or sont apparues dans de nombreuses publications démontrant des propriétés catalytiques dans diverses réactions telles que l'hydrogénation sélective des liaisons C-C et N-O, la formation de peroxyde d'hydrogène ainsi que l'oxydation des alcools en acides ou en aldéhydes (Lemire *et al.*, 2004, Bond et Thompson 2006, Corma et Garcia 2008).

De la même façon, les propriétés optiques de l'or à l'état massif ne sont pas les mêmes que celles à l'échelle nanométrique. Les NP d'or possèdent des propriétés optiques nouvelles et

extrêmement intéressantes parmi lesquelles une grande capacité à absorber et à diffuser la lumière incidente.

L'origine physique de ces propriétés est liée aux interactions entre la lumière et les électrons libres, proches de la surface du métal. Quand les NP d'or sont exposées à une source de lumière, le champ électrique de la lumière induit une oscillation cohérente des électrons de la bande de conduction des NP d'or qui donne lieu à un phénomène qui s'appelle la résonnance plasmonique de surface (*surface plasmon resonance*, SPR) (Mie, 1908).

La position spectrale et la largeur de la bande à laquelle la SPR survient dépend de la taille, de la forme (El-Sayed, 2001, Kelly *et al.*, 2003), des interactions interparticulaires (Su *et al.*, 2003), ainsi que du milieu environnant dans lequel se trouvent les NP (Daniel et Astruc, 2004, Huang *et al.*, 2007). Cette propriété a permis l'utilisation des NP d'or pour la détection et pour le suivi dans l'organisme de biomolécules (Alivisatos, 2004, Haes *et al.*, 2004, Rosi et Mirkin, 2005) ainsi que pour l'imagerie (Sokolov *et al.*, 2003, El-Sayed *et al.*, 2005) et la thérapie photothermique (Pissuwan *et al.*, 2006), offrant la possibilité de remplacer les chromophores et fluorophores classiques.

Une description plus détaillée à propos de la SPR des NP métalliques peut être trouvée dans un grand nombre de revues (El-Sayed, 2001, Link et El-Sayed, 2003, Huang *et al.*, 2007, Jain *et al.*, 2007).

I.1.4 Stabilisation des nanoparticules d'or contre l'agrégation

L'utilisation des NP d'or dans le domaine médical (en diagnostique et en thérapeutique) requiert une grande stabilité de la structure nanoparticulaire.

Le terme « stabilité » peut avoir plusieurs connotations selon les applications. Par exemple, un médicament stable peut être défini comme son aptitude à conserver ses propriétés physico-chimiques, microbiologiques et biologiques. Quand il est appliqué aux NP d'or, ces dernières correspondent à des particules résistant à l'agrégation et, de ce fait, possédant une longue stabilité. Le terme « agrégation » est utilisé dans ce manuscrit au sens large pour caractériser l'union de particules en suspension pour en former de plus grosses.

De nombreuses stratégies pour limiter l'agrégation des NP en solution après leur formation ont été étudiées. Pour cela, la présence d'un agent stabilisant à la surface métallique est nécessaire. Comme cela a déjà été évoqué dans le paragraphe décrivant les méthodes de synthèse des NP d'or, le stabilisant permet d'une part de contrôler la taille, la forme, la composition de surface et d'autre part d'éviter l'agrégation des NP lors de leur préparation et à long terme.

Cependant, aucune tendance générale ne se dégage sur le choix de l'agent stabilisant, qui doit donc être adapté à l'application. Par exemple, pour des applications biomédicales à visée thérapeutique, il est nécessaire d'utiliser un agent stabilisant qui permette à la fois de préparer des NP dispersibles dans l'eau et de réduire la réactivité de la surface métallique vis-à-vis de biomolécules. Ainsi pour remplir ce cahier des charges, l'agent destiné à stabiliser les NP sera choisi en fonction de son mécanisme de stabilisation et de son interaction avec la surface métallique de la NP. Dans les prochains paragraphes, nous allons décrire brièvement et indépendemment ces deux objectifs en les illustrant par des exemples.

I.1.4.1 Mécanismes de stabilisation

L'action stabilisante de l'agent stabilisant utilisé pour les NP d'or présente le même mécanisme que pour toutes les suspensions colloïdales. Dans la littérature, trois modèles de stabilisation sont proposés pour expliquer cette action : (i) la stabilisation électrostatique par des molécules chargées adsorbées à la surface, (ii) la stabilisation stérique par de larges molécules encombrées, et (iii) la stabilisation « électrostérique » (la somme des deux mécanismes précédents) (figure 4).

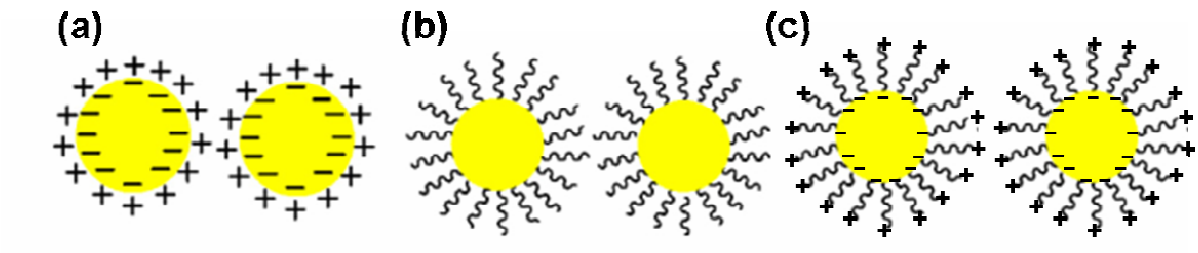

Figure 4. Représentation schématique de la stabilisation (a) électrostatique, (b) stérique et (c) « électrostérique » des nanoparticules d'or.

Stabilisation électrostatique

Les mécanismes généraux de la stabilisation électrostatique des colloïdes sont donnés par la théorie de Derjaguin, Landau, Verwey, Overbeek (DLVO). Elle suggère que la stabilité d'une particule dans une solution correspond à l'équilibre entre deux types de forces d'interaction inter-particulaire, les forces attractives de Van der Waals et les forces répulsives électrostatiques (Derjaguin et Landau, 1941, Verwey et Overbeek, 1948). En effet, les NP d'or s'agrègent pour

donner le métal massif en l'absence de ces forces répulsives opposées aux forces de Van der Waals (Zhou *et al.*, 2009). Ainsi la stabilisation électrostatique est basée sur le principe de la répulsion entre deux NP portant des charges de surface identiques. Cette stratégie de stabilisation est le résultat de :

(i) l'adsorption d'entités chargées à la surface des NP d'or, ce qui entraîne une répulsion entre les NP d'or de même charge, comme c'est le cas de l'adsorption de l'hydrazine et des ions citrate, à la surface de NP d'or qui vont s'ioniser au contact de l'eau (Zhu *et al.*, 2003, Balasubramanian *et al.*, 2010a, Tatarchuk *et al.*, 2011).

(ii) l'ionisation de groupements chimiques de certaines espèces, présents à la surface des NP d'or, par modification du pH (Selvakannan *et al.*, 2003). En effet, nous pouvons prendre l'exemple des NP d'or stabilisées par la lysine qui sont dispersibles dans l'eau à pH 3 car la fonction amine primaire libre est sous forme d'ammonium, ce qui empêche l'agrégation des NP par répulsion électrostatique ; elles précipitent à pH 10 car les groupements carboxylate formés sont en interaction (liaisons hydrogène électrostatiques) avec les groupements amine de la molécule de lysine voisine (figure 5).

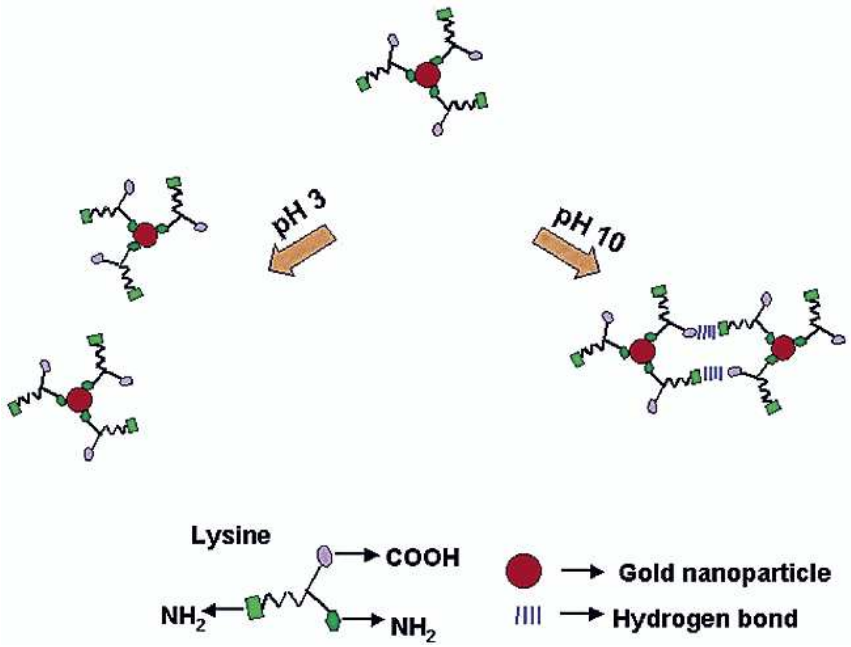

Figure 5. Représentation schématique des nanoparticules d'or stabilisées par la lysine dispersibles dans l'eau à pH 3 et précipitant à pH 10 (Selvakannan *et al.*, 2003).

Stabilisation stérique

Le second moyen de protéger les NP d'or contre l'agrégation est la répulsion stérique. Il s'agit de diminuer la réactivité de surface des NP d'or soit par des ligands organiques soit par l'adsorption de macromolécules qui forment une couche protectrice en surface.

De plus, la stabilisation stérique est efficace en milieux organique et aqueux, contrairement à la stabilisation électrostatique qui n'est efficace qu'en milieu aqueux. Ce type de stabilisation est aussi beaucoup moins sensible à la présence d'électrolytes en solution comparativement à la stabilisation électrostatique. Par ailleurs elle offre la possibilité d'ajouter certaines fonctions à la surface des NP, ce qui la rend particulièrement attrayante pour les applications biologiques.

Les ligands couramment employés pour la stabilisation stérique sont les suivants :

(i) des polymères, des copolymères (Sakai et Alexandridis, 2004, Alexandridis et Tsianou, 2011) et des dendrimères (Esumi *et al.*, 2004, Peng *et al.*, 2011) ;

(ii) des ligands contenant du soufre, tels que des xanthates (Tzhayik *et al.*, 2002), des disulfures (Porter *et al.*, 1998, Yonezawa *et al.*, 2001), des mono- (Zhang *et al.*, 2010), di- (Roux *et al.*, 2005), tri- (Garg *et al.*, 2010), et tétrathiols (Felidj *et al.*, 2003).

Stabilisation « électrostérique »

La combinaison des deux précédentes approches de stabilisation, électrostatique et stérique, est appelée répulsion « électrostérique ». En général, ce mécanisme de stabilisation est obtenu avec un composé organique chargé qui se lie à la surface de la NP, celle-ci bénéficiant à la fois de l'effet de cette charge et de l'effet d'encombrement stérique (Chapel et Berret, 2012). Les molécules les plus décrites dans la littérature sont :

(i) des polymères chargés tel que les polyacrylates (Note *et al.*, 2005) et la polyéthylèneimine (Kim *et al.*, 2011) ;

(ii) des tensioactifs, comme le Pluronic® (copolymère tribloc : poly(oxyde d'éthylène-poly(oxyde de propylène)-poly(oxyde d'éthylène) (Alexandridis et Tsianou, 2011) et le CTAB (Sobhan *et al.*, 2010).

Ces molécules possèdent un groupement polaire générant un effet électrostatique et une longue chaîne latérale lipophile créant un effet stérique.

Parmi ces trois approches, la stabilisation stérique ou « électrostérique » sont les mécanismes de stabilisation les plus utilisés pour assurer la stabilité des NP d'or à long terme ainsi que dans des milieux complexes (citons le milieu de culture cellulaire). Ces stratégies sont faiblement sensibles à la nature des espèces présentes dans le milieu, alors que dans le cas de la stabilisation électrostatique, la double couche ionique est facilement altérable.

I.1.4.2 Interactions entre la surface d'une nanoparticule et l'agent stabilisant

La force des interactions entre l'agent stabilisant et la surface métallique des NP d'or joue un rôle important dans la stabilité de la suspension obtenue (Sperling et Parak, 2010). Celles-ci sont décrites brièvement ci-dessous.

Interactions avec un niveau d'énergie faible

Ce type d'interactions englobe les agents stabilisants portant des groupements amine, hydroxyle et acide carboxylique en bout de chaîne capables d'interagir avec l'or par des interactions électrostatiques (Zhang *et al.*, 2012). Une stratégie consiste à adsorber physiquement les polymères (par exemple, les polyélectrolytes) ou encore à encapsuler des NP dans des objets formés par les polymères (par exemple des dendrimères). Parmi ces dernières, la stabilisation électrostatique par les ions citrate est la plus couramment utilisée pour l'élaboration de NP d'or.

Ces stratégies laissent la surface accessible et/ou facilement fonctionnalisable, ce qui peut être un avantage pour des applications en catalyse (Biswas *et al.*, 2012). Cependant, pour des applications biomédicales, une interaction plus forte avec la surface métallique est une stratégie plus intéressante.

Interactions avec un niveau d'énergie forte

Les dérivés de thiols sont décrits dans la littérature comme étant capables d'établir de fortes interactions avec les NP d'or (*ca.* 50 kcal/mol) (Love *et al.*, 2005). Cette liaison est souvent décrite comme étant une liaison covalente. Cependant, la nature microscopique et le mécanisme exact de cette interaction chimique font encore l'objet de discussions (Love *et al.*, 2005). En outre, de nombreux dérivés de thiols possédant un groupement hydrophile en bout de chaîne ont été utilisés pour la stabilisation de NP d'or, particulièrement sur les NP à visée thérapeutique (figure 6). Ces ligands thiols peuvent s'écrire sous la forme X-R-SH : le groupement thiol forme une liaison covalente avec la surface de la NP et la fonction X (X = -COOH, -OH, $-NH_2$) permet l'interaction avec le milieu aqueux. Des acides aminés tels que la cystéine, et des peptides tels que le glutathion, qui portent un groupement thiol, sont fréquemment utilisés pour stabiliser les NP d'or. De plus, le groupement amine de ces ligands permet la fonctionnalisation ultérieure avec des molécules pharmacologiquement actives (Zhang *et al.*, 2012).

D'une façon générale, plus un ligand assurera une forte interaction avec la surface d'une NP et plus les NP seront stables au cours du temps (Sperling et Parak, 2010). Ainsi, certains auteurs ont utilisé un ligand polydenté pour assurer une plus forte interaction de l'agent stabilisant avec le centre métallique. Citons par exemple les ligands dithiolés (Garcia *et al.*, 2005, Roux *et al.*, 2005). De plus cette stratégie présente l'avantage supplémentaire de réduire la réactivité de la surface de la NP avec le milieu environnant, ce qui peut être un avantage pour des applications dans le domaine biomédical.

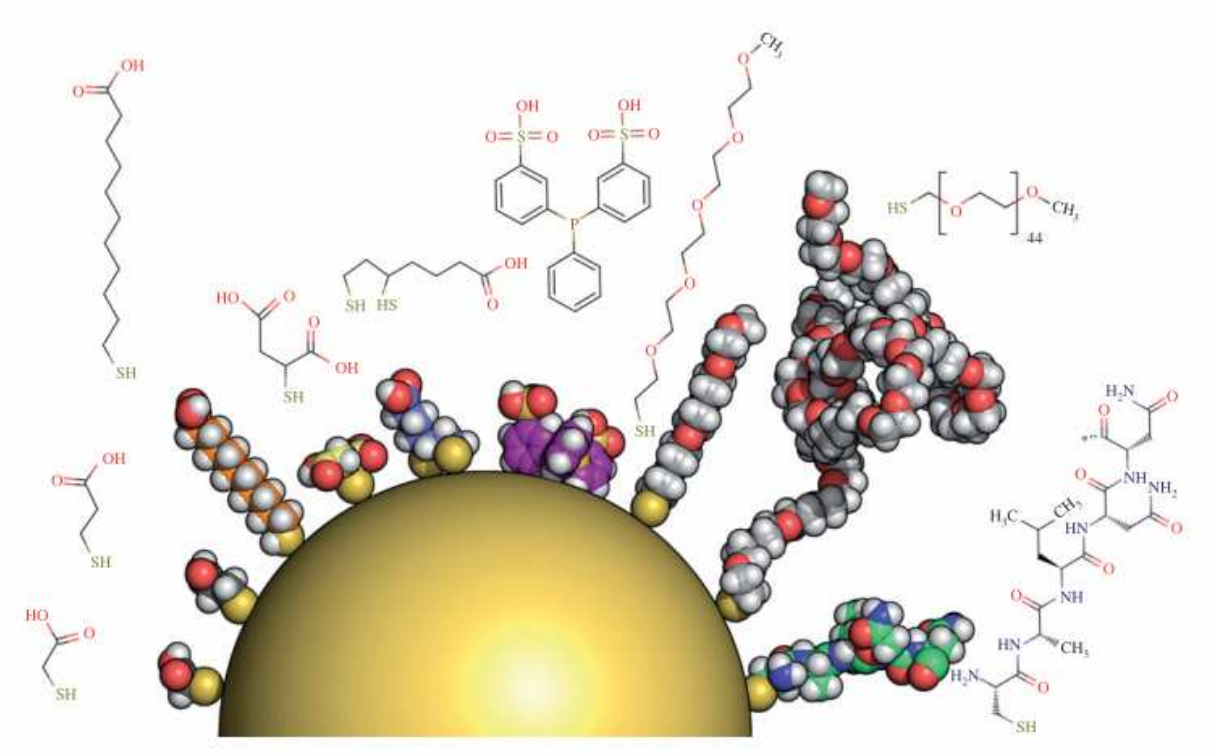

Figure 6. Représentation d'une nanoparticule d'or avec différents ligands décrits dans la littérature comme stabilisants en milieu aqueux. La particule est idéalisée comme une sphère lisse, les molécules et la particule ne sont pas à la même échelle. De gauche à droite : l'acide mercaptoacétique, l'acide mercaptopropionique, l'acide mercaptoundécanoïque, l'acide mercaptosuccinique, l'acide dihydrolipoïque, la bis-sulfonate triphénylphosphine, les $mPEG_5$-SH, $mPEG_{45}$-SH (2000 g/mol), et un petit peptide (Sperling et Parak, 2010).

I.1.4.3 Stratégies pour étudier la stabilité des nanoparticules d'or

Comme mentionnée précédemment, la stabilité des NP d'or est fortement liée au(x) mécanisme(s) de stabilisation mis en jeu ainsi qu'à la force de l'interaction entre l'agent stabilisant et la surface métallique. Ainsi différentes stratégies expérimentales ont été développées pour prévoir la stabilité des NP d'or en fonction du temps sous l'effet de divers paramètres. Ce sont : (i) l'échange de ligands avec les ligands pré-greffés, (ii) la température, (iii) la concentration en ions de

la solution, (iv) le changement du pH.

Dans ces études, il est nécessaire d'évaluer plusieurs caractéristiques physico-chimiques telles que la taille, le potentiel zêta, le λ_{max}, l'absorbance à λ_{max}, la concentration en NP ainsi que l'état de la surface (présence et densité de ligands en surface). Les différentes techniques utilisées pour déterminer ces paramètres sont résumées dans le tableau 2.

Tableau 2. Différentes techniques de caractérisation des nanoparticules d'or

Technique	**Propriétés caractérisées**	**Intérêts et limites de la mesure**
Diffusion dynamique de la lumière	- Rayon hydrodynamique - Distribution de la taille - Etat d'agrégation	- Mesure non destructive qui permet d'accéder à la taille de NP en suspension dans un liquide ; - Donne des informations relatives à la stabilité des NP en fonction du temps ; NP dans différents milieux (PBS, milieu de culture,...) ; - Fournit la taille hydrodynamique des NP (diamètre du cœur métallique + l'épaisseur de la couronne).
Microscopie électronique à transmission	- Taille géométrique - Distribution de taille et forme - Etat d'agrégation - Composition élémentaire de l'échantillon (TEM couplé avec spectrométrie de rayons X)	- Technique destructive qui permet la mesure directe des propriétés morphologiques et structurales des NP, y compris la composition élémentaire ; - Impose des techniques de préparation particulières ; - Analyse réalisée sous vide.
Microscopie à force atomique	Taille et distribution de la taille - Morphologie, texture de la surface et rugosité - Etat d'agrégation	- Visualisation en trois dimensions de la surface analysée ; - Permet d'obtenir des informations sur les propriétés physiques et les forces d'interaction des NP d'or ; - La mesure peut se faire sans vide.
Spectrophotométrie d'absorption UV-Visible	- Taille - Etat d'agrégation	- Le suivi dans le temps de λ_{max} et de l'absorbance à λ_{max} permet de donner des informations relatives à la stabilité des NP d'or.
Spectrométrie de masse à source plasma à couplage inductif	- Composition élémentaire de l'échantillon	- Dosage de l'or et d'autres éléments contenus dans les NP d'or ; - Mesure rapide ; - Sensibilité élevée ; - Technique coûteuse et peu disponible dans la majorité des laboratoires.
Spectrophotocolori-métrie	- Dosage de l'or	- Dosage de l'or contenu dans les NP d'or ; - Permet de calculer le rendement de synthèse ; - Concentration et absorbance molaires des NP d'or (en utilisant le diamètre obtenu par TEM) ; - Sensibilité moins élevée que par ICP-MS ; - Mesure rapide.
Electrophorèse capillaire	- Taille - Charge des particules	- Détermination de la taille ainsi que de la charge des NP (potentiel zêta) ; - Utilisation de volumes d'échantillons réduits ; - Mesure rapide et à bas coûts.
Spectrométrie de photoélectrons induits par rayons X	- Etat de la surface	- Identification et quantification des éléments présents à la surface des NP d'or ; - Informations sur l'environnement chimique de l'élément détecté tel que le type de liaisons, l'état d'oxydation, la fonction chimique, etc... ; - Technique coûteuse et peu disponible dans la majorité des laboratoires.

Les réactions d'échanges de ligands avec les ligands pré-greffés

Afin de prévoir la stabilité de NP d'or en fonction du temps, une méthode employée par de nombreux auteurs consiste à ajouter un ligand (citons le GSH, le DHLA, la cystéine et le dithiothréitol (DTT)) à la solution contenant les NP stabilisées par d'autres ligands (Kim *et al.*, 2005, Roux *et al.*, 2005, Chompoosor *et al.*, 2008, Zhang *et al.*, 2009).

Le ligand greffé est difficilement échangeable s'il se lie fortement à la surface métallique. Comme évoqué précédemment, les ions citrate sont liés à la surface métallique par des interactions électrostatiques. Ainsi, ces ions peuvent être facilement échangeables en solution par le DTT (Zhang *et al.*, 2009). Contrairement aux NP stabilisées par les ions citrate, les NP stabilisées par des ligands de type thiol (forte interaction avec la surface métallique) conduisent à un taux d'échange de ligand très faible voire nul (Zhang *et al.*, 2009).

La réactivité chimique des NP d'or vis-à-vis d'autres molécules est également liée à leur charge en solution. Des études réalisées par Chompoosor *et al.* (2008) ont montré que les dérivés de monothiols chargés positivement sont plus facilement échangeables avec des molécules chargées négativement (comme le GSH, le DHLA et la cystéine) que les monothiols chargés négativement. En effet, ces dernières molécules présentent une forte répulsion électrostatique avec les thiols étudiés (figure 7).

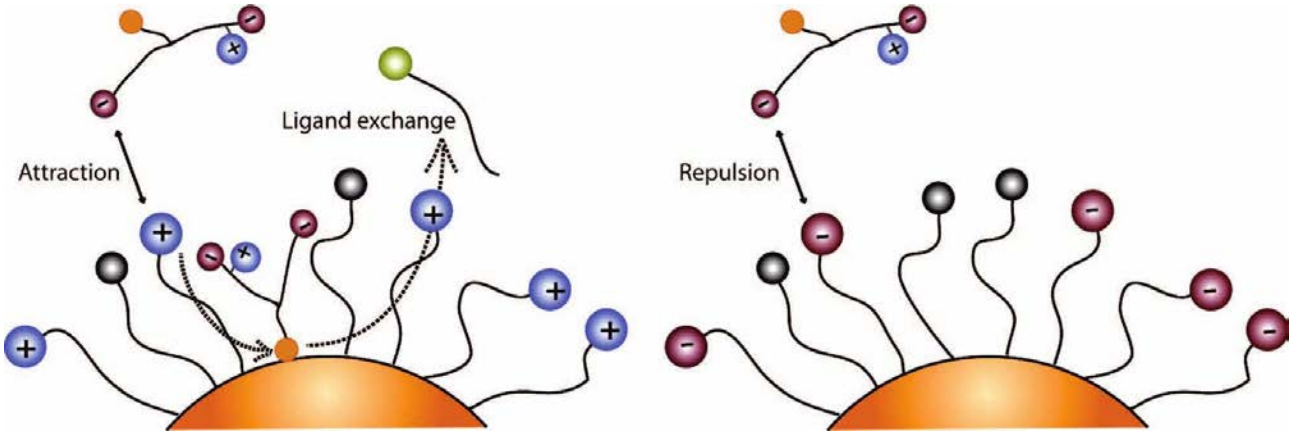

Figure 7. Effet de la charge des nanoparticules d'or sur leur réactivité vis-à-vis des molécules chargées négativement (Chompoosor *et al.*, 2008).

Les méthodes d'accélération pour la prédiction de la stabilité des nanoparticules d'or

La stabilité des NP d'or peut être étudiée par modification de la température, du pH ou de la force ionique par ajout d'un sel neutre.

Parmi les méthodes d'accélération, les méthodes thermiques sont souvent employées et consistent à augmenter la température afin d'accélérer la déstabilisation. En effet, les NP d'or stabilisées par de faibles interactions sont fortement sensibles à la hausse de la température. Par exemple, des NP d'or stabilisées par les ions citrate sont stables (pas de modification du rayon hydrodynamique) pendant 21 jours à 4°C et deviennent instables (augmentation du rayon hydrodynamique) à partir du sixième jour à 23°C (Balasubramanian *et al.*, 2010a). En revanche, des NP d'or stabilisées par des polymères monothiols (HS-PEG) sont stables de 4°C à 70°C (pas de modification de λ_{max} et de l'absorbance à λ_{max}) (Zhang *et al.*, 2007).

La plupart des agents stabilisants actuellement utilisés pour limiter l'agrégation des NP d'or possèdent un groupement hydrophile en bout de chaîne (par exemple : -COOH, -OH, $-NH_2$). Cependant, ces ligands sont très sensibles aux variations de pH. Par exemple, les NP d'or fonctionnalisées par le DHLA ne sont pas chargées en surface pour des valeurs de pH < pKa (-COOH) = 4,85, et de ce fait s'agrègent (Roux *et al.*, 2005).

La stabilité des NP d'or peut aussi être évaluée par la modification d'autres facteurs, comme la force ionique de la solution. Comme pour la température, les NP d'or établissant de faibles interactions avec l'agent stabilisant sont plus sensibles à la présence de sels dans la solution que les NP d'or fortement liées à l'agent stabilisant (Zhang *et al.*, 2007).

I.2 Risques potentiels des nanoparticules d'or sur la santé

Si la stabilité des suspensions de NP d'or est une condition *sine qua non* à leur utilisation dans le domaine médical, la connaissance des conséquences pour l'organisme exposé à ce type de particules est primordiale. Cette problématique est commune à toutes les particules auxquelles un organisme peut être exposé. En effet, la présence des NP dans les produits de notre quotidien est aujourd'hui un fait de plus en plus courant. A l'heure actuelle, selon la base de données Nanowerk, plus de 2834 produits contenant des NP sont déjà commercialisés. Cependant, peut-être en conséquence des expériences du passé dans d'autres domaines industriels néfastes pour l'Homme, il existe une incertitude et une crainte réelle quant à leurs risques pour la santé. La législation européenne vise à réglementer et à contrôler l'utilisation et l'exposition aux nanomatériaux (European commission, 2012). En France, à compter du 1er janvier 2013 (décret n° 2012-233 du 17

février 2012), tout fabricant, importateur et distributeur de substances contenant des NP au delà de 100 g/an, sera tenu de déclarer au Ministère de l'Environnement les quantités et les types de NP utilisées; toutefois, cette déclaration ne mentionnera pas leurs conséquences éventuelles pour la santé. De plus, il n'existe, pour l'instant, ni protocole standard, ni NP de référence adaptées aux études toxicologiques.

Malheureusement, une très faible proportion des recherches sur les NP s'intéresse à leurs risques, ce qui retarde la mise en place de leurs règles d'utilisation par les autorités compétentes. Cette tâche s'avère très lourde et complexe en raison du grand nombre de NP existantes, mais surtout en raison du grand nombre de caractéristiques physico-chimiques (taille, forme, état de surface, fonctionnalisation,...) qui peuvent influencer leurs effets biologiques. De plus, les tests biologiques classiquement utilisés et conçus pour évaluer la toxicité de substances chimiques se révèlent parfois non adaptés aux NP et trompeurs, ceci en raison d'interférences découlant de leurs propriétés nouvelles et pour certaines de leur insolubilité dans l'eau (Kroll *et al.*, 2009, Dhawan et Sharma, 2010, Kroll *et al.*, 2011, Kroll *et al.*, 2012).

Dans les prochains paragraphes, nous allons tout d'abord décrire les principaux effets biologiques connus des NP et plus particulièrement des NP d'or. De plus, de nombreux travaux ont souligné l'implication du stress oxydant dans la toxicité des NP inorganiques observée sur les cellules. Ainsi les techniques couramment utilisées pour évaluer l'induction du stress oxydant par les NP, les éventuelles difficultés rencontrées lors de leur application et l'influence des caractéristiques physico-chimiques des NP sur ces tests seront ensuite détaillées et discutées dans une revue en préparation pour soumission à Talanta.

I.2.1 Effets biologiques des nanoparticules d'or à l'échelle cellulaire et moléculaire

Comme souligné plus haut, différents types des NP sont déjà mis sur le marché et leurs effets sur la santé dépendent de leurs caractéristiques (taille, potentiel zêta, etc...). Ainsi pour évaluer leurs effets biologiques, les études *in vitro* semblent être une première étape indispensable car elles sont particulièrement adaptées aux tests d'un très grand nombre de conditions et de variables. De plus, ces études livrent une grande quantité d'informations sur la toxicité aiguë (à court terme) des NP ainsi que sur leur mécanisme de toxicité au niveau cellulaire et moléculaire (à plus long terme).

Les études de toxicité *in vitro* sont généralement conduites sur des cellules en culture issues des différents organes du corps. Les cellules épithéliales et les macrophages, par exemple, sont

couramment utilisés comme modèles *in vitro* car ils reproduisent respectivement les caractéristiques des barrières présentes dans le corps et propres au système immunitaire.

Afin de connaître l'interaction des NP d'or avec les cellules et donc de prévoir et comprendre leur mécanisme d'action, l'internalisation et la localisation intracellulaire des NP d'or sont souvent étudiées (tableau 3). L'internalisation des NP d'or par les cellules dépend principalement de la nature de l'agent stabilisant utilisé, se trouvant en surface (Goodman *et al.*, 2004, Hutter *et al.*, 2010). Cependant, quel que soit le type de NP d'or testé, ces dernières sont localisées dans des vésicules qui sont probablement des vésicules d'endocytose (Shukla *et al.*, 2005, Arnida et Ghandehari, 2010, Brandenberger *et al.*, 2010). Dans ces différentes études, aucune NP d'or n'a été retrouvée libre dans le cytoplasme, dans les organites ou dans le noyau.

Tableau 3. Différentes études de l'internalisation des nanoparticules d'or décrites dans la littérature

Agent stabilisant	Propriétés		Cellule			Résultats		Références
	Size (nm)	ζ (mV)	Modèle cellulaire	Incubation Dose	Incubation Temps	Internalisation	Méthodes	
Lysine	3-8	*ND*	Macrophages (RAW 264.7)	50 µM	24 h	Oui	AFM CFLSM TEM	Shukla *et al.* (2005)
				50 µM	24 h			
PEG	50 (sph) 10x45 (r)	-27 +1		10 µg	6 h		TEM ICP-MS	Arnida *et al.* (2011)
Citrate Cys SAP Cys AGIP	12 12 17	-36 +2 -7	Macrophages murins de moelle osseuse	Quantité de NP d'or qui transporte 10^{-6} M du peptide	6 h	Non Oui (récepteur spécifique) Oui (récepteur spécifique)	TEM	Bastús *et al.* (2009a)
Citrate	15	*ND*	Co-culture de cellules : épithéliales, dendritiques et macrophages primaires.	[Au] = 200-2000 µM	4 et 24 h	Oui	TEM	Brandenberger *et al.* (2010)
PEG CTAB	23 77 12 23 77 12	-22 -9 -23 +42 +39 +46	Cellules microgliales (N9)	[NP] = 10^3-10^{11} NP/mL	24 h	Non Oui Non Oui Oui Oui	Microscope à fond noire TPL images TEM ICM-AES	Hutter *et al.* (2010)
AVA L-DOPA Mélatonine Sérotonine	35 35-45 35-45 *ND*	*ND*	Macrophages	10 mM	0,5 h (6 h*)	Oui Non* Oui Oui	TEM Microscopie confocale	Krpetic *et al.* (2010)
CTAB HS-PEO-OH HS-PEO-COOH HS-PEO-NH_2	15 x 50 (r)	+90 -4.6 -20.2 +21.3	Monocytes humains et macrophages	≤ 1 DO	1 h	Oui	TEM ICP-MS	Bartneck *et al.* (2010)
CTAB		+90	Cellules épithéliales humaines (HeLa)			Oui (1 %)		
Citrate CALNN PEG*	16	*ND*	Cellules épithéliales humaines (HeLa)	5 nM	2h 24 h*	Oui Oui Non	TEM AES	Nativo *et al.* (2008)

PEG - polyéthylène glycol, sph- sphérique, r - barre, *ND* - non déterminé, AFM - microscope à force atomique (*atomic force microscopy*), CFL-SM - microscope confocal à balayage laser (*confocal-laser scanning microscopy*), TEM- microscope électronique à transmission (*transmission electron microscopy*), ICP-MS - spectrométrie de masse à source plasma à couplage inductif (*Inductively coupled plasma mass spectrometry)*, DO – densité optique, SAP- sweet arrow peptide, AGIP- peptide inhibiteur de la croissance amyloïde (*amyloid growth inhibitory peptide*), CTAB- bromure de cétyltriméthylammonium (*cetyl trimethylammonium bromide*), TPL- Luminescence par deux photons (*Two-Photon Luminescence*), ICP-AES- spectroscopie d'émission atomique avec plasma à couplage inductif (*Inductively coupled plasma- atomic emission spectroscopy*), AVA - acide 5-aminovalérique, PEO - oxyde de polyéthylène, CALNN - ligand du type pentapeptide (Cys-Ala-Leu-Asn-Asn), AES - spectroscopie d'émission atomique (*Atomic Emission Spectroscopy*)

Les effets des NP d'or sur la viabilité cellulaire ont été décrits dans plusieurs études. Un effet cytotoxique a parfois été constaté. L'intensité de ces effets dépend de plusieurs paramètres comme le modèle cellulaire (Patra *et al.*, 2007), la nature du stabilisant utilisé (Hutter *et al.*, 2010), leur taille (Pan *et al.*, 2009), leur dose (Goodman *et al.*, 2004, Patra *et al.*, 2007) ou encore leur potentiel de surface (Goodman *et al.*, 2004). Un des principaux effets notés suite à une exposition aux NP d'or est l'activation de facteurs proinflammatoires comme les cytokines (Bastús *et al.*, 2009a, Hutter *et al.*, 2010). Ce sont des facteurs qui favorisent l'inflammation c'est-à-dire la réponse immunitaire. Ainsi ces NP ne sont pas inertes pour l'organisme. Cependant, certaines études ne montrent pas de réponse proinflammatoire (Shukla *et al.*, 2005).

En raison de leur activité catalytique reconnue (Esumi *et al.*, 2003), l'hypothèse de la génération d'espèces réactives de l'oxygène (ROS) a été vérifiée par différents auteurs. Cette production de ROS a été corrélée à des dommages membranaires et à des dommages oxydatifs de l'ADN et donc elle pourrait expliquer l'origine des autres dommages à l'ADN constatés comme les micronoyaux (Li *et al.*, 2010). Cependant, il faut noter qu'il n'y a pas toujours de dommages à l'ADN (Alkilany et Murphy, 2010). Le tableau 4 résume les principaux résultats des études citées. Les mécanismes d'action et les conséquences aux échelles cellulaire et moléculaire d'une exposition à des NP d'or semblent donc dépendre de beaucoup de paramètres et demandent à être éclaircis.

Cependant, le panel de techniques à disposition pour étudier le stress oxydant occasionné par l'exposition à des NP d'or, et plus généralement à des particules inorganiques, se heurte à des difficultés d'ordre analytique menant parfois à des résultats contradictoires tel que cela est constaté dans la littérature. La revue présentée ci-dessous tente de répertorier ces techniques mais aussi d'alerter et de donner des solutions aux expérimentateurs pour suppléer ces difficultés.

I.2.2 Article 1. Tournebize J., Sapin-Minet A., Boudier A., Bartosz G. and Leroy P. Pitfalls of assays devoted to evaluation of oxidative stress induced by inorganic nanoparticles. En préparation pour soumettre à *Talanta*.

.

Tableau 4. Effets biologiques des nanoparticules d'or décrits dans des études *in vitro*

Agent stabilisant	Propriétés			Cellule							Toxicité	Références
				Modèle cellulaire	Incubation		Statut redox					
	Taille (nm)	ζ (mV)	Forme		Dose	Temps	RNS/ ROS	GSH	Cytokines	Expression de gènes		
Citrate DHLA	5	-50 -40	Sphérique	Macrophages (NR8383)	[NP] = 10 nM	24h	RNS = (-)	*ND*	*ND*	*ND*	> 80 %	Leroy *et al.* (2011)
PEG	23	-22	Sphérique	Cellules microgliales (N9)	[NP] = 10^6–10^{11} NP d'or/mL	24h	RNS = (-)	*ND*	GM-CSF (+) IL-1α (non)	TLR-2 (non)	80 %	Hutter *et al.* (2010)
	77	-9	Oursin						GM-CSF (+) IL-1α (+)	TLR-2 (+)	100 %	
	12	-23	Barre						GM-CSF (+) IL-1α (non)	TLR-2 (+)	100 %	
CTAB	23	+42	Sphérique						*ND*	*ND*	0 %	
	77	+39	Oursin						IL-1α (+)	TLR-2 (-)	100 %	
	12	+46	Barre						*ND*	*ND*	> 90 %	
Citrate	8	*ND*	Sphérique	Hépatocytes (HL7702)	[NP] = 5 – 50 nM	12 – 72 h	ROS = (+)	30 % (72h)	*ND*	*ND*	40 %	Gao *et al.* (2011)
	37						*ND*	*ND*			> 85 %	
Citrate	12	-36	Sphérique	Macrophages murins de moelle osseuse	Quantité de NP d'or qui transporte 10^{-6} M du peptide	6 h	*ND*	*ND*	*ND*	Non	> 90 %	Bastús *et al.* (2009a), Bastús *et al.* (2009b)
Cys SAP (petit peptide)	12	+2								TNF-α (+) IL-1ß (+) IL-6 (+) NOS2 (+)		
Cys AGIP (peptide long)	17	-7										
Citrate	33	*ND*	Sphérique	Cellules rénales de hamster (BHK21)	[NP] = 10 – 120 nM	72 h	*ND*	*ND*	*ND*	*ND*	100 %	Patra *et al.* (2007)
				Carcinome de foie humain (Hep2G)		72 h					100 %	
				Carcinome de foie humain (A549)		36 h					50 %	
Sérum de veau fœtal	35	- 11	Sphérique	Fibroblastes pulmonaires	[NP] = 1 nM	72 h	*ND*	*ND*	*ND*	Surexpression de différents gènes impliqués dans le stress oxydant	*ND*	Li *et al.* (2010)

Tableau 4. *Suite*

Agent stabilisant	Propriétés			Cellule							Toxicité	Références
				Modèle cellulaire	Incubation		Statut redox					
	Taille (nm)	ζ (mV)	Forme		Dose	Temps	RNS/ ROS	GSH	Cytokines	Expression de gènes		
Citrate	15	*ND*	Sphérique	Co-culture de cellules : épithéliales, dendritiques et macrophages primaires.	[Au] = 200 – 2000 µM	4 et 6 h	*ND*	*ND*	Non (IL-1 , IL-2, IL-4, IL-6, IL-8, IL-10, GM-CSF, TNF-α, INF-γ)	Non (TNF-α, IL-8, iNOS, HO-1, SOD-2)	*ND*	Brandenberger *et al.* (2010)
Citrate	18	*ND*	Sphérique	Cellules épithéliales humaines (HeLa)	[NP] = 0,2 – 2 nM	3 – 6 h	*ND*	*ND*	*ND*	Non (puces à gènes)	100 %	Khan *et al.* (2007)
Lysine	37	*ND*	Sphérique	Macrophages (RAW 264.7)	[Au] = 10 – 100 µM	24h 48h 72h	RNS (-) RNS (-) *ND*	*ND*	TNF-α (non) IL-ß (non) *ND*	TNF-α (no) *ND*	> 90 % > 90 % 85 %	Shukla *et al.* (2005)

Pourcentage (%) déterminé à la dose maximale en NP d'or; Non - pas d'induction ; (-) - diminution; (+) - augmentation; *ND* - non déterminé; SAP : *sweet arrow peptide*; AGIP - peptide inhibiteur de la croissance amyloïde (*amyloid growth inhibitory peptide*); PEG - poly (éthylène glycol); CTAB - bromure de cétyltriméthylammonium.

Pitfalls of assays devoted to evaluation of oxidative stress induced by inorganic nanoparticles

Juliana TOURNEBIZE[1], Anne SAPIN-MINET[1], Ariane BOUDIER[1], Grzegorz BARTOSZ[2] and Pierre LEROY[1*]

[1] *Université de Lorraine, CITHEFOR, EA 3452, Nancy, 54001, France*

[2] *Department of Molecular Biophysics, University of Lodz, Lodz, Poland*

[*] pierre.leroy@pharma.uhp-nancy.fr

En préparation pour soumettre à *Talanta*.

Abstract

During the last years, there has been a remarkable increase in the use of inorganic nanoparticles (NP) in different applications, including consumer and medical products. Despite these exciting applications, the extremely small size of NP allows them to penetrate cells and can interact with cellular structures causing serious side effects. A number of studies showed that NP predominantly causes adverse effects via induction of oxidative stress – an imbalance between damaging oxidants and protective antioxidants – resulting in inflammation, immune response, cell damage, genotoxicity, etc… Most of the *in vitro* methods used for measurement of oxidative stress biomarkers were designed and standardized for conventional organic, inorganic and biochemical compounds. More recently, these methods have been adapted to studies related to various nanomaterials. Thus, this review is an attempt to highlight some current methods employed in and to provide a critical analysis of the major challenges and issues faced in this emerging field.

Table of contents

1. Introduction

In recent years, an increasing number of nanomaterials have entered the market of products directly related to human use. For instance, NP are frequently used in products which range from cosmetics (TiO_2, Fe_2O_3) to wound dressing (AgNP). Nanoparticles also offer an extraordinary opportunity for applications in medicine [1]. Today, more that 25 nanomedicines have already been approved for human use, such as AmBisome® (nanoformulated Amphotericin B) and Feridex IV® (FeO NP as a magnetic imaging contrast media). These applications were mentioned in recent papers and will not be discussed in this review [2-3]. These NP carry out the drug, offer drug protection or the ability of drug sustained release. Advanced FDA-approved use of NP includes also quantum dots (QDs) in living cell imaging, and zirconium oxides in bone replacement and prosthetic devices.

Based on their composition, NP can be grouped into the following categories: (i) organic NP (polymers, dendrimers…); and (ii) inorganic NP (Ag, Au, Fe, Pt, TiO_2, QDs, silica NP, carbon nanotube,…) [3]. The surface of NP can be modified by multiple ligands such as target molecules, polyethyleneglycols, thiols, leading to the increase of NP stability and the decrease of their surface reactivity toward molecules and cell components (Fig. 1 A).

Comparing to the large number of studies interested in NP in the literature, the biological effects of NP have received little attention, where the focus seems to be mainly synthesis and characterization of new nanomaterials. However, there are several recent reports in which oxidative stress has been identified as an important mechanism for toxicity of all types of NP [4-6]. Furthermore, the evaluation of oxidative stress biomarkers may be a useful way to identify which physico-chemical properties of NP are associated with the biological insults, to permit targeted screening and allow materials scientists to generate new and safer NP with this structure-toxicity information in mind.

Oxidative stress describes various deleterious processes resulting from an imbalance between protective antioxidants and damaging oxidants, reactive oxygen and nitrogen species (ROS and RNS, respectively). High levels of ROS or RNS are deleterious to all classes of cell components: lipids, proteins, nucleic acids, and other macromolecules (Fig. 1B). However, these species are also formed in normal physiology reacting with cellular components, leading to the activation of intracellular signaling pathways, nuclear transcription factors, inducing gene expression and cell responses such as repair, adaptation or transformation; this process is known as redox signaling. Excellent descriptions of the individual molecules and their scavengers can be found in a number of reviews [7-9] and in a book [10].

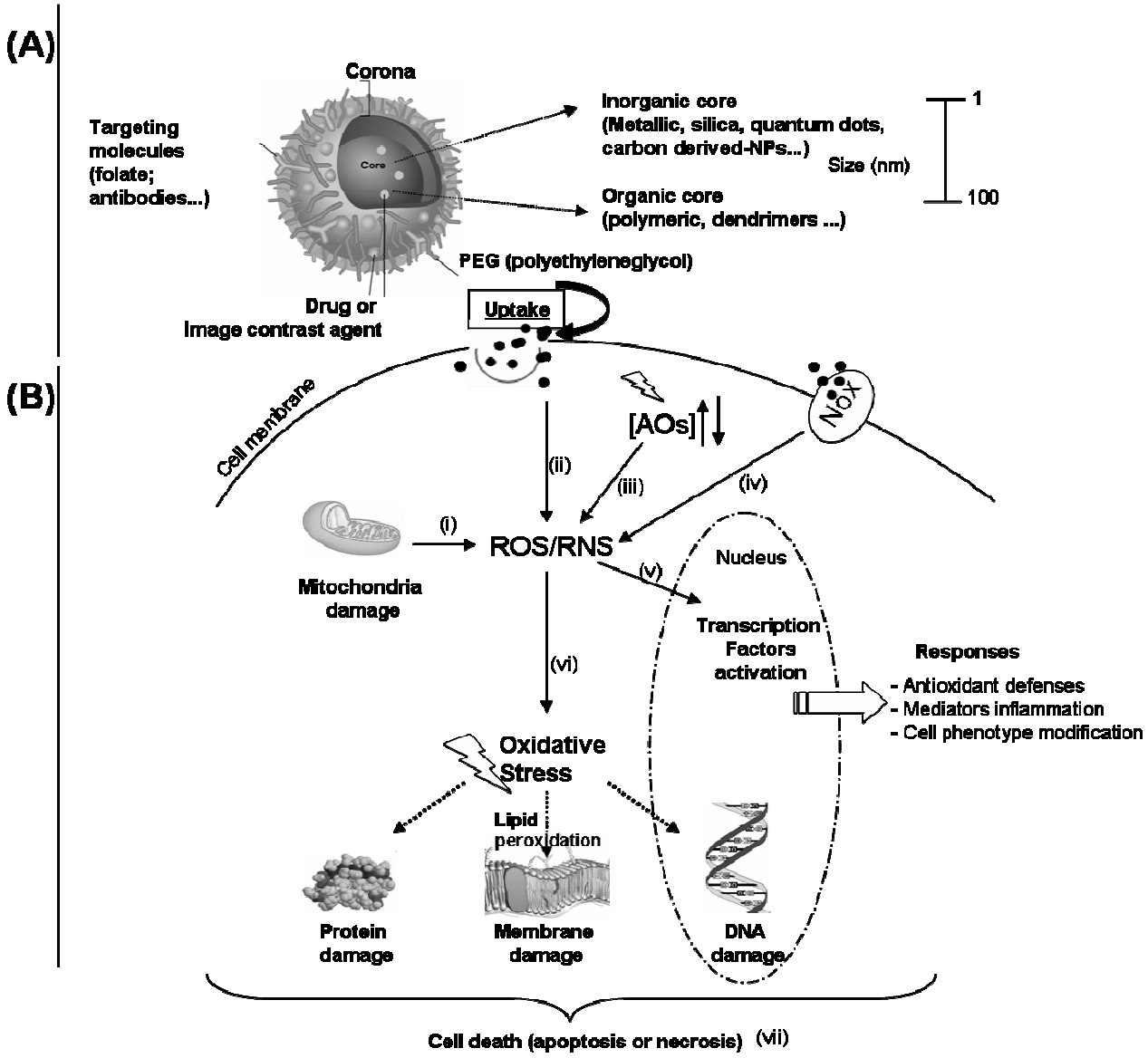

Fig. 1. Interaction of nanoparticles (NP) with cells. (A) Schematic representation of NP types and structures; (B) Interaction of NP with cellular constituents: interaction with mitochondria (i), generation of ROS/RNS by NP due to their surface reactivity (ii), interaction with antioxidants (iii), and NADPH oxidase (NOX) protein family (iv) are shown. Transcription factor activation (v) and damages of cell components (vi, vii).

Currently, most of the methods proposed in the literature to evaluate if NP can induce oxidative stress have been carried out by classical oxidative stress assays. However, these techniques designed for testing established drugs and chemicals are not always adapted to evaluate NP impact. Indeed, some NP can interfere with assay components and readout systems, leading to conflicting reports and the generation of unreliable data, due to their unsual physicochemical

properties, including: (i) high surface area, leading to increased adsorption capacity; (ii) different optical properties that interfere with fluorescence or visible light absorption detection systems; (iii) increased catalytic activity due to enhanced surface energy; and (iv) magnetic properties that make them redox active and thus interfere with methods based on redox reactions [6, 11-20].

On the basis of literature, the potentially most relevant mechanisms of inorganic NP for the protection or for the induction of oxidative stress *in vitro* are presently reviewed. Then, this review is limited to explain the *in vitro* methods used to evaluate these interactions and in particular, the interferences of NP with classic oxidative stress assays.

Among the different types of NP, in this review we chose to study only the inorganic NP which, due to their high surface reactivity, are more likely to have interferences with classical oxidative stress methods, leading to confuse results.

2. How nanoparticles induce and/or prevent oxidative stress

The following sections provide a brief overview of the possible targets of NP in cells and explain the ability of some inorganic NP – due their surface reactivity – to decrease or increase the levels of ROS/RNS.

2.1. Interaction of nanoparticles with cells: target structures

As shown in Fig. 1B, NP may interact with different cell structures and species in cells, including: plasma membrane, mitochondria, endoplasmatic reticulum, antioxidant compounds, proteins and nucleus. These interactions can lead to changes in cellular redox potential that could lead to benefit or adverse effects [21].

Nanoparticles interfere with plasma membrane in different manners. Transmembrane proteins, such as NOX enzymes, can be activated by NP, thus inducing the activation of intracellular signaling pathways [22-24]. Nanoparticles can also be internalized by different mechanisms depending on the physico-chemical properties of NP and the exposed cell type (phagocytes *versus* other cell types). These possible pathways have already been reviewed [25] which provide an extensive overview of these mechanisms and will not be presently discussed.

Once the NP are internalized into the cell, it interact with organelles, *e.g.* mitochondria (source of $O_2^{\bullet-}$, H_2O_2, Ca^{2+}) and endoplasmatic reticulum (source of Ca^{2+}), can lead to further ROS and RNS production. The enhanced generation of ROS, the presence of NP (TiO_2, carbon black, fullerol, and polystyrene) inside mitochondria of exposed cells as well as their consequent damage

has been reported [4]. The interaction of NP with mitochondria and/or endoplasmic reticulum may also cause the dysregulation of Ca^{2+} levels following the NOX activation and resulting $^{\bullet}NO$ production, which, at high concentrations, induces peroxynitrite ($ONOO^-$) formation in presence of $O_2^{\bullet-}$.

Due to their high surface reactivity, citrate-stabilized AuNP interact directly with antioxidants, *e.g.* reduced glutathione (most abundant antioxidant inside cells), present as well as in cell-free conditions [26] as in cells [5], resulting in deregulation of the redox balance and overproduction of ROS/RNS.

Depending on the level of ROS/RNS induced by NP outside or inside the cells, NP can lead to the activation of intracellular signaling pathways (*e.g.* MAPK), nuclear transcription factors (*e.g.* AP-1, NF-kB or Nrf2), and altered gene expression following the induction of adaptive responses including release of inflammation mediators, antioxidant defence activation, and cell phenotype modification [21]. The oxidative stress resulting from an excess of ROS/RNS overwhelms the antioxidant capacities of the cells and could lead to injuries of cell components, *e.g.* lipid peroxidation, oxidation of protein and DNA damages, following cell death by apoptosis or necrosis.

2.2. Surface reactivity of nanoparticles

Due their high surface reactivity, some NP (*e.g.* fullerenes, CeO_2, AuNP,…) could act as scavenger and/or generator of ROS/RNS in cell-free conditions and/or in living organisms [26-27].

As shown in Fig. 2, the reactivity of NP with ROS and RNS species depends on: (i) the catalytic potency of NP surface; (ii) partial dissolution of NP and resulting release of metallic ions, and (iii) adsorption of molecules onto their surface.

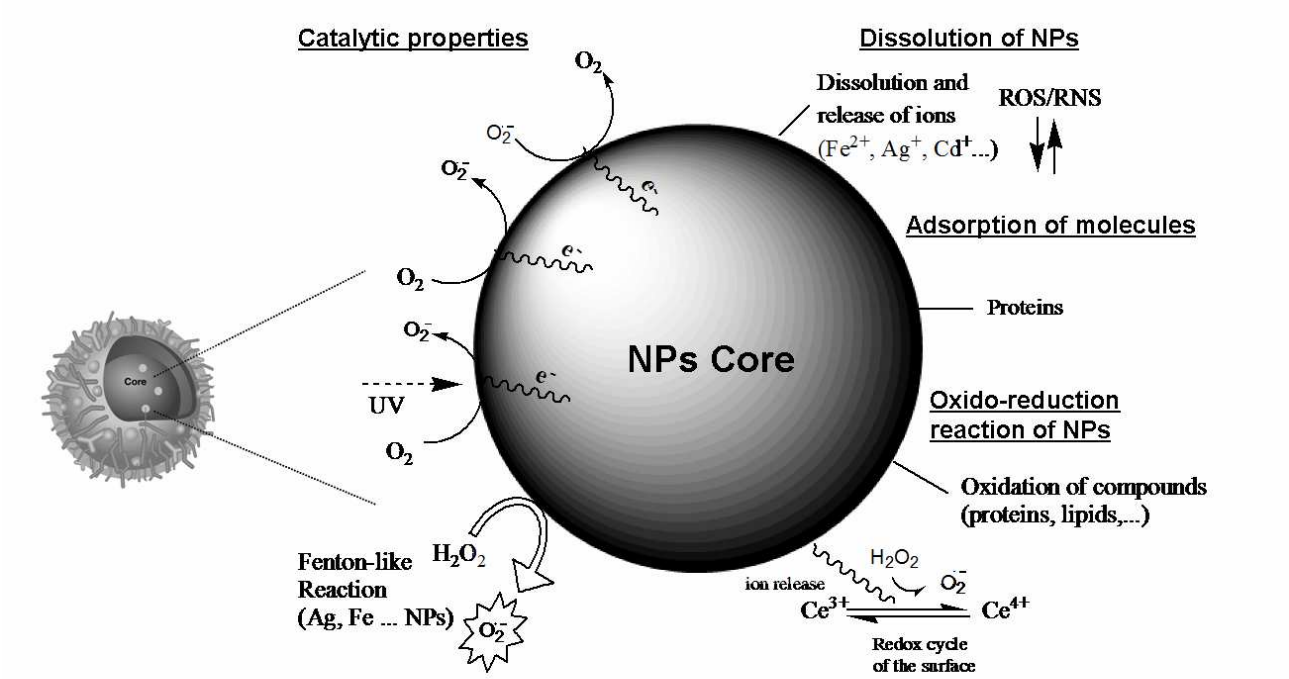

Fig. 2. Surface reactivity of nanoparticles. Electronic and/or ionic transfer occurring during the catalytic, dissolution and redox reactions of nanoparticles in cell-free conditions or during cell exposure

2.2.1 Nanoparticles as radical scavengers

Free radicals can be scavenged by NP after catalytic reaction on their surface. For instance, AgNP coated with green components (*e.g.* aqueous extract of orange peel) have shown anti-microbial and free radical scavenging properties [28]. It was showed that bimetallic NP consisting of Au and Pt [29] and metal oxide NP, such as CeO_2, Al_2O_3, Y_2O_3 [30], exhibit scavenging ROS activity through catalytic reaction.

Some publications have shown the antioxidant effect of AuNP stabilized by chitosan [31-32] and dendrimers [33]. Indeed, these NP were capable of scavenging $^{\bullet}OH$. Recently, it has been demonstrated that the antioxidant activity of CeO_2 NP is pH-dependent and these latter NP do not present any antioxidant properties at acidic pH [27]. Among the metallic and oxide NP, inorganic carbon nanotubes (CNT) [34] and fullerene derivatives [35] exhibit a remarkable radical scavenging capacity in aqueous solution aimed at $O_2^{\bullet -}$ and $^{\bullet}OH$.

Nanoparticles can also act as antioxidant delivery systems improving the scavenging properties of the antioxidant alone. For instance, metallic and metal oxide NP have been studied as potential antioxidant delivery systems. Inded, AuNP enhance the antioxidant activity of Trolox® (soluble form of vitamin E) [36] and FeO NP may encapsulated antioxidant enzymes and protect cells against H_2O_2 induced death [37].

2.2.2 Nanoparticles as radical generators

Redox reactions following the dissolution of NP and the resulting release of ions catalyse Fenton-type reaction. In this context, two kinds of metallic NP can be distinguished: (i) fully or partially oxidized NP with a redox potential (Eh) higher that the Eh of most biological redox couples, including CeO_2, Mn_3O_4 and Co_3O_4 NP [30, 38-39], and (ii) fully or partially reduced NP characterized by an Eh lower that the Eh of most biological redox couples, including Fe°- and the Fe_3O_3-based NP [40]. As shown in Fig. 3, NP with Eh close to Eh of biological redox couples are chemically stable, whereas NP with higher or lower Eh are able to be oxidized, reduced or dissolved inducing cell damages.

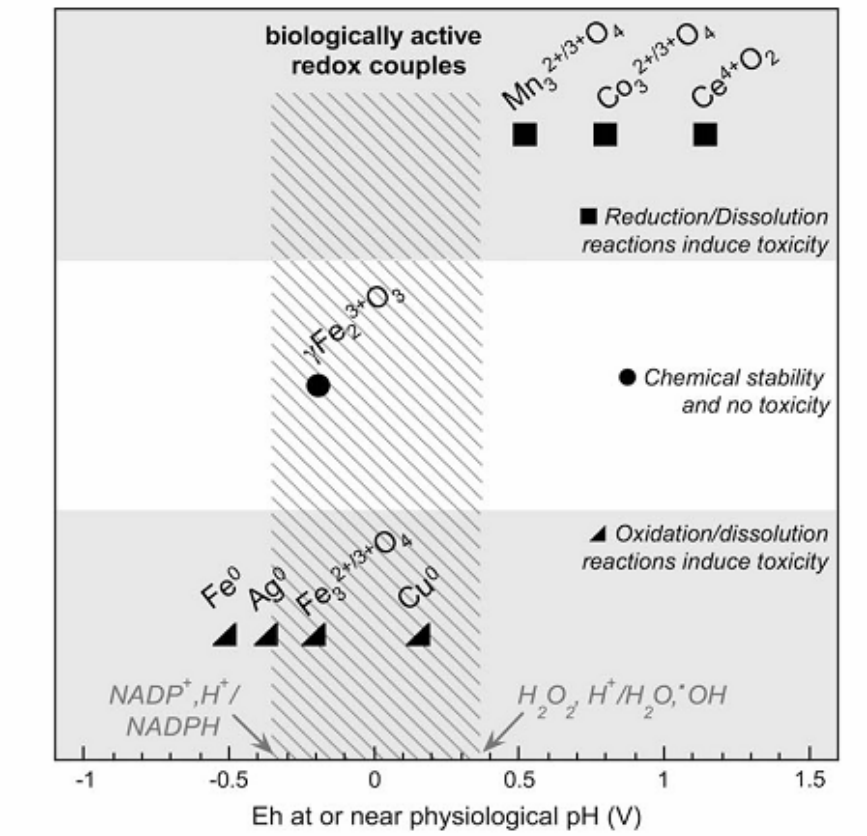

Fig. 3. Plot of the Eh values of various biological redox couples compared to the Eh characteristics of metallic nanoparticles. This figure shows the correlation between the ability of metallicnanoparticles to generate a potential toxicity when they are oxidized, reduced or dissolved in biological in vitro conditions (reproduced from [30]).

In another way, radicals can be generated by NP. For example, fullerenes catalyse the production of $^1O_2$ (in a non-polar environment) and $O_2^{\bullet-}$ (in polar solvents) upon photoexcitation with visible light [41]. Furthermore, AuNP act as a catalyst, causing the production of $^{\bullet}NO$ from

endogenous *S*-nitrosothiols in blood serum and this process is ascribed to the formation of the corresponding covalent Au-thiolate on the surface of AuNP [26, 42].

3. Strategies to investigate oxidative stress: interference of inorganic nanoparticles

The oxidative stress research community has provided a large number of commercial kits and standardised *in vitro* tests especially developed for molecular drugs and chemicals. These same methods have been applied to evaluate NP-induced oxidative stress. However, in many instances these assays are not suitable for investigation of NP, without prior adaptation, since NP can interfere with assay reagents released cellular markers or detection systems thereby generating false positive or negative results [6, 12, 15-16, 43]. In figure 4, we summarize the most common mechanism of NP interferences mentioned below with few examples.

This review part is specifically directed at identifying the problems (due to NP interferences) that researchers can encounter when assessing the NP-oxidative stress impact by the classical assays. In addition, the possible strategies to avoid them are also mentioned.

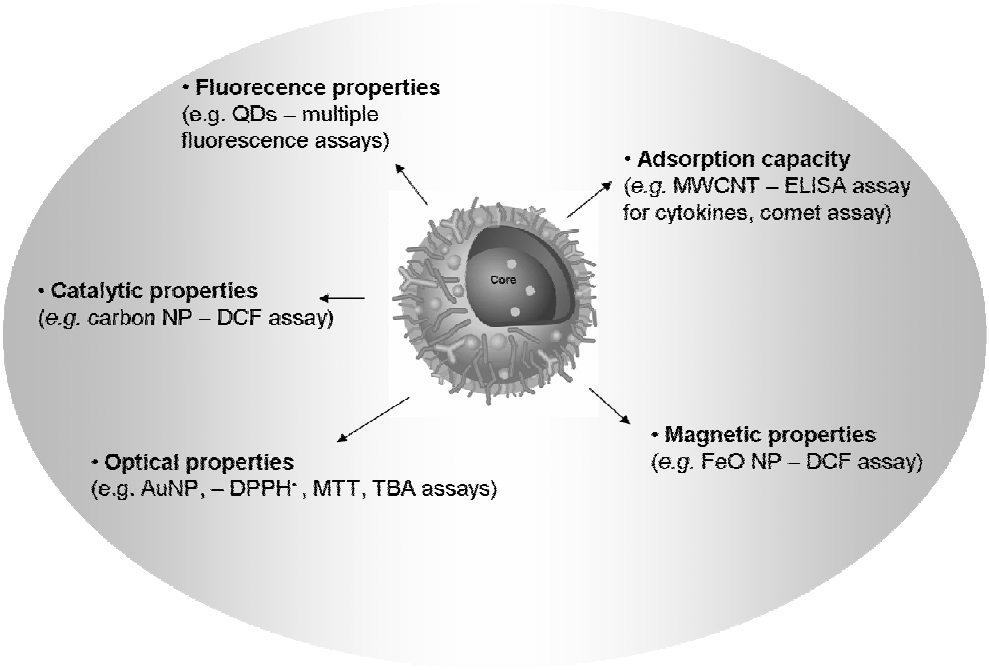

Fig. 4. Nanoparticles specific properties responsible for false-positive and false-negative results with some commonly used oxidative stress assays.

Examples are given as type of nanoparticle – assay in which they cause interference. Abbreviations: QDs, quantum dots; NP, nanoparticles; DPPH•, 1,1-diphenyl-2-picrylhydrazyl radical; MTT, 3-(4,5-dimethylthiazol-2-yl)-2,5-diphenyl tetrazolium bromide; *AuNP, gold nanoparticle; MWCNT, multiwall carbon nanotubes; DCF, dichlorofluorescein; FeO NP, iron oxide nanoparticles.*

3.1 Assays to evaluate the reactivity between inorganic nanoparticles and radicals under cell-free conditions

Numerous chemical assays have been reported to evaluate the capacity of antioxidants to scavenge free radicals; the most commonly used methods are based on the monitoring of blenching rate of coloured radicals: 2,2-azinobis(3-ethyl-benzothiazoline-6-sulfonic acid) ($ABTS^{\bullet+}$) and 1,1-diphenyl-2-picrylhydrazyl radical ($DPPH^{\bullet}$). These assays have also been transferred to the evaluation of NP ability to either scavenge or produce radicals.

3.1.1 Methods to evaluate scavenging of radicals by nanoparticles

The radical scavenging capacities of NP have been evaluated by treating them with coloured radicals or $OH^{\bullet}$ or $O_2^{\bullet-}$ previously produced by other sources. As far as coloured radicals are concerned, several authors used the stable $DPPH^{\bullet}$ [28, 36, 44-45], though the $ABTS^{\bullet+}$ was also used by Fang *et al.* [46]. $DPPH^{\bullet}$ is a free radical that is acquired directly without any preparation but is poorly water soluble, while $ABTS^{\bullet+}$ must be previously generated, *e.g.* by potassium persulfate oxidation [46] but it is soluble in both aqueous and organic media. As $DPPH^{\bullet}$ can only be dissolved in organic (especially alcoholic) media, it is an important limitation when interpreting the role of hydrophilic antioxidants. In all cases, the simplest method to estimate antioxidant activity is to measure spectrophotometrically the loss of the radical color due to its reaction with an antioxidant.

A common problem in the spectrophotometric $DPPH^{\bullet}$ assay is the interference caused by the optical properties of NP. For example, AuNP and AgNP absorb light at the same wavelength as the $DPPH^{\bullet}$ assay (*i.e.* 515 nm). Therefore, separation NP from the solution by including centrifugation [28, 47] or by filtration [48] before measuring $DPPH^{\bullet}$ absorbance, have been proposed to avoid this interference. In addition, electron spin resonance (ESR) has been described as an alternative technique to measure the antioxidant properties of AuNP functionalized with Trolox® and reacting with $DPPH^{\bullet}$ [36]. $DPPH^{\bullet}$ assay can also be performed by HPLC, and may be considered as an alternative approach to determine the antioxidant properties of NP (such as diamond and AuNP) as well as to investigate the mechanisms occurring with the free radical [49].

Others methods have been show to provide accurate evaluation of NP scavenging radical activity. For example, the radical scavenging activity of NP has been estimated by monitoring the elimination of $OH^{\bullet}$ and $O_2^{\bullet-}$ in presence of NP. Hydroxyl radicals can be generated by H_2O_2/UV light process [34] or Fenton reaction [31, 33-35] and their consumption by NP can be monitored by using spin trapping techniques in which the probe 5,5-dimethyl-1-pyrroline-*N*-oxide (DMPO) reacts with $OH^{\bullet}$ to form a stable adduct monitored by ESR. A competitive reaction occurs between DMPO and the NP to scavenge $OH^{\bullet}$.

This spin trapping technique was also described to evaluate the consumption by multiwall carbon nanotubes (MWCNT) and fullerenes of $O_2^{\bullet-}$ produced by xanthine/xanthine oxidase system [34-35]. Fenoglio *et al.* evaluated the reactivity of MWCNT with $O_2^{\bullet-}$ by monitoring the reduction of cytochrome c (spectrophotocolorimetry at $\lambda = 550$ nm). However, due to the high electron affinity and hydrophobic surface, MWCNT may react directly with cytochrome c as well as adsorb and inactivate both cytochrome c or xanthine oxidase. Thus, to exclude these hypotheses, others assays need to be performed [34].

3.1.2 Methods to evaluate the generation of radicals by nanoparticles

The generation of radicals by NP has been studied by different methods depending of the studied radical type.

Hydroxyl radicals ($OH^{\bullet}$) can be generated by the reaction between NP and H_2O_2 or deoxyribose and monitored by spin-trapping technique and thiobarbituric assay (TBA), respectively; NP, such as carbon NP and TiO_2, attack deoxyribose to form $OH^{\bullet}$ that, upon heating with TBA at low pH, yield a pink colour (absorbance recorded at 532 nm) [34, 47]. In these studies, the samples were centrifuged to remove NP, avoiding their optical interference.

Indeed, others methods can be used to evaluate the generation of radicals without interferences. For exemple, ABTS assay has also been reported to estimate the generation of $OH^{\bullet}$ by NP [50]. Cerium oxide NP in presence of H_2O_2 and ABTS catalysed the formation of $ABTS^{+\bullet}$. The production of $ABTS^{+\bullet}$ was measured at 420 nm with no interference of CeO_2 NP.

Superoxide anion ($O_2^{\bullet-}$) generated by the reaction between AgNP and H_2O_2 was monitored by using: indirect method, measuring the H_2O_2 concentrations, with Amplex® Red reagent (10-acetyl-3,7-dihydroxyphenoxazine) (react with H_2O_2 to produce highly fluorescent resorufin) [51] and direct method, measuring $O_2^{\bullet-}$concentration, with chemiluminescence-based Methyl *Cypridina* luciferin (2-methyl-6-phenyl-3,7-dihydroimidazo[1,2-a]pyrazin-3-one) analogue [51].

The reaction between NP and $^{\bullet}NO$ donors (for example *S*-nitrosothiols (RSNO) [26, 42] has been used to estimate the generation of the radical nitric oxide ($^{\bullet}NO$). In this case, a $^{\bullet}NO$ selective carbon fiber electrode was used and no interference of AuNP was mentioned.

3.1.3 Interaction of inorganic nanoparticles with molecules involved in redox homeostasis

Understanding the reactivity between molecules implied in redox homeostasis and NP is crucial to predict the NP fate in the human body. The reactivity of NP with proteins and reduced glutathione (GSH) has been often studied.

When enter in the body, NP immediately become coated in biological molecules, including proteins. The most commonly tested proteins are the albumin, insulin, γ–globulin, fibrinogen and other proteins present in human serum. Under cell-free conditions, the interaction of NP with theses proteins have been evaluated by different assays, including: measuring protein concentration by using bicinchinoninic acid assay [52], monitoring protein conformational change by: one and two dimensional gel electrophoresis [53], by measuring the fluorescence quenching [54-55], by circular dichromism techniques [55], and by monitoring the physico-chemical characteristics of NP by using dynamic light scattering [54, 56], transmission electronic microscopy or isothermal titration

calorimetry measurements (enthalpy and entropy analysis) [56]. In this studies no interference of NP was mentioned.

The interaction of NP with GSH under cell-free conditions has been investigated by using fluorogenic reagents, such as rhodamine-based organoselenium probes [5], and by determination of change on physico-chemical properties of NP by using resonance elastic light scattering – sensitive technique to monitor bioinorganic complexes – and UV-vis spectrophotometer [57-58].

However, the fluorescence intensity of probes can be significantly decreased by the presence of metallic NP, such as AuNP, giving the false impression of a diminution of GSH content caused by the NP. For example, our group showed that citrate-stabilized AuNP displayed interference with the fluorescence emission of the naphthalene-2,3-dicarboxyaldehyde (NDA)-GSH adducts (Fig. 5). Since both the excitation and the emission wavelengths of the NDA-GSH adduct (472 nm and 528 nm, respectively) lie within the spectrum of visible light, AuNP may absorb not only the emitted GSH-NDA fluorescence but also the excitation energy, thereby preventing excitation of the fluorophore. Thus, potential interferences with NP need to be considered if the investigators whish to reliably use the assays in a quantitative manner. To minimize particle interference, this assay was modified and NP were removed by precipiting the AuNP with acid solution (HCl 0.6 M) following centrifugation step and then the fluorescence intensity of the GSH-NDA adduct was measured, and an increase of GSH-NDA fluorescence (*i.e.* concentration remaining on GSH) was observed, showing the interference of AuNP with readout system.

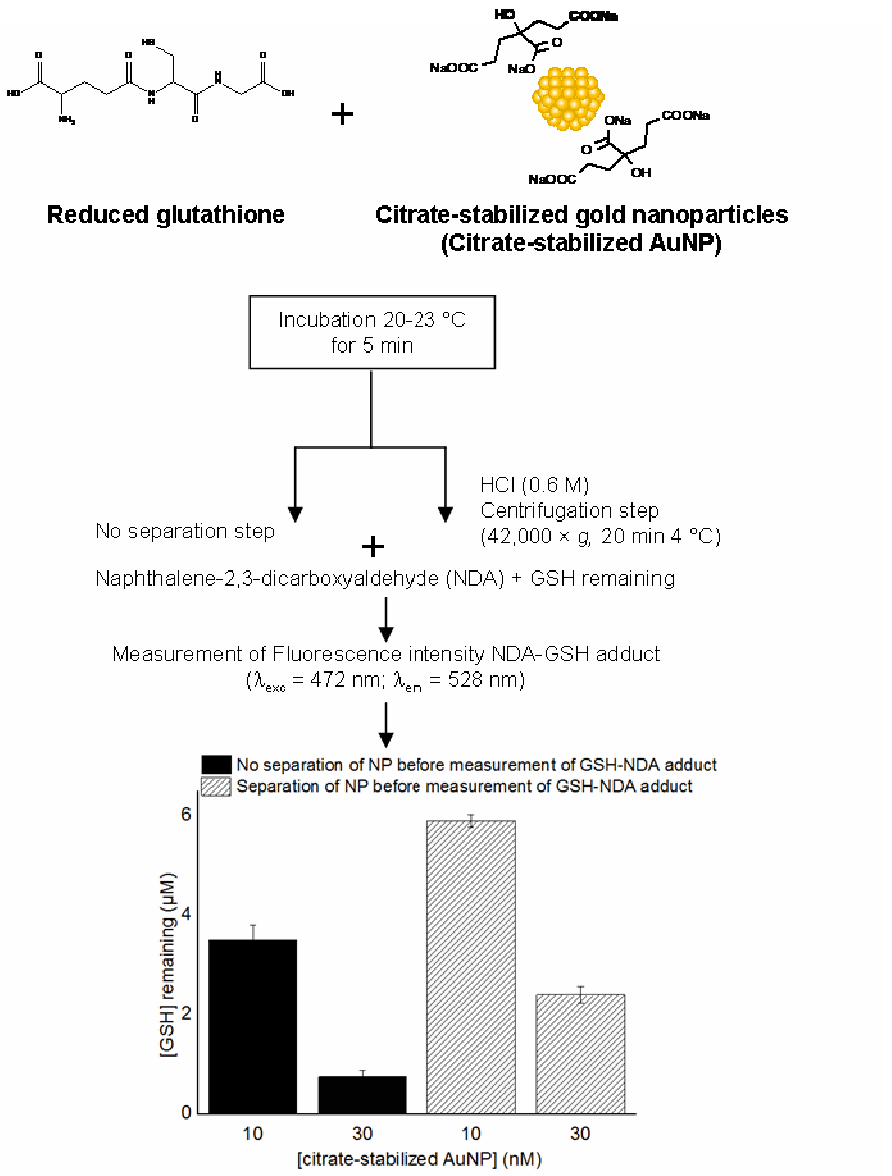

Fig. 5. Interaction in cell-free conditions between reduced glutathione (GSH) (6 µM) and citrate-stabilized gold nanoparticles (AuNP) (10 and 30 nM): interference of AuNP in fluorescence read out systems.

A solution of citrate-stabilized AuNP (550 µL) at a final concentration of 10 and 30 nM were mixed with 50 µL of GSH (72 µM). Samples were kept at room temperature (20 – 23°C) for 5 min. The NP were removed or no by precipitation (50 µL of HCl (0.6 M) were added to samples, and the resulting mixture was centrifuged at 42,000 × g for 20 min at 4°C). Then, the samples or the supernatant (600 µL) was mixed with 50 µL of NaOH (1 M), 140 µl of borate buffer (1 M, pH 9.2), and 10 µL of NDA (5.4 mM) prepared in ethanol and the mixture was incubated for an additional 10-min period at 4°C. Fluorescence intensity was read at λ_{exc} = 472 nm and λ_{em} = 528 nm by using a spectrofluorimeter (Hitachi F-2000, France). Concentrations of GSH were calculated using a calibration curve in the range 1.5 – 7.5 µM.

3.2 Assays to evaluate the reactivity between inorganic nanoparticles and cells

The presence of oxidative stress in cells may be evaluated by the direct measurement of different radicals, by the detection of antioxidant levels and gene expression and by the measurement of the resulting damage to cell components. Directly measuring radical species might seem the preferred method, but many ROS/RNS are extremely unstable and difficult to measure directly. Because of this, many scientists prefer to measure the levels of antioxidant enzymes and other redox molecules which serve to counteract radical species generated in the cell. Several genes that are induced during oxidative stress have been also analyzed. Another approach is to measure the damage on proteins, DNA, RNA, lipids, or other biomolecules. While this is an indirect approach, many markers of damage are extremely stable and therefore provide a more reliable method to measure oxidative stress. The *in vitro* assays used to evaluate these markers are discussed in the following sections.

3.2.1 Methods for measurement of ROS/RNS radicals produced by cells

The induction of oxidative stress by NP in cells may be evaluated by the measurement of radicals (ROS/RNS). As far as ROS are concerned, several fluorescent probes are frequently employed, including: 2'7'-dichlorodihydrofluorescein diacetate (H_2DCF-DA) [4, 47, 59-66], 5-(and-6)-chloromethyl-2',7'-dichlorodihydrofluorescein diacetate, acetyl ester (CM-H_2DCF-DA) [67-68], bis(*p*-methylbenzenesulfonate) dichlorofluorescein [5], hydroethidine [64] and dihydrorhodamine-1,2,3 [69]. In all assays, the simplest method is the incubation of NP treated cells with fluorogenic probes, which are taken up by cultured cells, and become fluorescent upon intracellular oxidation. Then the fluorescence intensity can be estimated by flow cytometry [47], by confocal microscopy [14], or by conventional spectrofluorometry [62].

A consideration when using fluorimetric dyes for quantifying inorganic NP induced oxidative stress is the possiblity of their direct interaction with the probe. For example, AuNP have been shown to quench DCF fluorescence upon NP-induced oxidative stress [70]. Doak *et al*., showed, in a cell-free system, that dextran-coated FeO NP interfere with the fluorescence emission of DCF, depending on the oxidation state of the iron (the interference was more pronounced with Fe_3O_4 than Fe_2O_3 NP) [14]. They suggested that adsorption could be a reason for the quenching of the fluorescence response [14]. Some studies noted fluorescence quenching by carbon black NP while detecting ROS generation *via* DCF assay [6, 71]. Carbon black NP can also react directly with H_2DCF-DA due their catalytic activity. This phenomenon have been observed to be incubation-time dependent. In cell-free systems, after 1h incubation of carbon black NP with the substrate H_2DCF-DA, DCF fluorescence was not detectable. However, after 4h of incubation of NP

with H_2DCF-DA, carbon black had produced significant amounts of fluorescent DCF (Kroll *et al.*, 2012).

To minimize particle interference, the classical DCF assay has been modified and NP dispersions have been removed by washing the NP-treated cells prior to the incubation with DCF [6, 43]. In addition, given the fact that the interference of NP is concentration dependent and that all NP cannot be removed entirely from the solution by separation techniques, NP dispersions applied should also be limited to concentrations that do not interfere with the measurement of DCF signals.

As far as RNS are concerned, the levels of nitrite in culture media are frequently used as an index of $^{\bullet}$NO production. The most frequently applied method to nitrite measurement consists in Griess colorimetric technique [59, 72-73]. Since nitrite is present in supernatant of cells, NP cannot be removed by washing prior to the measurement. Thus, limiting NP concentrations to a maximum that does not interfere with colorimetric assays is of particular importance to evade false results.

3.2.2 Methods for measurement of antioxidants in cells

Endogenous antioxidants such as GSH, are considered to be the first line of cellular defence against ROS. In recent studies, variations of GSH levels after exposure to NP have been investigated using either the colorimetric Ellman's reagent (5,5'-dithio-bis-2-nitrobenzoic acid, DTNB) [65, 68, 74-75], or fluorogenic reagents, such as rhodamine-based organoselenium fluorescent probe [5] and orthophthaldialdehyde (OPA) [62].

Depletion of GSH has been observed in cells exposed to $NiFe_2O$ NP [65], AgNP [74], CuNP [68, 75]. Due to their optical properties, in these studies a separation step by centrifugation was performed to avoid the optical interference of NP. In others studies, depletion of GSH by NP was evaluated by using fluorescence-based assays, limiting the optical interference of AuNP [5] and silica NP [62].

3.2.3 Methods for measurement of oxidation products in cells

The generation of ROS, depletion of antioxidants and decrease of antioxidant enzymes activity is inevitably linked to increased risk of oxidative damages to molecules such as lipids and DNA, and this can be evaluated by using *in vitro* cell assays.

The lipid peroxidation products, such as malonyldialdehyde (MDA), can be measured by using the TBA assay [68, 74, 76] and western blot analysis [77], whereas DNA damage can be assessed by a number of different assays, such as by 8-hydroxy-2-deoxyguanosine (8-OH-dG)

detection, by comet assay [47, 78-79], and by fluorescence *in situ* hybridization assay based on peptide nucleic acid probes [79].

Some studies have showed the interference of inorganic NP such as carbon black, TiO_2 and MWCNT with the comet assay [80-81]. This assay relies on a fluorescent microscopy read-out and agglomerates of these NP used clearly either quench or enhance fluorescence intensity. In conclusion critical concentrations above which NP massively agglomerate, should not be exceeded. Furthermore, alternative methods are needed to circumvent these problems.

In order to exclude NP that interfere with the oxidative stress assays, cell-free controls were assayed for each concentration of NP, and the corresponding absorbance was subtracted from the absorbance of cell groups [76].

3.2.4 Nanoparticles perturb multiple signal transduction pathways

The impact of NP on gene expression of transcription factors (mainly NF-κB pathways) has been studied by qualitative methods (electrophoretic mobility shift assay (EMSA) [63], semiquantitative [59] or quantitative real time reverse transcriptase-polymerase chain reaction (RT-PCR) analysis [77, 82].

Enzyme-liked immunosorbent technique (ELISA) was used to quantify inflammatory markers in cell culture supernatants after exposure to various inorganic NP including, AgNP [61], AuNP [59], SiO_2 NP [63], carbon black [6, 83-84] and quantum dots [82].

Many studies have reported that inorganic NP, due to their high adsorptive capacities, have the potential to adsorb cytokines released from cells leading to false-negative results. For example, metal oxide NP such as TiO_2 and SiO_2 have found to cause artefacts in immunoassays by adsorbing the proinflammatory cytokine IL-6 (Veranth *et al.*, 2007), and carbon black was found to bind several different cytokines, for example, GM-CSF, TGF-ß, TNF-α, IL-6 and IL-8 (Monteiro-Riviere and Inman, 2006, Kocbach *et al.*, 2008, Brown *et al.*, 2010). Recently, it was reported that the presence of serum proteins could reduce cytokine binding to metal oxide and carbon black NP (Kroll *et al.*, 2012). Moreover, limiting NP concentrations to a maximum that does not display cytokine binding is of particular importance to avoid misinterpretation (Kroll *et al.*, 2012).

3.2.5 Methods for cell viability evaluation

A classic approach to assess acute cytotoxicity of NP involves the use of tetrazolium salts, such as 3-(4,5-dimethylthiazol-2-yl)-2,5-diphenyl tetrazolium bromide (MTT), 2,3-bis-(2-methoxy-4-nitro-5-sulfophenyl)-2H-tetrazolium-5-carboxanilide (XTT) and 2-(4-iodo-phenyl)-3-(4-nitrophenyl)-5-(2,4-disulfophenyl)-2H tetrazolium, monosodium salt (WST-1), that are cleaved in

the mitochondria of metabolically active cells to form colored water insoluble (MTT) and soluble (XTT and WST-1) formazan salts (which are proportional to the number of living cells) [5, 12, 47, 59-63, 65, 68, 74, 76]

However, NP may interact with the formazan salts, causing an under-estimation of the number of viable cells. For exemple, single-walled carbon nanotubes (SWCNTs) can adsorb MTT-formazan crystals and stabilize their chemical structure, and, as a consequence, these crystals cannot be solubilised in organic solvents (SDS, acetone,…), mimicking a cytotoxic effect [12, 18, 85-86]. In addition, it appears that the insolubility of the MTT-formazan is crucial for attachment to the carbon NP and disturbance of the test. Indeed, no interference was observed with water-soluble formazan salts, such as WST-1 or XTT [12].

Since tetrazolium-based assays are based on colorimetric dyes, quantified by light absorption measurement, NP have a potential wavelength-dependent absorbance artefacts, leading the false impression of an improved number of viable cells caused by the NP [16, 87]. For example, our group showed that citrate-stabilized AuNP interfere with light absorption of MTT assay (Fig. 6A). To confirm this artefact, the data were validated by traditional trypan blue exclusion assay. In comparison to trypan blue manual counting, the MTT assay appeared to have consistently overestimated ($p < 0.024$) when high concentrations of AuNP were used (> 20 nM). Thus, we showed that the decreased formation of formazan (due to reduced cell metabolism) was masked by the strong absorption of AuNP near 520 nm (Fig. 6B), providing a false impression of lack of toxicity. This interference with formazan assays is not confined to AuNP alone; it has also been reported for others metallic (AgNP) and metal oxide (AgO, Fe_3O_4, CeO_2, TiO_2 and CoO) NP, which also absorb at the wavelengths used in these tests: 340, 380, 405, 440, 540 or 550 nm [14, 76, 88-89], providing a false result of lack of toxicity.

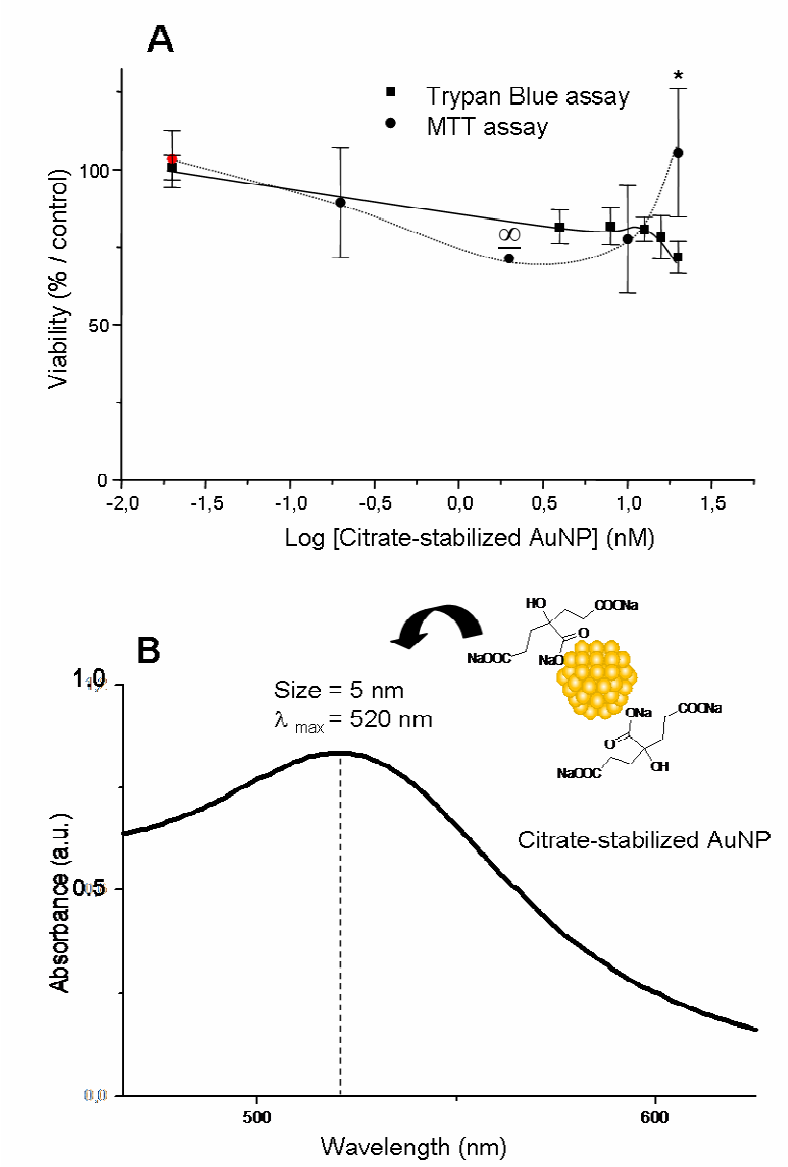

Fig. 6. Interference of citrate-stabilized gold nanoparticles (AuNP) with MTT assay. (A) Viability studies of rat alveolar macrophages (NR8383) (at $1 \times 10^{+5}$ cell/mL) after 24-h exposure with citrate-stabilized gold nanoparticles (citrate-stabilized AuNP) by using MTT assay (•) (96-well plates) (MTT-formazan production measured spectrophotometrically at λ = 540 nm) and Trypan Blue assay (■) (24-well plates) (observation by optical microscopy) Control cells (unexposed cells with NP) were taken as 100% viability (0% cytotoxicity). Data are expressed as mean and standard error of n > 3 replicates in n > 3 separate experiments. $\underline{\infty}$ (n = 1). The non-parametric Mann and Whitney randomised test was performed for statistical calculations. (B) Normalized UV-vis absorption spectra of citrate-stabilized AuNP (band plasmon band at 520 nm).

Some strategies to avoid these interferences are: (i) development of assays using wavelengths of 700 – 800 nm, (ii) remove NP from the cell monolayer prior to the incubation with

formazan salts [6], (iii) use alternative methods that are not based on optical readouts (*e.g.* flow cytometry, trypan blue assay, clonogenic assay,…) [88, 90].

Another common cell viability assay is the lactate dehydrogenase (LDH). In this assay, the level of extracellular LDH released from damaged cells is measured using a colorimetric test based on the convertion of pyruvic acid to lactic acid [6]. Lactate dehydrogenase catalyses the NAD^+-dependent reaction from lactate to pyruvate. In a second step, the enzyme diaphorase transfers H/H^+ from $NADH/H^+$ to the yellow tetrazolium salt (2-[4-iodophenyl]-3-[4-nitrophenyl]-5-phenyltetrazolium chloride) (INT), which is reduced to formazan (red) and can be measured by spectrophotometry at 492 nm.

The reliability of this assay, when used for measuring NP toxicity, could be influenced by several factors: (i) NP (*e.g.* ZnO NP) could cause a decrease in LDH activity by metal-catalyzed oxidation of LDH [6], (iii) NP (*e.g.* TiO_2, AgNP, CuNP) could be a target on which LDH molecules are adsorbed [91], (iv) certain NP (like AuNP and PtNP) could catalyse NADH oxidation [22, 24], (v) INH salts also absorbs in the spectrum of visible light, the mechanisms underlying this interference might be similar to those discussed above for the NP-increased formazan salts light absorption.

Since LDH is present in supernatant of cells, NP cannot be removed by washing prior to the measurement. In addition, removal of NP by centrifugation depends highly on the NP type and might only be applicable when individual particles are tested [91].

4. Conclusions

In the last years, pre-existing oxidative stress methods, currently used to evaluate the potential of drugs to induce an oxidative stress, have also been used to evaluate inorganic NP safety. However, many studies showed that because of the unique properties of inorganic NP, traditional oxidative stress assays should be used with caution, adapted and sometimes can not be used otherwise.

The NP interference in oxidative stress assays depends on the type of NP (due to the spectific NP properties related below) and the suitability of the assay for assessing NP impact should be examined case by case to avoid false results. Some strategies to avoid this interference when traditional oxidative stress are used, such as: (i) introduction of a separation step to reduce the amount of NP, (ii) restriction of NP amount below interfering levels if NP cannot be entirely removed, and (iii) use of assays not based in optical detection.

With this review, we aimed to adapt these methods underlying possible artefacts due to nanomaterials, to generate new and safer NP.

5. References

[1] J.M. Irache, I. Esparza, C. Gamazo, M. Agüeros, S. Espuelas, Vet. Parasitol. 180 (2011) 47-71.
[2] E. Paszko, C. Ehrhardt, M.O. Senge, D.P. Kelleher, J.V. Reynolds, Photodiagn. Photodyn. 8 (2011) 14-29.
[3] Y. Teow, P.V. Asharani, M.P. Hande, S. Valiyaveettil, Chem. Commun. 47 (2011) 7025-7038.
[4] T. Xia, M. Kovochich, J. Brant, M. Hotze, J. Sempf, T. Oberley, C. Sioutas, J.I. Yeh, M.R. Wiesner, A.E. Nel, Nano Lett. 6 (2006) 1794-1807.
[5] W. Gao, K. Xu, L. Ji, B. Tang, Toxicol. Lett. 205 (2011) 86-95.
[6] A. Kroll, M. Pillukat, D. Hahn, J. Schnekenburger, Arch. Toxicol. (2012) 1-14.
[7] C.K. Sen, Biochem. Pharmacol. 55 (1998) 1747-1758.
[8] R.G. Allen, M. Tresini, Free Radical Biol. Med. 28 (2000) 463-499.
[9] J.H. Forman, M. Torres, Mol. Aspects Med. 22 (2001) 189-216.
[10] C. Jacob, P.G. Winyard Redox Signaling and Regulation in Biology and Medicine, Wiley-VCH Verlag GmbH & Co. KGaA, Weinheim, 2009.
[11] N.A. Monteiro-Riviere, A.O. Inman, Carbon 44 (2006) 1070-1078.
[12] J.M. Worle-Knirsch, K. Pulskamp, H.F. Krug, Nano Lett. 6 (2006) 1261-1268.
[13] K. Pulskamp, S. Diabate, H.F. Krug, Toxicol. Lett. 168 (2007) 58 – 74.
[14] S.H. Doak, S.M. Griffiths, B. Manshian, N. Singh, P.M. Williams, A.P. Brown, G.J.S. Jenkins, Mutagenesis 24 (2009) 285-293.
[15] A. Kroll, M.H. Pillukat, D. Hahn, J. Schnekenburger, Eur. J. Pharm. Biopharm. 72 (2009) 370-377.
[16] N.A. Monteiro-Riviere, A.O. Inman, L.W. Zhang, Toxicol. Appl. Pharmacol. 234 (2009) 222-235.
[17] M.M. Song, W.J. Song, H. Bi, J. Wang, W.L. Wu, J. Sun, M. Yu, Biomaterials 31 (2010) 1509 – 1517
[18] A. Dhawan, V. Sharma, Anal. Bioanal. Chem. 398 (2010) 589-605.
[19] C. Hoskins, L. Wang, W. Cheng, A. Cuschieri, Nanoscale Res. Lett. 7 (2012) 1-12.
[20] O.P. Sharma, T.K. Bhat, Food Chem. 113 (2009) 1202-1205.
[21] F. Marano, S. Hussain, F. Rodrigues-Lima, A. Baeza-Squiban, S. Boland, Arch. Toxicol. 85 (2011) 733-741.
[22] X. Huang, I.H. El-Sayed, X. Yi, M.A. El-Sayed, J. Photochem. Photobiol. B 81 (2005) 76-83.
[23] A.E. Nel, L. Madler, D. Velegol, T. Xia, E.M.V. Hoek, P. Somasundaran, F. Klaessig, V. Castranova, M. Thompson, Nat. Mater. 8 (2009) 543-557.
[24] K. Hikosaka, J. Kim, M. Kajita, A. Kanayama, Y. Miyamoto, Colloids Surf B 66 (2008) 195-200.
[25] K. Unfried, C. Albrecht, L.O. Klotz, A. Von Mikecz, S. Grether-Beck, R.P.F. Schins, Nanotoxicology 1 (2007) 52-71.
[26] H.Y. Jia, Y. Liu, X.J. Zhang, L. Han, L.B. Du, Q. Tian, Y.C. Xu, J. Am. Chem. Soc. 131 (2009) 40-41.
[27] A. Karakoti, S. Singh, J.M. Dowding, S. Seal, W.T. Self, Chem. Soc. Rev. 39 (2010) 4422-4432.
[28] R. Konwarh, B. Gogoi, R. Philip, M.A. Laskar, N. Karak, Colloid Surface B 84 (2011) 338-345.
[29] M. Kajita, K. Hikosaka, M. Iitsuka, A. Kanayama, N. Toshima, Y. Miyamoto, Free Radic. Res. 41 (2007) 615-626.
[30] M. Auffan, J. Rose, M.R. Wiesner, J.Y. Bottero, Environ. Pollut. 157 (2009) 1127-1133.
[31] K. Esumi, N. Takei, T. Yoshimura, Colloid Surface B 32 (2003) 117-123.

[32] N.O. Yakimovich, A.A. Ezhevskii, D.V. Guseinov, L.A. Smirnova, T.A. Gracheva, K.S. Klychkov, Russ. Chem. B+ 57 (2008) 520-523.
[33] K. Esumi, H. Houdatsu, T. Yoshimura, Langmuir 20 (2004) 2536-2538.
[34] I. Fenoglio, M. Tomatis, D. Lison, J. Muller, A. Fonseca, J.B. Nagy, B. Fubini, Free Rad. Biol. Med. 40 (2006) 1227-1233.
[35] L.L. Dugan, D.M. Turetsky, C. Du, D. Lobner, M. Wheeler, C.R. Almli, C.K.F. Shen, T.Y. Luh, D.W. Choi, T.S. Lin, Proc. Natl. Acad. Sci. U.S.A. 94 (1997) 9434-9439.
[36] Z. Nie, K.J. Liu, C.J. Zhong, L.F. Wang, Y. Yang, Q. Tian, Y. Liu, Free Radic. Biol. Med. 43 (2007) 1243-1254.
[37] M. Chorny, E. Hood, R.J. Levy, V.R. Muzykantov, J. Control. Release 146 (2010) 144-151.
[38] K.-I. Fukui, Y. Namai, Y. Iwasawa, Appl. Surf. Sci. 188 (2002) 252-256.
[39] N.V. Skorodumova, S.I. Simak, B.I. Lundqvist, I.A. Abrikosov, B. Johansson, Phys. Rev. Lett. 89 (2002) 1-4.
[40] M. Auffan, W. Achouak, J. Rose, M.A. Roncato, C. Chaneac, D.T. Waite, A. Masion, J.C. Woicik, M.R. Wiesner, J.Y. Bottero, Environ Sci Technol 42 (2008) 6730-6735.
[41] Y. Yamakoshi, N. Umezawa, A. Ryu, K. Arakane, N. Miyata, Y. Goda, T. Masumizu, T. Nagano, J. Am. Chem. Soc. 125 (2003) 12803-12809.
[42] H.Y. Jia, X. Han, Z.W. Li, Q. Tian, X.X. Miao, L.B. Du, Y. Liu, Talanta 85 (2011) 1871-1875.
[43] A. Kroll, C. Dierker, C. Rommel, D. Hahn, W. Wohlleben, C. Schulze-Isfort, C. Gobbert, M. Voetz, F. Hardinghaus, J. Schnekenburger, Part. Fibre Toxicol. 8 (2011) 9-23.
[44] T. Endo, T. Fukunaga, T. Yoshimura, K. Esumi, J. Colloid Interface Sci. 302 (2006) 516-521.
[45] A. Watanabe, M. Kajita, J. Kim, A. Kanayama, K. Takahashi, T. Mashino, Y. Miyamoto, Nanotechnology 20 (2009) 1-9.
[46] R. Fang, H. Jing, Z. Chai, G.H. Zhao, S. Stoll, F.Z. Ren, F. Liu, X.J. Leng, J. Nanobiotechnology 9 (2011) 1-14.
[47] L. Tiano, T. Armeni, E. Venditti, G. Barucca, L. Mincarelli, E. Damiani, Free Radic. Biol. Med. 49 (2010) 408-415.
[48] R. Isono, T. Yoshimura, K. Esumi, J. Colloid Interf. Sci. 288 (2005) 177-183.
[49] A. Boudier, J. Tournebize, G. Bartosz, S. El Hani, R. Bengueddour, A. Sapin-Minet, P. Leroy, Anal. Chim. Acta 711 (2012) 97-106.
[50] E.G. Heckert, S. Seal, W.T. Self, Environ Sci Technol 42 (2008) 5014-5019.
[51] D. He, A.M. Jones, S. Garg, A.N. Pham, T.D. Waite, J. Phys. Chem. C 115 (2011) 5461-5468.
[52] C. Schulze, U.F. Schaefer, C.A. Ruge, W. Wohlleben, C.M. Lehr, Eur. J. Pharm. Biopharm. 77 (2011) 376-383.
[53] Z.J. Deng, G. Mortimer, T. Schiller, A. Musumeci, D. Martin, R.F. Minchin, Nanotechnology 20 (2009).
[54] F. Jin, Mater. Sci. Forum 694 (2011) 396-398.
[55] S.H.D. Lacerda, J.J. Park, C. Meuse, D. Pristinski, M.L. Becker, A. Karim, J.F. Douglas, ACS Nano 4 (2010) 365-379.
[56] S.J. Liu, Y.C. Han, R.R. Qiao, J.F. Zeng, Q.J. Jia, Y.L. Wang, M.Y. Gao, J. Phys. Chem. C 114 (2010) 21270-21276.
[57] P.K. Sudeep, S.T.S. Joseph, K.G. Thomas, J. Am. Chem. Soc. 127 (2005) 6516-6517.
[58] M. Stobiecka, K. Coopersmith, M. Hepel, J. Colloid Interface Sci. 350 (2010) 168-177.
[59] R. Shukla, V. Bansal, M. Chaudhary, A. Basu, R.R. Bhonde, M. Sastry, Langmuir 21 (2005) 10644-10654.
[60] S.M. Hussain, K.L. Hess, J.M. Gearhart, K.T. Geiss, J.J. Schlager, Toxicol. In Vitro 19 (2005) 975-983.
[61] C. Carlson, S.M. Hussain, A.M. Schrand, L.K. Braydich-Stolle, K.L. Hess, R.L. Jones, J.J. Schlager, J. Phys. Chem. B 112 (2008) 13608-13619.

[62] E.J. Park, K. Park, Toxicol. Lett. 184 (2009) 18-25.
[63] X. Liu, J.A. Sun, Biomaterials 31 (2010) 8198-8209.
[64] S. Hussain, L.C.J. Thomassen, I. Ferecatu, M.-C. Borot, K. Andreau, J.A. Martens, J. Fleury, A. Baeza-Squiban, F. Marano, S. Boland, Part. Fibre Toxicol. 7 (2010) 1-17.
[65] M. Ahamed, J.M. Akhtar, M.A. Siddiqui, J. Ahamad, J. Musarrat, A.A. Al-Khedhairy, M.S. Alsalhi, S.A. Alrokayan, Toxicology 283 (2011) 101-108.
[66] Y.X. Zhao, X.H. Gu, H.Z. Ma, X.G. He, M. Liu, Y. Ding, J. Phys. Chem. C 115 (2011) 12797-12802.
[67] J. Park, D.H. Lim, H.J. Lim, T. Kwon, J.S. Choi, S. Jeong, I.H. Choi, J. Cheon, Chem. Commun. 47 (2011) 4382-4384.
[68] M. Valodkar, R.N. Jadeja, M.C. Thounaojam, R.V. Devkar, S. Thakore, Mater. Chem. Phys. 128 (2011) 83-89.
[69] H. Lee, K. Lee, I.-K. Kim, T.G. Park, Adv. Funct. Mater. 19 (2009) 1884-1890.
[70] T. Pfaller, V. Puntes, E. Casals, A. Duschl, G.J. Oostingh, Nanotoxicology 4 (2010) 138-138.
[71] B.B. Aam, F. Fonnum, Arch. Toxicol. 81 (2007) 441-446.
[72] E. Hutter, S. Boridy, S. Labrecque, M. Lalancette-Hébert, J. Kriz, F.M. Winnik, D. Maysinger, ACS Nano 4 (2010) 2595-2606.
[73] P. Leroy, A. Sapin-Minet, A. Pitarch, A. Boudier, J. Tournebize, R. Schneider, Nitric Oxide-Biol. Chem. 25 (2011) 54-56.
[74] S. Arora, J. Jain, J.M. Rajwade, K.M. Paknikar, Toxicol. Lett. 179 (2008) 93-100.
[75] M. Valodkar, P.S. Rathore, R.N. Jadeja, M. Thounaojam, R.V. Devkar, S. Thakore, J. Hazard Mater. 201-202 (2011) 244-249.
[76] Y. Liu, Z. Chen, J. Wang, J Nanopart Res 13 (2011) 199-212.
[77] J.J. Li, D. Hartono, C.-N. Ong, B.-H. Bay, L.-Y.L. Yung, Biomaterials 31 (2010) 5996-6003.
[78] K. Bhattacharya, M. Davoren, J. Boertz, R.P.F. Schins, E. Hoffmann, E. Dopp, Part. Fibre Toxicol. 6 (2009) 1-11.
[79] J.J. Li, S.L. Lo, C.T. Ng, R.L. Gurung, D. Hartono, M.P. Hande, C.N. Ong, B.H. Bay, L.Y.L. Yung, Biomaterials 32 (2011) 5515-5523.
[80] C. Hirsch, J.-P. Kaiser, F. Wessling, K. Fischer, M. Roesslein, P. Wick, H.F. Krug, J. Phys.: Conf. Ser. 304 (2011) 012053.
[81] Z. Magdolenova, D. Bilanicova, G. Pojana, L.M. Fjellsbo, A. Hudecova, K. Hasplova, A. Marcomini, M. Dusinska, J. Environ. Monit. 14 (2012) 455-464.
[82] H.-M. Lee, D.-M. Shin, H.-M. Song, J.-M. Yuk, Z.-W. Lee, S.-H. Lee, S.M. Hwang, J.-M. Kim, C.-S. Lee, E.-K. Jo, Toxicol. Appl. Pharmacol. 238 (2009) 160-169.
[83] D.M. Brown, C. Dickson, P. Duncan, F. Al-Attili, V. Stone, Nanotechnology 21 (2010) 2155104-215113.
[84] A. Kocbach, A.I. Totlandsdal, M. Låg, M. Refsnes, P.E. Schwarze, Toxicol. Lett. 176 (2008) 131-137.
[85] A. Casey, E. Herzog, M. Davoren, F.M. Lyng, H.J. Byrne, G. Chambers, Carbon 45 (2007) 1425–1432.
[86] L. Belyanskaya, P. Manser, P. Spohn, A. Bruinink, P. Wick, Carbon 45 (2007) 2643–2648.
[87] N. Lewinski, V. Colvin, R. Drezedk, Small 4 (2008) 26–49.
[88] G. Oostingh, E. Casals, P. Italiani, R. Colognato, R. Stritzinger, J. Ponti, T. Pfaller, Y. Kohl, D. Ooms, F. Favilli, H. Leppens, D. Lucchesi, F. Rossi, I. Nelissen, H. Thielecke, V. Puntes, A. Duschl, D. Boraschi, Part. Fibre Toxicol. 8 (2011) 8.
[89] V. Wilhelmi, U. Fischer, D. van Berlo, K. Schulze-Osthoff, R.P.F. Schins, C. Albrecht, Toxicol. In Vitro 26 (2012) 323-334.

[90] M. Horie, K. Nishio, H. Kato, K. Fujita, S. Endoh, A. Nakamura, A. Miyauchi, S. Kinugasa, K. Yamamoto, E. Niki, Y. Yoshida, Y. Hagihara, H. Iwahashi, J. Biochem. 150 (2011) 461-471.
[91] X.L. Han, R. Gelein, N. Corson, P. Wade-Mercer, J.K. Jiang, P. Biswas, J.N. Finkelstein, A. Elder, G. Oberdorster, Toxicology 287 (2011) 99-104.

Chapitre II.

Nanoparticules d’or fonctionnalisées par l’acide dihydrolipoïque : synthèse, caractérisation physico-chimique et étude de stabilité

II.1 Introduction

Les objectifs du présent chapitre sont les suivants : (i) synthétiser en phase aqueuse des NP d'or stabilisées par un dithiol, (ii) améliorer leur stabilité, et (iii) développer des techniques de routine qui permettent de les caractériser.

Pour ce faire, nous avons choisi de travailler avec des NP d'or stabilisées par l'acide dihydrolipoïque (DHLA) et nous avons essayé de comprendre l'origine de la meilleure stabilisation des NP d'or par ce ligand. Le DHLA a été choisi pour deux raisons principales :

- il s'agit tout d'abord d'un composé non toxique. Le DHLA est notamment un puissant antioxydant endogène et peut piéger les radicaux libres, chélater les métaux et régénérer d'autres antioxydants (Goraca *et al*., 2011).
- le DHLA présente une grande affinité pour la surface des NP d'or grâce à ses deux groupements fonctionnels thiols.

Des NP d'or fonctionnalisées par le DHLA (NP Au@DHLA) ont été synthétisées auparavant par Roux *et al.* (2005) en phase organique, en se basant sur la synthèse de Brust *et al.* (1994). L'inconvénient de cette méthode est l'utilisation d'un solvant organique (méthanol ou toluène) difficile à éliminer par la suite pour une utilisation dans des milieux biologiques. Dans ce contexte, nous avons cherché à développer de nouvelles stratégies de stabilisation des NP Au@DHLA en l'absence de solvant organique. Pour ce faire, une première étape de synthèse consiste à synthétiser des NP d'or stabilisées par les ions citrate selon la méthode de Turkevich *et al.* (1951). Lors d'une seconde étape de synthèse, les NP d'or stabilisées par les ions citrate ont été fonctionalisées par le DHLA par échange de ligands.

Afin de prouver la fonctionnalisation de surface par le DHLA, les propriétés physico-chimiques des NP d'or (taille, charge, rapport [S]/[Au],...) ont été évaluées. De plus, afin de mieux appréhender l'effet du rapport [DHLA]/[Au] sur la stabilité des NP, nous avons procédé de la façon suivante : nous avons utilisé quatre concentrations différentes de DHLA, toutes en excès par rapport à la concentration en Au présent en surface (*i.e.* ×28, ×56, ×140 et ×222) lors de la 2ème étape de synthèse et nous avons suivi la stabilité des NP d'or en fonction du temps (durée de 50 j) par spectroscopie UV-visible et par diffusion dynamique de la lumière (*DLS, dynamic light scattering*). Nous avons également examiné l'évolution des spectres d'absorption, après ajout d'un sel à forte concentration (NaCl 1 M) et d'un autre dithiol, *i.e.* le dithiotréitol (DTT), pendant 2 h. Nous avons aussi étudié l'impact de la densité de couverture des NP d'or sur leur interaction avec des composés choisis pour représenter une possible bioréactivité. Notre hypothèse de travail a été la suivante : les

NP d'or sont d'autant plus réactives vis-à-vis des molécules qu'elles sont faiblement stabilisées par le ligand greffé. Différentes molécules ont été choisies pour vérifier cette hypothèse :

- l'albumine de sérum bovin (BSA, *bovine serum albumin*), protéine majoritaire du sang : la BSA peut se lier à la surface métallique des NP d'or soit par adsorption soit par formation de liaisons covalentes (*via* le résidu cystéine).
- le sel d'ammonium de l'acide 2',2'-azinobis(3-éthylbenzothiazoline)-6-sulfonique ($ABTS^{\bullet+}$), modèle de radical libre couramment utilisé pour évaluer le pouvoir radicalaire des antioxidants. Parmi d'autres types de radicaux libres, (tel que le 1,1-diphényl-2-picrylhydrazyle ($DPPH^{\bullet}$)), l'$ABTS^{\bullet+}$ a été choisi en raison de sa solubilité en milieu biphasique et de son absorption dans le visible (maximum d'absorbance à 734 nm), ce qui permet d'évaluer le pouvoir réducteur des NP d'or solubles dans l'eau par spectrophotométrie visible sans interférence de la SPR. L'$ABTS^{\bullet+}$ peut interagir avec les NP d'or soit par adsorption soit par interaction entre son électron non apparié et les électrons de conduction de l'or.

Cette étude a permis de parfaitement définir une plateforme nanoparticulaire fonctionnalisée en surface et stable en fonction du temps, et elle fait l'objet d'un manuscrit en préparation pour soumettre à *Macromolecules* (**article 2**). Brièvement, parmi les différents rapports [DHLA]/[Au] utilisés lors de la $2^{ème}$ étape de synthèse, seules les valeurs ×140 et ×222 conduisent à des NP ($Au@DHLA_{140}$ et $Au@DHLA_{222}$) stables pendant 50 j dans un milieu physiologique PBS ainsi que dans une solution de NaCl 1 M pendant 2 h. En effet, aucune variation a été observée, ni sur le rayon hydrodynamique, ni sur la valeur de λ_{max}. Nous avons également démontré que toutes les NP Au@DHLA préparées par échange de ligand sont insensibles à une réaction d'échange avec un autre dithiol, le DTT.

De plus, ces NP présentent une plus faible réactivité vis-à-vis de la BSA et de l'espèce radicalaire $ABTS^{\bullet+}$, en comparaison avec les NP moins couvertes par le DHLA (×28 et ×56) ainsi qu'avec les NP d'or stabilisées par les ions citrate.

Ces NP d'or, stables dans les milieux testés et peu réactives, présentent donc un fort potentiel pour des applications biologiques futures (pour par exemple véhiculer un principe actif greffé en surface).

La caractérisation physico-chimique des NP d'or est nécessaire pour valider le mode de synthèse des NP d'or et mieux prévoir les effets biologiques et les applications à venir. Parmi les techniques couramment utilisées et citées dans le chapitre I, il est crucial de disposer de techniques de quantification de l'or contenu dans ces NP afin de déterminer la concentration de ces entités. La

spectrométrie de masse et la spectrométrie d'émission optique avec source plasma à couplage inductif sont les outils le plus utilisés pour mesurer la teneur en or dans les NP (Allabashi *et al.*, 2009, Scheffer *et al.*, 2008, Yu et Andriola, 2010). Malgré leur limite de détection très basse (de l'ordre de 0,01 µM pour l'or), ces techniques sont coûteuses et peu disponibles dans la majorité des laboratoires. Pour cette raison, nous nous sommes intéressés au développement d'une méthode spectrophotocolorimétrique de l'or simple qui permet de calculer la concentration des NP d'or. Cette étude originale a fait l'objet d'un manuscrit accepté le 5 décembre 2010 dans *Talanta* **(article 3)**. Cette méthode comprend deux étapes : (i) l'or des NP est oxydé en $AuCl_4^-$ par l'emploi d'une solution de dibrome 7×10^{-4} M dans HCl 5×10^{-2} M ; (ii) la concentration en $AuCl_4^-$ est déterminée par formation d'une paire d'ions entre l'anion $AuCl_4^-$ et le cation coloré Rhodamine B^+. La paire d'ions est extraite dans un solvant organique et l'absorbance lue est proportionnelle à la quantité initiale d'or contenue dans les NP.

La méthode a été appliquée à l'ensemble des NP d'or mais seules les NP d'or stabilisées par les ions citrate et les NP $Au@DHLA_{222}$ ont été décrites dans l'article 3. Nous avons déterminé la teneur en or des NP ainsi que la concentration en NP en utilisant le diamètre obtenu par microscopie électronique à transmission.

Pour compléter leur caractérisation, un deuxième test permettant d'apprécier le pouvoir antiradicalaire des NP d'or a été réalisé. Son utilisation et l'optimisation de la méthode à fait l'objet d'un article publié dans *Anal. Chim. Acta* en 2012; il repose sur la réaction entre les NP et le 1,1-diphényl-2-picrylhydrazyle ($DPPH^\bullet$). Le $DPPH^\bullet$ est un radical stable avec un atome d'azote central; il présente une bande d'absorption à λ = 515 nm ($\varepsilon = 12{,}5\ mM^{-1}\ cm^{-1}$) (couleur violet). Ce radical est couramment utilisé pour évaluer la capacité de piégeage des radicaux libres par des antioxidants synthétiques et naturels. Cependant, ce test peut poser des difficultés d'interprétation lorsque les composés testés possèdent une bande d'absorption intense dans le visible, vers 515 nm (tel est le cas des NP), interférant avec celle du $DPPH^\bullet$. Pour cette raison, nous nous sommes intéressés au développement d'une méthode CLHP permettant de suivre simultanément la consommation du $DPPH^\bullet$ et la formation du composé réduit correspondant, le DPPH-H. Cette méthode analytique a permis d'étudier sans interférence le mécanisme de la réaction entre le $DPPH^\bullet$ et différents types d'antioxydants ainsi que d'évaluer le pouvoir antiradicalaire de matrices complexes et de nanomatériaux (NP de diamant et d'or).

II.1.1 Article 2. Tournebize J., Boudier A., Sapin-Minet A., Maincent P., Leroy P., Schneider R. Role of gold nanoparticles capping density on stability and surface reactivity to design a drug delivery platform. En préparation pour soumettre à *Macromolecules*.

II.1.2 Article 3. Tournebize J., Sapin-Minet A., Schneider R., Boudier A., Maincent P., Leroy P. Simple spectrophotocolorimetric method for quantitative determination of gold in nanoparticles, *Talanta*. 83: 1780-1783 (2011).

II.1.3 Article 4. Boudier A., Tournebize J., Bartosz G., El Hani S., Bengueddour R., Sapin-Minet A., Leroy P. High-performance liquid chromatographic method to evaluate the hydrogen atom transfer during reaction between 1,1-diphenyl-2-picryl-hydrazyl radical and antioxidants. *Anal. Chim. Acta*. 711: 97-106 (2012).

Role of gold nanoparticles capping density on stability and surface reactivity to design drug delivery platforms

Juliana TOURNEBIZE[a], Ariane BOUDIER[a], Anne SAPIN-MINET[a], Philippe MAINCENT[a], Pierre LEROY[a], Raphaël SCHNEIDER[b]*

[a] *Université de Lorraine, CITHEFOR EA 3452 « Cibles thérapeutiques, formulation et expertise préclinique du médicament », Faculty of Pharmacy, BP 80403, 54001 Nancy Cedex, France*
[b] *Université de Lorraine Laboratoire Réactions et Génie des Procédés, UPR 3349, CNRS, 1, rue Grandville, BP 20451, 54001 Nancy Cedex, France*

* Corresponding author.
E-mail address: Raphael.schneider@univ-lorraine.fr

Abstract

Five-nanometer sized gold nanoparticles (AuNP) stabilized with citrate ions have been reacted with various excess (× 28, × 56, × 140, × 222) of dihydrolipoic acid (DHLA). Ligand exchange between citrate and the dithiol resulted in DHLA capped AuNP which degree of inertia was found to be in relationship with the density of capping. Indeed, the results revealed the importance of DHLA density to enhance the colloidal stability and modulate the reactivity towards free radicals and proteins of biological relevance. Thus, AuNP capped with the highest amount of DHLA were found to be the ones, first, the most resistant to environmental changes, then, characterized by the lowest residual catalytic reactivity of their metallic core and finally the lowest interacting with proteins through non-specific adsorption. The physico-chemical properties conferred to AuNP prepared with the × 222 excess were therefore very interesting for further pharmaceutical development of nanoparticle platforms.

Keywords: Gold nanoparticles; Dihydrolipoic acid; Capping density; Stability; Reactivity; Bovine serum albumin; Free radical.

Table of Contents graphic:

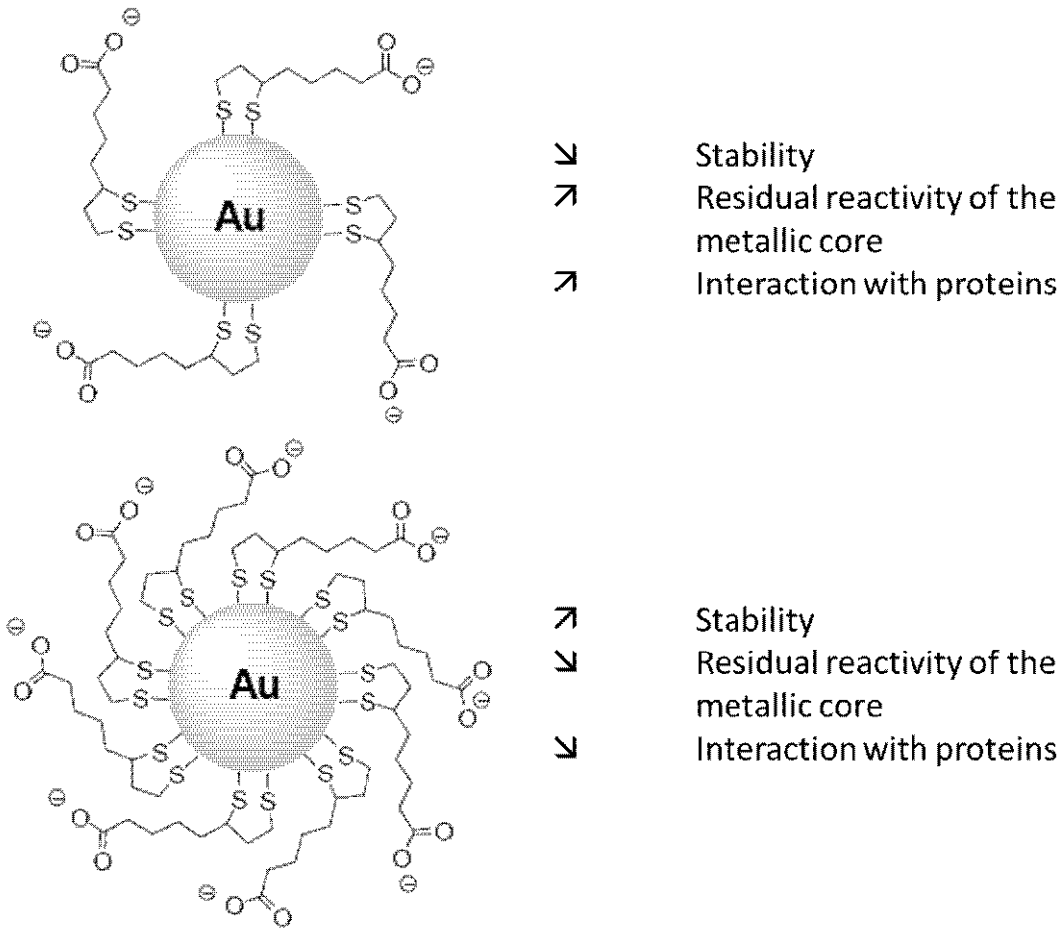

1. Introduction

Functionalized noble metal nanoparticles (NP), which specifically interact with cellular targets, are of great interest in biotechnology and medicine.[1-3] Among these metal NP and due to their inertia as well as weakly toxic nature, controllable size and ease of functionalization with various ligands, gold NP (AuNP) have been intensively studied over the last years for diagnostic,[4-5] including tomography and magnetic resonance imaging[6] as well as for drug delivery.[7-9] However, the essential parameters affecting the successful use of AuNP for biological purposes are their stability in physiological conditions as well as their surface reactivity towards molecules encountered in living organisms.

The stability of AuNP suspension strongly depends on nano-object surface charge as well as pH and ionic strength of the medium. Because of these concerns, extensive research is focusing on the improvement of the AuNP stability and the development of methods to evaluate the stability of AuNP prior to their biological use (Table 1). The most common strategy to disperse AuNP in aqueous medium and to get access to NP valuable for bio-applications is the use of a protective agent, which not only prevents the NP against aggregation, but also leads to functionalized objects.[10] So far, thiol-containing compounds have been widely used as protective agents for obtaining stable monolayer-protected AuNP, due to the strong affinity of sulfur to gold.[11] In many cases, the AuNP are synthesized using the Turkevich's method[12] or modifications of this method[13-14] and functionalized *via* a two-step approach, referred to cap-exchange (or ligand exchange). This involves replacing the native citrate cap with bifunctional hydrophilic ligands that contain a thiol group for anchoring the ligand to the nanocrystal surface and a second module that not only promotes aqueous dispersibility[15-16] but also can ease the grafting of a drug *via* carboxylic acid groups for example.[17] Regardless of the cap-exchange method used, small hydrodynamic diameters (< 25 nm) and good colloidal stability are prerequisite for developing AuNP with great potential utility in biological applications. The success of these applications largely depends on the ligand used to cap the nanocrystal surface.

Indeed, depending on the targeted application, the ligand type and the density of capping should differ. Thus, as far as catalysis domain is concerned, it was previously shown that whatever the selected ligand, the capping limits AuNP catalytic activity. Moreover, increasing the capping density was related to a decrease of the catalytic efficiency.[18] On the contrary, for biological purposes, a total inertia is required to ensure biocompatibility; therefore an absence of any residual catalytic activity parallel to an optimized capping density is needed.

Among the various ligand used, dihydrolipoic acid (DHLA), the reduced form of α-lipoic acid (LA) (Scheme 1), and the poly(ethylene glycol)esters of DHLA are known to afford NP, like quantum dots, higher colloidal stability than monothiol ligands because of the higher affinity of the dithiol function towards metal atoms present at the nanocrystal surface (Table 1).[17, 19-21]

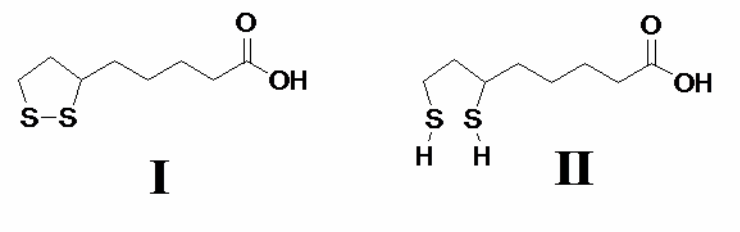

Scheme 1. Molecular structures of α-lipoic acid (I) and dihydrolipoic acid (II).

Table 1. Stability studies of citrate- and thiol-capped AuNP, reported in the literature, as a function of time and various environmental parameters.

Ligand or stabilizing agent	Storage conditions	Modified factor to trigger aggregation	Parameter or method used to monitor stability	Main conclusions	Ref
• Citrate	Synthesis medium	benzyl mercaptan (bm)	D_h[1] d_c[2] Zeta potential[3] Color Maximum absorbance and wavelength[4]	Fast aggregation of the AuNP upon bm addition.	22-23
• Citrate	4 and 23°C, in the dark	-	D_h[1]: initial standard deviation (± 2.8 nm)	A standard deviation > 2.8 nm from the average size was notified as instability. Stable during 21 days at 4°C or stable for less than 6 days at 23 °C.	24
• 1-pentanethiol tetraethylene glycol (MT^7) • 1-pentanethiol trimethyl ammonium terminated tetra ethylene glycol (MT^7) • 1-pentanethiol carboxylate-terminated tetraethylene glycol (MT^7) • 1-pentanethiol fluorescein isothiocyanate-terminated tetraethylene glycol (MT^7)	Dry powders	glutathione DHLA Cysteine	Fluorescence intensity[6]	Stability towards thiol is governed by the surface charge of AuNP.	25
• Hexa-(ethyleneglycol)-terminated thiol (MT^7)	Temperature from 5 to 70°C NaCl 0 to 1.0 M pH from 1.3 to 12.4	NaCl temperature pH	Maximum absorbance and wavelength[4]	AuNP were stable during the analyses into all the conditions.	26
• Citrate • 2-mercaptosuccinic acid (MT^7)	Dialysis against water just before the analysis	pH cyanide dissolution	Maximum absorbance and wavelength[4] Resonance angle[5]	Less instability for 2-mercaptosuccinic acid NP than for the citrate ones.	27
• Cystamine • 2-mercaptoethanesulfonic acid (MT^7) • 3-mercaptopropionic acid (MT^7)	water	Density of the capping was varied	D_h[1] d_c[2]	Optimisation of the gold salt/stabilizer ratio is important for the stability. Satisfying stability for 2-mercaptoethanesulfonic acid.	28
• Thio-polyethylene glycols (HS-PEG) (MT^7)	water PBS (pH = 7.4) Serum	-	Maximum absorbance[4]	Better stability with high molecular weight (>2000 Da). Stable for at least 3 weeks in all media.	29
• mercapto alkane bearing polyethylene oxide moieties:	NaCl 0 to 2 M	NaCl Density of the capping was varied	D_h[1], Zeta potential[3], Maximum absorbance[4],	Better stability for alkane derivatives than citrate AuNP. Best stability with HS-$(CH_2)_{11}$-PEO_6-	16

((HS-$(CH_2)_n$-PEO_m-X with n = 5 to 11, m = 0 to 6 and X = -OH or –COOH) (MT^7)				COOH derivatives.	
• Mercaptoundecanoic acid (MT^7) • DHLA (DT^7)	NaOH adjusted to the desired value with HCl or buffer at pH=8.2 NaCl 0.01 M Room temperature	pH DTT at 40 °C	Maximum absorbance and wavelength[4] Color and precipitate occurrence D_h[1] d_c[2] Zeta potential[3]	Instability under acidic pH but 2 weeks of stability at pH 10. Less stability against DTT in the case of the monothiol as compared to DHLA.	17
• Citrate • HS-PEG (MT^7) • DHLA-PEG (DT^7)	PBS, under inert atmosphere, 40°C PBS	Dithiothreitol (DTT) 10% Fetal calf serum, 37°C	Maximum absorbance and wavelength[4] D_h[1]	DHLA-PEG AuNP were more stable than PEG AuNP after the use of DTT (no stability for citrate-stabilized AuNP). Hypothesis on the capping density to explain the lower stability of the 80-nm AuNP as compared to the 20- or 40-nm ones.	30

Methods used for the measurement of parameters were DLS[1] (for hydrodynamic diameters, D_h), TEM[2] (for core diameters d_c), laser-doppler evaluation[3], UV-visible spectra set on the surface plasmon resonance absorbance band[4], surface plasmon resonance spectroscopy[5], spectrofluorimeter[6]. The ligands were classified as MT for monothiols and DT for dithiol[7].

DHLA, its derivatives and other multiple thiol-anchor ligands have also proved to be valuable ligands for stabilizing and inhibiting aggregation of AuNP in aqueous solution.[31] Furthermore, DHLA is a physiological compound, with antioxidant activity, already administered to humans.[32] As a consequence, this molecule is of high potential as AuNP ligand.

Although DHLA-capped AuNP are a substantial improvement in term of stability and also biocompatibility,[33] compared to monothiol-stabilized ones, no systematic study devoted to the influence of the [DHLA]/[Au] molar ratio during the cap-exchange on the properties of produced AuNP has been undertaken. In fact, high molar excess of DHLA or its derivatives are generally used to saturate NP surfaces. In this work, cap-exchange reactions of physisorbed bound citrate ions present at the surface of small-sized (*ca.* 5 nm in diameter) AuNP prepared *via* the Turkevich's method by using DHLA were investigated. The influence of the molar ratio of DHLA to Au on the aggregation behaviour of AuNP in phosphate buffer solution and in presence of salt excess was studied. Next, we investigated the role of DHLA capping density on the reactivity with various molecules, a dithiol, a free radical and a protein of biological relevance: albumin. This work highlights how important is the packing density to build a stable and inert platform for the design of drug delivery systems.

2. Experimental section

2.1. Chemicals. All reagents and solvents were of analytic grade and used without further purification. Tetrachloroauric acid trihydrate ($HAuCl_4 \bullet 3H_2O$) and α-lipoic acid were purchased from Sigma-Aldrich (France). Phosphate-buffered saline (PBS) solution was prepared as follows: $[Na_2HPO_4] = 4 \times 10^{-2}$ M, $[KH_2PO_4] = 4 \times 10^{-3}$ M, and $[NaCl] = 1 \times 10^{-1}$ M, final pH was adjusted to 7.4. Ultrapure deionized water (>18.2 MΩ.cm) was used to prepare all solutions. Before synthesis, all glassware was thoroughly using *aqua regia* (3:1 HCl/HNO_3) and rinsed with ultrapure water prior to use.

2.2. Preparation of citrate-stabilized gold sols. Gold colloids were prepared at room temperature by sodium borohydride reduction of $HAuCl_4 \bullet 3H_2O$ in the presence of sodium citrate as described by Brown and co-workers.[14] Briefly, at room temperature, 1 mL of a 1 % (w/v) $HAuCl_4 \bullet 3H_2O$ solution in water was added to 90 mL of water. After 1 min of stirring, 2.0 mL of a 38.8 mM sodium citrate solution in water were added. One minute later, 1.0 mL of a freshly prepared 0.075 % (w/v) $NaBH_4$ solution in a 38.8 mM sodium citrate solution was quickly injected in the reaction flask. The reaction medium was stirred for an additional 5-min period and

the resulting deep red colloidal solution immediately stored in the dark at 4 ºC for a maximum period of 2 months in polypropylene tube.

2.3. Synthesis and purification of DHLA-capped gold nanoparticles (Au@DHLA). $Au@DHLA_{28}$, $Au@DHLA_{56}$, $Au@DHLA_{140}$ and $Au@DHLA_{222}$ NP were prepared by adding respectively 90, 150, 375 and 600 µmol of α-lipoic acid, solubilized in respectively 1.5, 2.5, 5 and 10 mL of 0.5 M aqueous NaOH solution, to 25 mL of freshly prepared citrate-capped AuNP. The reaction mixture was stirred for 24 h at 20-23 °C before dialysis. The non-reacted α-lipoic acid remaining in the solution after the cap-exchange was removed by dialysis against PBS for 48 h using a dialysis bag (regenerated cellulose with a molecular weight cut-off of 10 kDa (Roth®, France)). The dialysis medium was changed once to fresh PBS after 24 h. The resulting Au@DHLA NP suspension was stored in the dark at 4 °C for a maximum period of 2 months in polypropylene tube.

2.4. Characterization of gold nanoparticles. A double-beam UV-visible spectrophotometer (model Uvikon 932, Kontron) was used for spectra recordings and absorbance measurements. All measurements were performed at 20-23 °C using quartz cuvettes of 1-cm path length. The scanning wavelength range was from 200 to 900 nm with 0.4 nm interval. Molar absorbance values of AuNP were calculated as previously published.[34] The results are the followings: $1{,}20 \pm 0{,}10 \times 10^7$, $0{,}43 \pm 0{,}10 \times 10^7$, $0{,}43 \pm 0{,}10 \times 10^7$, $0{,}42 \pm 0{,}10 \times 10^7$, $0{,}50 \pm 0{,}20 \times 10^7$ $M^{-1}cm^{-1}$, for citrate-stabilized AuNP, $Au@DHLA_{28}$, $Au@DHLA_{56}$, $Au@DHLA_{140}$, and $Au@DHLA_{222}$ NP, respectively.

Transmission electronic microscopy (TEM) images were recorded using a Philips CM20 instrument with a LaB_6 cathode operating at 200 kV. AuNP solutions were deposited onto a 400 mesh carbon film copper grids. The average diameter of the gold core was calculated for each AuNP sample by counting *ca.* 200 individual particles from TEM images. From these observations, the number of Au surface atoms (N_s) on a single AuNP was calculated using: $N_S = \frac{4\Pi R_{NP}^2}{\Pi R_{atom}^2}$, where R_{NP} is the radius obtained by TEM and R_{atom} = 0.137 nm[35].

The hydrodynamic diameter (D_h) and surface charge of AuNP were measured using a Zetasizer Nano ZS (Malvern Instruments, UK). These measurements were performed at 20 ºC using low volume polystyrene and disposable capillary cells, respectively. All D_h reported are volume average values, based on three independent measurements of two AuNP batches. Prior to zeta potential measurements, Au@DHLA NP were dialysed against ultra pure water for 24 h. All surface charges reported are averages based on three measurements of one batch of AuNP.

X-ray photoelectron spectroscopy (XPS) measurements were performed at a residual pressure of 10^{-9} mbar, using a Kratos Axis Ultra electron energy analyzer (Kratos Analytical, UK) operating with a monochromatic Al Kα source.

2.5. Gold and sulfur content. Gold content of the various kinds of gold nanoparticles was determined using the previously reported methodology.[34] Sulfur content of the various batches was determined by Inductively Coupled Plasma-Optical Emission Spectrometer (ICP-OES A VARIAN 720-ES).

2.6. Stability studies. Effects of [DHLA] / [Au] ratio on stability of AuNP were evaluated based on changes in the λ_{max} of the surface plasmon resonance (SPR) band and D_h of AuNP which were stored at 4 ºC in physiological medium PBS (150 mM) and in polypropylene tubes for 50 days. The AuNP were wrapped with aluminium foil and stored in the dark throughout the measurement period. The effects of dithiothreitol (DTT) and high concentration of salt on the stability of the various [DHLA] / [Au] ratio were also evaluated. Briefly, DTT and NaCl were added to each preparation of AuNP to a final concentration of 0.1 M and 1 M, respectively. The solution was incubated at 40 °C for 1 min and stored in the dark at room temperature (20 – 23 °C) in low volume polystyrene cuvettes for 100 min. For all stability studies, citrate-capped AuNP were used as control sample.

2.7. Interaction of gold nanoparticles with 2,2'-azino-di(3-ethylbenzothiazoline-6-sulphonate) and bovine serum albumin. 2,2'-azino-di(3-ethylbenzthiazoline-6-sulphonate), $ABTS^{\bullet+}$, stock solution was prepared mixing 5.4 mM ABTS with 1.7 mM potassium persulfate in PBS and placed in the dark at room temperature for 16 h to give a dark blue solution. Molar concentrations of $ABTS^{\bullet+}$ were calculated using molar absorbance value previously reported (*i.e.* $\varepsilon_{734nm} = 1.5 \times 10^4\ M^{-1}cm^{-1}$.[36] The interaction between $ABTS^{\bullet+}$ and AuNP was studied as follows: 1125 µL of Au@DHLA NP and citrate-stabilized AuNP were reacted with 375 µL of 200 µM $ABTS^{\bullet+}$ solution in PBS. After 2-h incubation at 20 – 23°C, the absorbance of reaction medium was measured at 734 nm.

Aliquots (500 µL) of a 1.6 µM BSA solution prepared in PBS were mixed with AuNP in PBS (500 µL); the resulting mixtures were incubated at 37°C for 1 h. The interaction between BSA and AuNP was monitored measuring the intrinsic tryptophan fluorescence of BSA (λ_{exc} = 280 nm, λ_{em} = 355 nm)[37] with a spectrofluorimeter (Hitachi F-2000, France). Fluorescence intensities with and without AuNP (*I* and *I°)* were measured and Stern-Volmer equation was used to calculate the

related constant: $I°/I = 1 + K_{SV}[Q]$ where K_{SV} is Stern-Volmer constant and [Q] the AuNP concentration which is the quencher.[38]

2.8.. Statistical analyses. One-way analysis of variance (SigmaStat® 3.1) was used for statistical analyses. For each sample group the equal variance (Levene median) and normality (Kolmogorov–Smirnov) tests were performed.

3. Results and discussion

3.1. Proof of the variation of the surface packing density. Citrate-stabilized AuNP were first synthesized by reduction of $HAuCl_4$ using sodium borohydride at room temperature. Using TEM, the average diameter of these NP was found to be 5.3 ± 1.1 nm (Figure 1), which is consistent with the synthetic method employed.[14]

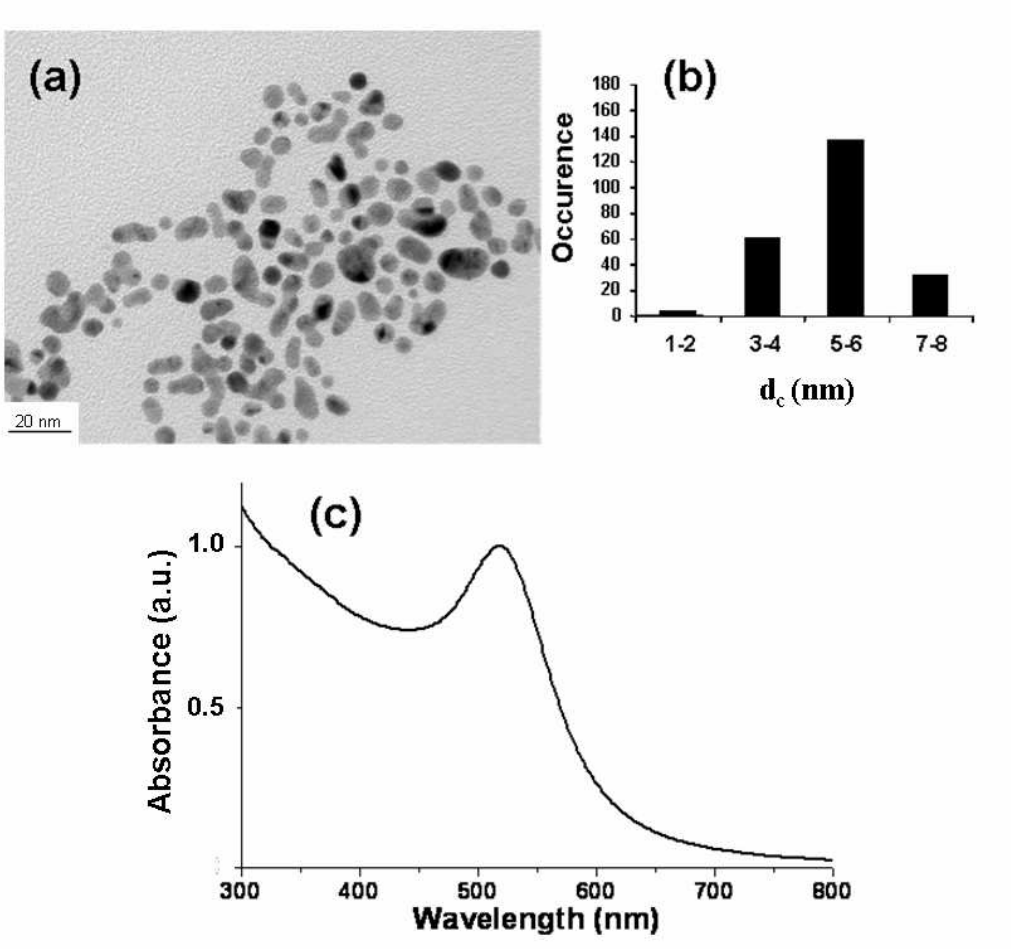

Figure 1. Characteristics of citrate-stabilized AuNP (a) TEM image (scale bar is 20 nm), (b) the corresponding size distribution (n > 200) and (c) their UV-vis absorption spectrum.

The UV-*vis* absorption spectrum of the citrate-stabilized AuNP shows a narrow plasmon bandwidth, centered at 517 nm, confirming the small diameter and the weak polydispersity observed by TEM (Figure 1). Using a molar absorbance ε of 1.2×10^7 $M^{-1}cm^{-1}$ for these *ca.* 5 nm-sized AuNP,[34] the concentration of the citrate-stabilized AuNP solution was found to be 5.89×10^{16} NP per liter. An average diameter of 5.3 nm represents about 1147 cubic face-centered structural units in each nanocrystal (using a theoretical lattice parameter *a* of 0.408 nm), and 4588 Au atoms per nanocrystal. The number of Au surface atoms on a single AuNP was estimated to be 1104.

The citrate ions were next displaced by incubation for one day with LA in aqueous medium. The process used was different from Roux et al.[17] who prepared Au@DHLA NP in a one-step reaction directly with DHLA in organic solvent, which may not allow a good compatibility for further pharmaceutical application. After reaction, the dispersion color changed from pink-red to purple red during the reaction of AuNP with LA. The 5-membered heterocycle of LA containing the dithiolane ring exhibits a strong absorption at 334 nm. This absorption decreases after treatment with AuNP. Because dialkylsulfide absorption on gold yields unstable complexes,[39] a cleavage of the S-S bond of LA by using $NaBH_4$ remaining in the reaction medium is more likely, as already suggested by Roux et al.[17] Using this synthetic protocol, four samples were prepared with different theoretical [DHLA] / [surface Au atoms] molar ratios (28/1, 56/1, 140/1 and 222/1) to evaluate the influence of the ligand coverage on the properties of AuNP. These samples are noted $Au@DHLA_{28}$, $Au@DHLA_{56}$, $Au@DHLA_{140}$, and $Au@DHLA_{222}$, respectively.

After reaction between NP and LA, unbound LA was removed by dialysis against PBS buffer. Upon dialysis, the complete disappearance of the dithiolane ring absorption at 334 nm was observed. Figure 2 depicts results obtained for $Au@DHLA_{222}$ NP.

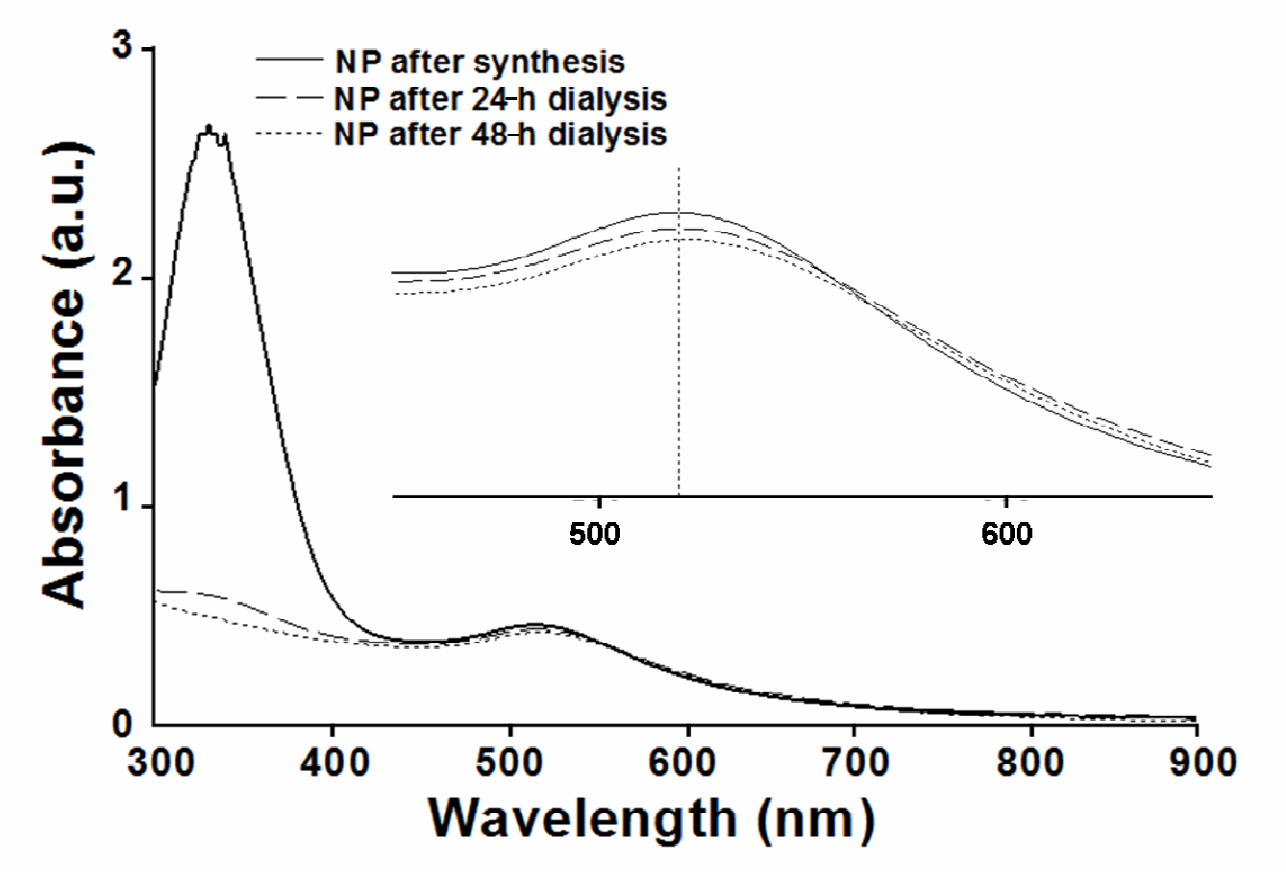

Figure 2. Evolution of the UV-vis spectra of Au@DHLA$_{222}$ NP as a function of dialysis time: NP in reaction medium and after 24-h and 48-h dialysis. Inset: magnification of the AuNP surface plasmon resonance band.

Removal of LA excess was in all cases accompanied by a small bathochromic shift of the surface plasmon resonance (SPR) band depending on the NP ligand coverage. UV-vis absorption spectra showed that after dialysis, except Au@DHLA$_{28}$ NP, all NP exhibit an absorption peak near 520 nm, which is characteristic of the SPR band of AuNP with an average diameter of 4-5 nm (Figure 3).

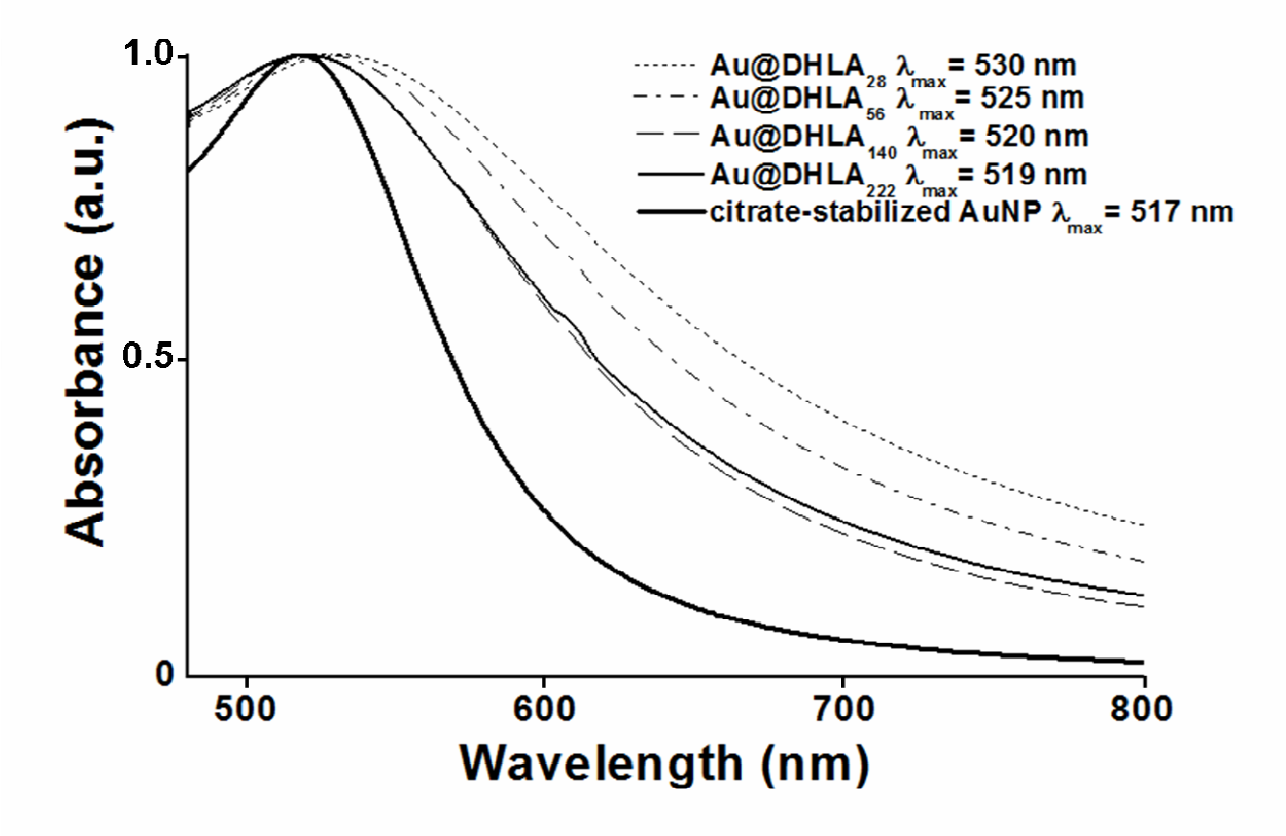

Figure 3. Normalized UV-vis absorption spectra for the several [DHLA]/[Au] molar ratios used during the cap-exchange reaction.

Compared to the SPR band of citrate-stabilized AuNP (λ_{max} = 517 nm), ligand-exchanged Au@DHLA$_{140}$, and Au@DHLA$_{222}$ NP exhibit only a slight red shift ($\Delta\lambda$ = 2-3 nm) originating from the NP surface modification (changes in the surface dielectric constant of the NP associated with the adsorption of the thiol functions of DHLA). This weak red shift also demonstrates that there is no significant particle aggregation during the cap exchange process. Some degree of aggregation was observed for Au@DHLA$_{56}$ NP with a red shift of 8 nm. With the lowest [DHLA]/[Au] ratio used (Au@DHLA$_{28}$ NP), a more pronounced red shift was observed ($\Delta\lambda$ = 13 nm) indicating a more marked increase of the NP diameters during the cap exchange.

X-ray photoelectron spectroscopy **(**XPS) was first used to confirm the chemical bonding between AuNP and DHLA. High-resolution spectra collected for Au 4f, S 2p and C 1s are given in Figure 4. The Au, S and C signals were compared, and they were found to be similar in shape and position for the four materials prepared by capping exchange. The C 1s peak can be deconvoluted into 3 peaks associated with C-C bonds (at 284.6 eV), carbon bound to sulphur (285.5 eV), and carbon bound to two oxygen atoms (COOH function at 287.6 eV). The presence of these signals corresponds with those expected to be observed after covalent anchorage of DHLA at the surface of

AuNP. The Au 4f region shows a pair of peaks at 83.25 eV and 87.6 eV assigned to the Au $4f_{7/2}$ and Au $4f_{5/2}$ peaks, respectively, that are originating from the metal gold cores. The peaks of S $2p_{3/2}$ and S $2p_{1/2}$ originating from S atoms bound to AuNP are observed at 162.3 eV (the signal of S 2p was not deconvoluted), confirming that the S element is linked to the Au surface as thiolate species.[40] A peak centred at *ca.* 167.8 eV assigned to oxidized forms of sulfur could also be observed on XPS spectra. This oxidation probably originates from air-drying of the NP for XPS analyses. Another element detected on the XPS survey scan was O. Gold, C, S, and O are consistent with the exclusive structure of the Au@DHLA NP proposed.

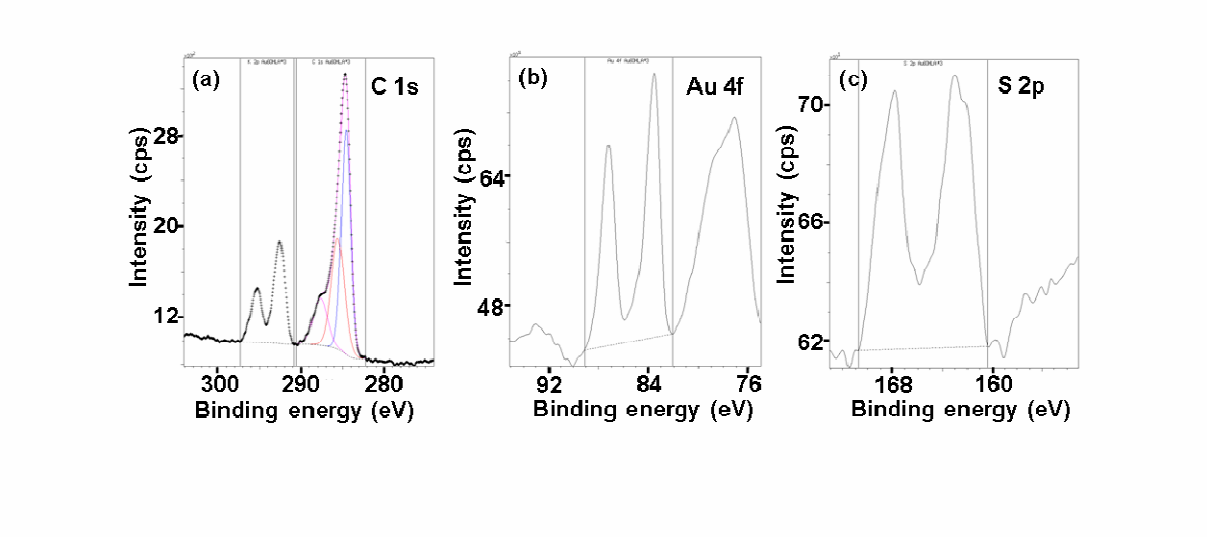

Figure 4. XPS binding energy spectra of Au@$DHLA_{222}$: (a) C 1s, (b) Au 4f and (c) S 2p.

The [S]/[Au] ratio was determined for each Au@DHLA NP using ICP-OES for S and a spectrophotometric assay based on the reaction of $AuCl_4^-$ with the cationic form of a probe (Rhodamine B) to give a coloured ion pair complex,[34] respectively. The results presented in Table 2 showed that more DHLA was added, more the Au@DHLA NP were capped, as expected.

Transmission electron microscopy (TEM), DLS and zeta potential measurements were further used to determine the physicochemical properties of DHLA-functionalized AuNP. TEM micrographs (Figure 5) show that spherical shapes dominate in dispersions of Au@$DHLA_{56}$, Au@$DHLA_{140}$, and Au@$DHLA_{222}$ NP and that these NP are monodisperse and unaggregated (Figure 5).

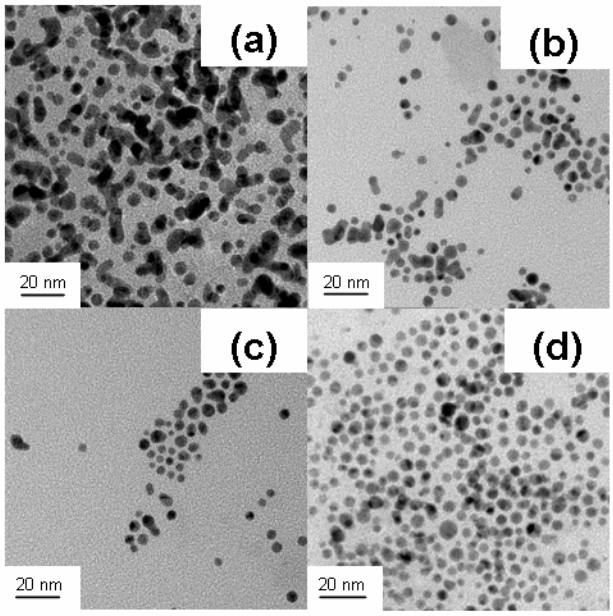

Figure 5. TEM images of (a) Au@DHLA$_{28}$, (b) Au@DHLA$_{56}$, (c) Au@DHLA$_{140}$ and (d) Au@DHLA$_{222}$ NP. All scale bars are 20 nm.

The average diameters extracted from the TEM images (n > 200) are listed in Table 2. Higher inhomogeneities in nanoparticles shape and size dispersion can be observed for Au@DHLA$_{28}$ NP dispersions (Figure 5) than for Au@DHLA$_{56}$, Au@DHLA$_{140}$, and Au@DHLA$_{222}$ NP, respectively, which confirmed the results observed by UV-vis absorption. For that small ligand coverage, TEM studies indicate that the inter-particle distance is reduced and that NP start to coalesce and aggregate, with the extent of aggregation increasing as a function of storage time (*vide infra*). Moreover, we also noticed that solutions of Au@DHLA$_{28}$ NP turned to a dark-gray color after a few days of storage, indicating particle irreversible aggregation.[41]

Table 2. Characterization of synthesized gold nanoparticles *(values are expressed as mean ± standard deviation of n independent measurements).*

	[S]/[Au]	d_c [a] (nm) (n > 200)	D_h [b] (nm) (n = 3)	ζ [c] (mV) (n = 3)
Citrate-stabilized AuNP	-	5.3 ± 1.1	6.5 ± 0.5	-51 ± 3
Au@DHLA$_{28}$	0.26	6.5 ± 3.5	15.0 ± 0.7	-44 ± 1
Au@DHLA$_{56}$	0.29	4.0 ± 1.0	7.7 ± 0.4	-56 ± 0
Au@DHLA$_{140}$	0.33	3.9 ± 1.0	7.7 ± 0.1	-66 ± 5
Au@DHLA$_{222}$	0.41	3.5 ± 1.3	7.2 ± 0.8	-64 ± 4

[a] d_c : average core diameter determined by TEM; [b] D_h = hydrodynamic diameter determined by DLS; [c] All ζ potential measurements were conducted at pH = 7.4;

Hydrodynamic diameters of citrate-stabilized and DHLA-functionalized AuNP obtained one day after the ligand exchange were also determined (Table 2). All AuNP exhibit appropriate D_h, which were larger than the metallic core (due to drying process before TEM observations and solvatation layers in aqueous medium). The derived DLS size distributions (data not shown) were found to be monomodal with a relatively narrow distribution, confirming the absence of aggregation after the capping exchange and subsequent purification step of all AuNP. Hydrodynamic diameters measured for Au@DHLA NP were however found not to be uniform and to strongly depend on the [DHLA]/[Au] ratio used for the ligand exchange. Au@DHLA$_{28}$ NP exhibit a D_h of about 15 nm, which is approximately 2.3 times larger than the native citrate-stabilized AuNP (6.5 nm). A strong decrease of D_h was observed when the [DHLA]/[Au] ratio increased. Au@DHLA$_{56}$, Au@DHLA$_{140}$ and Au@DHLA$_{222}$ NP have D_h close to that of the starting citrate-stabilized AuNP, indicating that the ligand exchange was homogeneous onto these AuNP and the lack of AuNP coalescence during the capping exchange reaction.

The electric potential, referred to as zeta potential (ζ), which controls the colloidal stability and interparticle interactions, was also determined for the 5 sets of AuNP (Table 2). ζ values obtained confirmed the presence of negative charges on the surfaces of the AuNP, due to the carboxylate groups of the citrate or DHLA ligands. After dialysis and at pH = 7.4, citrate-stabilized AuNP have a high negative charge of -51 mV. At the same pH value, the ζ potential values measured for Au@DHLA$_{28}$, Au@DHLA$_{56}$, Au@DHLA$_{140}$, and Au@DHLA$_{222}$ NP are -44, -56, -66 and -64 mV, respectively. These values confirmed, as well, the increase of capping density by the DHLA ligand when increasing the [DHLA]/[Au] ratio during the ligand exchange reaction.

3.2. Colloidal stability of Au@DHLA NP. Two kinds of experimentations were led in order to assess the colloidal stability of Au@DHLA NP either in their final medium of synthesis (*i.e.* PBS) or in presence of a factor able to trigger aggregation (Table 1) such as salt (NaCl) and another dithiol (dithiothreitol).

Firstly, for AuNP coated by a layer of thioacid like DHLA, strong electrostatic forces should prevent the particles from contacting and aggregation above pH = 4.8. These electrostatic forces are however sensitive to salts present in the medium, which can cause bridging between NP, thus leading to aggregation. Evaluation of the stability of Au@DHLA NP in an electrolytic environment like PBS (pH = 7.4, ionic strength = 150 mM) should not only provide information on how AuNP potentially behave in biological media, but also allow to assess the ligand binding affinity to the nanocrystals.

DLS and UV-vis spectroscopy were first used to monitor the stability of AuNP over a period of 50 days in PBS at 4°C (Figure 6).

Starting citrate-stabilized AuNP were found to be highly sensitive to saline media and precipitated completely in 24 h when added to PBS. The density of the capping layer was found to have marked effects on the stability of Au@DHLA NP in PBS. The measured D_h of Au@DHLA$_{28}$ NP was found to increase with storage time in PBS and reached about 150 nm after 50 days, indicating a clear aggregation of the native material (Figure 6). This result is supported by the red-shift of the SPR band to 547 nm (Figure 6) and confirms TEM data recorded for these NP just after the purification step. Moreover, dispersions of these NP became progressively unstable with time and changed color to dark-purple. Macroscopic precipitation was also observed after few days of storage at 4 °C.

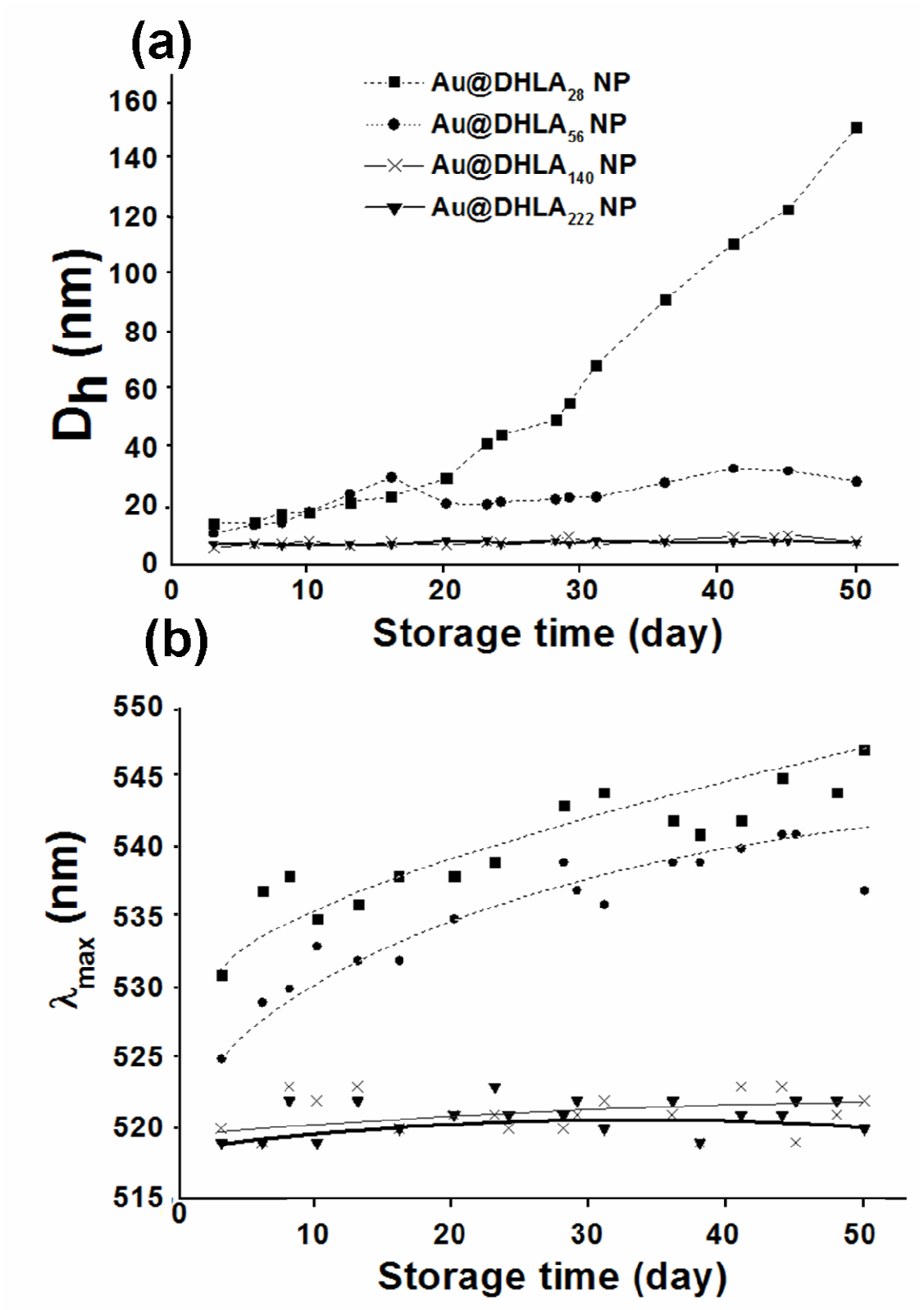

Figure 6. Stability studies of the different AuNP (Au@DHLA28 (■), Au@DHLA56 (•), Au@DHLA140 (×), Au@DHLA222 (▼)) stored at 4°C in PBS versus storage time: evolution of (a) hydrodynamic diameters (Dh) and (b) surface plasmon resonance band maxima (λ_{max}).

Degree of aggregation was also found to be marked for Au@DHLA$_{56}$ NP. Although a marked red shift from 522 at day 0 to more than 540 nm at day 45 was observed by UV-vis spectroscopy (Figure 6), the increase of D_h is significantly less pronounced than that observed for Au@DHLA$_{28}$ NP ($D_h \approx 30$ nm idem after 50 days storage) (Figure 6). Neither a bathochromic shift of the SPR band maximum nor an increase of the D_h were observed for Au@DHLA$_{140}$ and Au@DHLA$_{222}$ NP, which were essentially unaffected in PBS medium over 50 days storage and exhibit the best colloidal stability.

Secondly, we explored the effects of adding an excess of NaCl on the colloidal stability of Au@DHLA NP prepared using the various [DHLA] / [Au] described above. Figure **7** shows evolution of the SPR band upon addition of Au@DHLA NP in a 1 M NaCl solution (citrate-stabilized AuNP were used as control sample).

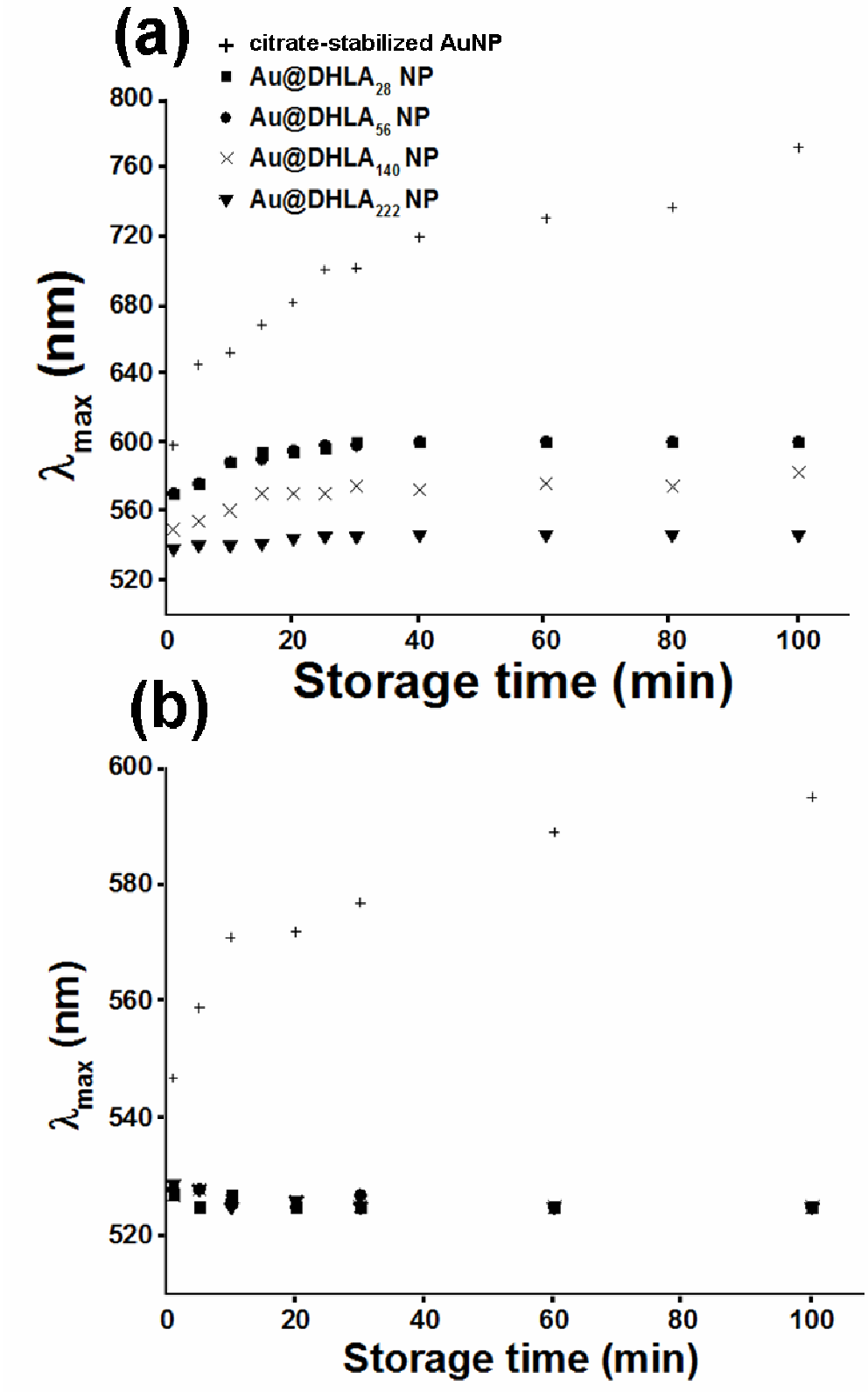

Figure 7. Time-dependent λ_{max} evolution upon addition of citrate-capped AuNP (+) and Au@DHLA NP (Au@DHLA$_{28}$ (■), Au@DHLA$_{56}$ (•), Au@DHLA$_{140}$ (×), Au@DHLA$_{222}$ (▼)) (a) in a 1 M NaCl solution and (b) in a 0.1 M DTT solution.

The citrate-stabilized AuNP changed color from red to violet immediately upon mixing with the salt solution and precipitated within 30 min. As shown in Figure **7**, the addition of 1 M NaCl caused a gradual shift of Au@DHLA$_{28}$ and Au@DHLA$_{56}$ NP SPR band from *ca.* 530 nm to 600 nm over 100 min. In comparison, suspensions of Au@DHLA$_{140}$ and Au@DHLA$_{222}$ NP were found to be more stable. The bathochromic shifts of the SPR band maxima were found to be less pronounced (from 532 nm to 583 and 547 nm for Au@DHLA$_{140}$ and Au@DHLA$_{222}$ NP, respectively) and Au@DHLA$_{222}$ NP remained dispersed and aggregate-free in 1 M NaCl solution at least for 24 h.

At last, we evaluated the formation of AuNP aggregates in presence of a 0.1 M 1,4-dimercapto-2,3-butanediol (also called dithiothreitol, DTT) solution. Since DTT has a great affinity for AuNP, DHLA displacement by DTT should alter the photophysical properties of the AuNP, including a red-shift and a decrease of the SPR band and a change in the NP dispersion color.[42-45] For citrate-stabilized AuNP, the SPR band maximum is red-shifted in 10 min from 522 to 570 nm (Figure 7). A λ_{max} value of 595 nm was attained after 100 min, which suggests formation of aggregates. Under the same experimental conditions, no color change and no sign of aggregation were observed for all Au@DHLA NP, indicating a higher colloidal stability. More interestingly, a gradual shift of the SPR band maximum was observed for all NP from *ca.* 530 to 525 nm after treatment with DTT (Figure 7). These data clearly show that DHLA is not displaced from the periphery of AuNP upon mixing with the 0.1 M DTT solution and that the surface of Au@DHLA NP can probably accommodate the DTT ligand, which further behaves as a protective agent of the Au core.

Results obtained after these three stability tests demonstrate firstly that due its two anchoring groups to the Au metallic surface, DHLA provides enhanced stability to AuNP in aqueous solution as compared to single thiol ligands-capped AuNP, which are far less stable in electrolytic environments.[15, 43-45] Secondly, the surface packing density of DHLA is a crucial parameter to enhance the stability of Au@DHLA NP in aqueous solution, a high surface coverage affording NP with the best colloidal stability.

3.3. Surface packing density of DHLA controls NP reactivity with a free radical and bovine serum albumin. Understanding the reactivity between molecules of biological relevance and AuNP is crucial to predict the AuNP fate in human body. Because of the rising interest of AuNP for biomedical applications, research is investigating the detailed interactions between AuNP and some molecules and their precise mechanisms. Two kinds of molecules were presently tested: a free radical, 2,2'-azino-di(3-ethylbenzthiazoline-6-sulphonate, ABTS) to check the residual catalytic activity of AuNP and a protein of biological relevance, bovine serum albumin (BSA). Again, the influence of the surface packing density of Au@DHLA NP on the behavior of nano-object towards

the molecules was evaluated. In all of these assays, Au@DHLA$_{28}$ was not tested due to its low stability highlighted in the stability tests.

Previous works have already reported that gold and other noble metal NP can react directly with free radicals for example 1,1-diphenyl-2-picrylhydrazyl (DPPH$^{\bullet}$).[46-48] Nevertheless, the reaction with this radical is usually followed at a wavelength of 515 nm which interact with the the SPR band maxima. Novel methods were therefore devoted to limit this phenomenon *via* HPLC analysis for instance.[48] In this study, a hydrogen atom transfer between the probe and AuNP was proven. Although DPPH$^{\bullet}$ reaction requires an organic medium, the other radical, ABTS$^{\bullet+}$, also widely used to evaluate the radical scavenging properties of antioxidants, can react in aqueous solution, which mimics more accurately the physiological environment. Therefore, this *in situ* generated radical was chosen to evaluate the residual AuNP metallic core reactivity. In this study, the surface capping density of AuNP is hypothesized to minimize the interaction of free radicals with AuNP surface.[18] To support this hypothesis, AuNP at different concentrations (10 – 90 nM) were reacted in ABTS$^{\bullet+}$ solution. As shown in Figure 8, the initial concentration of ABTS$^{\bullet+}$ gradually decreased when AuNP concentration increased for all types of particles.

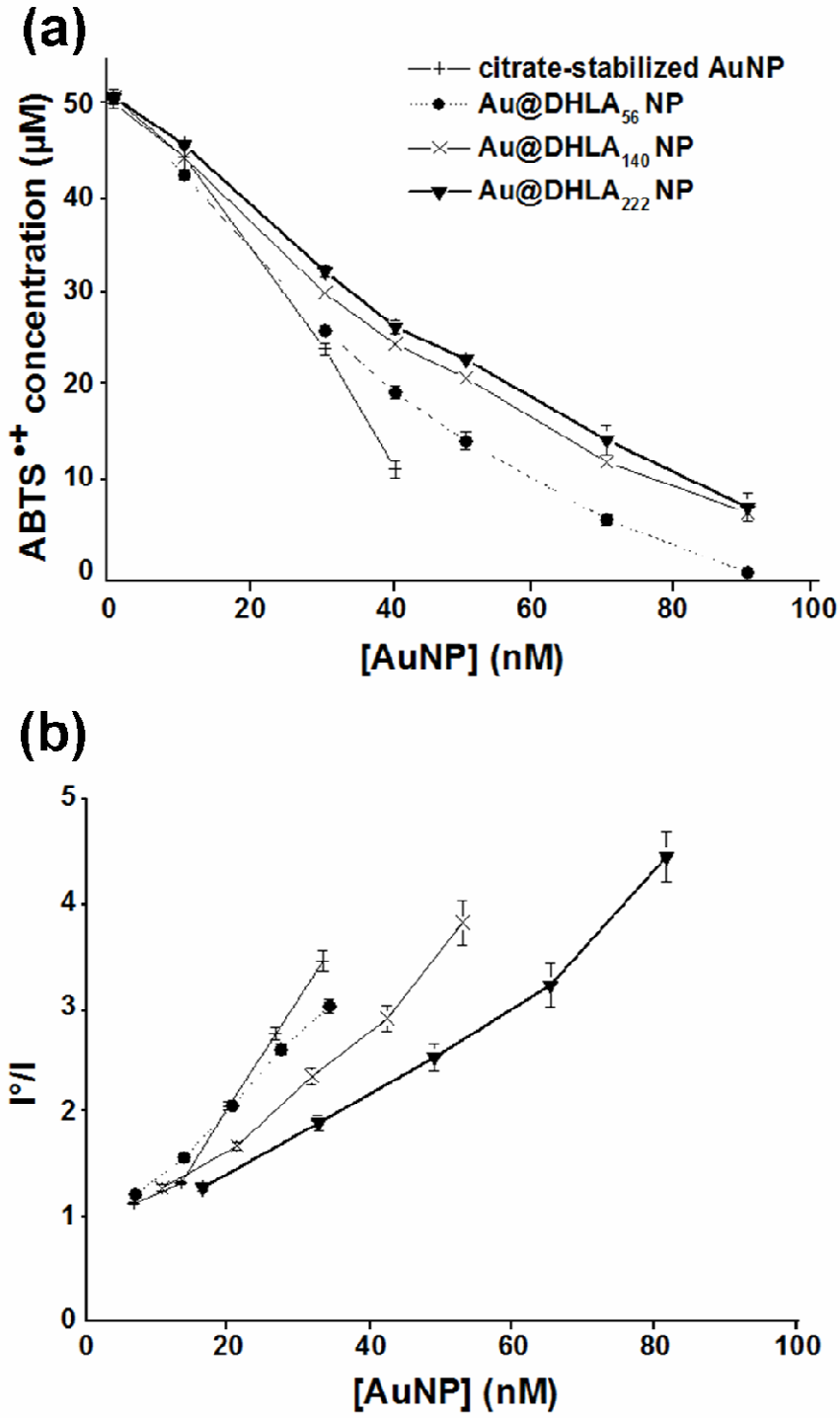

Figure 8. Reactivity between gold nanoparticles (citrate-capped AuNP (+) and Au@DHLA NP: Au@DHLA$_{56}$ (•), Au@DHLA$_{140}$ (×), Au@DHLA$_{222}$ (▼)) and (a) 2,2'-azino-bis(3-ethylbenzothiazoline-6-sulphonic acid) radical $ABTS^{\bullet+}$ and (b) bovine serum albumin (BSA). Fluorescence intensities of the protein were recorded in absence (I°) and in presence (I) of AuNP.

The half-maximum values (EC50) of the concentration–response curves were calculated and the results were as follow: 11 ± 1, 19 ± 1, 24 ± 1, 26 ± 1 nM for citrate-stabilized AuNP, Au@DHLA$_{56}$,

Au@DHLA$_{140}$ and Au@DHLA$_{222}$ NP, respectively. The obtained values of citrate-stabilized AuNP, Au@DHLA$_{56}$ were significantly different of what was calculated for Au@DHLA$_{140}$ and Au@DHLA$_{222}$ ($p < 0.05$). Moreover, no statistically difference was highlighted between the two last cited AuNP. Therefore, DHLA capping seems to bring a better inertia towards highly reactive molecules. Moreover, the surface capping density is a key to control the reaction between AuNP and free radicals.

The interaction of particles with albumin is usually the first step to predict the object becoming in blood stream since it is quantitatively the most important circulating protein (38 to 48 g/L) with a fundamental role into oncotic pressure, transport of molecules and antioxidant property.[49] In this work, we evaluated how AuNP surface packing density influences the reactivity towards bovine serum albumin (BSA) which possesses 76 % homology as compared to the human protein.[50] BSA fluorescence quenching as a function of AuNP concentration for each type of nano-object was studied (Figure 8). The results showed that whatever the AuNP, they all interact with BSA. Nevertheless, the Stern-Volmer constant after linear regression were calculated as: 0.091 ± 0.003, 0.068 ± 0.002, 0.056 ± 0.003 and 0.047 ± 0.003 nM^{-1} for citrate-stabilized AuNP, Au@DHLA$_{56}$, Au@DHLA$_{140}$ and Au@DHLA$_{222}$ NP, respectively. Stern-Volmer constant obtained in the case of the densest surface packing (Au@DHLA$_{222}$) was significantly different ($p < 0.001$) as compared to all other cappings. It is well-known that the quenching between BSA and AuNP occurs *via* an interaction with tryptophan located at 212 position, in a hydrophobic domain, which changes its fluorescence after modification of its molecular environment.[50] Two mechanisms are nowadays highlighted to understand how AuNP can bind BSA and as a consequence, quenches the amino acid fluorescence:[51]

- First, the electrostatic binding, which is based on the fact that even though BSA is globally negatively charged at physiological pH, 60 positively charged lysine residues are located on the protein surface able to interact with oppositely charged groups through electrostatic interactions;
- Second, the displacement mechanism, in which AuNP capping ligand is displaced after adsorption of BSA onto the gold core.

As regards citrate-stabilized AuNP, the interaction occurs mainly through the first mechanism but the second one is not excluded.[51] If DHLA capping is now considered, capping ligand displacement may not occur because of the presence of two sulfur atoms that covalently binds AuNP core. Therefore, this gives superiority to DHLA over citrate as capping ligand, especially if the packing density of Au@DHLA$_{222}$ is taken into consideration. Moreover, even if Au@DHLA NP binds BSA, the most important capping was able to limit this interaction in some extent. These

experimentations are of main importance to test these nanoparticle platforms as future drug delivery systems, since it is now well-described that protein binding on nano-objects induces fast internalization by cells through multiple receptor uptake.[52] Indeed, this phenomenon helps antigen-presenting cells recognition, (macrophages, B cells and dendritic cells which are efficient in non-self internalization), and finally, induces fast clearance from blood stream.[53] Therefore, protein binding on nanoparticle surface will directly influence the pharmacokinetic behavior of a nano-object (half-life and distribution to the targeted site for instance). But, thanks to the presence of the carboxylic acid groups of DHLA on AuNP surface, these particles offer the possibility to be further functionalized by the grafting of a drug of therapeutic relevance and also polyethylene glycol (PEG). Indeed, this polymer is usually used to create a steric barrier to avoid protein adsorption on NP in order to improve the object half-life in blood stream.[53] As a consequence, Au@DHLA$_{222}$ will be chosen and chemically modified to finally investigate the impact on macrophage physiology of this platform, offering both, a pharmaceutical application and stealthiness towards the antigen-presenting cells.

4. Conclusions

Citrate-capped AuNP with an average diameter of *ca.* 5 nm were coated with DHLA using a cap-exchange method. The influence of the molar ratio of DHLA to Au on the properties and on the stability of Au@DHLA NP produced was investigated. Among the four sets of AuNP prepared (Au@DHLA$_{28}$, Au@DHLA$_{56}$, Au@DHLA$_{140}$, and Au@DHLA$_{222}$), Au@DHLA NP with the highest ligand surface density exhibit the best colloidal stability under *in vitro* physiological conditions. The superior stability of Au@DHLA$_{140}$ and Au@DHLA$_{222}$ NP in saline medium results from the combined effects of (*i*) the tight binding offered by the bidentate dithiol group of DHLA on AuNP surfaces, and (*ii*) the more homogeneous surface coverage of AuNP provided by high [DHLA]/[Au] ratios. Finally, Au@DHLA$_{222}$ showed the best inertia towards a free radical and albumin, thus it becomes an ideal candidate for further biomedical application.

Acknowledgements

Authors gratefully acknowledge Dr Lavinia Balan (IS2M, LRC 7228, Université de Haute Alsace, Mulhouse, France) for TEM measurements and Debora Gościk (Poznan University of Medical Sciences, Poznan) for technical assistance during stability studies.

Notes

The authors declare no competing financial interest.

References

(1) De, M.; Ghosh, P. S.; Rotello, V. M. *Adv. Mater.* **2008,** *20*, 4225-4241.
(2) Rosi, N. L.; Mirkin, C. A. *Chem. Rev.* **2005,** *105*, 1547-1562.
(3) Alivisatos, P. *Nat. Biotechnol.* **2004,** *22*, 47-52.
(4) Haes, A. J.; Hall, W. P.; Chang, L.; Klein, W. L.; Van Duyne, R. P. *Nano Lett.* **2004,** *4*, 1029.
(5) Boisselier, E.; Astruc, D. *Chem. Soc. Rev.* **2009,** *38*, 1759-1782.
(6) Warsi, M. F.; Adams, R. W.; Duckett, S. B.; Chechik, V. *Chem. Commun.* **2010,** *46*, 451-453.
(7) Gupta, A. K.; Gupta, M. *Biomaterials* **2005,** *26*, 3995-4021.
(8) Joshi, P.; Chakraborty, S.; Dey, S.; Shanker, V.; Ansari, Z. A.; Singh, S. P.; Chakrabarti, P. *J. Colloid Interface Sci.* **2011,** *355*, 402-409.
(9) Paciotti, G. F.; Kingston, D. G. I.; Tamarkin, L. *Drug. Dev. Res.* **2006,** *67*, 47-54.
(10) Rao, C. N. R.; Mèuller, A.; Cheetham, A. K., *The chemistry of nanomaterials : synthesis, properties and applications in 2 volumes*. Weinheim: Wiley-VCH: Allemagne, 2004.
(11) Templeton, A. C.; Wuelfing, W. P.; Murray, R. W. *Acc. Chem. Res.* **2000,** *33*, 27-36.
(12) Turkevich, J.; Stevenson, P. C.; Hillier, J. *Discuss. Faraday Soc.* **1951,** *11*, 55-75.
(13) Kimling, J.; Maier, M.; Okenve, B.; Kotaidis, V.; Ballot, H.; Plech, A. *J. Phys. Chem. B* **2006,** *110*, 15700-15707.
(14) Brown, K. R.; Walter, D. G.; Natan, M. J. *Chem. Mater.* **1999,** *12*, 306-313.
(15) Brust, M.; Walker, M.; Bethell, D.; Schiffrin, D. J.; Whyman, R. *J. Chem. Soc. Chem. Comm.* **1994**, 801-802.
(16) Jans, H.; Stakenborg, T.; Jans, K.; de Broek, B. V.; Peeters, S.; Bonroy, K.; Lagae, L.; Borghs, G.; Maes, G. *Nanotechnology* **2010,** *21*, 285608-285616.
(17) Roux, S.; Garcia, B.; Bridot, J.-L.; Salomé, M.; Marquette, C.; Lemelle, L.; Gillet, P.; Blum, L.; Perriat, P.; Tillement, O. *Langmuir* **2005,** *21*, 2526-2536.
(18) Biswas, M.; Dinda, E.; Rashid, M. H.; Mandal, T. K. *J. Colloid Interf. Sci.* **2012,** *368*, 77-85.
(19) Mattoussi, H.; Mauro, J. M.; Goldman, E. R.; Anderson, G. P.; Sundar, V. C.; Mikulec, F. V.; Bawendi, M. G. *J. Am. Chem. Soc.* **2000,** *122*, 12142-12150.
(20) Stewart, M. H.; Susumu, K.; Mei, B. C.; Medintz, I. L.; Delehanty, J. B.; Blanco-Canosa, J. B.; Dawson, P. E.; Mattoussi, H. *J. Am. Chem. Soc.* **2010,** *132*, 9804-9813.
(21) Aldeek, F.; Mustin, C.; Balan, L.; Roques-Carmes, T.; Fontaine-Aupart, M. P.; Schneider, R. *Biomaterials* **2011,** *32*, 5459-5470.
(22) Kim, T.; Lee, C. H.; Joo, S. W.; Lee, K. *J. Colloid. Interface Sci.* **2008,** *318*, 238-243.
(23) Kim, T.; Lee, K.; Gong, M. S.; Joo, S. W. *Langmuir* **2005,** *21*, 9524-9528.
(24) Balasubramanian, S. K.; Yang, L.; Yung, L.-Y. L.; Ong, C.-N.; Ong, W.-Y.; Yu, L. E. *Biomaterials* **2010,** *31*, 9023-9030.
(25) Chompoosor, A.; Han, G.; Rotello, V. M. *Bioconjugate Chem.* **2008,** *19*, 1342-1345.
(26) Zhang, F.; Skoda, M. W. A.; Jacobs, R. M. J.; Zorn, S.; Martin, R. A.; Martin, C. M.; Clark, G. F.; Goerigk, G.; Schreiber, F. *J. Phys. Chem. A* **2007,** *111*, 12229-12237.
(27) Zhu, T.; Vasilev, K.; Kreiter, M.; Mittler, S.; Knoll, W. *Langmuir* **2003,** *19*, 9518-9525.
(28) Gofberg, I.; Mandler, D. *J. Nanopart Res.* **2010,** *12*, 1807 1811.
(29) Bogliotti, N.; Oberleitner, B.; Di-Cicco, A.; Schmidt, F.; Florent, J. C.; Semetey, V. J. *Colloid Interf. Sci.* **2011,** *357*, 75-81.
(30) Zhang, G.; Yang, Z.; Lu, W.; Zhang, R.; Huang, Q.; Tian, M.; Li, L.; Liang, D.; Li, C. *Biomaterials* **2009,** *30*, 1928-1936.
(31) Li, Z.; Jin, R.; Mirkin, C. A.; Letsinger, R. L. *Nucleic Acids Res.* **2002,** *30*, 1558-62.

(32) Moini, H.; Packer, L.; Saris, N. E. L. *Toxicol. Appl. Pharm.* **2002,** *182*, 84-90.
(33) Leroy, P.; Sapin-Minet, A.; Pitarch, A.; Boudier, A.; Tournebize, J.; Schneider, R. *Nitric Oxide-Biol. Chem.* **2011,** *25*, 54-56.
(34) Tournebize, J.; Sapin-Minet, A.; Schneider, R.; Boudier, A.; Maincent, P.; Leroy, P. *Talanta* **2011,** *83*, 1780-1783.
(35) Lewis, D. J.; Day, T. M.; MacPherson, J. V.; Pikramenou, Z. *Chem. Comm.* **2006,** *13*, 1433-1435.
(36) Re, R.; Pellegrini, N.; Proteggente, A.; Pannala, A.; Yang, M.; Rice-Evans, C. *Free Radic. Biol. Med.* **1999,** *26*, 1231-1237.
(37) Pramanik, S.; Banerjee, P.; Sarkar, A.; Bhattacharya, S. C. *J. Lumin.* **2008,** *128*, 1969-1974.
(38) Möller, M.; Denicola, A. *Biochem. Mol. Biol. Educ.* **2002,** *30*, 175-178.
(39) Vargas, M. C.; Giannozzi, P.; Selloni, A.; Scoles, G. *J. Phys. Chem. B* **2001,** *105*, 9509-9513.
(40) Vance, A. L.; Willey, T. M.; Nelson, A. J.; van Buuren, T.; Bostedt, C.; Terminello, L. J.; Fox, G. A.; Engelhard, M.; Baer, D. *Langmuir* **2002,** *18*, 8123-8128.
(41) Link, S.; El-Sayed, M. A. *J. Phys. Chem. B* **1999,** *103*, 4212-4217.
(42) Mei, B. C.; Oh, E.; Susumu, K.; Farrell, D.; Mountziaris, T. J.; Mattoussi, H. *Langmuir* **2009,** *25*, 10604-10611.
(43) Oh, E.; Susumu, K.; Goswami, R.; Mattoussi, H. *Langmuir* **2010,** *26*, 7604-7613.
(44) Qiao, F. Y.; Liu, J.; Li, F. R.; Kong, X. L.; Zhang, H. L.; Zhou, H. X. *Appl. Surf. Sci.* **2008,** *254*, 2941-2946.
(45) Kim, J.-Y.; Lee, J.-S. *Nano Lett.* **2009,** *9*, 4564-4569.
(46) Isono, R.; Yoshimura, T.; Esumi, K. *J. Colloid Interf. Sci.* **2005,** *288*, 177-83.
(47) Nie, Z.; Liu, K. J.; Zhong, C. J.; Wang, L. F.; Yang, Y.; Tian, Q.; Liu, Y. *Free Radic. Biol. Med.* **2007,** *43*, 1243-54.
(48) Boudier, A.; Tournebize, J.; Bartosz, G.; El Hani, S.; Bengueddour, R.; Sapin-Minet, A.; Leroy, P. *Anal. Chim. Acta* **2012,** *711*, 97-106.
(49) Candiano, G.; Petretto, A.; Bruschi, M.; Santucci, L.; Dimuccio, V.; Prunotto, M.; Gusmano, R.; Urbani, A.; Ghiggeri, G. M. *J. Proteomics* **2009,** *73*, 188-195.
(50) Chakraborty, S.; Joshi, P.; Shanker, V.; Ansari, Z. A.; Singh, S. P.; Chakrabarti, P. *Langmuir* **2011,** *27*, 7722-7731.
(51) Brewer, S. H.; Glomm, W. R.; Johnson, M. C.; Knag, M. K.; Franzen, S. *Langmuir* **2005,** *21*, 9303-9307.
(52) Chithrani, B. D.; Ghazani, A. A.; Chan, W. C. W. *Nano Lett.* **2006,** *6*, 662-668.
(53) Owens III, D. E.; Peppas, N. A. *Int. J. Pharmaceut.* **2006,** *307*, 93-102.

Talanta 83 (2011) 1780–1783

Contents lists available at ScienceDirect

Talanta

journal homepage: www.elsevier.com/locate/talanta

Short communication

Simple spectrophotocolorimetric method for quantitative determination of gold in nanoparticles

Juliana Tournebize[a], Anne Sapin-Minet[a], Raphaël Schneider[b], Ariane Boudier[a], Philippe Maincent[a], Pierre Leroy[a,*]

[a] EA 3452 Cibles thérapeutiques, formulation et expertise précliniqe du médicament, Faculty of Pharmacy, Nancy-University, BP 80403, 54001 Nancy Cedex, France
[b] Laboratoire Réactions et Génie des Procédés, UPR 3349, Nancy-University, CNRS, 1, rue Grandville, BP 20451, 54001 Nancy Cedex, France

ARTICLE INFO

Article history:
Received 22 June 2010
Received in revised form
24 November 2010
Accepted 5 December 2010
Available online 13 December 2010

Keywords:
Gold nanoparticles
Bromine oxidation
Rhodamine B
Ion-pair colorimetric method

ABSTRACT

A simple spectrophotocolorimetric method devoted to the measurement of gold content in nanoparticles (NPs) was developed. It includes two steps: (i) metal gold NPs (Au NPs) are oxidized into the $AuCl_4^-$ anion using a 5×10^{-2} M HCl–1.5×10^{-2} M NaCl–7×10^{-4} M Br_2 solution, next (ii) $AuCl_4^-$ concentration is measured using a spectrophotometric assay based on the reaction of $AuCl_4^-$ with the cationic form of Rhodamine B to give a violet ion pair complex. This latter is extracted with diisopropyl ether and the absorbance of the organic complex is measured at 565 nm. The method is linear in the range 6–29 μM of $AuCl_4^-$ with a limit of detection of 4.5 μM.

The analytical method was optimized with respect of bromine excess to obtain complete Au NPs oxidation. The method was applied to two types of Au NPs currently under investigation: citrate-stabilized Au NPs and Au NPs capped with dihydrolipoic acid (Au@DHLA). Both the gold content of Au NPs and the concentration of NPs (using NP diameter measured by transmission electron microscopy) have been calculated.

1. Introduction

Bulk gold is one of the most noble of all the metals, being unreactive to oxygen, sulphur, concentrated acids or bases even at elevated temperatures. However, gold reacts readily with halogens and dissolves in solutions containing or generating chlorine such as aqua regia to form tetrachloroauric acid ($HAuCl_4$). The preparation of biologically active gold (oxidation states: +I and +III) species for the treatment of diseases including rheumatoid arthritis and various cancers has been reported earlier [1]. Mild reduction of $AuCl_4^-$ solutions by various reducing agents such as sodium citrate or sodium borohydride gives highly coloured solutions containing gold NPs (Au NPs) [2]. The ease of synthesizing Au NPs and their affinity for binding many compounds make them attractive candidates as carriers for the delivery of various biologically active molecules such as proteins, DNA, RNA, drugs and antioxidants. Gold NPs became the most intensively studied nanosized materials and their potential for application in a wide spectrum of areas that include biology and medicine has been reviewed [2–8].

Among the numerous parameters needed for the full characterization of Au NPs (physical and hydrodynamic diameter, morphology, surface functionalization, zeta potential, ...), determination of their gold content is of main importance [9]. However, there is a lack of simple assays easily available in most laboratories working within this nanotechnological area. The most frequently reported method for the measurement of gold content in NPs needs a hyphenated and expensive technique: inductively coupled plasma associated or not with mass spectrometry or optical emission spectroscopy (ICP, ICP-MS, ICP-OES) [9–11]. The present report concerns the development of a simple and low-cost assay coupling chemical oxidation of gold in NPs and spectrophotocolorimetric measurement of gold; this alternative method was applied to two common kinds of Au NPs-stabilized either with citrate or dihydrolipoic acid.

2. Experimental

2.1. Chemicals

All solvents were of analytic grade and used without further purification. Sodium citrate tribasic dihydrate, tetrachloroauric acid trihydrate ($HAuCl_4 \cdot 3H_2O$), sodium borohydride, α-lipoic acid, Rhodamine B, and bromine were purchased from Sigma–Aldrich (France), diisopropyl ether was obtained from Carlo Erba Reactifs-SDS (France). Phosphate-buffered saline (PBS) solution was prepared as follows: $[Na_2HPO_4] = 4 \times 10^{-2}$ M, $[KH_2PO_4] = 4 \times 10^{-3}$ M,

* Corresponding author. Tel.: +33 3 83 68 23 67; fax: +33 3 83 68 23 01.
E-mail address: pierre.leroy@pharma.uhp-nancy.fr (P. Leroy).

0039-9140/$ – see front matter © 2010 Elsevier B.V. All rights reserved.
doi:10.1016/j.talanta.2010.12.005

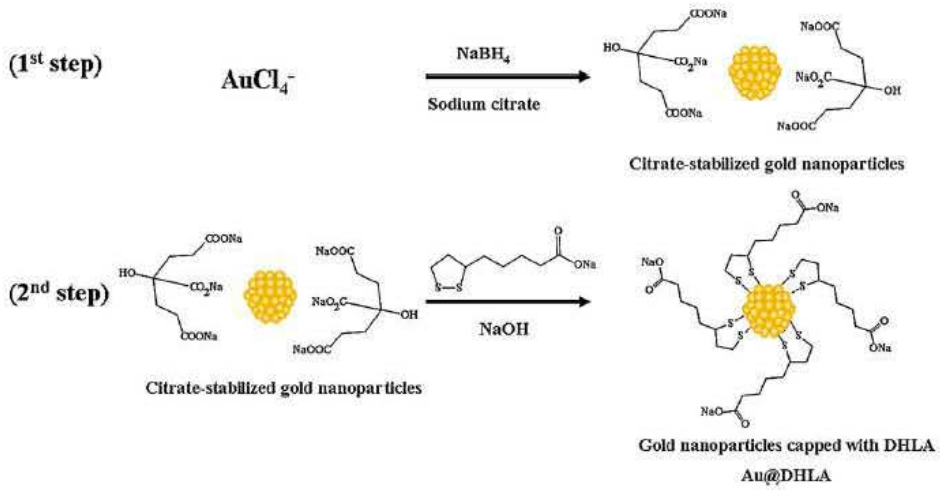

Fig. 1. Schematic representation of synthesis of gold nanoparticles stabilized with citrate (1st step) and capped with dihydrolipoic acid (DHLA) (2nd step).

and [NaCl] = 1×10^{-1} M, final pH was adjusted to 7.4. Ultrapure deionized water (>18.2 MΩ cm^{-1}) was used for all solution preparations. All glassware was cleaned with 37% HCl (w/v) and rinsed thoroughly with ultrapure deionized water prior to use. All handling conditions required to prevent any risk of toxicity and injury during NPs synthesis and oxidation (use of gloves, glasses, fume hood) were taken into consideration.

2.2. Synthesis of citrate-stabilized gold nanoparticles

Gold NPs were prepared as previously reported [12]. Briefly, at room temperature, to 90 mL of H_2O, 1 mL of 1% (w/v) $HAuCl_4 \cdot 3H_2O$ in H_2O was added. After 1 min of stirring, 2.0 mL of a 38.8 mM sodium citrate solution was added. One minute later, 1.0 mL of freshly prepared 0.075% (w/v) $NaBH_4$ in 38.8 mM sodium citrate solution was added. The reaction medium was stirred for an additional 5 min period and the resulting deep red colloidal solution was stored in the dark at 4 °C for a maximum period of 2 months.

2.3. Synthesis of gold nanoparticles capped with dihydrolipoic acid (Au@DHLA NPs)

A 600-μmol portion of α-lipoic acid in 10 mL of NaOH 0.5 M solution was added to 25 mL of freshly prepared citrate-capped Au NPs under stirring at room temperature (20–23 °C). After 24 h, Au NPs capped with dihydrolipoic acid (DHLA), obtained from α-lipoic acid reduction, were dialyzed against PBS for 48 h using a 10 kDa cut-off dialysis bag (Interchim®, France). The dialysis medium was changed once to fresh PBS after 24 h. The resulting Au@DHLA NPs solution was stored in the dark at 4 °C for a maximum period of 2 months.

2.4. Instrumentation

An UV–visible spectrophotometer (model Uvikon 932, Kontron) was used for spectra recordings and absorbance measurements. The transmission electron microscopic (TEM) images were recorded using a Philips CM20 instrument with a LaB_6 cathode operating at 200 kV. Gold NP solutions were deposited onto a 400-mesh carbon film copper grids. The average of gold core diameter was calculated for each Au NPs sample by counting 200 particles from the TEM images.

2.5. Determination of gold content in nanoparticles

One millilitre of Au NPs was mixed with 1 mL of 5×10^{-2} M HCl and 1.5×10^{-2} M NaCl solutions containing Br_2 at a concentration ranging from 1 to 7×10^{-4} M to ensure that the Au NPs oxidation was complete. The mixture was incubated for 20 min at room temperature, next it was placed at 60 °C for 30 min to remove any remaining bromine. Then the colorimetric assay was performed as previously described [13]: 0.5 mL of the solution resulting from the oxidation process, 0.5 mL of water (blank), or 0.5 mL of a standard solution were mixed with 9.5 mL of water, 2.5 mL of 20% (w/v) HCl solution, 5 mL of 30% (w/v) NH_4Cl solution, and 2.5 mL of 0.84×10^{-3} M Rhodamine B solution prepared in water. The result-

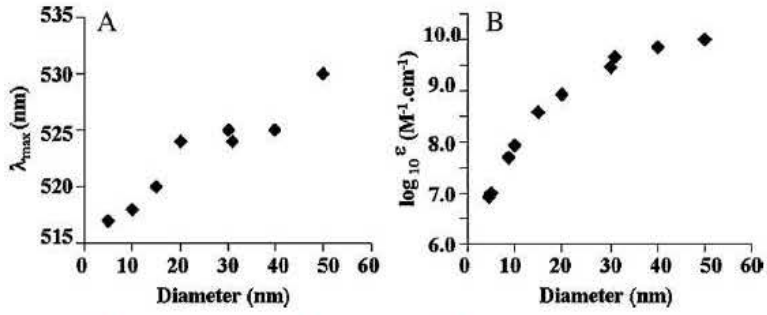

Fig. 2. Variation of λ_{max} (A) and molar absorbance (B) of citrate-stabilized gold nanoparticles as a function of diameter according to data literature [14,18–21].

ing mixture was shaken for 30 s with 5 mL of diisopropyl ether. The organic phase was separated and its absorbance was measured at 565 nm using 1-cm path glass cuvettes.

Calibration curve was operated using a series of dilutions of the $HAuCl_4 \cdot 3H_2O$ stock solution (1 mg mL^{-1}; 3 mM) prepared in water, in the range 60–290 μM.

2.6. Calculation

The number of gold atoms per AuNP (n_{atom}) was determined using the average size of the particle determined by TEM. Assuming a spherical shape and a face-centered cubic AuNP structure (fcc) [11,14,15], n_{atom} for each type of Au NPs was calculated using Eq. (1), where N_A is the Avogadro number (6.022×10^{23}), ρ is the density for fcc gold (19.3 g cm^{-3}), D is the diameter of the Au NPs in cm, and M stands for atomic mass of gold (197 g mol^{-1}):

$$n_{atom} = \frac{N_A \pi \rho D^3}{6M} \quad (1)$$

The number of NPs per liter (nAuNPs) was calculated according to Eq. (2), where $CAuCl_4^-$ corresponds to the result of colorimetric determination:

$$nAuNPs = \frac{CAuCl_4^- \times N_A}{n_{atom}} \quad (2)$$

This concentration was then divided by Avogadro number to get the final molar concentration of Au NPs, i.e. CAuNPs.

The molar absorbance ε of each type of Au NPs was determined according to Lambert–Beer law (Eq. (3)) where A is the Au NPs maximum absorbance at λ_{max}, l is the path length, and CAuNPs is the Au NPs concentration (M):

$$A = \varepsilon \times l \times CAuNPs \quad (3)$$

3. Results and discussion

Citrate-stabilized Au NPs were prepared by reduction of $AuCl_4^-$ using sodium borohydride in the presence of citrate ions [12,16]. The citrate-capped Au NPs were further functionalized with dihydrolipoic acid (DHLA), obtained from α-lipoic acid reduction, using a [DHLA]/[Au] ratio of 222/1 to yield water soluble Au NPs capped with DHLA (Au@DHLA) (Fig. 1). The NPs stabilized by DHLA offer better stability than citrate-stabilized Au NPs and can be coupled to biomolecules to obtain new delivery platforms [17].

Accurate determination of the concentration of NPs is essential to fully characterize the prepared solutions. Besides, quantifying the amount of gold reduced during the synthesis of Au NPs is also important to evaluate the stability of these materials [11]. Since Au NPs have strong plasmon absorption bands in the visible domain, the use of their molar absorbances should be the easiest way to estimate Au NPs concentrations. Several authors estimated the size and concentration of Au NPs by their UV–vis absorbance spectra, mainly focusing on the position of the λ_{max} and molar absorbance, respectively (Fig. 2A and B) [14,18–21]. Although increase of core diameter of Au NPs introduces continuous increase of molar absorbance (Fig. 2B), the estimation of the diameter using λ_{max} is imprecise. When the Au NPs diameter increases from ca. 5 to 50 nm, a narrow and imprecise bathochromic shift of λ_{max} from ca. 517 to 534 nm is observed [14,19,20]. The position of λ_{max} cannot therefore be used as a conclusive and accurate diagnostic for determining the diameter and the concentration of NPs (Fig. 2A). Thus, in most cases, this approach gives unreliable results because the position of the plasmon resonance is affected by multiple factors, like environment dielectric properties, physical or chemical interactions on particles surface, surface charge, interparticle distance, and aggregation [2].

The accurate and simple quantification of gold contained into Au NPs is still a challenge. In the present work, a spectrophotocolorimetric assay is reported as an interesting low-cost alternative to more hyphenated techniques [9–11]. It permits calculation of gold content in Au NPs, yield of NPs obtained after each synthesis step, and accurate concentration of NPs (using NP diameter measured by TEM).

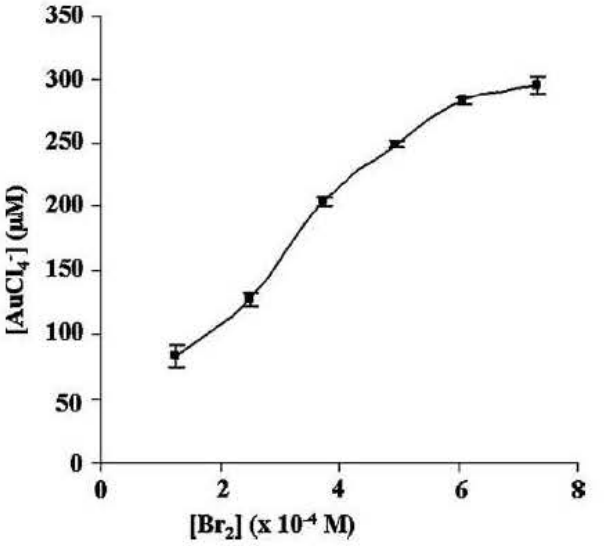

Fig. 3. Effect of bromine concentration on conversion of gold nanoparticles into the anionic species $AuCl_4^-$ (each point is the mean ± standard deviation of three independent measurements).

3.1. Optimization of bromine oxidation

A HCl–NaCl–Br_2 solution, which proved to be more efficient than other solutions such as HNO_3–HCl, NaCl–Br_2, HCl–NaCl or HCl–Br_2 solutions [21–25], was selected to oxidize gold NPs into $AuCl_4^-$. Further studies were carried in order to optimize the concentration of Br_2 required for complete conversion (Fig. 3). Using citrate-capped Au NPs, a plateau was obtained at concentrations higher than 6×10^{-4} M and the retained Br_2 concentration was 7×10^{-4} M. The complete dissolution of Au NPs was also verified by the full disappearance of surface plasmon resonance peak observed at around 520 nm (Fig. 4). Similar data were obtained using Au@DHLA NPs (data not shown). Full recovery of an $AuCl_4^-$ solution treated with bromine solution was observed (105 ± 5%, n = 6), confirming the accuracy of the present assay.

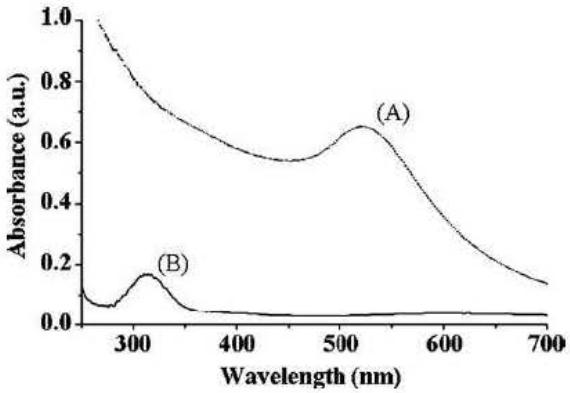

Fig. 4. UV–visible spectra of citrate-stabilized gold nanoparticles before (A) and after (B) oxidative treatment using the optimized bromine/chloride solution (5×10^{-2} M HCl–1.5×10^{-2} M NaCl–7×10^{-4} M Br_2).

Table 1
Different characteristics of synthetized gold nanoparticles (values are expressed as mean ± standard deviation of *n* independent measurements).

	Citrate-stabilized Au NPs	Au@DHLA
Diameter (nm) ($n=200$)	5.3 ± 1.1	3.5 ± 1.0
$CAuCl_4^-$ (μM) ($n=3$)	304 ± 13	116 ± 7
Yield (%) ($n=3$)	104 ± 5	56 ± 3
Number of NPs per liter (nAuNPs) ($n=3$)	$(4.0 \pm 0.2) \times 10^{16}$	$(5.0 \pm 0.3) \times 10^{16}$
CAuNPs (nM) ($n=3$)	66 ± 3	85 ± 5
ε ($M^{-1}\,cm^{-1}$) ($n=3$)	$(1.2 \pm 0.1) \times 10^7$	$(0.5 \pm 0.2) \times 10^7$

3.2. Method validation

Operating conditions previously reported [13,21], especially HCl concentration on which the intensity of the ion-pair colour is very dependent, were strictly observed. The linearity of the method was checked in the 6–29 μM (concentrations expressed in organic layer where absorbance is read) range and the corresponding equation of the regression line was: $A_{565\,nm} = 0.0569\,[AuCl_4^-] \pm 0.0017 - 0.2085 \pm 0.0439$; coefficient of determination, $r^2 = 0.9992$ (6 points, $n=4$). The inter-assay precision was determined using six different citrate-stabilized Au NPs batches: the value obtained was equal to 301 ± 7 μM.

The limit of detection (LOD) was calculated as follows [11]:

LOD = 3 sa0 (sa0: standard deviation of blank solution) ($A_{blank} = 0.041 \pm 0.016$, $n=6$, inter-day measurements). The value found for LOD was 4.5 μM, providing enough sensitivity for measuring gold content in different synthesized batches of Au NPs. LOD of the present assay at the micromolar level is 10,000-fold higher than LOD value obtained when using ICP-MS [10]. The main advantage of ICP-MS remains very low sample volume. Nonetheless, the present method represents an easy to use alternative that can become a routine protocol in a laboratory.

Otherwise, cetyltrimethylammonium bromide (CTAB) is frequently used as capping reagent of Au NPs [26] and its potential interference was presently tested with the colorimetric method. This hydrophobic cationic species could interfere during ion-pairing formation between $AuCl_4^-$ and the cationic form of Rhodamine B. We added CTAB in the protocol at two concentration levels, 200 and 1000 μM, corresponding to a [CTAB]/[$AuCl_4^-$] ratio of 1× and 5×, and we observed no interference.

3.3. Quantification of Au NPs

It is generally assumed that the reduction of $AuCl_4^-$ by $NaBH_4$ in the presence of citrate ions is complete [11,14,19]. As can be seen in Table 1, the gold concentration in citrate-stabilized Au NPs is 304 ± 13 μM, and it is consistent with the initial gold concentration used in the synthesis (292 μM), thus confirming the accuracy of this method. Indeed, the measured concentration of citrate-stabilized Au NPs is in line with what has been reported by others authors [12,14,20]. For example, the molar absorbance value for 5.3 nm diameter citrate-stabilized NPs obtained in this study is $1.2 \times 10^7\ M^{-1}\,cm^{-1}$, and similar NPs (diameter = 5.0 nm) described by Pellegrino et al. is $1 \times 10^7\ M^{-1}\,cm^{-1}$ [20].

From Table 1, another important result to notice is that the increase in core diameter of Au NPs introduces decrease of Au NPs concentration and increase in the molar absorbance of Au NPs, the same tendencies were previously observed [7,14].

4. Conclusion

In the routine laboratory practice, it would be desirable to have a simple, fast, and low-cost method for rapid monitoring of the NPs concentration during all preparative stages. The present spectrophotocolorimetric assay meets these goals and could be easily applied to all types of Au NPs varying by capping ligands or active molecules attached to their surface.

Acknowledgement

Authors gratefully acknowledge Dr Lavinia BALAN (IS2M, LRC 7228, Université de Haute Alsace, Mulhouse, France) for realizing TEM measurements.

References

[1] C.J. Murphy, A.M. Gole, J.W. Stone, P.N. Sisco, A.M. Alkilany, E.C. Goldsmith, S.C. Baxter, Acc. Chem. Res. 41 (2008) 1721–1730.
[2] M.C. Daniel, D. Astruc, Chem. Rev. 104 (2004) 293–346.
[3] D. Astruc, M.C. Daniel, J. Ruiz, Chem. Commun. 23 (2004) 2637–2649.
[4] D. Pissuwan, T. Niidome, M.B. Cortie, J. Control. Release, in press.
[5] C.-K. Kim, P. Ghosh, V.M. Rotello, Nanoscale 1 (2009) 61–67.
[6] H.M. Joshi, D.R. Bhumkar, K. Joshi, V. Pokharkar, M. Sastry, Langmuir 22 (2006) 300–305.
[7] B. Duncan, C. Kim, V.M. Rotello, J. Control. Release 148 (2010) 122–127.
[8] P. Ghosh, G. Han, M. De, C.K. Kim, V.M. Rotello, Adv. Drug Deliv. Rev. 60 (2008) 1307–1315.
[9] L. Yu, A. Andriola, Talanta 82 (2010) 869–875.
[10] A. Scheffer, C. Engelhard, M. Sperling, W. Buscher, Anal. Bioanal. Chem. 390 (2008) 249–252.
[11] R. Allabashi, W. Stach, A. de la Escosura-Muñiz, L. Liste-Calleja, A. Merkoçi, J. Nanoparticle Res. 11 (2009) 2003–2011.
[12] K.R. Brown, D.G. Walter, M.J. Natan, Chem. Mater. 12 (1999) 306–313.
[13] B.J. Macnulty, L.D. Wollard, Anal. Chim. Acta 13 (1955) 154–158.
[14] X. Liu, M. Atwater, J. Wang, Q. Huo, Colloids Surf. B Biointerfaces 58 (2007) 3–7.
[15] J.H. Lin, C.W. Chang, W.L. Tseng, Analyst 135 (2010) 104–110.
[16] J.M. Abad, S.F. Mertens, M. Pita, V.M. Fernandez, D.J. Schiffrin, J. Am. Chem. Soc. 127 (2005) 5689–5694.
[17] S. Roux, B. Garcia, J.L. Bridot, M. Salome, C. Marquette, L. Lemelle, P. Gillet, L. Blum, P. Perriat, O. Tillement, Langmuir 21 (2005) 2526–2536.
[18] P.K. Jain, K.S. Lee, I.H. El-Sayed, M.A. El-Sayed, J. Phys. Chem. B 110 (2006) 7238–7248.
[19] R.C. Mucic, J.J. Storhoff, C.A. Mirkin, R.L. Letsinger, J. Am. Chem. Soc. 120 (1998) 12674–12675.
[20] T. Pellegrino, R.A. Sperling, A.P. Alivisatos, W.J. Parak, J. Biomed. Biotechnol. 2007 (2007) 26796–26805.
[21] D. Hu, H. Han, R. Zhou, F. Dong, W. Bei, F. Jia, H. Chen, Analyst 133 (2008) 768–773.
[22] M.T. van Meersbergen, L. Lorenzen, J.S.J. van Deventer, Miner. Eng. 6 (1993) 1067–1079.
[23] A. Pal, J. Photochem. Photobiol. Chem. 142 (2001) 59–65.
[24] M.S. El-Shahawi, A.S. Bashammakh, S.O. Bahaffi, Talanta 72 (2007) 1494–1499.
[25] J. Zheng, W. Huang, S. Chen, Z. Niu, Z. Li, Electrochem. Commun. 8 (2006) 600–604.
[26] M.A. Sobhan, M.J. Withford, E.M. Goldys, Langmuir 26 (2010) 3156–3159.

II.1.2.1 Résultats complémentaires de la publication n°3

La méthode analytique utilisée pour le dosage de l'or contenu dans les NP et présentée dans l'article "Simple spectrophotocolorimetric method for quantitative determination of gold in nanoparticles" est simple, reproductible, peu coûteuse et rapide; elle permet de calculer le rendement de la synthèse des NP d'or, leur concentration et absorbance molaires. Néanmoins, la méthode que nous avons développée ici n'est pas une méthode de référence ou usuelle pour ce type d'application. C'est pourquoi nous avons cherché à comparer les résultats obtenus par cette méthode avec ceux résultant de la technique la plus utilisée pour le dosage des éléments métalliques (incluant l'or), *i.e.* la spectrométrie de masse à source plasma à couplage inductif (*Inductively coupled plasma mass spectrometry* - ICP-MS). Cependant, il est important de souligner que cette technique est très complexe à mettre en œuvre notamment en termes de préparation de l'échantillon et d'équipement (l'appareillage ICP-MS n'est pas disponible dans tous les laboratoires et la sous-traitance par un laboratoire qui en est doté est fréquemment nécessaire), le coût de la mesure est donc important. De ce fait, une fois démontrée l'équivalence des résultats obtenus par les deux techniques, ICP-MS (méthode de référence) et spectrophotocolorimétrie (méthode optimisée décrite dans l'article 3), le calcul de la concentration et de l'absorbance molaires des NP d'or sera réalisé en routine par cette dernière méthode, plus facile à mettre en œuvre.

II.1.2.1.1 Conditions opératoires

Les particules testées correspondent aux NP stabilisées par les ions citrate et les NP recouvertes de DHLA (Au@DHLA$_{222}$), synthétisées de la même manière que celle décrites prédédemment. Pour l'analyse par ICP-MS, les échantillons ont été dilués dans l'eau régale (mélange HCl + HNO_3 3 :1, V/V) et analysés au moyen d'un appareil ICP-MS Agilent série 7500cx (De Duve Institute; Catholic University of Leuven, Belgium). La droite d'étalonnage réalisée avec des étalons d'un sel d'or ($HAuCl_4$, Merck) est comprise entre 0,05 et 25 µM. La limite de détection de la méthode est de 0,015 µM.

II.1.2.1.2 Résultats et discussion

Comme le montre le tableau 5, la concentration de l'or dans les NP d'or stabilisées par les ions citrate et les NP Au@DHLA$_{222}$ déterminée par la technique ICP-MS est cohérente avec la concentration de l'or obtenue par la méthode colorimétrique, confirmant ainsi l'exactitude de cette dernière technique et son utilisation possible en routine.

Tableau 5. Détermination de la concentration molaire de l'or dans les NP d'or stabilisées par des ions citrate et les NP Au@DHLA$_{222}$ par colorimétrie et par ICP-MS.

Types de nanoparticules	Méthode spectrophotocolorimétrique (n = 3)	ICP-MS (n = 1)
[$AuCl_4^-$] pour les NP d'or stabilisées par des ions citrate (µM)	46 ± 3	42
[$AuCl_4^-$] pour les NP Au@DHLA$_{222}$ (µM)	13 ± 2	14

Nous avons ainsi appliqué la technique colorimétrique pour mesurer la concentration ainsi que l'absorbance molaire de l'ensemble des NP d'or (*i.e.* NP d'or stabilisées par des ions citrate, Au@DHLA$_{28,}$ Au@DHLA$_{56,}$ Au@DHLA$_{140}$ et Au@DHLA$_{222}$) juste après leur synthèse (j < 5). Comme le montre le tableau 6, la fonctionnalisation des NP d'or par le DHLA réduit de trois fois l'absorbance molaire des NP d'or. De plus, nous avons montré que la densité de couverture par le DHLA améliore le rendement de la synthèse et augmente la reproductibilité de la synthèse. En effet, les NP Au@DHLA$_{28}$ ont un rendement de synthèse faible et très varié (53 % ± 29), en comparaison avec les NP plus couvertes par le DHLA (*i.e* NP Au@DHLA$_{56}$ = 78 % ± 19 ; Au@DHLA$_{140}$ = 77 % ± 15 ; Au@DHLA$_{222}$ = 82 % ± 19)

Tableau 6. Détermination par la méthode spectrophotocolorimétrique, après synthèse (j < 5), de la concentration molaire de l'or (µM) dans les NP d'or stabilisées par les ions citrate et par l'acide dihydrolipoïque (DHLA) et de leur absorbance molaire ($M^{-1}.cm^{-1}$) (n expériences indépendantes).

Méthode spectrophotocolorimétrique		
Type de nanoparticules	**[$AuCl_4^-$] (n = 5) (µM)**	**Absorbance molaire (n = 5) ($M^{-1}.cm^{-1}$)**
NP d'or stabilisée par des ions citrate	345 ± 47	(1,20 ± 0,10) × 10^{+7}
Au@DHLA$_{28}$ NP	206 ± 68*	(0,43 ± 0,10) × 10^{+7}*
Au@DHLA$_{56}$ NP	236 ± 46	(0,43 ± 0,10) × 10^{+7}
Au@DHLA$_{140}$ NP	220 ± 40	(0,42 ± 0,10) × 10^{+7}
Au@DHLA$_{222}$ NP	202 ± 33	(0,40 ± 0,20) × 10^{+7}

* (n = 3)

Analytica Chimica Acta 711 (2012) 97–106

Contents lists available at SciVerse ScienceDirect

Analytica Chimica Acta

journal homepage: www.elsevier.com/locate/aca

High-performance liquid chromatographic method to evaluate the hydrogen atom transfer during reaction between 1,1-diphenyl-2-picryl-hydrazyl radical and antioxidants

Ariane Boudier[a], Juliana Tournebize[a], Grzegorz Bartosz[b,1], Safae El Hani[c], Rachid Bengueddour[c], Anne Sapin-Minet[a], Pierre Leroy[a,*]

[a] CITHEFOR - EA 3452, Faculté de Pharmacie, Nancy-Université, 5 Rue Albert Lebrun, BP 80403, 54001 Nancy Cedex, France
[b] Department of Molecular Biophysics, University of Lodz, Lodz, Poland
[c] Laboratoire de Nutrition et Santé, Biology Department, Faculty of Sciences, Ibn Tofail University, Kenitra, Morocco

ARTICLE INFO

Article history:
Received 27 July 2011
Received in revised form 24 October 2011
Accepted 30 October 2011
Available online 9 November 2011

Keywords:
1,1-Diphenyl-2-picrylhydrazyl
1,1-Diphenyl-2-picrylhydrazine
HPLC
Antioxidants
Complex matrices
Nanoparticles

ABSTRACT

1,1-Diphenyl-2-picrylhydrazyl (DPPH•) is a stable nitrogen centred radical widely used to evaluate direct radical scavenging properties of various synthetic or natural antioxidants (AOs). The bleaching rate of DPPH• absorbance at 515 nm is usually monitored for this purpose. In order to avoid the interference of complex coloured natural products used as antioxidant supplements or cosmetics, HPLC systems have been reported as alternative techniques to spectrophotometry. They also rely upon measurement of DPPH• quenching rate and none of them permits to identify and measure 1,1-diphenyl-2-picryl-hydrazine (DPPH-H), the reduced product of DPPH• resulting from hydrogen atom transfer (HAT), which is the main mechanism of the reaction between DPPH• and AOs. We presently report an HPLC method devoted to the simultaneous measurement of DPPH• and DPPH-H. Both were fully separated on a C18 column eluted with acetonitrile–10 mM ammonium citrate buffer pH 6.8 (70:30, v/v) and detected at 330 nm. Adsorption process of DPPH• onto materials of the HPLC system was pointed out. Consequently, the linearity range observed for DPPH• was restricted, thus a much lower limit of detection was obtained for DPPH-H than for DPPH• using standards (0.02 and 14 μM, respectively). The method was applied to three commonly used AOs, *i.e.* Trolox®, ascorbic acid and GSH, and compared with spectrophotometry. Further application to complex matrices (cell culture media, vegetal extracts) and nanomaterials demonstrated (i) its usefulness because of higher selectivity than colorimetry, and (ii) its help to investigate the mechanisms occurring with the free radical.

1. Introduction

Antioxidant supplementation through the use of nutraceuticals has been stimulated over the last two decades, by observations that free radicals are involved in many pathophysiological conditions [1]. Numerous chemical assays have been reported to estimate antioxidant capacities of pure chemicals and natural products, including 2,2-azinobis(3-ethyl-benzothiazoline-6-sulfonic acid) (ABTS), 1,1-diphenyl-2-picrylhydrazyl radical (DPPH•) decolorization assay, ferric reducing antioxidant power (FRAP), and oxygen radical absorption capacity (ORAC) [2–5]. DPPH• has been extensively used for this purpose. It is a stable nitrogen centred radical (Fig. 1) discovered by Goldsmith and Renn in 1922 [6], and later introduced to evaluate direct radical scavenging properties of antioxidants (AOs) [7]. DPPH• exhibits an absorption band at 515 nm ($\varepsilon = 12.5\ mM^{-1}\ cm^{-1}$) and its bleaching rate is monitored in the presence of various synthetic or natural AOs. The results may be expressed either as the percentage of remaining DPPH• or as Trolox® Equivalent Antioxidant Capacity [8].

From the mechanistic point of view, AOs can quench DPPH• by: hydrogen atom transfer (HAT) (Eq. (1)), single electron transfer (SET) (Eq. (2)) [8], or sequential proton loss electron transfer (SPLET) [9,10] (Eq. (3)), as follows:

$$DPPH^{\bullet} + AH \rightarrow DPPH - H + A^{\bullet} \quad (Eq.\ (1)) \qquad (HAT)$$

$$\begin{pmatrix} DPPH^{\bullet} + AH \rightarrow DPPH^{-} + AH^{+\bullet} & (Eq.\ (2.1)) \\ AH^{+\bullet} \rightarrow AH^{\bullet} + H^{+} & (Eq.\ (2.2)) \\ DPPH^{-} + H^{+} \rightarrow DPPH - H & (Eq.\ (2.3)) \end{pmatrix} \qquad (SET)$$

* Corresponding author. Tel.: +33 3 83 68 23 77; fax: +33 3 83 68 23 01.
E-mail address: pierre.leroy@pharma.uhp-nancy.fr (P. Leroy).
[1] Guest Professor at Nancy-University.

0003-2670/$ – see front matter © 2011 Elsevier B.V. All rights reserved.
doi:10.1016/j.aca.2011.10.063

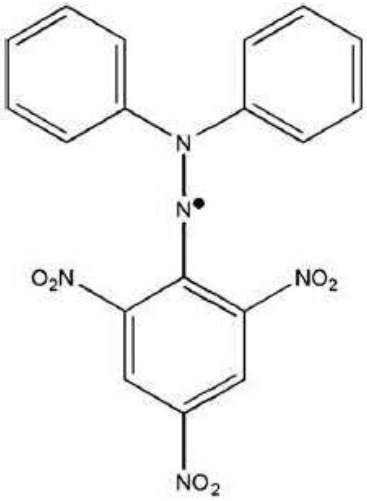

Fig. 1. Structure of 1,1-diphenyl-2-picrylhydrazyl radical (DPPH•).

$$\left(\begin{array}{ll} AH \rightarrow AH^- + H^+ & (Eq.\ (3.1)) \\ AH^- + DPPH^\bullet \rightarrow AH^\bullet + DPPH^- & (Eq.\ (3.2)) \\ DPPH^- + H^+ \rightarrow DPPH - H & (Eq.\ (3.3)) \end{array}\right) \quad (SPLET)$$

As already noted [11], different mechanisms occur according to structure of reagent and reaction medium. In non-aqueous medium, the SET and SPLET mechanisms are predominant due to the capacity of organic solvents to form strong hydrogen bonds with AOs [9,10,12]. However, in aqueous medium, the HAT mechanism prevails. As a conclusion, the net result of all mechanisms is the same, *i.e.* formation of 1,1-diphenyl-2-picrylhydrazine (DPPH-H).

Similar mechanisms are observed in oxidation pathways in which AOs can play a preventive role by scavenging reactive species, thus counteracting oxidative stress. The first is HAT, illustrated in the case of lipid peroxidation involving radical generation and hydroperoxide formation. Another possible mechanism by which AOs can deactivate a free radical is electron transfer, in which the radical cation is first formed followed by rapid and reversible deprotonation in solution.

A wide variety of AOs has been tested by using DPPH•: hydroxylated aromatic compounds like polyphenols [8], flavonoids [13], aniline derivatives [14], indolic compounds [15], thiols [11], and reactive oxygen species [16]. More recently, nanostructures were also evaluated for their potential antioxidant properties by using DPPH• assay: platinum nanoparticles (NPs) [17], Au/TiO_2 NPs [18], silver NPs [19], and gold NPs functionalized with Trolox® [20].

A common problem in the spectrophotometric DPPH• assay is the interference by coloured compounds used as AO supplements or cosmetics, therefore HPLC and electron spin resonance (ESR) systems have been proposed as alternative techniques to the classical colorimetric assay [21–26].

Previously reported DPPH• assays using HPLC rely upon: (i) the measurement of remaining DPPH• in a reversed phase HPLC system after off-line reaction of AOs with the probe [27]; it is claimed that this assay suppresses interferences linked to colours of natural extracts tested [21], (ii) on-line post-column addition of DPPH• in order to separate and identify which fractions or pure compounds in complex extracts exhibit antioxidant activity [25,26,28,29]. This later approach frequently uses another detection mode, such as diode array detection [27] or mass spectrometry [26], in order to identify in complex matrices, the compounds offering a high reactivity for DPPH• [27].

Controversies appeared in literature about the stability of DPPH• [30], the precision of methods based on its quenching rate and problems with the linearity of the HPLC detection of the radical. The corresponding reduced product DPPH-H is more stable than DPPH•, thus the availability of a method relying upon DPPH-H measurement rather than disappearance monitoring of DPPH• would present a major advantage for the accuracy of the DPPH• assay.

In this paper, a simple and rapid HPLC method for the simultaneous measurement of DPPH• and DPPH-H was developed and validated. This method was first applied to the monitoring of HAT mechanism between DPPH• and three commonly used AOs, *i.e.* Trolox® (the water-soluble form of vitamin E), ascorbic acid and reduced glutathione (GSH), and resulting data were compared with those obtained using the classical spectrophotometric method. Then, reactivity of complex matrices (cell culture media, vegetal extracts, *i.e.* marine alga extracts and fruit juice) was studied by using the present method. Finally, the capacities for nanomaterials to scavenge free radicals were investigated.

2. Experimental

2.1. Chemicals

All solvents, standards and reagents were of analytical grade and used without further purification. 1,1-Diphenyl-2-picrylhydrazyl (DPPH•), 1,1-diphenyl-2-picrylhydrazine (DPPH-H), Trolox® (6-hydroxy-2,5,7,8-tetramethylchroman-2-carboxylic acid), ascorbic acid, reduced glutathione (GSH), citric acid monohydrate, gallic acid, acetonitrile, Dulbecco's modified Eagle medium (DMEM), phenol red, sodium citrate tribasic dihydrate, tetrachloroauric acid trihydrate ($HAuCl_4 \cdot 3H_2O$), sodium borohydride, diamond nanopowder and other chemicals were purchased from Sigma–Aldrich (France). Methanol was purchased from Carlo Erba (France). Folin–Ciocalteu's phenol reagent was provided by Merck Chemicals (France). Ultrapure deionized water (>18.2 MΩ cm) was used for all solutions.

2.2. Instrumentation

A double beam UV-visible spectrophotometer (model UV-1700, Shimadzu France) was used for spectra recordings and absorbance measurements. The HPLC equipment consisted of a Hitachi model L6000 pump, a Rheodyne® model 7125 injector equipped with a 50-μL loop, a Croco-Cil® column oven, and a LKB model 2151 spectrophotometric UV-visible detector. Separations were isocratically performed by using either a LiChrospher® RP 18e (particle size: 5 μm; 250 mm × 4 mm; Merck Darmstadt, Germany) or an Interchrom C18 Nucleosil (particle size: 3 μm; 150 mm × 4 mm; Interchim, France) column, eluted with a mixture of acetonitrile and 10 mM ammonium citrate buffer pH 6.8 (70:30, v/v) at a flow rate of 0.8 mL min^{-1}. The temperature of the column was 40 °C and the resulting back-pressure were *ca.* 110 bar for LiChrospher® RP 18e and 180 bar for Interchrom C18 Nucleosil. The spectrophotometric detection was operated at either 330 or 515 nm. Alternatively, a photodiode array detector (Beckman model 168 associated with Beckman System Gold® software) was used to obtain on-line spectra. The wash out step was realized using a mixture acetonitrile–water (70:30, v/v) at a flow rate of 0.8 mL min^{-1} for 15 min.

2.3. Reactivity studies between reference antioxidants and DPPH• monitored by HPLC and spectrophotometry

Trolox® (57 μM), ascorbic acid (57 μM), and GSH (114 μM) stock solutions were daily prepared in methanol–10 mM ammonium citrate buffer pH 7.4 (60:40, v/v). One milliliter of each antioxidant

solution was mixed with 1 mL of a DPPH• stock solution freshly prepared at a concentration of 142 μM in methanol–10 mM ammonium citrate buffer pH 7.4 (60:40, v/v), using vortex for 20 s, then the resulting mixture was kept in the dark at room temperature (20–23 °C) for 10 min. The reaction was also performed in Dulbecco's modified Eagle medium (DMEM) added or not with phenol red as pH indicator (0.016 g L^{-1}) as follows: 500 μL of Trolox® at a concentration of 40 μM in methanol was mixed with 400 μL of medium. Then, the resulting solutions were mixed with 100 μL of DPPH• solution prepared in methanol at a concentration of 710 μM, and kept in the same reaction conditions as above. The reaction is completed at this time, and the absorbance was measured at 515 nm and HPLC analysis was performed in parallel (n = 3).

DPPH• calibration curve was realized in the range 27–71 μM using a series of dilutions of the 142 μM DPPH• daily prepared stock solution. The highest concentration of the calibration curve was injected 5-fold before injecting other standard solutions and samples. DPPH-H calibration curve was realized in the range 7–71 μM using either the commercially available standard or a series of dilutions of the DPPH• stock solution reacted with a 5-fold excess of either GSH or Trolox®, for 10 min. The relative standard deviation of peak area corresponding to the highest concentration of the calibration curve for each analyte, was less than 1.5% (n = 3; considered as the suitability test of the assay).

2.4. Marine algae collection and treatment

The studied algae, *i.e. Ulva lactuca* and *Gracilaria multipartita*, were collected on the coastal region of Rabat within North latitude of 34°03′ and a west longitude of 6°46′ with an altitude of 79 m. The beach of Rabat is located 35 km away from Kenitra city, on the left bank of the mouth of Bouregreg river. It is bordered by the Atlantic Ocean to the west. The algae were stripped of their epiphytes and debris adhering to their fronds, rinsed on site with seawater and then placed in plastic bags. Upon arrival at the laboratory, algae were again rinsed with distilled water and dried in the open air, in a direct contact with the sun to ensure a complete dehydration. The dried seaweed was then crushed to reduce their size, and obtain a very fine powder which served for the remainder of our study.

2.5. Reactivity studies between marine algae extract or fruit juice, and DPPH•

One gram of the powder resulting from preparation of the algae was extracted with 50 mL of methanol–ammonium citrate buffer pH 7.4 (60:40, v/v), using magnetic stirring at 500 rpm, in the dark, at room temperature (20–23 °C) and for 4 h. The resulting suspension was filtered using a 0.45 μm membrane (Durapore®, Millipore). A commercially available fruit juice (specific gravity 1.06 kg L^{-1}) made of apples, grapes, blackcurrants, blackberries and cranberries was also analysed. The filtrate or the fruit juice was diluted using methanol–ammonium citrate buffer pH 7.4 (60:40, v/v) to obtain the appropriate concentration and the DPPH• assay was applied as follows: equal volumes of the diluted solution resulting from algae extracts or fruit juice and DPPH• solution prepared in methanol–ammonium citrate buffer pH 7.4 (60:40, v/v) at a concentration of 142 μM, were mixed and kept in the dark, at room temperature (20–23 °C), for 2 h. The reaction medium was next analysed either by spectrophotometry or injected into the HPLC system (n = 3).

2.6. Determination of total phenol content

Total phenol content in natural products presently studied was evaluated by using Folin's method described by the International Organization for Standardization (ISO) 14502-1 [31] using gallic acid as the standard. Briefly, 1 mL of the diluted alga extracts in methanol–ammonium citrate buffer pH 7.4 (60:40, v/v) or fruit juice (in water) was mixed with 5 mL of a 1/10 dilution Folin–Ciocalteu's phenol reagent in water. Then 4 mL of a sodium carbonate solution (7.5%, w/v) was added. After shaking and incubating for 60 min in the dark at room temperature (20–23 °C), the absorbance was read at 765 nm. A calibration curve was built with gallic acid solutions with concentrations ranging from 10 to 100 μg mL^{-1} either diluted in water (in the case of fruit juice) or in methanol–ammonium citrate buffer pH 7.4 (60:40, v/v) (in the case of alga extracts), in order to avoid any matrix interference. The total phenol content was expressed as gallic acid equivalents in g 100 g^{-1}.

2.7. Reactivity studies between nanoparticles and DPPH•

Citrate-capped gold NPs were prepared as previously reported [32] by the reduction of a gold salt using citrate ions and $NaBH_4$. Then, the as-synthesized gold NPs were dialyzed against methanol–10 mM ammonium citrate buffer pH 7.4 (60:40, v/v) for 3 h using a 10 kDa cut-off dialysis bag (Interchim®, France). The gold content of NPs was measured using the previously reported method [32]. The interaction with DPPH• was studied as follows: 900 μL of gold NPs were reacted with 100 μL of 710 μM DPPH• solution in methanol. After 10 min incubation, the reaction medium was analysed by spectrophotometry and HPLC (n = 3).

Ten mg of a diamond NPs powder was suspended with 1 mL of methanol–ammonium citrate buffer pH 7.4 (60:40, v/v) applying ultrasonic bath for 5 min. The reaction between DPPH• and diamond NPs, with final concentrations of respectively 71 μM and 1 mg mL^{-1}, was performed for 1 h at room temperature (20–23 °C). The medium was then centrifuged at 42,000 × g for 20 min (Biofuge Stratos Heraeus, Thermo Scientific). The supernatants were analysed using spectrophotometry and HPLC (n = 3).

2.8. Software and statistical analyses

ChemDraw Ultra 8.0 soft was used to estimate the partition coefficient of the compounds. One-way analysis of variance (SigmaStat 3.1) was used to compare the half-maximum values (EC_{50}) of the concentration–response curves and for each sample group; the equal variance (Levene median) and normality (Kolmogorov–Smirnov) tests were performed.

3. Results and discussion

3.1. Selection of reaction conditions between antioxidants and DPPH•

The choice of reaction medium was performed with the following criteria: DPPH• assay has been mainly realized in pure methanol because standard AOs and extracts from natural products usually tested are poorly water soluble. The compounds responsible of DPPH• reduction frequently correspond to hydroxylated aromatic structures, *e.g.* polyphenolic compounds [33]. Recent studies have revisited this assay by using mixtures of methanol and aqueous buffers [34]. This approach permits to take into account the pH influence during the reaction between the radical and the AOs, especially according to their ionization constant. A pH value close to 7 is frequently selected to mimic physiological conditions. Among different salts present in buffer composition, ammonium citrate was claimed to give rise to the highest difference between spectral properties of the two components of the redox couple DPPH•/DPPH-H [25]. However, the reagent DPPH• presents a high hydrophobicity ($_c$log P = 4.52), making the presence of an organic

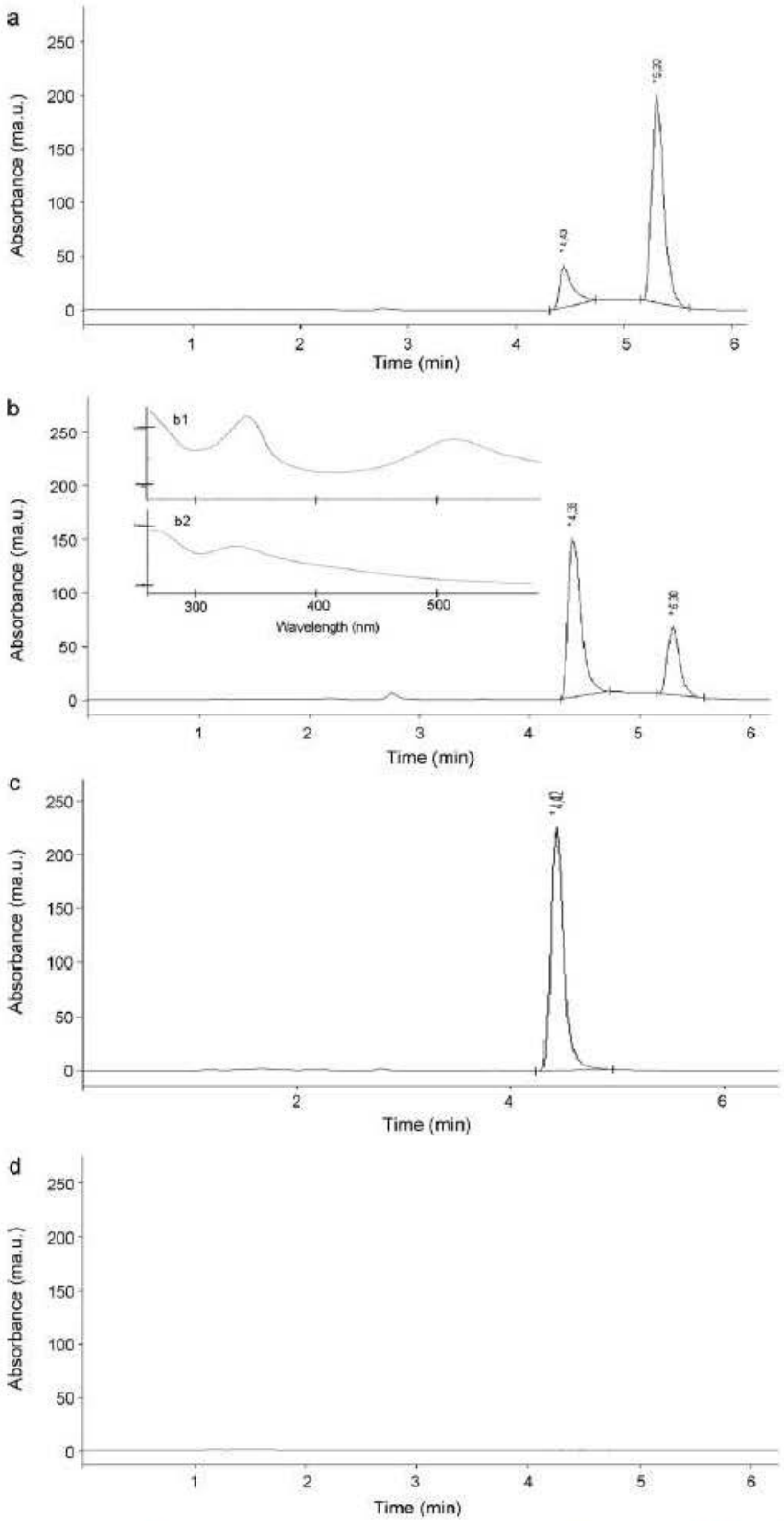

Fig. 2. Typical chromatograms corresponding to: (a) DPPH• standard solution (71 μM), (b) reaction between DPPH• (71 μM) and Trolox® (18 μM) (insert graph: spectra (b1) and (b2) recorded, respectively at 5.3 min and 4.4 min), (c) reaction between DPPH• (71 μM) and Trolox® (29 μM), and (d) Trolox® (18 μM). Detection was set at 330 nm using Interchrom C18 (3 μm) column.

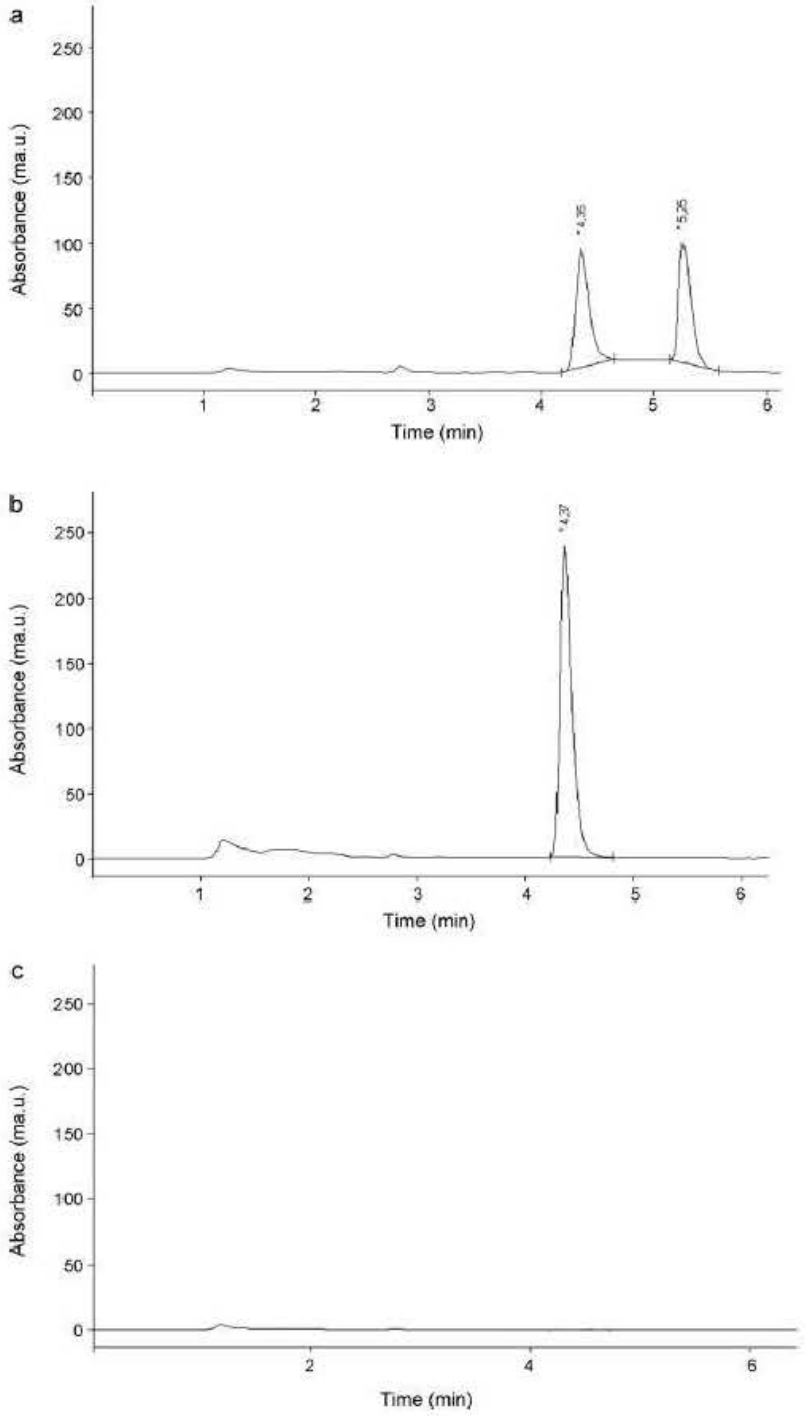

Fig. 3. Typical chromatograms corresponding to reaction products between DPPH• (71 μM) and marine alga extracts of (a) 1.88 mg L^{-1}, (b) 3.76 mg L^{-1} gallic acid equivalent, and (c) extract alone at 1.88 mg L^{-1}.

solvent necessary: at least 60% of methanol is required to prevent any precipitation. In our case, we selected a mixture of methanol–10 mM ammonium citrate buffer pH 7.4 for all experiments involving standard AOs, natural products and nanomaterials. For experiments with cell culture media, ammonium citrate buffer was changed to DMEM.

DPPH• assay was run in order to reach a plateau of DPPH• consumption and DPPH-H production (10 min for standard AOs or gold NPs, 1 h for diamond NPs, and 2 h for extracts of natural products).

Selected AOs in our study present various structures resulting in a wide range of polarity and pK_a values (Table 1). They were also selected by considering their pivotal role in cellular redox control

Table 1
Characteristics of reference antioxidants reacting with DPPH•.

Structure of AO (reduced form)	pK	cLog P[a]	Redox couple	E°′ [b] (V)	$(EC_{50})^c$ (μM)	Stoichiometry of the reaction DPPH•/AO
–	–	4.5	DPPH•/DPPH-H	+0.54	–	–
Ascorbic acid 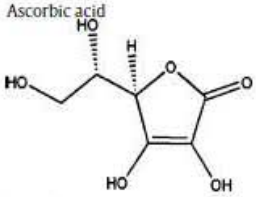	4.2[g]	−3.4	DHA•/HASC⁻	+0.28	22 ± 2[d,#] 18 ± 1[e,#] 22 ± 2[f,#]	1/2
Trolox® 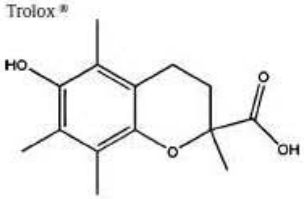	3.6[g]	3.0	Q•/QH$_2$	+0.19 [35]	21 ± 1[d,‡] 18 ± 2[e,‡] 22 ± 2[f,‡]	1/2
Reduced glutathione 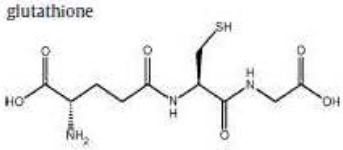	8.7[g]	−3.2	GS•/GSH	−0.24	42 ± 2[d,‡] 34 ± 4[e,‡] 38 ± 4[f,‡]	1/1

[a] Calculated using Chem Draw soft.
[b] *vs.* standard hydrogen electrode.
[c] Efficient concentration 50 (after reaction with 71 μM DPPH•).
[d] Determined by colorimetry.
[e] Determined by HPLC measuring DPPH.
[f] Determined by HPLC measuring DPPH-H.
[g] pK of the –COOH group for ascorbic acid and Trolox® and the –SH group for reduced glutathione.
[#,‡] Half-maximum values (EC_{50}) were not significantly different ($p > 0.05$).

Table 2
Characteristics of the two analyte peaks in the HPLC system (calculated according to the European Pharmacopoeia).

	Retention factor (t_0 evaluated by disturbance baseline)	Number of theoretical plates	Asymmetry factor	Resolution
DPPH•	3.37	16,000	1.39	5.35
DPPH-H	2.58	11,000	1.33	

Table 3
(a) Calibration curves of colorimetric and HPLC methods and (b) validation parameters for DPPH• and DPPH-H measurement by using HPLC method.

(a)

Analyte	Method	Concentration range (μM)	Slope ± S.D.[a]	Intercept ± S.D.[a]	Determination coefficient (r^2)
DPPH•	Colorimetry at 515 nm	27–71	0.0115 ± 0.0010	0.0015 ± 0.0005	0.999
	HPLC at 330 nm	27–71	30 ± 4	−380 ± 70	0.998
DPPH-H	HPLC at 330 nm	7–71	29 ± 2	40 ± 20	0.999

(b)

Analyte	Repeatability (R.S.D.[b] of 6 determinations at 44 μM)	Intermediate precision (R.S.D.[b] of 3 injections at 44 μM on two days)	Accuracy (3 concentrations, $n = 5$)	LOQ[c] (μM)	LOD[d] (μM)
DPPH•	1.9%	2.5%	102.1 ± 3.8%	27	14
DPPH-H	1.8%	0.5%	99.3 ± 3.3%	0.20	0.02

[a] Standard deviation.
[b] Relative standard deviation.
[c] Limit of quantification was determined experimentally based on a signal-to-noise ratio.
[d] Limit of detection was determined experimentally based on a signal-to-noise ratio.

and their efficiency to fight oxidative stress: (i) ascorbic acid or vitamin C; (ii) Trolox® a water soluble form of α-tocopherol, vitamin E [35]; (iii) reduced glutathione (GSH). A redox cycle between tocopherol located in the plasma membrane and ascorbic acid in the cytoplasm or outside the cell permits oxidized α-tocopherol to be regenerated to its reduced form by reacting with ascorbic acid. Glutathione is the main low molecular weight thiol in the cell and is believed to act as the main intracellular redox buffer aside other numerous actions [36]. These three AOs are the reduced forms of the following redox couples: $Dha^{\bullet}/HAsc^{-}$, $Q^{\bullet}/QH_2$, and $GS^{\bullet}/GSH$, reacting with DPPH• to produce DPPH-H. Their redox potential values vary with pH and their corresponding apparent redox potential values ($E^{\circ\prime}$) at pH 7.4 (this value was chosen for the present experiments in order to obtain the ionization state of the AOs corresponding to that under physiological conditions) are lower than $E^{\circ\prime}$ of the redox couple DPPH•/DPPH-H, which is *ca.* 0.54 V *vs.* standard hydrogen electrode, according to recent electrochemical studies [37].

3.2. Development and validation of the DPPH-HPLC method

Initial conditions reported in the literature for the elution of DPPH• in a reversed phase system were methanol–water (70:30, v/v) [21] or (80:20, v/v) [24]. Presently, the components of mobile phase were selected to be close to the reaction medium in order to minimize the disturbance in the reaction equilibrium during chromatographic process. Two modifications between reaction medium and mobile phase were introduced: (i) pH value of the citrate buffer was lowered from pH 7.4 to 6.8 to increase lifetime of the reversed phase column (in our hands, more than 300 injections were performed without any performance loss); (ii) methanol (an 80% in the mobile phase was necessary to obtain elution of both analytes, *i.e.* DPPH• and DPPH-H, in a 10 min range) was substituted for another organic solvent, *i.e.* acetonitrile (70%). No variation of retention time was observed following these two modifications. Acetonitrile is routinely preferred because it generates lower back-pressure on column than methanol. Two different kinds of C18 stationary phase, LiChrospher® RP 18e (5 μm) and Interchrom C18 Nucleosil (3 μm), were tested with the same mobile phase. Both gave rise to baseline separation between the two considered analytes with similar retention factors and other chromatographic parameters (Fig. 2 and Table 2).

Diode array detector (DAD) gives on-line spectra of the two studied analytes (Fig. 2, insert graph b1 and b2), providing identification of both the reagent (DPPH•) and the product (DPPH-H) of the reaction. The wavelength of 330 nm was selected, permitting to simultaneously detect DPPH• and DPPH-H with similar response factor (molar absorbance: 19 and 12 $mM^{-1}\,cm^{-1}$ for DPPH• and DPPH-H, respectively), and to obtain full selectivity when analyzing standard AOs (Fig. 2) and diluted extracts of natural products (Fig. 3). All previous HPLC studies realized on complex natural antioxidant products only detect DPPH• in the visible range (*ca.* λ = 515 nm) [24,25]. We can conclude that shifting detection wavelength from visible to UV range should permit to measure DPPH• and DPPH-H on the same chromatogram without affecting selectivity.

When investigating validation parameters of the HPLC method, several problems arose. First, one with non-reproducibility obtained with the DPPH• peak area. All previously reported HPLC methods devoted to DPPH• assay do not measure its concentration by using a calibration curve built with DPPH• standard, but with one of the tested AOs, thus no data exist concerning DPPH• linearity range and corresponding precision.

DPPH• needs four successive injections of a standard solution at a high concentration level (71 μM) to reach a constant value of its peak area (Fig. 4a). Such phenomenon was not observed with

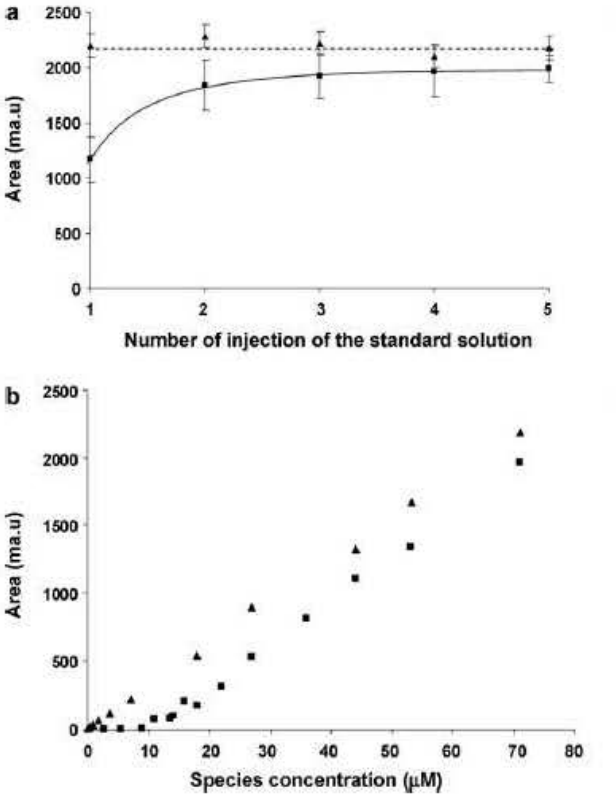

Fig. 4. (a) Dependence of the peak area of DPPH• (■) and DPPH-H (▲) on the number of successive injections of the DPPH• and DPPH-H standard solutions (71 μM). Each point corresponds to the mean ± SD of 4 consecutive processes consisting in re-starting the HPLC system (a washing step was operated at the end of each process). (b) Linearity studies of DPPH• (■) and DPPH-H (▲) in the HPLC system.

DPPH-H. This is probably due to an adsorption process of DPPH• onto metallic parts of the HPLC system and silica particles of the stationary phase not fully capped with alkyl groups. Adding EDTA (0.5 mM) to the mobile phase did not correct this process (data not shown). Consequently, the observed linearity range for DPPH-H is broader than for DPPH• (Fig. 4b and Table 3a) and the detection limit obtained with standards is 700-fold lower (15-fold lower than in the colorimetric assay – limit of detection of 0.3 μM – performed in batch) (Table 3b).

We observed consistently the reduced form DPPH-H (identified with DAD) in all chromatograms corresponding to DPPH• standards, at a constant ratio between the oxidized and reduced forms (Fig. 2a). The exact reason for this phenomenon is still unknown but can be linked to the lack of high purity of the purchased reagent, as already mentioned in the literature [30]. Three different batches of DPPH• were tested and the same ratio between the two peaks was observed. Thus, the peak area corresponding to this residual DPPH-H content was subtracted in all calculations.

Main validation parameters are summarized in Table 3b. A lower LOQ was obtained for DPPH-H (0.20 μM) than for DPPH• (27 μM). As already mentioned, this may be due to the reactivity of the DPPH• radical with the stationary phase and metallic parts of the HPLC system, precluding measurements of low concentrations of DPPH•. A high repeatability was obtained and the inter-day precision was associated with acceptable RSD: less than 2 and 3% for DPPH-H and DPPH•, respectively.

All AOs tested gave rise to the same product as the commercially available standard DPPH-H and the stoichiometric ratio of the

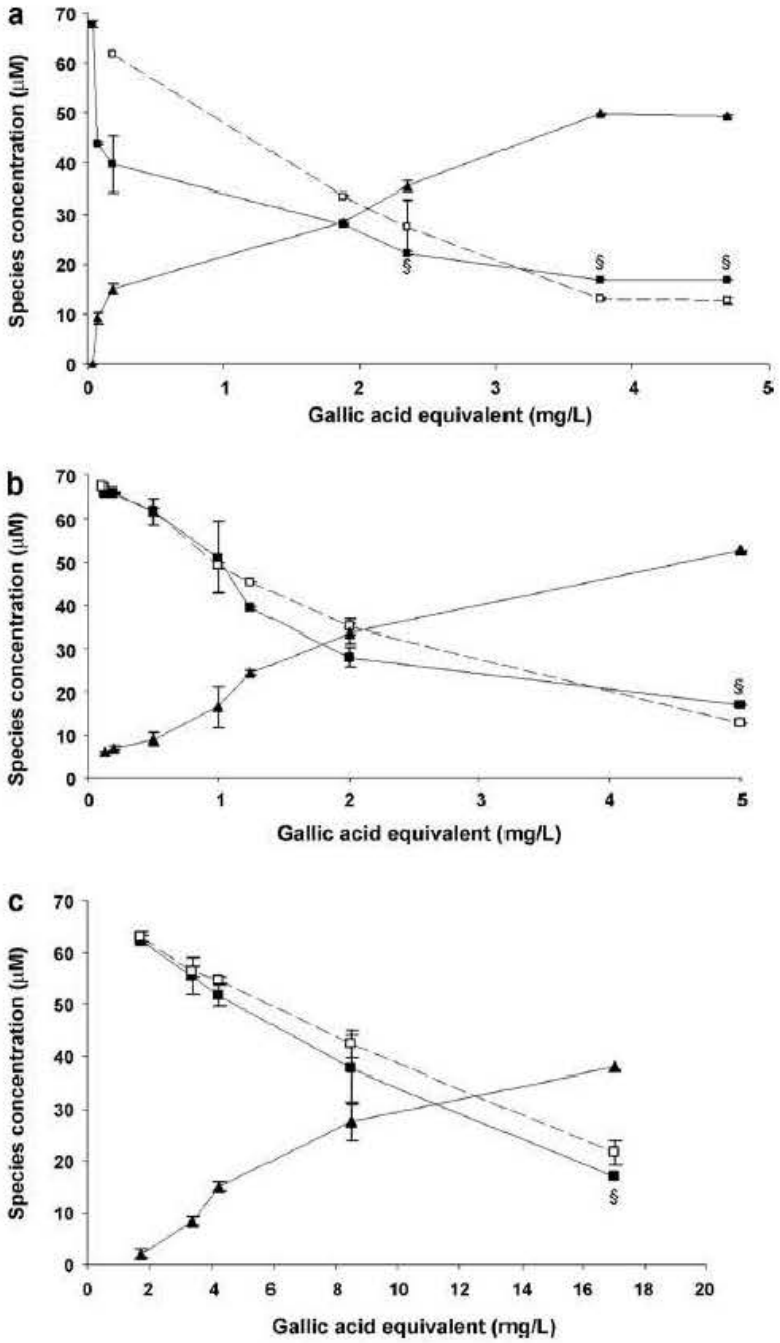

Fig. 5. DPPH• and DPPH-H concentrations (mean ± SD of three independent injections) evaluated by spectrophotometry (□) and HPLC (concentrations of DPPH• (■) and DPPH–H (▲)) measured after reaction with (a) fruit juice, (b) *U. lactuca* and (c) *G. multipartita* algae extracts. Values indicated by § are approximate data (between LOQ and LOD of the method).

reaction with DPPH• was confirmed: 1:1 (GSH), and 1:2 (ascorbic acid and Trolox®) [8,11,34] (Table 1). No significant difference between half-maximum values (EC_{50}) of the concentration–response curves were observed when measuring DPPH• consumption by using either spectrophotometry or HPLC, and DPPH-H production by HPLC, which fully validates the usefulness of the present assay for all types of AOs (Table 1). The HPLC method was then tested into complex matrices (cell culture media, natural products) and nanomaterials, in order to explore the new possibilities given by this method.

Firstly, the exact contribution of an AO, *i.e.* Trolox®, added to a cell culture media (Dulbecco's modified Eagle medium (DMEM), containing or not phenol red as pH indicator), was evaluated by using both spectrophotometry and HPLC. Because of DMEM components (amino acids, vitamins, inorganic salts, phenol red, etc.), this matrix strongly interferes in colorimetric assay. As a matter of fact, the blanks corresponding to DMEM and DMEM with

Table 4
DPPH• and DPPH-H concentrations measured by colorimetry and HPLC after reaction between DPPH• (71 μM) and nanoparticles.

Nanoparticles	Colorimetry	HPLC	
	DPPH• remaining (μM)	DPPH-H production (μM)	DPPH• remaining (μM)
Diamond (1 mg mL^{-1})	57 ± 1	20 ± 3	43 ± 1
Gold, citrate-capped (gold content: 0.07 mg mL^{-1})	Not determinable	11 ± 1	60 ± 2

phenol red (DPPH• omitted) represented 25% and 44%, respectively, of DPPH• absorbance at EC_{50} value calculated for Trolox® (20 μM). No interference was noted by using HPLC and the measured EC_{50} value corresponds to the expected one.

Secondly, as far as natural products are concerned (*i.e.* algae and fruit juice), their reaction with DPPH• (Fig. 5) gave EC_{50} values, not significantly different ($p > 0.05$), of 2.8 ± 0.5, 2.2 ± 0.4 and 2.5 ± 0.2 mg gallic acid equivalents L^{-1} for *U. lactuca* extract, 11.1 ± 1.0, 9.9 ± 2.1 and 13.0 ± 1.4 mg gallic acid equivalents L^{-1} for *G. multipartita*, and eventually 3.7 ± 1.8, 2.4 ± 0.8 and 2.7 ± 0.3 mg gallic acid equivalents L^{-1} for fruit juice, using colorimetric method and HPLC monitoring DPPH• and DPPH-H, respectively. Using the Folin–Ciocalteau's method, *U. lactuca* and *G. Multipartita* algae, and the juice were characterised by 188 ± 4 mg of gallic acid equivalents 100 g^{-1}, 170 ± 3 mg of gallic acid equivalents 100 g^{-1}, and 236 ± 9 mg gallic acid equivalents 100 g^{-1}, respectively. As far as *U. lactuca* extract is concerned, the ratio EC_{50} (given by DPPH assay whatever the test considered) over the total phenol content, was in accordance with previously reported results on natural antioxidants [38].

Lastly, the presently developed HPLC method was applied to nanomaterials. Indeed, there is an increasing interest in NPs and their involvement in redox reactions [39,40]. For this purpose, the colorimetric DPPH• assay is frequently used [17–19]. In our study, the radical scavenging capacities of two different kinds of NPs were evaluated. Such NPs exhibited the following physico-chemical properties: a diameter of 5.3 nm for gold NPs and surface plasmon resonance band centred at 517 nm [32] and a diameter of 10 nm for diamond NPs (as given by the supplier). Nevertheless, a complete physico-chemical characterisation of the NPs in the reaction medium is currently under investigation. Indeed, this medium (methanol–10 mM ammonium citrate buffer pH 7.4 (60:40, v/v)) with a 4-fold lower content of citrate ions as compared to the synthesis medium, may affect these citrate capped gold NPs properties. The results of the reaction between DPPH• and NPs are presented in Table 4. As far as gold NPs are concerned, their reaction with DPPH• could only be analysed using the HPLC method due to the high interference of gold NPs because of the surface plasmon resonance band which represented 229% of DPPH• absorbance at EC_{50}. Nevertheless, via the HPLC analyses, a good correlation between DPPH• consumption and DPPH-H production (respectively 60 μM and 11 μM for an initial concentration of 71 μM) was observed and a HAT mechanism was suggested. As a contrast, the interaction between diamond NPs did not lead to a correspondence between DPPH• consumption and DPPH-H production. These interesting results may suggest that other mechanisms can occur such as adsorption of the free radical onto the nanomaterial as it was previously highlighted in the literature with other NPs [39,41]. The adsorption process onto the diamond NPs surface is currently under further investigation. As a conclusion of this part, the HPLC method represents a powerful tool to investigate various mechanisms occurring during DPPH• reaction via the assessment of a balance between DPPH• and DPPH-H.

4. Conclusion

To the best of our knowledge, it is the first report of a HPLC method devoted to DPPH-H measurement. It appears as a simple, fast, and reliable tool to study HAT mechanism during reaction between DPPH• and various classes of AOs. The reaction product is measured with a broader linearity range and lower quantification limit than the reagent consumption could be. Moreover, the method was highlighted as a powerful tool to investigate interaction between the free radical probe and nanomaterials.

Acknowledgment

The authors would like to thank Miss Rima Kahla for her technical support.

References

[1] A. Sanz, G. Barja, R. Pamplona, C. Leeuwenbugh, in: C. Jacob, P.G. Winyard (Eds.), Redox Signaling and Regulation in Biology and Medicine, Wiley-VCH Verlag GmbH & Co. KGaA, Weinheim, 2009, pp. 433–464.
[2] I.F.F. Benzie, J.J. Strain, Anal. Biochem. 239 (1996) 70–76.
[3] J.K. Moon, T. Shibamoto, J. Agric. Food Chem. 57 (2009) 1655–1666.
[4] R.L. Prior, X. Wu, K. Schaich, J. Agric. Food Chem. 53 (2005) 4290–4302.
[5] K. Thaipong, U. Boonprakob, K. Crosby, L. Cisnero-Zevallos, D. Hawkins Byrne, J. Food Comp. Anal. 19 (2006) 669–675.
[6] S. Goldschmidt, K. Renn, Chem. Ber. 55 (1922) 628–643.
[7] M.S. Blois, Nature 181 (1958) 1199–1200.
[8] W. Brand-Williams, M.E. Cuvelier, C. Berset, Food Sci. Technol. 28 (1995) 25–30.
[9] M. Musialik, G. Litwinienko, J. Org. Chem. 7 (2005) 4951–4954.
[10] M.C. Foti, C. Daquino, I.D. Mackie, G.A. DiLabio, K.U. Ingold, J. Org. Chem. 73 (2008) 9270–9282.
[11] S. Viirlaid, R. Mahlapuu, K. Kilk, A. Kuznetsov, U. Soomets, J. Järv, Bioorg. Chem. 37 (2009) 126–132.
[12] T. Noipa, S. Srijaranai, T. Tuntulani, W. Ngeontae, Food Res. Int. 44 (2011) 798–806.
[13] P. Trouillas, P. Marsal, A. Svobodová, J. Vostálová, R. Gažák, J. Hrbáč, P. Sedmera, V. Křen, R. Lazzaroni, J.L. Duroux, D. Walterová, J. Phys. Chem. A 112 (2008) 1054–1063.
[14] E. Baciocchi, A. Calcagni, O. Lanzalunga, J. Org. Chem. 73 (2008) 4110–4115.
[15] A. Cano, O. Alcaraz, M.B. Arnao, Anal. Bioanal. Chem. 376 (2003) 33–37.
[16] P. Ionita, Chem. Pap. 59 (2005) 11–16.
[17] A. Watanabe, M. Kajita, J. Kim, A. Kanayama, K. Takahashi, T. Mashino, Y. Miyamoto, Nanotechnology 20 (2009) 1–9.
[18] R. Isono, T. Yoshimura, K. Esumi, J. Colloid Interface Sci. 288 (2005) 177–183.
[19] R. Konwarh, B. Gogoi, R. Philip, M.A. Laskar, N. Karak, Colloids Surf. B 84 (2011) 338–345.
[20] Z. Nie, K.J. Liu, C.J. Zhong, L.F. Wang, Y. Yang, Q. Tian, Y. Liu, Free Radic. Biol. Med. 43 (2007) 1243–1254.
[21] T. Yamaguchi, H. Takamura, T. Matoba, J. Terao, Biosci. Biotechnol. Biochem. 62 (1998) 1201–1204.
[22] H. Ukeda, Y. Adachi, M. Sawamura, Talanta 58 (2002) 1279–1283.
[23] K.P. Suja, A. Jayalekshmy, C. Arumughan, J. Agric. Food Chem. 52 (2004) 912–915.
[24] D. Chandrasekar, K. Madhusudhana, S. Ramakrishna, P.V. Diwan, J. Pharm. Biomed. Anal. 40 (2006) 460–464.
[25] A. Bartasiute, B.H. Westerink, E. Verpoorte, H.A.G. Niederländer, Free Radic. Biol. Med. 42 (2007) 413–423.
[26] N. Nuengchamnong, K. Ingkaninan, Food Chem. 118 (2010) 147–152.
[27] Y. Zhang, S. Shi, Y. Wang, K. Huang, J. Chromatogr. B 879 (2011) 191–196.
[28] M. Kosar, H.J.D. Dorman, O. Bachmayer, K.H.C. Baser, R. Hiltunen, Chem. Nat. Compd. 39 (2003) 161–166.
[29] H.A. Niederländer, T.A. van Beek, A. Bartasiute, I.I. Koleva, J. Chromatogr. A 1210 (2008) 121–134.
[30] N.D. Yordanov, A.G. Christova, Fresenius J. Anal. Chem. 358 (1997) 610–613.
[31] ISO14502-1: Determination of Substances Characteristic of Green and Black Tea. Part 1. Content of Total Polyphenols in Tea – Colorimetric Method Using Folin–Ciocalteu Reagent, 2005.
[32] J. Tournebize, A. Sapin-Minet, R. Schneider, A. Boudier, P. Maincent, P. Leroy, Talanta 83 (2011) 1780–1783.
[33] E.J. Lien, S. Ren, H.H. Bui, R. Wang, Free Radic. Biol. Med. 26 (1999) 285–294.
[34] O.P. Sharma, T.K. Bhat, Food Chem. 113 (2009) 1202–1205.
[35] E. Cadenas, G. Merényi, J. Lind, FEBS 253 (1989) 235–238.
[36] G.R. Buettner, Arch. Biochem. Biophys. 300 (1993) 535–543.

[37] Q. Zhuang, F. Scholz, F. Pragst, Electrochem. Commun. 1 (1999) 406–410.
[38] H.H. Abd El-Baky, F. El-Baz, G.S. El-Baroty, Int. J. Food Sci. Technol. 44 (2009) 1688–1695.
[39] P. Ionita, F. Spafiu, C. Ghica, J. Mater. Sci. 43 (2008) 6571–6574.
[40] M. Auffan, J. Rose, M.R. Wiesner, J.-Y. Bottero, Environ. Pollut. 157 (2009) 1127–1133.
[41] Z. Zhang, A. Berg, H. Levanon, R.W. Fessenden, D. Meisel, J. Am. Chem. Soc. 125 (2003) 7959–7963.

II.1.3.1 Résultats complémentaires de la publication n°4

Les résultats présentés dans l'article "High-performance liquid chromatographic method to evaluate the hydrogen atom transfer during reaction between 1,1-diphenyl-2-picryl-hydrazyl radical and antioxidants" montrent un test fiable pour évaluer le pouvoir antiradicalaire de matrices complexes (*i.e.* milieu culture cellulaire et extrait d'algues) ainsi que celui de NP d'or et de diamant. De plus, cette méthode CLHP est plus sélective que la spectrocopie UV-visible et intéressante pour évaluer le mécanisme de la réaction entre le $DPPH^{\bullet}$ et différents types d'antioxydants.

Après avoir précisé un point concernant les propriétés physico-chimiques des NP d'or stabilisées par des ions citrate, d'autres expériences non décrites dans cet article sont présentées ci-après. En effet, nous avons optimisé une méthode CLHP pour évaluer sans interférence par le test $DPPH^{\bullet}$ le pouvoir réducteur des NP d'or cependant lors de ces expériences un problème d'instabilité des NP d'or en milieu organique a été constaté ce qui confirme que cette méthode n'est pas réellement adaptée à celles-ci.

Caractéristiques physico-chimiques des nanoparticules d'or dans le milieu réactionnel

Les NP d'or stabilisées par les ions citrate, après dialyse contre le tampon méthanol-citrate (60:40; V/V) pendant 2 h, sont caractérisées par spectrophotométrie UV-visible et par diffusion dynamique de la lumière. Comme nous pouvions nous y attendre d'après certaines études (Zhang *et al.*, 2007, Kim *et al.*, 2008, Balasubramanian *et al.*, 2010a), l'étape de dialyse a provoqué une augmentation du rayon hydrodynamique (34 fois) et un déplacement bathochromique ($\Delta\lambda$ = 533 – 517 = 16 nm), indiquant l'existence probable d'une forte agrégation des NP d'or stabilisées par les ions citrate (tableau 7).

Tableau 7. Modifications des caractéristiques physico-chimiques des nanoparticules d'or induites par la dialyse lors du test au $DPPH^{\bullet}$.

	NP d'or stabilisées par les ions citrate	
	Après synthèse	Après dialyse contre méthanol-citrate (60:40; V/V)
Rayon hydrodynamique (nm)	6,5	223
λ_{max} (nm)	517	533

Cette agrégation est provoquée par la faible force ionique du milieu utilisé. Ainsi, ce test n'est pas adapté et pose des difficultés pour l'analyse des NP stables en milieu aqueux que nous utilisons, car le DPPH$^{\bullet}$ n'est soluble qu'en présence d'au moins 60 % d'méthanol. Ces conditions entraînent une agrégation de nos NP. Ainsi, le test ABTS$^{\bullet+}$, décrit précédemment dans l'article 2, est plus adapté pour l'étude des substances hydrophiles car le radical cationique ABTS$^{\bullet+}$ est soluble en milieux organique et aqueux. De plus, l'ABTS$^{\bullet+}$ présente un spectre d'absorption dans le visible avec trois maxima à 645, 734 et 815 nm permettant ainsi, contrairement au DPPH$^{\bullet}$, d'évaluer le pouvoir réducteur des NP d'or par spectrophotométrie visible sans interférence (figure 8).

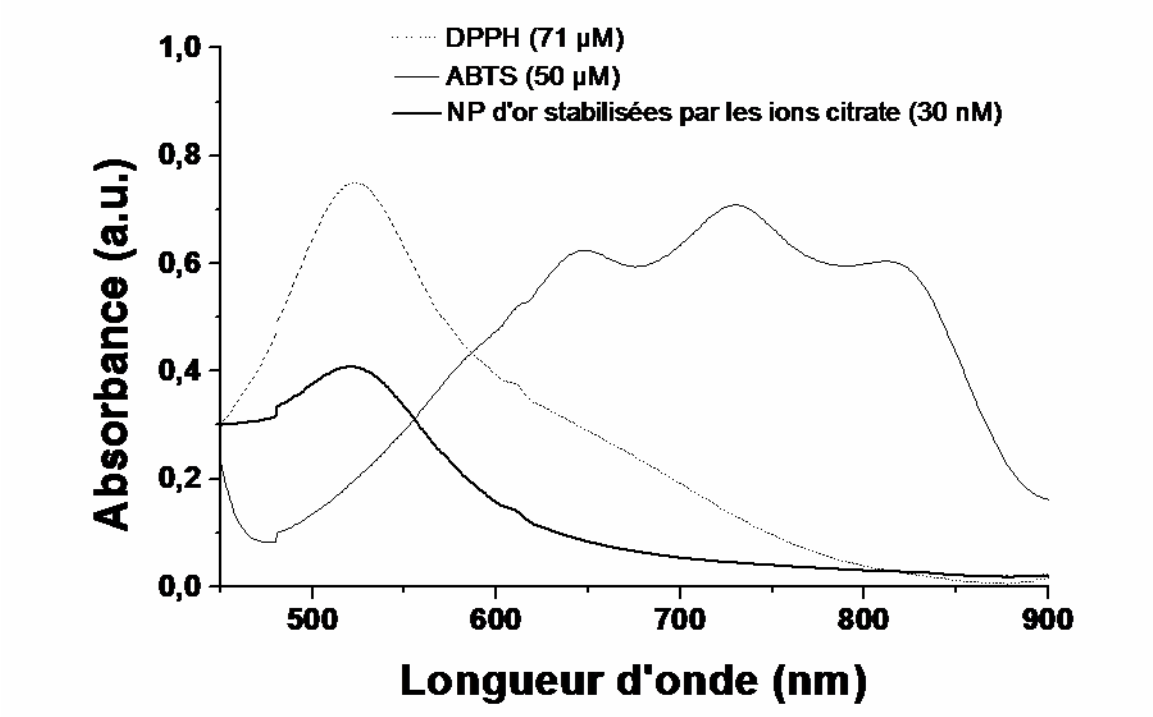

Figure 8. Spectres d'absorption UV-visible du DPPH$^{\bullet}$ (dans PBS), de l'ion radicalaire ABTS$^{\bullet+}$ (dans PBS), et des NP d'or stabilisées par les ions citrate (dans l'eau).

Les résultats du pouvoir antiradicalaire des NP vis-à-vis de l'ABTS$^{\bullet+}$ figurent dans l'article n° 2. Dans cet article, nous avons démontré que les NP d'or stabilisées par de faibles interactions avec le ligand sont capables d'interagir plus fortement avec l'ABTS$^{\bullet+}$. En effet, les NP d'or stabilisées par les ions citrate ont une surface plus accessible et elles réagissent plus facilement avec l'ABTS$^{\bullet+}$ que les NP Au@DHLA. De plus, nous avons remarqué que le test ABTS$^{\bullet+}$ est plus adapté pour évaluer la bioréactivité de composés hydrophiles tels que les NP d'or et présente moins d'interférences spectrales par rapport à l'emploi de DPPH$^{\bullet}$.

Chapitre III.

Effet de la fonctionnalisation de surface des nanoparticules d’or sur l’homéostasie redox cellulaire

III.1 Introduction

Dans nos travaux de synthèse et de caractérisation des NP d'or (chapitre II), nous avons montré que leur densité de couverture par le DHLA améliore leur stabilité et diminue leur réactivité vis-à-vis de la BSA et d'une espèce radicalaire modèle. Parmi les différents rapports [DHLA]/[Au] étudiés, les NP Au@DHLA$_{140}$ et Au@DHLA$_{222}$ sont les plus stables en fonction du temps et en solution de force ionique élevée (NaCl 1 M) et moins réactives vis-à-vis de la BSA et de l'ABTS$^{\bullet+}$.

Toutefois, la possibilité d'utiliser des NP d'or dans des applications biologiques, nécessite l'absence de cytotoxicité. Dans ce chapitre, nous nous sommes intéressés à l'impact biologique des NP Au@DHLA$_{222}$ (notées dans ce chapitre de façon simplifiée : NP Au@DHLA) ainsi que celui des NP d'or stabilisées par les ions citrate.

Comme évoqué précédemment, la plupart des travaux disponibles dans la littérature s'intéresse à la toxicité aiguë des NP d'or, et, en outre, ces travaux apparaissent contradictoires (Shukla *et al.*, 2005, Jia *et al.*, 2009, Pan *et al.*, 2009, Ma *et al.*, 2010, Li *et al.*, 2010, Gao *et al.*, 2011, Zhao *et al.*, 2011). D'après certains auteurs, les NP d'or seraient toxiques pour certaines cellules mais pas pour d'autres (Connor *et al.*, 2005, Unfried *et al.*, 2007, Alkilany et Murphy, 2010, Soenen *et al.*, 2011). De plus, de nombreuses caractéristiques influencent les risques de toxicité induite par les NP d'or, telles que la taille (Pan *et al.*, 2007), la forme (Hutter *et al.*, 2010), la charge (Goodman *et al.*, 2004), la fonctionnalisation de surface (Goodman *et al.*, 2004, Shukla *et al.*, 2005, Takahashi *et al.*, 2005, Hauck *et al.*, 2008). Par contre, certaines études (Shukla *et al.*, 2005, Ma *et al.*, 2010) ont conclu à la biocompatibilité des NP d'or, celles-ci ne provoquant pas d'altération du système immunitaire (Shukla *et al.*, 2005). Récemment, Ma *et al.* (2010) ont observé que l'exposition des macrophages à des NP d'or entraîne une diminution et une inhibition de la production de $^{\bullet}$NO induite par LPS.

Ces résultats émanant de la littérature sont discutables et difficilement comparables en raison d'un manque d'informations sur les caractéristiques des NP d'or, ce qui nous a conduit à écrire une lettre à l'éditeur **(article 5, Leroy *et al., Letter to the Editor, Nitric Oxide-Biol Chem.,* 2011 (25); 54-56)**, pour alerter et mettre en garde contre toute conclusion hâtive qui attribuerait aux NP d'or un comportement général au contact des cellules. En effet, contrairement aux résultats de la littérature, nous avons montré que lors d'une exposition pendant 24 h des macrophages aux NP d'or utilisées dans nos études (stabilisées par des ions citrate ou stabilisées par le DHLA), il n'y a ni diminution, ni inhibition de la production d'oxyde nitrique ($^{\bullet}$NO) induite par le LPS. Ces résultats restent cependant propres aux NP de notre étude, et dans chaque type d'étude, une bonne connaissance des NP utilisées par le biais d'une caractérisation détaillée est donc nécessaire.

Au vu de ces résultats, deux questions se posent : les NP d'or sont-elles vraiment capables de perturber directement ou indirectement l'équilibre redox cellulaire? La fonctionnalisation de surface joue-t-elle un rôle?

Pour répondre à ces questions, nous avons évalué l'impact de ces NP sur l'homéostasie redox soit en absence de cellules, soit en présence de cellules. Ces résultats originaux font l'objet d'un manuscrit soumis dans *International Journal of Pharmaceutics,* Mai 2012 **(article 6)**. Dans un premier temps, en absence de cellules, nous avons développé différents tests pour évaluer l'interaction de NP d'or avec le GSH, la BSA et le GSNO. Ces molécules ont été choisies en raison de leur rôle important dans la régulation de l'homéostasie redox. Le GSH est un tripeptide considéré comme le thiol principal maintenant le potentiel redox cellulaire et capable d'éliminer les ROS et de se conjuguer avec les xénobiotiques électrophiles (Sies, 1999). Le groupement thiol du GSH peut être nitrosé, conduisant à la formation du GSNO, qui est une molécule endogène impliquée dans le stockage et dans le transport du $^{\bullet}$NO (Al-Sa'Doni et Ferro, 2000). L'albumine, comme mentionné précédement, est la protéine majoritaire dans le sang ; elle intervient dans le transport de multiples substances et dans le maintien du potentiel redox dans les fluides extracellulaires (Era *et al.*, 1995).

Nos résultats montrent que l'interaction entre les NP d'or et ces molécules dépend des caractéristiques physico-chimiques des NP, notamment de leur fonctionnalisation de surface. Les NP Au@DHLA ne réagissent pas avec le GSH et le GSNO, même à une concentration de 30 nM, la valeur la plus élevée testée, tandis que les NP d'or stabilisées par les ions citrate interagissent avec les deux types de molécules, par échange de ligands et par libération de $^{\bullet}$NO à partir du GSNO. De même, les NP d'or stabilisées par les ions citrate sont deux fois plus réactives vis-à-vis de la BSA que les NP Au@DHLA.

Dans un second temps, nous avons étudié l'interaction entre les NP d'or et les cellules, en considérant plus particulièrement l'influence de la fonctionnalisation de surface des NP sur leur internalisation ainsi que sur leur impact dans l'homéostasie redox des macrophages. Les macrophages sont considérés comme un modèle cellulaire de choix pour l'évaluation préliminaire des risques des NP (Soenen *et al.*, 2011). Les macrophages sont dérivés de la cellule souche hématopoïétique et ils jouent un rôle essentiel dans l'immunité innée. Ils constituent donc la première ligne de défense de l'organisme. Toute particule (microorganismes, particules inorganiques ou polymériques, …) entrant dans l'organisme (par n'importe quelle voie) est prise en charge par ces cellules circulantes ou présentes dans les tissus. Dans cette étude, nous avons voulu comprendre la réponse précoce des macrophages à une exposition à une faible concentration en NP d'or, *i.e.* 10 nM, valeur correspondant à une viabilité cellulaire de 80 % . Cette valeur est également

plus représentative d'une dose susceptible d'être utilisée ultérieurement en thérapeutique. Nous avons étudié la localisation cellulaire des NP d'or et nous avons déterminé la quantité de NP d'or internalisées par les macrophages afin de connaître leur interaction avec ce type de cellules et donc de prévoir et comprendre leur mécanisme d'action. Quel que soit le type de ligand, les NP d'or sont localisées dans des vésicules qui sont probablement des vésicules d'endocytose. Nos résultats montrent que les NP d'or stabilisées par les ions citrate sont internalisées deux fois plus que les NP Au@DHLA, confirmant la faible réactivité mentionnée dans le chapitre II.

Ensuite nous avons évalué le statut redox cellulaire suite à l'exposition de macrophages à des NP d'or par le suivi de biomarqueurs qui sont les plus à même de donner une réponse précoce à une modification de l'état redox. Les effets pro-oxydants des NP d'or ont été mis en évidence par le dosage intracellulaire du GSH et des ROS. En outre, les effets des NP sur l'expression des gènes liés à la réponse inflammatoire (*tnfα*) et au stress oxydant (*ncf1*) ont été aussi évalués. Plutôt que les LPS, nous avons tenu à utiliser un contrôle positif nanoparticulaire (de caractéristiques physico-chimiques néanmoins différentes des NP d'or) : des NP d'Eudragit® RS **(article 7, Eidi *et al., Int. J. Pharmaceut.* 2012 (422); 495-503)**.

Aucune modification du contenu intracellulaire en GSH n'a été observée après exposition aux NP Au@DHLA. En revanche, lorsque les cellules sont exposées aux NP d'or stabilisées par les ions citrate, une diminution de 20% du contenu cellulaire en GSH est observée. Du fait de cette diminution de GSH, on peut s'attendre à une production de ROS accrue. Curieusement, aucune augmentation de génération de ROS en GSH n'a été mise en évidence dans notre étude ; au contraire, une diminution de 28% du contenu cellulaire en ROS a été observée. De plus, nous avons constaté la même diminution avec les cellules exposées aux NP Au@DHLA.

Comme décrit précédemment dans le chapitre II, de nombreuses études suggèrent que les NP d'or présentent une très forte réactivité avec les radicaux libres, ce qui pourrait expliquer la diminution du contenu cellulaire en ROS (Esumi *et al.*, 2004, Isono *et al.*, 2005).

Au niveau transcriptionnel, nous n'avons pas mis en évidence de relation entre la diminution du GSH intracellulaire et l'activation des gènes impliqués dans la réponse inflammatoire et dans le stress oxydant. En revanche, nous avons observé que les NP Au@DHLA entraînent une sous-régulation de l'activité du facteur de transcription NF-κB. Dans la littérature, l'or à l'état métallique est réputé pour réduire l'expression du facteur de transcription NF-κB et en conséquence pour diminuer l'activité des nombreux gènes impliqués dans la production de RNS et ROS (Jeon *et al.*, 2000). Les mêmes mécanismes de sous-régulation pouraient être déclenchés par les NP Au@DHLA.

Ainsi, les NP Au@DHLA pourraient présenter un effet antiradicalaire par une action indirecte (sous-régulation du *nfκb*2 par les cellules, donc sous-expression des cascades de production de RNS et ROS) et par une action directe de piégeur de radicaux (démontrée en absence de cellules par l'utilisation de l'$ABTS^{\bullet+}$).

Ce travail démontre l'influence de l'état de surface des NP d'or sur leur comportement en présence de composés biologiques et de cellules. La faible réactivité des NP d'or présentant du DHLA en surface est vérifiée dans ces conditions expérimentales particulières, laissant envisager des applications médicales pour cette plateforme nanoparticulaire. Cette étude ne démontre pas pour autant une toxicité importante des particules stabilisées par les ions citrate, particules très souvent décrites dans la littérature. Enfin, la difficulté à mettre en évidence une modulation du statut redox, en dehors d'un stress oxydant, est clairement démontrée dans ce travail.

III.1.1 Article 5. Leroy P., Sapin-Minet A., Pitarch-Sierra A., Boudier A., Tournebize J., and Schneider R. Interactions between gold nanoparticles and macrophages : activation or inhibition ? Letter to the Editor. *Nitric Oxide-Biol. Chem.* **25 (1): 54 –56** (2011).

III.1.2 Article 6. Tournebize J., Boudier A., Joubert O., Eidi H., Bartosz G., Leroy P., Sapin-Minet A. Impact of gold nanoparticle coating on redox homeostasis. Soumis dans *International Journal of Pharmaceutics*, Mai 2012.

III.1.3 Article 7. Eidi H., Joubert O., Némos C., Grandemange S., Mograbi B., Foliguet B., Tournebize J., Maincent P., LeFaou A., Aboukhamis I., and Rihn B.H. Drug delivery by polymeric nanoparticles induces autophagy in macrophages. *Int. J. Pharmaceut.* 422: 495-503 (2012).

Nitric Oxide 25 (2011) 54–56

Contents lists available at ScienceDirect

Nitric Oxide

journal homepage: www.elsevier.com/locate/yniox

Letter to the Editor

Interactions between gold nanoparticles and macrophages: Activation or inhibition?

We read with great interest the study of interactions between gold nanoparticles (GNP) and macrophages recently published by Ma et al. [1]. They observed inhibition of NO-macrophage production after successive exposure of cultured cells to lipopolysaccharides (LPSs) and GNP. Variations of other biomarkers of inflammation have confirmed their observation. This work is questionable because of a lack of information on GNP characteristics. The use of polyethylene glycol (PEG)-coated GNP (diameter: 10–15 nm) is indicated in abstract and the reference "[17]" mentioned in experimental section does not describe any PEG-coated GNP but GNP stabilized with citrate. Main GNP properties that play a role in cell interactions are size, shape, surface charge (zeta potential), solubility, and surface layer. This latter mostly influences the immediate protein coating of GNP upon contact with biological matrices. This process leads to a protein corona, creating a "molecular signature", which is recognized by immune cells and determines the route of particle internalization. PEG-coated GNP have low interaction with proteins in comparison with citrate-stabilized GNP, thus a limited uptake by cells of the reticuloendothelial system is usually observed [2].

Several recent reports in the literature describe interactions between different kinds of GNP and macrophage cell lines, using various operating conditions, expressing nanoparticle concentrations in different ways and selecting concentrations with or without indicating their relationship with cell-viability (Table 1). Even marked differences appear between these studies, most of them have concluded to an activation process.

We have tested two kinds of GNP, quite similar related to their shape (spherical), hydrodynamic diameter (6–8 nm), but different with their surface chemistry, and consequently their zeta potential (ζ): (i) citrate ions which are most frequently used to stabilize the metallic core ($\zeta = -50$ mV), and (ii) dihydrolipoic acid (DHLA) which leads to a high capping density and stability of the corresponding GNP (covalent bond between DHLA and gold atoms of the core) ($\zeta = -40$ mV). These GNP were synthesized using a previously reported method [3] with some modifications [4], and were fully characterized [4]. The two sorts of GNP were exposed to macrophages at a concentration of 10 nM, which corresponds to a higher viability than 80%. These values were obtained using Trypan Blue assay (MTT assay could not be applied because of high absorbance of GNP in visible range interfering with probe measurement). Periods of contact for "inhibition" experiments were similar to previous ones [1].

Resulting data (Fig. 1) demonstrate neither significant activation, nor significant inhibition for both tested GNP, confirming previous studies [7].

In conclusion, the debate "Do GNP activate or inhibit NO-production in macrophages?" is still opened and it will need further experiments with closer and better described operating conditions than actual ones reported in the literature. There is a need to evaluate the real opportunity to use GNP as "safe" delivery platforms for diagnostic reagents and drugs.

References

[1] J.S. Ma, W.J. Kim, J.J. Kim, T.J. Kim, S.K. Ye, M.D. Song, H. Kang, D.W. Kim, W.K. Moon, K.H. Lee, Gold nanoparticles attenuate LPS-induced NO production through the inhibition of NF-KB and IFN-β/STAT1 pathways in RAW264.7 cells, Nitric Oxide 23 (2010) 214–219.
[2] P. Aggarwal, J.B. Hall, C.B. McLeland, M.A. Dobrovolskaia, S.E. McNeil, Nanoparticle interaction with plasma proteins as it relates to particle biodistribution, biocompatibility and therapeutic efficacy, Adv. Drug Deliv. Rev. 61 (2009) 428–437.
[3] S. Roux, B. Garcia, J.L. Bridot, M. Salome, C. Marquette, L. Lemelle, P. Gillet, L. Blum, P. Perriat, O. Tillement, Synthesis, characterization of dihydrolipoic acid capped gold nanoparticles, and functionalization by the electroluminescent luminol, Langmuir 21 (2005) 2526–2536.
[4] J. Tournebize, A. Sapin-Minet, R. Schneider, A. Boudier, P. Maincent, P. Leroy, Simple spectrophotocolorimetric method for quantitative determination of gold in nanoparticles, Talanta 83 (2011) 1780–1783.
[5] N.G. Bastús, E. Sánchez-Tilló, S. Pujals, C. Farrera, M.J. Kogan, E. Giralt, A. Celada, J. Lloberas, V. Puntes, Peptides conjugated to gold nanoparticles induce macrophage activation, Mol. Immunol. 46 (2009) 743–748.
[6] N.G. Bastús, E. Sánchez-Tilló, S. Pujals, C. Farrera, M.J. Kogan, E. Giralt, A. Celada, J. Lloberas, V. Puntes, Homogeneous conjugation of peptides onto gold nanoparticles enhances macrophage response, ACS Nano. 3 (2009) 1335–1344.
[7] C. Brandenberger, B. Rothen-Rutishauser, C. Mühlfeld, O. Schmid, G.A. Ferron, K.L. Maier, P. Gehr, A.G. Lenz, Effects and uptake of gold nanoparticles deposited at the air–liquid interface of a human epithelial airway model, Toxicol. Appl. Pharmacol. 242 (2010) 56–65.
[8] E. Hutter, S. Boridy, S. Labrecque, M. Lalancette-Hébert, J. Kriz, F.M. Winnik, D. Maysinger, Microglial response to gold nanoparticles, ACS Nano. 4 (2010) 2595–2606.

Pierre Leroy
Anne Sapin-Minet
Anna Pitarch
Ariane Boudier
Juliana Tournebize
EA 3452 Cibles Thérapeutiques, Formulation et Expertise Préclinique du Médicament, Faculty of Pharmacy, Nancy-University, BP 80403, 54001 Nancy Cedex, France
E-mail address: pierre.leroy@pharma.uhp-nancy.fr (P. Leroy)

Raphaël Schneider [b]
Laboratoire Réactions et Génie des Procédés, UPR 3349, Nancy-University, CNRS, 1, rue Grandville, BP 20451, 54001 Nancy Cedex, France

Available online 3 May 2011

1089-8603/$ - see front matter
doi:10.1016/j.niox.2011.04.012

Table 1
Literature data concerning interactions between various kinds of gold nanoparticles and cultured macrophage-cell types.

Particles					Cells			Results				References
Surface ligand	Properties				Cell type	Incubation		Toxicity	Internalization	Macrophages Activation	Inhibition of LPS activation	
	Size (nm)	Zeta potential (mV)	Shape	λ_{max} (nm)		Dose	Time (h)					
Citrate (PEG?)	10–15	ND	Spherical	ND	Murine macrophages (RAW264.7)	[Au] = 10–40 μg/mL	22	40% [GNP] = 80 μg/mL	ND	ND	Yes (dose dependent manner)	[1]
Citrate	12	−36	Spherical	518	Murine bone marrow macrophages	Quantity of particles delivering 10^{-6} M of peptide	6	<10%	No	No proliferation No secretion of pro-inflammatory cytokines	ND	[5,6]
Cys SAP (short peptide)	12	+2	Spherical	528				<10%	Yes (specific receptor)	Decrease of proliferation Secretion of pro-inflammatory cytokines	ND	
Cys AGIP (long peptide)	17	−7	Spherical	526				<10%	Yes (specific receptor)	Decrease of proliferation Secretion of pro-inflammatory cytokines	ND	
Citrate	15	ND	Spherical	ND	Human triple cell co-culture (epithelial cells A549/ primary macrophages/ primary dendritic cells)	[Au] = 200–2000 μM	4 and 24	*ND*	Yes (20%)	No secretion of pro-inflammatory cytokines	No inhibition	[7]
PEG	23	−22	Spherical	524	Microglia cells (N9)	[GNP] = 10^3–10^{11} GNP/mL	24	20% ([GNP] = 10^6 GNP/mL)	No	Secretion of pro-inflammatory cytokines	ND	[8]
	77	−9	Urchin	610				0%	Yes			
	12	−23	Rod	514				0%	No			
CTAB	23	+42	Spherical	522				>90% [GNP] = 10^6 GNP/mL	Yes	No production of Nitric oxide		
	77	+39	Urchin	618				20% [GNP] = 10^{11} GNP/mL	Yes			
	12	+46	Rod	512				0%	Yes			

ND: Not determined.
SAP: sweet arrow peptide (prolin rich cell penetrating peptide); AGIP: amyloid growth inhibitory peptide; PEG: poly(ethylene glycol); CTAB: cetyltrimethylammonium bromide.

Letter to the Editor / Nitric Oxide 25 (2011) 54–56

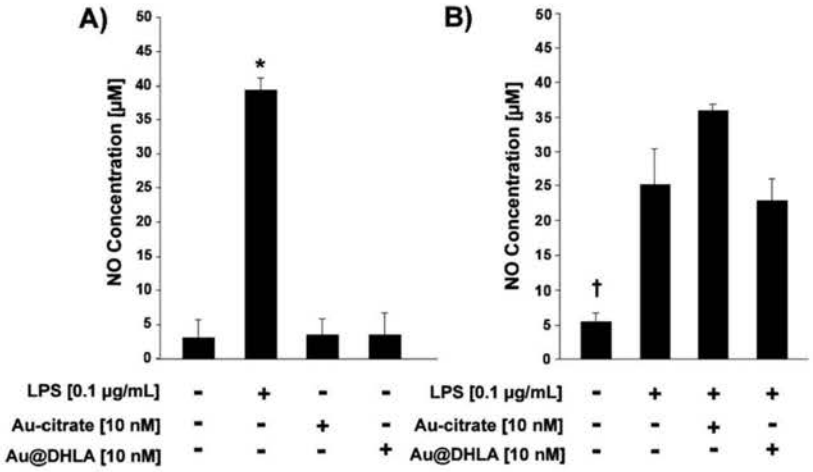

Fig. 1. Activation (A) and inhibition (B) studies of rat alveolar macrophages (NR8383) incubated with gold nanoparticles stabilized with citrate ions (Au-citrate) and capped with dihydrolipoic acid (Au@DHLA) at a concentration of 10 nM. Cells were exposed to GNP: for a 24-h period (A); successively to GNP (4 h) and LPS (18 h) (B). Nitric oxide concentrations in culture medium were measured by using conventional Griess colorimetric method. Values correspond to mean ± standard deviation of 3 independent experiments. $p < 0.05$ in relation to the control (without LPS and GNP) * (A) and to LPS-treated cells but not exposed to GNP † (B) when all the experiments were compared and the non-parametric Mann and Whitney randomised test were performed for calculations.

Elsevier Editorial System(tm) for International Journal of Pharmaceutics
Manuscript Draft

Manuscript Number:

Title: Impact of gold nanoparticle coating on redox homeostasis

Article Type: Research Paper

Section/Category: Pharmaceutical Nanotechnology

Keywords: gold nanoparticles; redox status; reduced glutathione; S-nitrosoglutathione; macrophages; cell uptake.

Corresponding Author: Dr. Anne Sapin-Minet,

Corresponding Author's Institution:

First Author: Juliana Tournebize

Order of Authors: Juliana Tournebize; Ariane Boudier; Olivier Joubert; Housam Eidi; Grzegorz Bartosz; Philippe Maincent; Pierre Leroy; Anne Sapin-Minet

Abstract: Gold nanoparticles (AuNP) hold great potential for biomedical applications. This study was aimed at examination of the effect of AuNP coating on the redox status of their environment. Two kinds of AuNP were tested, similar by shape and size, but with different surface coating: either stabilized with citrate or functionalized with dihydrolipoic acid (Au@DHLA NP). Interestingly, whereas citrate-stabilized AuNP interact in vitro with reduced glutathione (GSH) and S-nitrosoglutathione, Au@DHLA NP do not interfere with both biomolecules. Albumin exhibits higher affinity toward citrate-stabilized AuNP than Au@DHLA NP, increasing their hydrodynamic diameter (8.0- and 1.3-fold, respectively). Furthermore, the AuNP coating affects also their internalization by macrophages (which was two fold higher for citrate-stabilized AuNP), following an exposure to a subtoxic NP concentration (10 nM, 80 % viability). Citrate-stabilized AuNP were found to decrease the intracellular GSH level (ca. 20 %), with no increase in reactive oxygen species production. Furthermore, these AuNP did not induce apoptosis (as shown by caspase-3 activity and nfkb2 transcription factor), and also did not activate gene expression related to oxidative stress (ncf1) and inflammatory response (tnfα). The present data highlight that the functionalization of AuNP with DHLA decreases their reactivity with biomolecules and cells, resulting in a promising medical platform.

Suggested Reviewers: Stéphane Roux Pr
Professor, Université de Franche-Comté
stephane.roux@univ-fcomte.fr

Sylvie Bégu MCU
Assistant Professor, Institut Charles Gerhardt Montpellier, Université de Montpellier
sylvie.begu@enscm.fr

Edmond Creppy Pr
Professor, Laboratoire de Toxicologie, Université Victor Segalen Bordeaux 2 U.F.R. des Sciences Pharmaceutiques
edmond.creppy@tox.u-bordeaux2.fr

Chapitre III

Arnaud Beduneau Dr
Assistant Professor, Laboratory of Pharmaceutical Engineering University Franche-Comté
arnaud.beduneau@univ-fcomte.fr

Cover Letter

Dr Anne SAPIN-MINET
CITHEFOR-EA3452,
"Cibles thérapeutiques, formulation et expertise préclinique du médicament"
Faculté de Pharmacie
5, rue Albert Lebrun
BP 80403
F-54001 NANCY Cedex
FRANCE
Phone : + 33 3 83 68 22 97; fax : +33 3 83 68 23 01
e-mail: anne.sapin@pharma.uhp-nancy.fr

Nancy, May 04th 2012

To the Editor-in-Chief of International Journal of Pharmaceutics,

Sir,

Please find enclosed a manuscript by J. Tournebize *et al.* entitled "*Impact of gold nanoparticle coating on redox homeostasis*" for submission to your journal.

Gold nanoparticles are widely described for therapeutic carrier potentialities. The manuscript deals with the impact of gold nanoparticles (AuNP) onto intracellular redox homeostasis. Despite the number studies available on acute cytotoxicity of gold nanoparticles (AuNP), to our knowledge, there is a concern about the potential impact of AuNP, used in sub-lethal concentrations exposure, on the early events of cellular cytotoxicity. Based on the above facts, in this original manuscript we evaluated how AuNP coating influences cells uptake and redox status. To that end, we have prepared two kinds of AuNP previously described in the literature, with different surface coating, either stabilized with citrate or functionalized with dihydrolipoic acid. Our results revealed the importance of AuNP coating to modulate the uptake by macrophages and reactivity towards redox-regulating molecules, two crucial parameters for drug delivery carrier development.

All authors have read the present manuscript and approved its submission to International Journal of Pharmaceutics; the manuscript, or part of it, has neither been published nor is currently under consideration for publication by any other *journal*.

Waiting for the reviewers' comments

Yours faithfully,

Anne Sapin-Minet

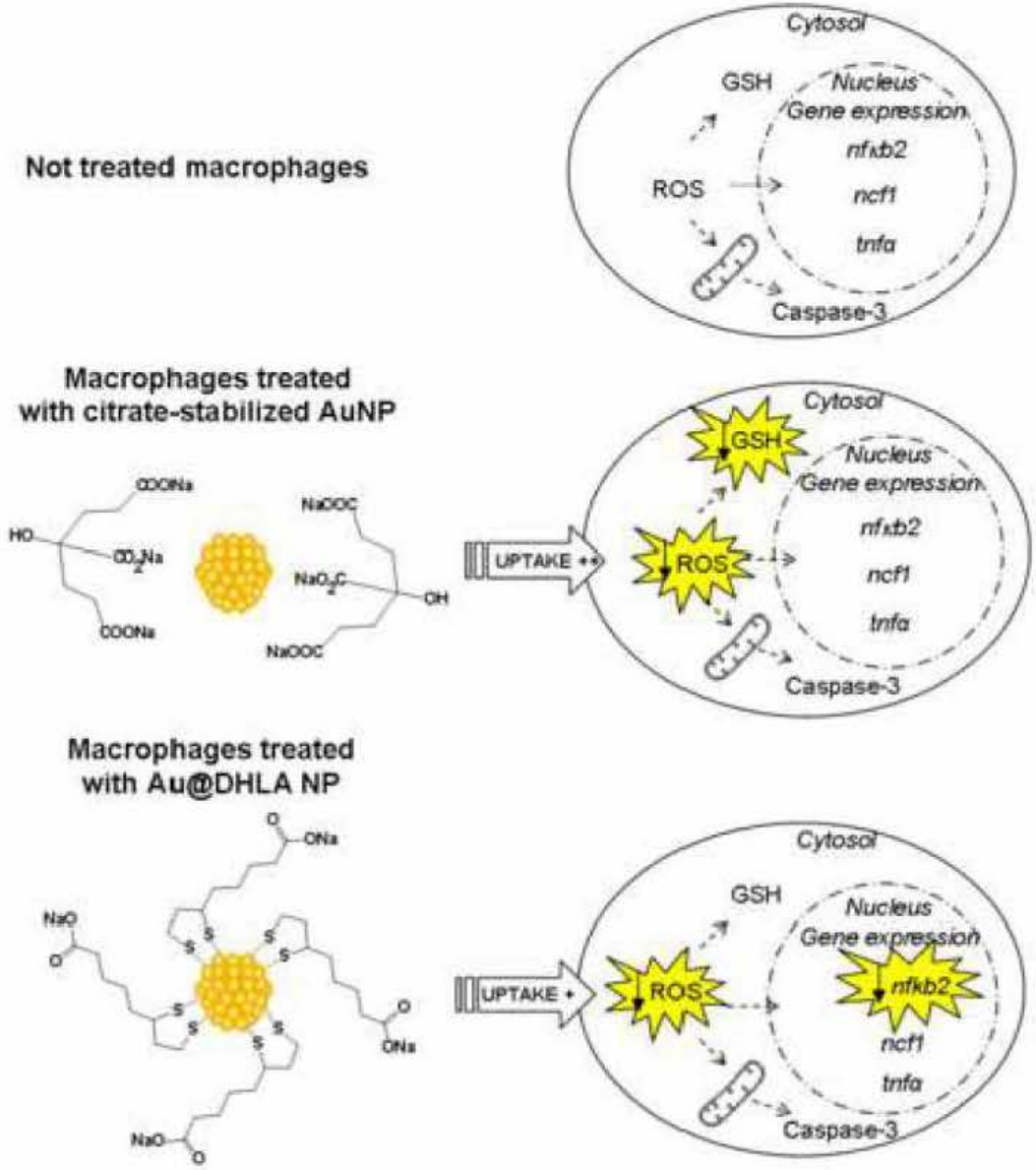
Not treated macrophages
Cytosol
GSH
Nucleus
Gene expression
nfκb2
ROS
ncf1
tnfa
Caspase-3
Macrophages treated with citrate-stabilized AuNP
UPTAKE ++
Macrophages treated with Au@DHLA NP
UPTAKE +

Impact of gold nanoparticle coating on redox homeostasis

J. Tournebize[a], A. Boudier[a], O. Joubert[a], H. Eidi[a], G. Bartosz[b,†], P. Maincent[a], P. Leroy[a], A. Sapin-Minet[a,*]

[a] *CITHEFOR, EA 3452, « Cibles thérapeutiques, formulation et expertise préclinique du médicament », Faculty of Pharmacy, Université de Lorraine, Nancy, France*

[b] *Department of Molecular Biophysics, University of Lodz, Lodz, Poland*

[†] Guest Professor at Université de Lorraine

* Corresponding author:

e-mail: anne.sapin@pharma.uhp-nancy.fr

Phone: + 33 3 83 68 22 97

Fax: +33 3 83 68 23 01

Abstract

Gold nanoparticles (AuNP) hold great potential for biomedical applications. This study was aimed at examination of the effect of AuNP coating on the redox status of their environment. Two kinds of AuNP were tested, similar by shape and size, but with different surface coating: either stabilized with citrate or functionalized with dihydrolipoic acid (Au@DHLA NP). Interestingly, whereas citrate-stabilized AuNP interact *in vitro* with reduced glutathione (GSH) and *S*-nitrosoglutathione, Au@DHLA NP do not interfere with both biomolecules. Albumin exhibits higher affinity toward citrate-stabilized AuNP than Au@DHLA NP, increasing their hydrodynamic diameter (8.0-and 1.3-fold, respectively). Furthermore, the AuNP coating affects also their internalization by macrophages (which was two fold higher for citrate-stabilized AuNP), following an exposure to a subtoxic NP concentration (10 nM, 80 % viability). Citrate-stabilized AuNP were found to decrease the intracellular GSH level (*ca.* 20 %), with no increase in reactive oxygen species production. Furthermore, these AuNP did not induce apoptosis (as shown by caspase-3 activity and *nfkb2* transcription factor), and also did not activate gene expression related to oxidative stress (*ncf1*) and inflammatory response (*tnfα*). The present data highlight that the functionalization of AuNP with DHLA decreases their reactivity with biomolecules and cells, resulting in a promising medical platform.

Keywords: gold nanoparticles; redox status; reduced glutathione; *S*-nitrosoglutathione; macrophages; cell uptake.

Abbreviations: AuNP, gold nanoparticles; citrate-stabilized AuNP, gold nanoparticles stabilized with citrate ions; DHLA, dihydrolipoic acid; Au@DHLA NP, gold nanoparticles capped with dihydrolipoic acid; GSH, reduced glutathione; GSNO, *S*-nitrosoglutathione; BSA, bovine serum albumin; ROS, reactive oxygen species; NDA, naphthalene-2,3-dicarboxyaldehyde; DAN, 2,3-diaminonaphthalene; $DCFH_2$-DA, 2',7'-dichlorofluorescin diacetate; DCF, dichlorofluorescein; TEM, transmission electronic microscopy; D_h, hydrodynamic diameter; PBS, phosphate-buffered saline; K_{sv}, fluorescence quenching constants; DMEM, dulbecco's modified Eagle's medium; FCS, fetal calf serum; ICP-MS, inductively coupled plasma mass spectroscopy; qRT-PCR, reverse transcription quantitative real time PCR; DLS, dynamic light scattering; RNS, reactive nitrogen species; ABTS, 2,2'-azino-di(3-ethylbenzthiazoline-6-sulphonate; ANOVA, one-way analysis of variance; *nfkb2*, nuclear factor-kappa B transcription factor; *ncf1*, neutrophil cytosolic factor 1; *tnfα*, tumor necrosis factor-alpha.

1. Introduction

Gold nanoparticles (AuNP) are some of the most widely used nanomaterials due to their unique physico-chemical properties such as excellent absorbance and scattering of light, simple synthesis methods and ease of surface modification with many bioactive molecules (Paciotti et al., 2004). Gold NP are widely utilized for analytical purposes and are expected to be employed in therapy. They have been used, *e.g.* for sensitive detection of reactive oxygen species (ROS) (Lee et al., 2009), cysteine (Li and Li, 2009), Cu^{2+} (Lee et al., 2010) and Pb^{2+} (Chai et al., 2010), for monitoring of nuclease (Zhao et al., 2008) and hyaluronidase activity (Lee et al., 2008), and lastly for labeling of proteins and cells (Lin et al., 2009). Gold NP have been proposed for cancer imaging and death induction of cancer cells (Loo et al., 2005), for intracellular gene regulation (Rosi et al., 2006) but also as a vehicle for TNF-α delivery to tumor cells (Paciotti et al., 2004). A phase I clinical trial showed that high doses of TNF-α linked to AuNP could be safely given to 30 patients with various advanced solid tumors (Libutti et al., 2010). Recently, Swiss Regulatory Agency approved a phase I clinical trial study with insulin-coated AuNP for oral administration to healthy volunteers (Alan, 2011).

Despite the potential use of AuNP in therapy, recent literature contains conflicting data regarding AuNP cytotoxicity and disturbances of redox status. Size (Pan et al., 2007), surface functionalization or coating (Goodman et al., 2004; Hauck et al., 2008; Shukla et al., 2005; Takahashi et al., 2005), shape (Hutter et al., 2010) are some of decisive parameters that possibly induce cell damages (Alkilany and Murphy, 2010; Soenen et al., 2011; Unfried et al., 2007). Related to AuNP concentration used, studies suggested the oxidative stress as a key mechanism leading to toxicity (Gao et al., 2011; Jia et al., 2009; Karakoti et al., 2010; Pan et al., 2009; Zhao et al., 2011). Looking over the cytotoxicity assays commonly used, the studies cited above determined membrane damages or metabolic irregularities of cells after exposure

to high (and often unrealistic for a therapeutic approach) concentrations of AuNP. Therefore, deleterious effects following one or repetitive exposure to low amounts of AuNP are difficult to reveal and the use of early-warning signals becomes mandatory. In particular, redox homeostasis alterations and beginnings of oxidative stress are likely early events that can be observed at sub-lethal concentrations and under short exposure to AuNP.

To the best of our knowledge, there is no systematic study of the impact of AuNP on redox homeostasis using sub-lethal concentrations. Based on the above facts, we proposed to study two kinds of AuNP with considerable interest for biological applications and able to carry a pharmaceutical molecule. They differ in surface coating, being either stabilized with citrate (citrate-stabilized AuNP) or functionalized with a dithiol, *i.e.* dihydrolipoic acid (Au@DHLA NP). In a previous study, we observed that a concentration of 10 nM of either citrate-stabilized AuNP or Au@DHLA NP, which corresponds to 80 % of viability, did not activate nor inhibit NO-production by macrophages (Leroy et al., 2011). The aim of this study was to refine these preliminary observations, studying consequences of the exposure to AuNP with different coatings and at sub-lethal concentrations, onto redox homeostasis. To identify early-warning signals of an oxidative stress, an integrative approach was lead. First, effects of AuNP coating on redox-regulating molecules interactions, including: reduced glutathione (GSH), *S*-nitrosoglutathione (GSNO) and bovine serum albumin (BSA) were studied in cell-free conditions. Secondly, the effect of AuNP coating on macrophage uptake, and modifications of redox status biomarkers such as reactive oxygen species (ROS), GSH, and mRNA expression related to apoptosis (*nfκb2*), oxidative stress (*ncf1*) and inflammatory response (*tnfα*) in the cells were measured.

2. Materials and methods

2.1. Reagents and standards

All reagents and solvents were of analytic grade and used without further purification. Tetrachloroauric acid trihydrate ($HAuCl_4 \bullet 3H_2O$), α-lipoic acid, bovine serum albumin (BSA, fraction V), reduced glutathione (GSH), naphthalene-2,3-dicarboxyaldehyde (NDA), *S*-nitrosoglutathione (GSNO), 2,3-diaminonaphthalene (DAN), 2',7'-dichlorofluorescin diacetate ($DCFH_2$-DA), dichlorofluorescein (DCF), and 2,2'-azino-di(3-ethylbenzthiazoline-6-sulphonate (ABTS) were purchased from Sigma-Aldrich (France). Phosphate-buffered saline (PBS) solution was prepared as follows: $[Na_2HPO_4] = 4 \times 10^{-2}$ M, $[KH_2PO_4] = 4 \times 10^{-3}$ M, and $[NaCl] = 1 \times 10^{-1}$ M, final pH was adjusted to 7.4. Ultrapure deionized water (> 18.2 MΩ.cm) was used for the preparation of all solutions.

2.2. Synthesis of gold nanoparticles (Citrate-stabilized AuNP and Au@DHLA NP)

Before synthesis, all the glassware was thoroughly washed with *aqua regia* (3:1 HCl/HNO_3) and rinsed with ultrapure deionized water prior to use. Citrate-stabilized AuNP were prepared as previously reported (Brown et al., 1999). Briefly, at room temperature, 1 mL of 1 % (w/v) $HAuCl_4 \bullet 3H_2O$ in water was added to 90 mL of water. After 1 min of stirring, 2.0 mL of a 38.8 mM sodium citrate solution in water were added. One minute later, 1.0 mL of a freshly 0.075 % (w/v) $NaBH_4$ solution in a 38.8 mM sodium citrate solution was quickly injected into the reaction flask. The reaction medium was stirred for an additional 5-min period and the resulting deep red colloidal solution was immediately stored in the dark at 4ºC.

Gold nanoparticles capped with dihydrolipoic acid (Au@DHLA NP) were prepared as follows: a 600 µmoles of α-lipoic acid in 10 mL of 0.5 M aqueous NaOH solution was added to 25 mL of freshly prepared citrate-stabilized AuNP. The reaction mixture was stirred for 24 h at room temperature (20-23°C) before dialysis. The non-reacted α-lipoic acid remaining in the solution after the cap-exchange was removed by dialysis against PBS for 48 h using a dialysis bag made of regenerated cellulose with a molecular weight cut-off of 10 kDa (Roth®, France). The dialysis medium was changed once to fresh PBS after 24 h. The resulting Au@DHLA NP solution was stored in the dark at 4°C.

2.3. Physico-chemical characterisation of gold nanoparticles

A double-beam UV-visible spectrophotometer (model Uvikon 932, Kontron) was used for spectra recordings and absorbance measurements. Molar concentrations of AuNP were calculated using molar absorbance values previously reported (i.e. $\varepsilon_{\text{citrate-stabilized AuNP}} = 1.2 \times 10^7\ M^{-1}cm^{-1}$, $\varepsilon_{\text{Au@DHLA NP}} = 0.5 \times 10^7\ M^{-1}cm^{-1}$) (Tournebize et al., 2011).

Transmission electronic microscopy (TEM) images were recorded using a Philips CM20 instrument with a LaB_6 cathode operating at 200 kV. Gold NP solutions were deposited onto a 400 mesh carbon film copper grids. The average diameter of the gold core was calculated for each AuNP sample by counting *ca.* 200 individual particles from the TEM images.

The hydrodynamic diameter (D_h) and zeta potential of AuNP were measured using a Zetasizer Nano ZS (Malvern Instruments, UK) and these measurements were performed at 20ºC using low volume polystyrene and disposable capillary cells, respectively. All D_h reported are volume averages values, based on three independent measurements of two AuNP batches. Zeta potential measurements were carried out in ultrapure water (implying

preliminary dialysis of Au@DHLA NP for 24 h). All surface charges reported are averages based on three measurements of one batch of AuNP.

2.4. Interaction of gold nanoparticles with reduced glutathione and S-nitrosoglutathione

Aliquots of either GSH or GSNO solutions at a concentration of 72 µM were prepared in PBS and ultrapure deionized water, respectively. Then, 550 µL of AuNP solution at a final concentration of 5, 10, 20, and 30 nM were mixed with 50 µL of 72 µM of GSH or GSNO. Samples were kept at room temperature (20 – 23°C) for 5 min.

For the measurement of the remaining GSH, 50 µL of HCl (0.6 M) were added to samples previously described, and the resulting mixture was centrifuged at 42,000 × *g* for 20 min at 4°C. The supernatant (600 µL) was mixed with 50 µL of NaOH (1 M), 140 µL of borate buffer (1 M, pH 9.2), and 10 µL of NDA (5.4 mM) prepared in ethanol and the mixture was incubated for an additional 10-min period at 4ºC. Fluorescence intensity was read at λ_{exc} = 472 nm and λ_{em} = 528 nm (Lewicki et al., 2006) in a spectrofluorimeter (Hitachi F-2000, France). Concentrations of GSH were calculated using a calibration curve in the range of 1.5 – 7.5 µM.

For the measurement of the nitric oxide ($^{\bullet}$NO) released from GSNO, 60 µL of DAN (105 µM) prepared in HCl (0.6 M) were added to each diluted sample (2 – 10 times) and the resulting mixture was centrifuged at 42,000 × *g* for 20 min at 4°C. The supernatant (600 µL) was mixed with 40 µL of NaOH (1 M). Fluorescence intensity was read at λ_{exc} = 375 nm and λ_{em} = 415 nm (Cook et al., 1996) in a spectrofluorimeter (Hitachi F-2000, France). Concentrations of $^{\bullet}$NO were calculated by using a calibration curve of nitrite in the range of 0.05 – 0.5 µM.

2.5. Protein binding assay

Aliquots (500 µL) of a BSA solution prepared in PBS at a concentration of 106 mg.L^{-1} were mixed with AuNP prepared in PBS (500 µL); the resulting mixtures were kept at 37°C for 1 h. The interaction between BSA and AuNP was monitored by measuring the intrinsic tryptophan fluorescence of BSA (λ_{exc} = 280 nm, λ_{em} = 355 nm) (Pramanik et al., 2008). Stern-Volmer equation ($I°/I = 1 + K_{sv}$ [AuNP]) was applied to calculate the fluorescence quenching constants (K_{sv}) of the different kinds of AuNP. I° and I represent the fluorescence intensity in the absence and presence of AuNP, respectively. Hydrodynamic diameters of AuNP (10 nM) incubated with or without BSA were measured in purified water.

2.6. Reactivity studies between gold nanoparticles and 2,2'-azino-di(*3-ethylbenzthiazoline*-6-*sulphonate*) (ABTS)

An $ABTS^{\bullet+}$ stock solution was prepared by mixing 5.4 mM ABTS with 1.7 mM potassium persulfate in PBS, which was placed in the dark at room temperature for 16 h to give a dark blue solution. Molar concentrations of $ABTS^{\bullet+}$ were calculated using molar absorbance value reported previously (*i.e.* $\varepsilon_{734\,nm} = 1.5 \times 10^4\ M^{-1}cm^{-1}$) (Re et al., 1999). The interaction between $ABTS^{\bullet+}$ and AuNP was studied as follows: 1125 µL of Au@DHLA NP (in PBS) and citrate-stabilized AuNP (in water) were reacted with 375 µL of 200 µM $ABTS^{\bullet+}$ solution in PBS. After 2-h incubation at room temperature (20 – 23°C), the reaction medium was analysed by spectrophotocolorimetry at 734 nm.

2.7. Interaction of gold nanoparticles with cells

2.7.1. Cell culture

The NR8383 rat alveolar macrophage cell line was purchased from the American Type Culture Collection (CRL-2192, ATCC, Manassas, VA). Cells were grown in Dulbecco's modified Eagle's medium (DMEM: GIBCO, Invitrogen®, France) supplemented with 15 % (v/v) decomplemented fetal calf serum (FCS, Eurobio, Les Ullis, France) and a mixture of antibiotics/antimycotic compounds (0.25 $\mu g.mL^{-1}$ of amphotericin B, 100 $U.mL^{-1}$ of penicillin and 100 $\mu g.mL^{-1}$ of streptomycin) in humidified atmosphere of 5 % CO_2 and 95 % air at 37°C and split every 3 or 4 days.

2.7.2. Intracellular distribution of gold nanoparticles under transmission electron microscopy

Cells were dispensed (1×10^5 cells/well) into a 24-well microplate and grown overnight. Next, the tested AuNP suspensions at a concentration of 10 nM were added into the wells. After 24-h incubation, cells were washed three times with PBS solution (pH 7.4) and fixed with 0.1% glutaraldehyde in 0.1 M sodium cacodylate buffer (pH 7.4), then rinsed for 3 h in sodium cacodylate buffer and incubated for 30 min in 1 % osmium tetroxide in sodium cacodylate buffer, rinsed and dehydrated through a series of ethanol concentrations (50, 70, 80, 90 %), for 5 min at each step, then in 100 % ethanol for 3 × 20 min. The cells were then embedded in the epoxy resin. Cell monolayers on plastic wells were treated twice with 100% xylene and semi thin (1.5 mm) or ultra thin sections (70-90 nm) were performed. Cell sections were deposited onto a 400-mesh carbon film copper grid.

2.7.3. Uptake study of gold nanoparticles using inductively coupled plasma mass spectroscopy

To measure the intracellular concentration of AuNP, cells were dispensed (1×10^5 cells/well) into a 24-well microplate and grown overnight. Next, the cells were incubated with the tested AuNP suspensions at a concentration of 10 nM for different time periods (0.2, 0.5, 2, 6 and 24 h). After incubation, the cells were washed three times with PBS solution (pH 7.4), resuspended in 0.5 mL of ultrapure water and subsequently lysed by two cycles of freezing for 10 s in liquid nitrogen and then thawing in a 37°C water bath for 60 s. The lysates were digested with *aqua regia* (3:1 HCl/HNO_3) prior to measurement of gold content by inductively coupled plasma mass spectroscopy (ICP-MS) (Agilent 7500cx instrument, Belgium). Gold concentration in the sample was converted to the number of AuNP *per* liter by using the following equation 1, where $CAuCl_4^-$ corresponds to the value resulting from ICP-MS analysis which is divided by atomic mass of gold (197 $g.mol^{-1}$) and n_{atom} correspond to the number of gold atoms per AuNP (4595 and 1369 for citrate-stabilized AuNP and Au@DHLA NP, respectively) (Tournebize et al., 2011). Results were calculated as number of AuNP *per* mg of protein.

$$\mathbf{nAuNPs = (CAuCl_4^- \times N_A) / n_{atom}} \qquad \text{(Eq. 1)}$$

2.7.4. Intracellular reduced glutathione measurement

Reduced glutathione measurements were performed as previously described (Lewicki et al., 2006), with some modifications. Briefly, cells were dispensed (5×10^5 cells/well) into a 6-well microplate and grown overnight. Gold nanoparticles were added at a concentration

of 10 nM per well. After 24-h incubation, cells were washed three times with cold PBS solution (pH 7.4), resuspended in 1 mL of cold lysis solution (3.3 % perchloric acid, 0.1 M HCl and 2 mM EDTA) and then broken by vigorous vortexing for 2 min. Cells lysates were centrifuged at 10,000 × *g* at 4°C for 15 min and the pellet, containing proteins, was resuspended in 500 µL of 0.1 M NaOH. One hundred µL of supernatant, 400 µL of 0.1 M HCl and 2 mM EDTA, and 10 µL of NaOH 40 % (w/v) were mixed. Then, 60 µL of this mixture, 120 µL of borate buffer (0.4 M, pH 9.2) and 20 µL of NDA solution in ethanol were mixed in a 96-black well microplate and incubated in the dark at 4°C for 25 min. Fluorescence intensity was then measured at 485-nm excitation and 528-nm emission using a microplate reader (Biotek Synergy, USA). Concentrations of GSH were calculated using a calibration curve in the range of 0.7 – 3.2 µM. Results were calculated as nmol of GSH *per* mg of protein. Total protein amount in 0.1 M NaOH solution was determined by Lowry method (Lowry et al., 1951) using BSA as standard for calibration curve. Results are expressed as comparison to untreated cells (negative control) or cells exposed to polymer NP (Eidi et al., 2012) as positive control (Eudragit® RS, concentration equal to 100 $\mu g.mL^{-1}$ corresponding to 60% viability).

2.7.5. Intracellular ROS measurement

The production of intracellular ROS was measured using 2',7'-dichlorofluorescin diacetate ($DCFH_2$-DA). Briefly, cells were dispensed (5×10^5 cells/well) into 6-well microplates, grown overnight and AuNP were added (10 nM). Negative and positive controls corresponded to untreated cells and polymer NP, respectively. After 24-h incubation, the cells were washed three times with 1 mL PBS solution (pH 7.4), resuspended in 1 mL of 4 µM $DCFH_2$-DA solution, and incubated for 40 min at 37°C.

Then, the cells were pelleted by centrifugation (300 × *g* for 5 min at 20ºC) and lysed using a lysis buffer (0.5 M Tris in HCl, 1.5 M NaCl, 0.1% SDS, 1% Triton X-100 and 1 × protease inhibitor cocktail). The conversion of $DCFH_2$ to the fluorescent product (DCF) was measured using a microplate reader (Biotek Synergy, France), with 485-nm excitation and 528-nm emission, and a calibration curve of DCF in the range of 7.5 – 112 nM.

2.7.6. Detection of caspase-3 activity

Detection of caspase-3 activity in NR8383 macrophages was performed using the EnzChek Caspase-3 Assay kit #1 (Molecular Probes, Netherlands). Briefly, cells were dispensed (4×10^5 cells/well) and grown overnight into 6-well microplates. After 24-h incubation with the various AuNP (10 nM), the cells were washed three times in 1 mL PBS (pH 7.4), resuspended in 50 µL of lysis-buffer (200 mM Tris, pH 7.5, 2 M NaCl, 20 mM EDTA, 0.2 % Triton X-100), incubated on ice for 30 min, and centrifuged at 600 × g for 5 min at 4°C. Then 50 µL of Z-DEVD-AMC substrate was added and incubated for 30 min. Fluorescence was measured using a microplate reader (Biotek Synergy, France) with 340-nm excitation and 528-nm emission. Cells treated with 10 µM of camptothecin for 24 h served as the positive control. An Ac-DEVD-CHO inhibitor was used to confirm that the observed fluorescence signal in both induced and control cells populations is due to the activity of caspase-3-like proteases.

298 *2.7.7. Total RNA extraction, RNA reverse transcription and quantitative RT-PCR (qRT-*
299 *PCR)*
300
301 Cells were dispensed (5×10^5 cells/well) into 6-well microplates and grown overnight.
302 After 24-h incubation with AuNP (10 nM), the total RNA from cells was isolated using Trizol
303 (Invitrogen®, France) according to established protocols. RNA purity and concentration were
304 determined spectrophotometrically using a BioSpec-nano (Shimadzu, France). Total RNA
305 (1 µg) from control or treated cell samples were reverse-transcribed with 50 nmol of oligo
306 (dT) using M-MLV reverse transcriptase (RT) (EC 2.7.7.4.49, Invitrogen, France) following
307 manufacturer's protocol. qRT-PCR was performed with a Stratagene Mx3000p system and
308 Mesa Green qPCR MasterMix Plus for SYBR® (RT-SY2X-03-WOULR, Eurogentec, USA).
309 Briefly, 100 ng of reverse-transcripted RNA from each sample were mixed with appropriate
310 concentrations of tested gene primers (Table 1) and the Mesa Green qPCR Master Mix.
311 *MRPSI8a (s18)* was used as internal control gene. PCR amplifications were carried out as
312 follows: 5 min at 95°C; 45 cycles (15 s at 95°C, 40 s at 60°C and 40 s at 72°C). A standard
313 curve was made for each gene and the subsequent slope was used to calculate the PCR
314 reaction efficiency ($E=10^{(-1/slope)}$). For each sample, the gene expression level was calculated
315 from the threshold cycle (C_t), which is the number of cycles necessary for the first detection
316 of a PCR product.
317
318 *2.8. Statistical analysis*
319
320 Data were compared by *t*-Student test, one-way analysis of variance (ANOVA) and
321 Tukey HSD post-hoc test or Mann-Whitney U test. For each sample group, the homogeneity
322 of variance was calculated using the Levene's test. All statistical analyses were performed

323 with the SigmaStat 3.11 software package (Sistat Inc., USA). A value of $p < 0.05$ was
324 considered as statistically significant.

3. Results and discussion

The use of AuNP in biomedical fields requires stability in physiological media and no adverse effect toward living organisms. Several recent reports in the literature have shown that the safety of AuNP depends on their physico-chemical characteristics (Goodman et al., 2004; Hauck et al., 2008; Pan et al., 2009; Pan et al., 2007; Takahashi et al., 2005). Stability and understanding of interactions with cell compounds and compartments are crucial parameters to propose a platform for drug delivery.

Among different types of AuNP, citrate-stabilized AuNP are largely described as potential drug delivery systems (Paciotti et al., 2004; Zhao et al., 2008). Nevertheless, due to the strong reactivity of free electrons present on their surface, citrate-stabilized AuNP are sensitive to environmental factors (such as pH < 6, high electrolytes levels, organic solvent) having the tendency to easily aggregate when used in these conditions. To solve this issue, AuNP can be stabilized by a large variety of natural and synthetic surface groups (cysteine, glucose, biotin, dendrimers, cetyltrimethylammonium bromide,…) and the most efficient capping agents are thiol-modified ligands (*e.g.* dithiol (Roux et al., 2005), trithiol species (Li et al., 2002) or multithiolated – α, β and γ – cyclodextrin (2 – 7 nm) (Liu et al., 2000)), which renders the AuNP effectively more stable due to the simultaneous anchorage onto AuNP surface of most of the sulfur ends of the molecules.

Dihydrolipoic acid (DHLA) is a dithiol obtained by the reduction of lipoic acid; DHLA is an endogenous thiol with a major antioxidant role (Goraca et al., 2011). It also appears very attractive to limit the aggregation and helps to overcome the lack of stability of AuNP colloids. Gold NP stabilized with DHLA (Au@DHLA NP) have already been reported (Roux et al., 2005). However, to the best of our knowledge, there is no report in the literature about the impact that Au@DHLA NP might have on cell constituents. In the present study, we

employed two types of AuNP (citrate-stabilized AuNP and Au@DHLA NP) with the same core particle size to examine whether the surface coating could influence the redox homeostasis and modulate the AuNP interactions with low-molecular redox active compounds, *i.e.* GSH and GSNO, with proteins and with cells.

3.1. Synthesis and physico-chemical characterization of gold nanoparticles

Citrate-stabilized AuNP were first synthesized by reduction of $HAuCl_4$ using sodium borohydride in the presence of citrate ions. Next, the as-synthesized AuNP were functionalized with DHLA from the *in situ* reduction of lipoic acid. An aqueous NP suspension was directly obtained.

The size of the obtained particles was determined by a combination of TEM and dynamic light scattering (DLS) experiments. Using TEM, the core diameter of citrate-stabilized AuNP and Au@DHLA NP was found to be equal to 5.3 nm and 3.5 nm, respectively. A spherical shape, monodisperse and unaggregated distribution dominated in both NP types (Fig. 1). Gold NP exhibit hydrodynamic diameters (D_h) – 6.5 nm and 7.2 nm for citrate-stabilized AuNP and Au@DHLA NP, respectively – which were larger than the metallic core diameter. This can be explained by the thiol ligands outspread in aqueous solution while they are highly contractive after drying on TEM copper grids but also by the solvatation layer around the AuNP in aqueous media. The derived DLS size distributions were found to be monomodal with a relative narrow distribution, confirming the absence of aggregation after the capping exchange (Fig. 1).

The surface charge assessed by zeta potential measurements (ζ), which controls the colloidal stability and inter-particle interactions, confirms the presence of negative charges on the AuNP surfaces. A significant ($p < 0.05$) decrease of ζ potential values was observed for

375 Au@DHLA NP (-64 ± 4 mV) as compared to citrate-stabilized AuNP (-51 ± 3 mV), due to
376 the displacement of citrate ions by DHLA, confirming the functionalization of AuNP by this
377 ligand. Carboxylate groups on the DHLA and citrate structures confer negative charge on
378 AuNP.

379 Similar results were obtained by Roux *et al.* (2005), mentioning a hydrodynamic
380 diameter of 5 – 8 nm and a negative charge (-35 mV). The different value of zeta potential
381 could be due to the different ratio [DHLA]/[Au] surface used during synthesis (ratio equal to
382 9 instead of 222 in our study after optimisation).

383

384 *3.2. Interactions between AuNP and biomolecules implied on redox status in cell-free*
385 *conditions*

386

387 Understanding the reactivity between biomolecules and AuNP in cell-free conditions is a
388 first investigation to predict the AuNP fate in the human body. In this work, AuNP
389 interactions with reduced glutathione (GSH), *S*-nitrosoglutathione (GSNO) and bovine serum
390 albumin (BSA) were explored, because of their involvement in maintaining the redox
391 homeostasis.

392

393 Glutathione is the most effective agent used by cells for the detoxification of ROS and
394 electrophilic xenobiotics (Sies, 1999). Its thiol group can be nitrosylated, leading to GSNO, a
395 major endogenous molecule involved in storage and transport of $^{\bullet}$NO (Al-Sa'Doni and Ferro,
396 2000). As shown in Fig. 2a, a linear (r^2 = 0.9974) dose-response relationship was observed
397 after interaction of citrate-stabilized AuNP and GSH, and a decrease of 70 % of GSH initial
398 concentration was observed at a concentration of 30 nM. In contrast, Au@DHLA NP did not
399 react with GSH, even at 30 nM. Gold NP core affinity for the thiol group of GSH has already

been described in the literature and ligand exchange between GSH and citrate-stabilized AuNP are facilitated by the weak electrostatic binding between citrate and AuNP core (Zhao et al., 2011). On the contrary, DHLA established covalent bonds with gold atoms at the NP surface, involving its two thiol groups, and, as a consequence, further ligand exchange will not easily occur. Furthermore, this interaction is also limited by electrostatic repulsion between the carboxyl groups of GSH and DHLA.

As the affinity of AuNP to thiol groups is known, the propensity to attach the GSH moiety of GSNO through cleavage of S-N bond and $^{\bullet}$NO release is expected. As shown in Fig. 2b, a linear (r^2 = 0.9909) dose-response relationship was observed after interaction of citrate-stabilized AuNP with GSNO, and it was found that the higher concentration of citrate-stabilized AuNP is, the higher concentration of $^{\bullet}$NO is released. The same phenomenon was observed by Jia *et al.* (2009): a release of $^{\bullet}$NO from GSNO was observed in a lesser extent when interacting with GSH functionalized AuNP in comparison with citrate-stabilized AuNP. Interestingly, citrate-stabilized AuNP were found to exhibit higher (two times) reactivity with GSH when compared to GSNO. This can be explained by the fact that the cleavage of nitrogen-sulfur bond in GSNO is restricted by bond-dissociation energy (between 22 and 32 kcal/mol) (Baciu and Gauld, 2003). Our experiments implying GSH and GSNO demonstrated considerable higher resistance to redox molecule exchange of Au@DHLA NP compared to citrate-stabilized AuNP.

During last decade, albumin (Bovine Serum Albumin) has been the most widely used protein model to evaluate protein-NP interactions (Pramanik et al., 2008). Albumin, the main extracellular protein in the blood, participates in the maintenance of a constant redox potential in the extracellular fluids having certain redox buffer capacity (Era et al., 1995). Indeed, albumin exerts a redox buffering action in plasma, by a variety of thiol-exchange reactions (Summa et al., 2007). Albumin reactions rely on a conserved reactive cysteine-34 that has an

unusually low pK_a value, equal to 5-7 (Summa et al., 2007). The interaction between AuNP and BSA in PBS medium (pH 7.4) was explored by means of fluorescence and DLS techniques. Bovine serum albumin has an intrinsic fluorescence mainly originating from its tryptophan residues. The resulting fluorescence was quenched with addition of AuNP. Moreover, the fluorescence intensity decreased gradually when AuNP concentration increased (Fig.2c). The Stern-Volmer constant (K_{sv}) for citrate-stabilized AuNP and Au@DHLA NP was found to be 0.091 ± 0.003 nM^{-1} and 0.047 ± 0.003 nM^{-1} respectively, showing that BSA exhibits higher (2 times) affinity toward citrate-stabilized AuNP when compared to Au@DHLA NP. These observations were confirmed by measuring the D_h of AuNP in presence of BSA after incubation at 37°C for 1 h in PBS. First, we explored the effects of incubation at 37°C for 1 h on the colloidal stability of AuNP. As shown in Fig. 2d, the D_h of citrate-stabilized AuNP changed from 6 to 1180 nm. Under the same experimental conditions, no increase of D_h and no sign of aggregation were observed for Au@DHLA, indicating again higher colloidal stability. Second, we evaluated the effects of BSA on the D_h of AuNP. Interestingly, the addition of BSA caused a smaller increase of citrate-stabilized AuNP D_h from 6 to 40 nm, than Au@DHLA NP, where a increase of 7 to 10 nm was observed. These results demonstrate that due to its two anchoring groups to the Au metallic surface, DHLA provides enhanced stability to AuNP in PBS medium when compared to citrate-stabilized AuNP. Moreover, these data showed that the capping by DHLA decreased the interaction with BSA. Albumin acts in plasma by oxidation and thiol exchange: this reactivity could explain interactions with the citrate-stabilized AuNP core establishing covalent link with cysteine residue. For Au@DHLA NP and BSA interactions, possibilities of BSA thiol anchorage are limited by DHLA, but protein adsorption is nevertheless conceivable.

448 *3.3. Impact of AuNP coating on the intracellular redox homeostasis*

449

450 Change in redox status has been proposed to play an important role in the mechanism of
451 toxicity of a number of NP. For example, depletion of GSH and production of ROS have been
452 observed in cells exposed to $NiFe_2O$ NP (Ahamed et al., 2011), AgNP (Carlson et al., 2008),
453 CuNP (Valodkar et al., 2011), AuNP (Gao et al., 2011; Zhao et al., 2011) and polymeric
454 (Eudragit® RS) NP (Eidi et al., 2012). Interactions between AuNP and different structures in
455 cells (including plasma membrane, mitochondria, endoplasmic reticulum, proteins and
456 antioxidants) are today highlighted and they can lead to changes in cellular redox potential
457 that could lead to adverse effects (Unfried et al., 2007).
458 Nanoparticles can interfere with plasma membrane via different ways including
459 transmembrane enzyme activation (such as NADPH oxidase enzymes) and internalization
460 (Unfried et al., 2007). When AuNP enters intracellular compartment, their interaction with
461 organelles, *e.g.* mitochondria (source of $O_2^{\bullet-}$, H_2O_2, Ca^{2+}) and endoplasmic reticulum (source
462 of Ca^{2+}), can lead to further ROS and reactive nitrogen species (RNS) formation. Indeed, due
463 to the high surface reactivity, AuNP can also interact directly with antioxidants in cells (Gao
464 et al., 2011), *e.g.* GSH, resulting in disorder of the redox balance and production of ROS and
465 RNS. These disturbances can lead to the activation of intracellular signaling pathways (*e.g.*
466 MAPK), nuclear transcription factors (*e.g.* AP-1, NF-κB or Nrf2), and altered gene expression
467 following the induction of adaptive responses including release of inflammation mediators,
468 antioxidant defence activation, and cell phenotype modification (Unfried et al., 2007). The
469 oxidative stress resulting from an excess of ROS and RNS overwhelms the antioxidant
470 capacities of the cells and can lead to injuries of cell components, *e.g.* lipid peroxidation,
471 oxidation of protein and DNA damages, followed by cell death by necrosis or apoptosis. The
472 extent of disturbances depends on different factors, mainly NP concentration and their

physico-chemical properties. Studies cited above have been focused to assess the effect of the acute toxicity of AuNP in cells by using high NP concentration.

In the present study, we propose to evaluate the potential early-warning signals of redox balance impairment in macrophages in contact with citrate-stabilized AuNP and Au@DHLA NP. The tested AuNP concentration is equal to 10 nM, and it corresponds to a sub-toxic concentration (corresponding to 80 % of viability measured by Trypan Blue assay (Leroy et al., 2011)) which is far away from a potential therapeutic approach. As a matter of fact, the high possible rate of drug anchoring on AuNP surface should limit NP administration to very low doses (Soenen et al., 2011).

3.4. Dihydrolipoic acid coating decreases nanoparticle uptake by macrophages

Interactions of AuNP with cells were investigated on NR8383 rat alveolar macrophages. Macrophages correspond to a hematopoietic cell line that plays an essential role in innate immunity. This cell type is considered as a convenient cell model to analyze and verify whether NP can potentially cause adverse effects (Soenen et al., 2011). Nanoparticle uptake by macrophages may occur through various pathways (Alkilany and Murphy, 2010; Chithrani and Chan, 2007; Unfried et al., 2007), and physicochemical properties of NP (such as size, surface charge, shape and surface coating) influence particle internalization by macrophages (Boudier et al., 2011; Goodman et al., 2004; Hauck et al., 2008; Hutter et al., 2010; Pan et al., 2007; Shukla et al., 2005; Takahashi et al., 2005).

Transmission electronic microscopy studies were performed for probing AuNP internalization and they highlighted the impact of the AuNP coating on macrophage uptake. Macrophages treated with AuNP were morphologically similar to those untreated, what means that the presence of AuNP had no apparent adverse impact (Fig. 3).

Aggregates of citrate-stabilized AuNP were observed in intracellular compartment since few Au@DHLA NP were noticed (Fig. 3b-e). After 24-h exposure, AuNP are localized in endosomal compartments and they did not enter the nucleus, which correlates with previous findings and the extensive literature on this issue (Chithrani and Chan, 2007; Shukla et al., 2005).

To quantify the AuNP internalization, the amount of gold inside cells was determined by using ICP-MS. Macrophages were cultured for different time periods (15 min, 30 min, 2 h, 6 h, and 24 h) with both AuNP types. As shown in Figure 3f, the uptake of AuNP by macrophages was time dependent. On the one hand, low amounts of AuNP per cell were observed after 15 min, 30 min, 2 h and 6 h and no significant difference between citrate-stabilized AuNP and Au@DHLA NP was noticed. On the other hand, macrophages internalized two times less Au@DHLA than citrate-stabilized AuNP after 24-h exposure.

The surface coating mostly influences the immediate protein corona of AuNP formed upon contact with biological matrices. This phenomenon creates a “molecular signature”, which is recognized by immune cells and determines the route of particle internalization (Aggarwal et al., 2009). In this study, we suggest that Au@DHLA NP have low interaction rate with proteins in comparison with citrate-stabilized AuNP, thus a limited uptake by macrophages was observed. Chithrani and Chan proposed that serum proteins adsorb onto the AuNP surface and mediate their uptake (Chithrani and Chan, 2007). This hypothesis correlates with observations described above in cell-free conditions with GSH, GSNO and albumin (Fig 2): DHLA covalently linked to AuNP did not allow easily ligand exchange or adsorption. We also showed the influence of serum constituents on AuNP uptake by macrophages (data not shown). Uptake of AuNP decreased in the absence of serum in cell culture medium.

523 *3.5. Dihydrolipoic acid coated nanoparticles do not disturb intracellular redox homeostasis*

524

525 As internalization of citrate-stabilized AuNP and Au@DHLA NP by macrophages
526 reached different levels, consequences in redox balance are not absolutely identical for both
527 AuNP types.

528 We studied the redox status of macrophages after exposure to sub-toxic concentrations of
529 AuNP by using biomarkers, such as GSH level, ROS production, and mRNA expression
530 related to oxidative stress (*ncf1*) and inflammatory response (*tnfα*). Results are compared with
531 those obtained with untreated cells (negative control) and with cells exposed to unloaded
532 Eudragit® RS NP as a positive control (Eidi et al., 2012).

533 We have demonstrated above that the DHLA coating of AuNP preserves from the ligand
534 exchanges with GSH under cell-free conditions (Fig. 2). When macrophages are exposed to
535 AuNP, the citrate-stabilized AuNP significantly reduced the intracellular level of GSH (by 20
536 %; $p < 0.05$), whereas Au@DHLA NP did not deplete the GSH pool (Fig. 4a). Interestingly,
537 GSH depletion in macrophages exposed to citrate-stabilized NP was not implied with ROS
538 generation (Fig. 5a). Dichlorofluorescein (DCF) concentration (an indicator of intracellular
539 ROS level) slightly decreased (by 28 %; $p < 0.05$) after exposure to a 10 nM concentration of
540 citrate-stabilized AuNP. The same decrease of ROS levels was observed with Au@DHLA NP
541 (Fig. 5a).

542 The radical scavenging capacities of AuNP have been reported in previous works under
543 cell- free conditions (Esumi et al., 2004; Isono et al., 2005) and cell assays (Ma et al., 2010;
544 Shukla et al., 2005). It is not known, for instance, how AuNP deplete ROS levels, whether
545 they bind directly free radicals (adsorption on the AuNP surface or on the possibility of
546 exchange interaction between the unpaired electrons of the free radicals and the conduction-
547 band electrons of the metal) or induce indirectly the ROS scavenging by direct down-

548 regulation of transcription factors (such as AP-1 and NF-κB) involved in ROS production
549 (Jeon et al., 2000). To support the hypothesis of the direct scavenging of free radicals by
550 AuNP, we added citrate-stabilized AuNP and Au@DHLA NP at different concentrations (5 –
551 40 nM) to a 50 µM $ABTS^{\bullet+}$ solution, a free radical widely used to evaluate direct radical
552 scavenging properties of various antioxidants (Re et al., 1999; Tirzitis and Bartosz, 2010). As
553 showed in figure 5b, a dose-response relationship was observed after interaction of citrate-
554 stabilized AuNP and Au@DHLA NP with $ABTS^{\bullet+}$, and no significant difference between
555 citrate-stabilized AuNP and Au@DHLA NP was noticed within the NP concentration range of
556 5 - 20 nM. However, when higher concentrations (30 – 40 nM) were used, $ABTS^{\bullet+}$ exhibits
557 higher affinity toward citrate-stabilized AuNP than toward Au@DHLA NP. This study proves
558 that AuNP can scavenge directly free radicals. However, further experiments need to be
559 carried out to show the exact mechanism of $ABTS^{\bullet+}$ consumption by AuNP.
560
561 To refine redox balance impairment and to identify activated redox signaling pathway by
562 both AuNP types, mRNA level of the gene encoding Nuclear factor-kB transcription factor
563 (*nfkb2*) and mRNA levels of genes related to ROS production through the NADPH oxidase
564 complex (neutrophil cytosolic factor 1 – *ncf1*) and inflammation process (tumor necrosis
565 factor-alpha – *tnfα*) was monitored by using qRT-PCR assays. It is usually admitted in the
566 literature that genes which show more than a 2-fold or less than 0.5- fold expression level as
567 compared to control, were considered as up- or down-regulated, respectively (Lin et al.,
568 2003).
569 Nuclear factor-κB transcription factor plays a central role as a mediator of activation
570 (Baek et al., 2009) and inflammatory responses (Lee and Kim, 2007), as well as in the control
571 of cell proliferation or apoptosis (Quentmeier et al., 2001; Woods et al., 2007) in immune
572 cells. In essence, this transcription factor is considered as “instigator” of many cell signaling

pathways following stress exposure and translating redox balance disruption (Allen and Tresini, 2000). Interestingly, we observed a down-regulation of *nfκb2* gene (Fig. 6a) in the Au@DHLA NP treated macrophages. Gold compounds (for instance, sodium aurothiomalate and sodium aurothioglucose) have been shown to block the activation of AP-1 and NF-κB transcription factors, affecting the expression of many pro-inflammatory genes involved on the production of RNS and ROS (Jeon et al., 2000). The similar mechanism of down-regulation of genes implied in ROS generation might also be involved in Au@DHLA NP. Hence, Au@DHLA NP could exert, indirectly (down-regulation of *nfκb2*; Fig. 6a) and directly (consumption of $ABTS^{\bullet+}$; Fig. 5b) antioxidants effects on macrophages.

As expected, citrate-stabilized AuNP and Au@DHLA NP treated macrophages did not activate the *ncf1* gene which encodes a subunit of NADPH oxidase, as shown in Figure 6b (Dika Nguea et al., 2008). NADPH oxidase is a transmembrane protein, which can be activated by NP to produce superoxide (Nel et al., 2009). This explanation could corroborate the fact that no significant ROS production was observed after citrate-stabilized AuNP and Au@DHLA NP exposure. However, in spite of the GSH scavenging after citrate-stabilized AuNP treatment, we have not highlighted apoptosis or inflammation induction in macrophages (as already reported in our previous study (Leroy et al., 2011). In this study, citrate-stabilized NP and Au@DHLA NP were unable to activate *tnfα* gene (Fig. 6c) and caspase-3 (Fig. 6d). Cell signaling consequences that we explored did not reveal deleterious effect of AuNP following a unique exposure. Other signaling pathways could be turned on such as autophagy, a catabolic process involving the degradation of a cell's own components through the lysosomal machinery (Ma et al., 2011).

4. Conclusion

Despite the studies available on acute cytotoxicity of AuNP, to our knowledge, the present study is one of the few focusing on the early events of cellular cytotoxicity and accompanying redox status alterations caused by AuNP exposure.

In the present study, we used AuNP with similar morphology and diameter but different surface coating. Both of them are currently planed as drug delivery systems. Contrary to citrate-stabilized AuNP, Au@DHLA NP are stable and offer multiple possibilities of functionalization (Roux et al., 2005). These studies pointed out that changing the coating of AuNP from a low-molecular weight molecule (citrate) to a bidentate ligand (DHLA), the uptake by macrophages and reactivity towards redox signaling molecules are decreased, two essential parameters to preserve cellular integrity and body safety, and to assure pharmaceutical platform function.

Acknowledgements

Authors gratefully acknowledge Dr Lavinia BALAN (IS2M, LRC 7228, Université de Haute Alsace, Mulhouse, France) for realizing AuNP TEM measurements; Pr Bernard FOLIGUET and Mme CHANEL (Department of electron microscopy, Faculty of Medicine, Nancy, Université de Lorraine, France) for cell TEM images; Pr. Jean-François COLLET (Université Catholique de Louvain, Bruxelles, Belgique) and Pr. Vincent HAUFROID (Université Catholique de Louvain, Bruxelles, Belgique) for ICP-MS analysis. Authors would also like to acknowledge Miss Debora GOŚCIK and Mr Kevin DALLEAU for their technical support.

References

Aggarwal, P., Hall, J.B., McLeland, C.B., Dobrovolskaia, M.A., McNeil, S.E., 2009. Nanoparticle interaction with plasma proteins as it relates to particle biodistribution, biocompatibility and therapeutic efficacy. Adv. Drug Deliv. Rev. 61, 428-437.

Ahamed, M., Akhtar, J.M., Siddiqui, M.A., Ahamad, J., Musarrat, J., Al-Khedhairy, A.A., Alsalhi, M.S., Alrokayan, S.A., 2011. Oxidative stress mediated apoptosis induced by nickel ferrite nanoparticles in cultured a549 cells. Toxicology 283, 101-108.

Al-Sa'Doni, H., Ferro, A., 2000. S-nitrosothiols: A class of nitric oxide-donor drugs. Clin. Sci. 98, 507-520.

Alan, 2011. Trial of insulin-coated gold nanoparticles approved, Science Business. http://sciencebusiness.technewslit.com/?p=6957

Alkilany, A.M., Murphy, C.J., 2010. Toxicity and cellular uptake of gold nanoparticles: What we have learned so far? J. Nanopart. Res. 12, 2313-2333.

Allen, R.G., Tresini, M., 2000. Oxidative stress and gene regulation. Free Radical Biol. Med. 28, 463-499.

Baciu, C., Gauld, J.W., 2003. An assessment of theoretical methods for the calculation of accurate structures and s-n bond dissociation energies of s-nitrosothiols (RSNOs). J. Phys. Chem. A 107, 9946-9952.

Baek, Y.-S., Haas, S., Hackstein, H., Bein, G., Hernandez-Santana, M., Lehrach, H., Sauer, S., Seitz, H., 2009. Identification of novel transcriptional regulators involved in macrophage differentiation and activation in U937 cells. BMC Immunology 10, 18.

Boudier, A., Castagnos, P., Soussan, E., Beaune, G., Belkhelfa, H., Ménager, C., Cabuil, V., Haddioui, L., Roques, C., Rico-Lattes, I., Blanzat, M., 2011. Polyvalent catanionic vesicles: Exploring the drug delivery mechanisms. Int. J. Pharmaceut. 403, 230-236.

Brown, K.R., Walter, D.G., Natan, M.J., 1999. Seeding of colloidal au nanoparticle solutions. 2. Improved control of particle size and shape. Chem. Mater. 12, 306-313.

Carlson, C., Hussain, S.M., Schrand, A.M., Braydich-Stolle, L.K., Hess, K.L., Jones, R.L., Schlager, J.J., 2008. Unique cellular interaction of silver nanoparticles: Size-dependent generation of reactive oxygen species. J. Phys. Chem. B 112, 13608-13619.

Chai, F., Wang, C., Wang, T., Li, L., Su, Z., 2010. Colorimetric detection of Pb^{2+} using glutathione functionalized gold nanoparticles. ACS Appl. Mater. Inter. 2, 1466-1470.

Chithrani, B.D., Chan, W.C., 2007. Elucidating the mechanism of cellular uptake and removal of protein-coated gold nanoparticles of different sizes and shapes. Nano Lett. 7, 1542-1550.

Cook, J.A., Kim, S.Y., Teague, D., Krishna, M.C., Pacelli, R., Mitchell, J.B., Vodovotz, Y., Nims, R.W., Christodoulou, D., Miles, A.M., Grisham, M.B., Wink, D.A., 1996. Convenient colorimetric and fluorometric assays for S-nitrosothiols. Anal. Biochem. 238, 150-158.

Dika Nguea, H., De Reydellet, A., Lehuédé, P., De Meringo, A., Le Faou, A., Marcocci, L., Rihn, B.H., 2008. Gene expression profile in monocyte during in vitro mineral fiber degradation. Arch. Toxicol. 82, 355-362.

Eidi, H., Joubert, O., Némos, C., Grandemange, S., Mograbi, B., Foliguet, B., Tournebize, J., Maincent, P., Le Faou, A., Aboukhamis, I., Rihn, B.H., 2012. Drug delivery by polymeric nanoparticles induced autophagy in macrophages. Int. J. Pharmaceut. 422, 495-503.

677 Era, S., Kazuo, K., Imai, H., Nakamura, K., Hayashi, T., Sogami, M., 1995. Age-related
678 change in redox state of human serum albumin. Biochim. Biophys. Acta Protein Struct. Mol.
679 Enzymol. 1247, 12-16.
680
681 Esumi, K., Houdatsu, H., Yoshimura, T., 2004. Antioxidant action by gold-pamam dendrimer
682 nanocomposites. Langmuir 20, 2536-2538.
683
684 Gao, W., Xu, K., Ji, L., Tang, B., 2011. Effect of gold nanoparticles on glutathione depletion-
685 induced hydrogen peroxide generation and apoptosis in HL7702 cells. Toxicol. Lett. 205, 86-
686 95.
687
688 Goodman, C.M., McCusker, C.D., Yilmaz, T., Rotello, V.M., 2004. Toxicity of gold
689 nanoparticles functionalized with cationic and anionic side chains. Bioconjugate Chem. 15,
690 897-900.
691
692 Goraca, A., Huk-Kolega, H., Piechota, A., Kleniewska, P., Ciejka, E., Skibska, B., 2011.
693 Lipoic acid - biological activity and therapeutic potential. Pharm. Reports 63, 849-858.
694
695 Hauck, T.S., Ghazani, A.A., Chan, W.C.W., 2008. Assessing the effect of surface chemistry
696 on gold nanorod uptake, toxicity, and gene expression in mammalian cells. Small 4, 153-159.
697
698 Hutter, E., Boridy, S., Labrecque, S., Lalancette-Hébert, M., Kriz, J., Winnik, F.M.,
699 Maysinger, D., 2010. Microglial response to gold nanoparticles. ACS Nano 4, 2595-2606.
700
701 Isono, R., Yoshimura, T., Esumi, K., 2005. Preparation of Au/TiO_2 nanocomposites and their
702 catalytic activity for DPPH radical scavenging reaction. J. Colloid Interf. Sci. 288, 177-183.
703
704 Jeon, K.-I., Jeong, J.-Y., Jue, D.-M., 2000. Thiol-reactive metal compounds inhibit NF-κB
705 activation by blocking IκB kinase. J. Immunol. 164, 5981-5989.

706 Jia, H.Y., Liu, Y., Zhang, X.J., Han, L., Du, L.B., Tian, Q., Xu, Y.C., 2009. Potential
707 oxidative stress of gold nanoparticles by induced-NO releasing in serum. J. Am. Chem. Soc.
708 131, 40-41.

709
710 Karakoti, A., Singh, S., Dowding, J.M., Seal, S., Self, W.T., 2010. Redox-active radical
711 scavenging nanomaterials. Chem. Soc. Rev. 39, 4422-4432.

712
713 Lee, H., Lee, K., Kim, I.-K., Park, T.G., 2009. Fluorescent gold nanoprobe sensitive to
714 intracellular reactive oxygen species. Adv. Funct. Mater. 19, 1884-1890.

715
716 Lee, H., Lee, K., Kim, I.-K., Park, T.G., 2010. Bodipy-functionalized gold nanoparticles as a
717 selective fluoro-chromogenic chemosensor for imaging Cu^{2+} in living cells. Analyst 135,
718 2022-2027.

719
720 Lee, H., Lee, K., Kim, I.K., Park, T.G., 2008. Synthesis, characterization, and in vivo
721 diagnostic applications of hyaluronic acid immobilized gold nanoprobes. Biomaterials 29,
722 4709-4718.

723
724 Lee, M.S., Kim, Y.J., 2007. Signaling pathways downstream of pattern-recognition receptors
725 and their cross talk. Annu. Rev. Biochem. 76, 447-480.

726
727 Leroy, P., Sapin-Minet, A., Pitarch-Sierra, A., Boudier, A., Tournebize, J., Schneider, R.,
728 2011. Interactions between gold nanoparticles and macrophages : Activation or inhibition ?
729 Letter to the Editor, Nitric Oxide-Biol. Chem. 25, 54 -56.

730
731 Lewicki, K., Marchand, S., Matoub, L., Lulek, J., Coulon, J., Leroy, P., 2006. Development
732 of a fluorescence-based microtiter plate method for the measurement of glutathione in yeast.
733 Talanta 70, 876–882.

734

735 Li, L., Li, B., 2009. Sensitive and selective detection of cysteine using gold nanoparticles as
736 colorimetric probes. Analyst 134, 1361-1365.

737
738 Li, Z., Jin, R., Mirkin, C.A., Letsinger, R.L., 2002. Multiple thiol-anchor capped DNA-gold
739 nanoparticle conjugates. Nucleic Acids Res. 30, 1558-1562.

740
741 Libutti, S.K., Paciotti, G.F., Byrnes, A.A., Alexander, H.R., Gannon, W.E., Walker, M.,
742 Seidel, G.D., Yuldasheva, N., Tamarkin, L., 2010. Phase I and pharmacokinetic studies of
743 cyt-6091, a novel pegylated colloidal gold-rh TNF nanomedicine. Clin. Cancer Res. 16, 6139-
744 6149.

745
746 Lin, C.-A.J., Yang, T.-Y., Lee, C.-H., Huang, S.H., Sperling, R.A., Zanella, M., Li, J.K.,
747 Shen, J.-L., Wang, H.-H., Yeh, H.-I., Parak, W.J., Chang, W.H., 2009. Synthesis,
748 characterization, and bioconjugation of fluorescent gold nanoclusters toward biological
749 labeling applications. ACS Nano 3, 395-401.

750
751 Lin, Z., Fillmore, G.C., Um, T.H., Elenitoba-Johnson, K.S.J., Lim, M.S., 2003. Comparative
752 microarray analysis of gene expression during activation of human peripheral blood T cells
753 and leukemic jurkat T cells. Lab. Invest. 83, 765-776.

754
755 Liu, J., Ong, W., Román, E., Lynn, M.J., Kaifer, A.E., 2000. Cyclodextrin-modified gold
756 nanospheres. Langmuir 16, 3000-3002.

757
758 Loo, C., Lowery, A., Halas, N., West, J., Drezek, R., 2005. Immunotargeted nanoshells for
759 integrated cancer imaging and therapy. Nano Lett. 5, 709-711.

760
761 Lowry, O.H., Rosebrough, N.J., Farr, A.L., Randall, R.J., 1951. Protein measurement with the
762 folin-phenol reagents. J. Biol. Chem. 193, 265-275.

763

764 Ma, J.S., Kim, W.J., Kim, J.J., Kim, T.J., Ye, S.K., Song, M.D., Kang, H., Kim, D.W., Moon,
765 W.K., Lee, K.H., 2010. Gold nanoparticles attenuate lps-induced no production through the
766 inhibition of NF-κB and IFN-β/STAT1 pathways in RAW264.7 cells. Nitric Oxide-Biol.
767 Chim. 23, 214-219.
768
769 Ma, X., Wu, Y., Jin, S., Tian, Y., Zhang, X., Zhao, Y., Yu, L., Liang, X.-J., 2011. Gold
770 nanoparticles induce autophagosome accumulation through size-dependent nanoparticle
771 uptake and lysosome impairment. ACS Nano 5, 8629-8639.
772
773 Nel, A.E., Madler, L., Velegol, D., Xia, T., Hoek, E.M.V., Somasundaran, P., Klaessig, F.,
774 Castranova, V., Thompson, M., 2009. Understanding biophysicochemical interactions at the
775 nano-bio interface. Nat. Mater. 8, 543-557.
776
777 Paciotti, G.F., Myer, L., Weinreich, D., Goia, D., Pavel, N., McLaughlin, R.E., Tamarkin, L.,
778 2004. Colloidal gold: A novel nanoparticle vector for tumor directed drug delivery. Drug
779 Deliv. 11, 169-183.
780
781 Pan, Y., Leifert, A., Ruau, D., Neuss, S., Bornemann, J., Schmid, G., Wolfgang, B., Ulrich,
782 S., Willi, J.-D., 2009. Gold nanoparticles of diameter 1.4 nm trigger necrosis by oxidative
783 stress and mitochondrial damage. Small 5, 2067–2076.
784
785 Pan, Y., Neuss, S., Leifert, A., Fischler, M., Wen, F., Simon, U., Schmid, G., Brandau, W.,
786 Jahnen-Dechent, W., 2007. Size-dependent cytotoxicity of gold nanoparticles. Small 3, 1941-
787 1949.
788
789 Pramanik, S., Banerjee, P., Sarkar, A., Bhattacharya, S.C., 2008. Size-dependent interaction
790 of gold nanoparticles with transport protein. J. Lumin. 128, 1969-1974.
791

792 Quentmeier, H., Drexler, H.G., Fleckenstein, D., Zaborski, M., Armstrong, A., Sims, J.E.,
793 Lyman, S.D., 2001. Cloning of human thymic stromal lymphopoietin (tslp) and signaling
794 mechanisms leading to proliferation. Leukemia 15, 1286-1292.
795
796 Re, R., Pellegrini, N., Proteggente, A., Pannala, A., Yang, M., Rice-Evans, C., 1999.
797 Antioxidant activity applying an improved ABTS radical cation decolorization assay. Free
798 Radical Bio. Med. 26, 1231-1237.
799
800 Rosi, N.L., Giljohann, D.A., Thaxton, C.S., Lytton-Jean, A.K., Han, M.S., Mirkin, C.A.,
801 2006. Oligonucleotide-modified gold nanoparticles for intracellular gene regulation. Science
802 312, 1027-1030.
803
804 Roux, S., Garcia, B., Bridot, J.-L., Salomé, M., Marquette, C., Lemelle, L., Gillet, P., Blum,
805 L., Perriat, P., Tillement, O., 2005. Synthesis, characterization of dihydrolipoic acid capped
806 gold nanoparticles, and functionalization by the electroluminescent luminol. Langmuir 21,
807 2526-2536.
808
809 Shukla, R., Bansal, V., Chaudhary, M., Basu, A., Bhonde, R.R., Sastry, M., 2005.
810 Biocompatibility of gold nanoparticles and their endocytotic fate inside the cellular
811 compartment: A microscopic overview. Langmuir 23, 10644-10654.
812
813 Sies, H., 1999. Glutathione and its role in cellular functions. Free Radical Bio. Med. 27, 916-
814 921.
815
816 Soenen, S.J., Rivera-Gil, P., Montenegro, J.-M., Parak, W.J., Smedt, S.C.D., 2011. Cellular
817 toxicity of inorganic nanoparticles: Common aspects and guidelines for improved
818 nanotoxicity evaluation. Nanotoday 6, 446-465.
819

820 Summa, D., Spiga, O., Bernini, A., Venditti, V., Priora, R., Frosali, S., Margaritis, A.,
821 Giuseppe, D.D., Niccolai, N., Simplicio, P.D., 2007. Protein–thiol substitution or protein
822 dethiolation by thiol/disulfide exchange reactions: The albumin model. Proteins 69, 369-378.
823
824 Takahashi, H., Niidome, Y., Niidome, T., Kaneko, K., Kawasaki, H., Yamada, S., 2005.
825 Modification of gold nanorods using phosphatidylcholine to reduce cytotoxicity. Langmuir
826 22, 2-5.
827
828 Tirzitis, G., Bartosz, G., 2010. Determination of antiradical and antioxidant activity: Basic
829 principles and new insights. Acta Biochim. Pol. 57, 139-142.
830
831 Tournebize, J., Sapin-Minet, A., Schneider, R., Boudier, A., Maincent, P., Leroy, P., 2011.
832 Simple spectrophotocolorimetric method for quantitative determination of gold in
833 nanoparticles. Talanta 83, 1780-1783.
834
835 Unfried, K., Albrecht, C., Klotz, L.-O., Von Mikecz, A., Grether-Beck, S., Schins, R.P.F.,
836 2007. Cellular responses to nanoparticles: Target structures and mechanisms. Nanotoxicology
837 1, 52-71.
838
839 Valodkar, M., Rathore, P.S., Jadeja, R.N., Thounaojam, M., Devkar, R.V., Thakore, S., 2011.
840 Cytotoxicity evaluation and antimicrobial studies of starch capped water soluble copper
841 nanoparticles. J. Hazard Mater. 201-202, 244-249.
842
843 Woods, C.G., Burns, A.M., Bradford, B.U., Ross, P.K., Kosyk, O., Swenberg, J.A.,
844 Cunningham, M.L., Rusyn, I., 2007. Wy-14,643–induced cell proliferation and oxidative
845 stress in mouse liver are independent of NADPH oxidase. Toxicol. Sci. 98, 366-374.
846

847 Zhao, W., Lam, J.C.F., Chiuman, W., Brook, M.A., Li, Y., 2008. Enzymatic cleavage of
848 nucleic acids on gold nanoparticles: A generic platform for facile colorimetric biosensors.
849 Small 4, 810–816.
850
851 Zhao, Y., Gu, X., Ma, H., He, X., Liu, M., Ding, Y., 2011. Association of glutathione level
852 and cytotoxicity of gold nanoparticles in lung cancer cells. J. Phys. Chem. C 115, 12797-
853 12802.

Figure captions:

Fig. 1. Synthesis and physico-chemical properties of AuNP. (Top) schematic representation of synthesis of AuNP stabilized with citrate (citrate-stabilized AuNP) (1st step) and functionalized with dihydrolipoic acid (Au@DHLA NP) (2nd step). (Bottom) Hydrodynamic and geometric diameters, and zeta potential measurements of AuNP. Values correspond to mean ± standard deviation of three independent experiments.

*, $p < 0.05$ in relation to citrate-stabilized AuNP when all experiments were compared and the *t*-student test were performed for calculations.

Fig. 2. Interactions in cell-free conditions between AuNP and molecules implied on redox status: (a) concentration of GSH remaining, (b) concentration of $^{\bullet}$NO released from GSNO and (c) fluorescence quenching of bovine serum albumin after exposure to citrate-stabilized AuNP and Au@DHLA NP at different concentrations (5–30 nM), (d) hydrodynamic size of AuNP at 10 nM before and after interaction with BSA. Values correspond to mean ± standard deviation of three independent experiments.

*, $p < 0.05$ in relation to citrate-stabilized AuNP when all experiments were compared and the *t*-student test were performed for all calculations.

Fig. 3. Evaluation of AuNP uptake by NR8383 macrophages after exposure to 10 nM of citrate-stabilized AuNP and Au@DHLA NP by using transmission electron microscopy (TEM) images and inductively coupled argon plasma mass spectrometry (ICP-MS) measurements. Representative images taken from (a) not treated macrophages (negative control) (b-c) and macrophages treated for 24 h with citrate-stabilized AuNP (d-e) and Au@DHLA NP; arrow indicates internalized nanoparticles, (f) kinetics of cellular uptake of citrate-stabilized AuNP and Au@DHLA NP as a function of incubation time.

879 Values correspond to mean ± standard deviation of three independent experiments. *, $p < 0.05$
880 in relation to citrate-stabilized AuNP, when the experiments were compared and the non-
881 parametric Mann and Whitney randomised test were performed for calculations.
882
883 **Fig. 4.** Intracellular reduced glutathione level in NR8383 macrophage after treatment with
884 citrate-stabilized AuNP and Au@DHLA NP. Eudragit® RS NP (100 $\mu g.mL^{-1}$) was used as the
885 positive control.
886 Values correspond to mean ± standard deviation of three independent experiments.
887 *, $p < 0.05$ in relation to control, when the experiments were compared and the non-
888 parametric Mann and Whitney randomised test were performed for calculations.
889
890 **Fig. 5.** Reactivity of AuNP with radicals; (a) ROS production in NR8383 macrophage after
891 treatment with citrate-stabilized AuNP and Au@DHLA NP at a concentration of 10 nM.
892 Eudragit® RS NP (100 $\mu g.mL^{-1}$) was used as the positive control; (b) $ABTS^{\bullet+}$ concentration
893 (initial concentration: 50 µM) after reaction with AuNP (5 – 40 nM).
894 Values correspond to mean ± standard deviation of three independent experiments.
895 In cells experiments, *, $p < 0.05$ in relation to control -, when the experiments were compared
896 and the non-parametric Mann and Whitney randomised test were performed for calculations.
897 In $ABTS^{\bullet+}$ experiments, *, $p < 0.05$ in relation to citrate-stabilized AuNP when all
898 experiments were compared and the *t*-student test were performed for all calculations.
899

Fig. 6. Expression levels of (a) *nfκb2*, (b) *ncf1* and (c) *tnfα* genes estimated with qRT-PCR and (d) detection of caspase-3 activity after treatment of NR8383 macrophages with citrate-stabilized AuNP and Au@DHLA NP. In qRT-PCR measurements, the expression levels were normalized to *s18* levels. Genes which showed more than 2.0-fold or less than 0.5-fold intensity as compared to control, were considered as up- or down-regulated. In caspase-3 protein activity experiments, camptothecin (10 µM) was used as a caspase-3 inducer and Ac-DEVD-CHO inhibitor was used to confirm that the observed fluorescence signal in both induced and control cells populations is due to the activity of caspase-3-like proteases. Values correspond to mean ± standard deviation of three independent measurements. *, $p < 0.05$ in relation to control, when the experiments were compared and the non-parametric Mann and Whitney randomised test were performed for calculations.

Table 1. Primer sequences (Forward / Reverse) used for qRT-PCR experiments

Primers	Forward primer	Reverse primer
nfkb2	5'-TTCGGAACTGGGCAAATGTT-3'	5'-ACACGTAGCGGAATCGAAAT-3'
tnfα	5'-TAGCCCACGTCGTAGCAAAC-3'	5'-TGGTATGAAATGGCAAATCG-3'
ncf1	5'-TTCACAACTACGCAGGTGAA-3'	5'-TTATCTCCTCCCCAGCCTTC-3'
s18	5'-CGCCGCTAGACGTAGAATTCT-3'	5'-CATTCTTGGCAAATGCTTTGC-3'

Figure 1

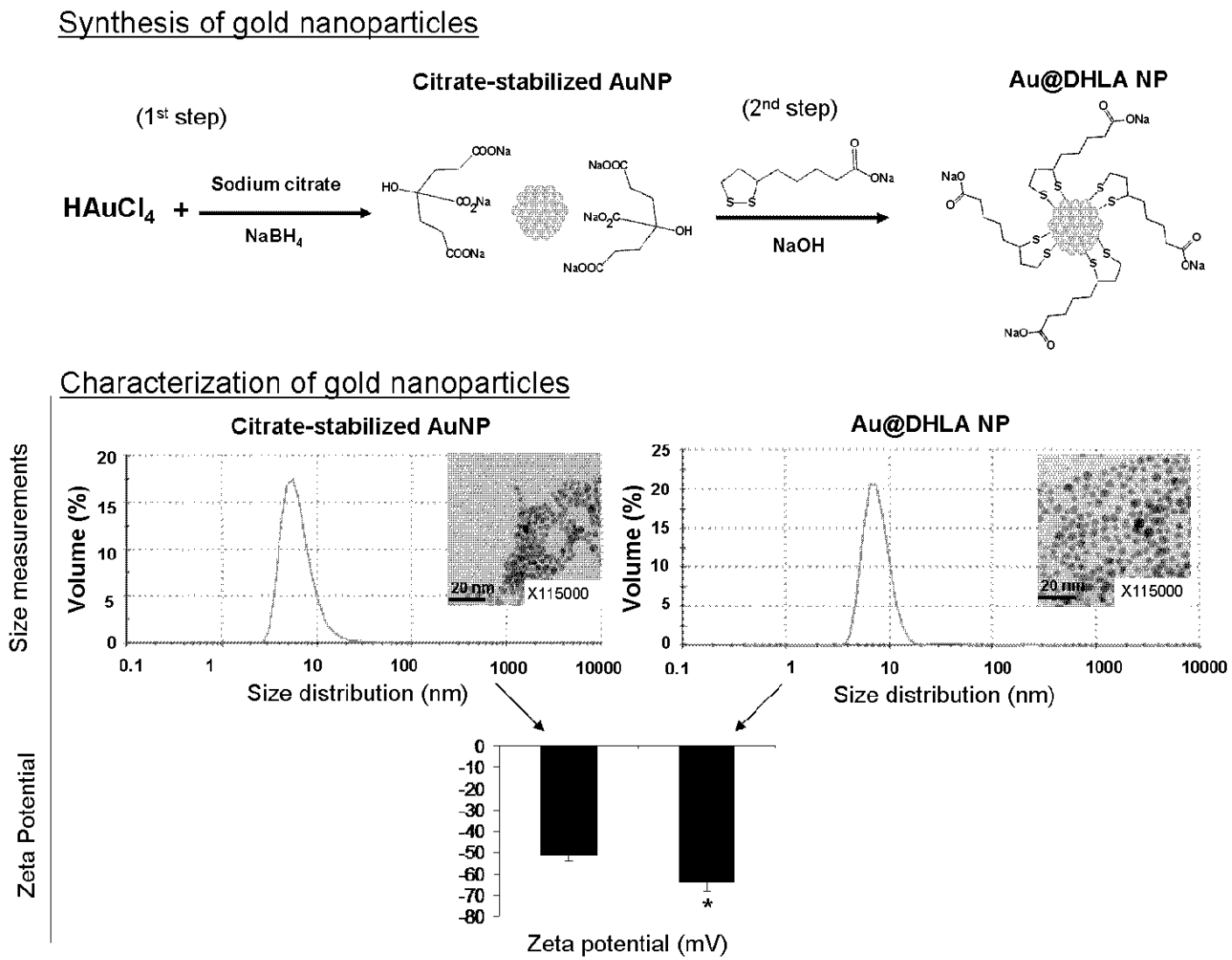
Synthesis of gold nanoparticles
Citrate-stabilized AuNP
Au@DHLA NP
(1st step)
(2nd step)
HAuCl4 +
Sodium citrate
NaBH4
NaOH
Characterization of gold nanoparticles
Size measurements
Zeta Potential
Citrate-stabilized AuNP
Au@DHLA NP
Volume (%)
Size distribution (nm)
20 nm
X115000
Zeta potential (mV)

Figure 2

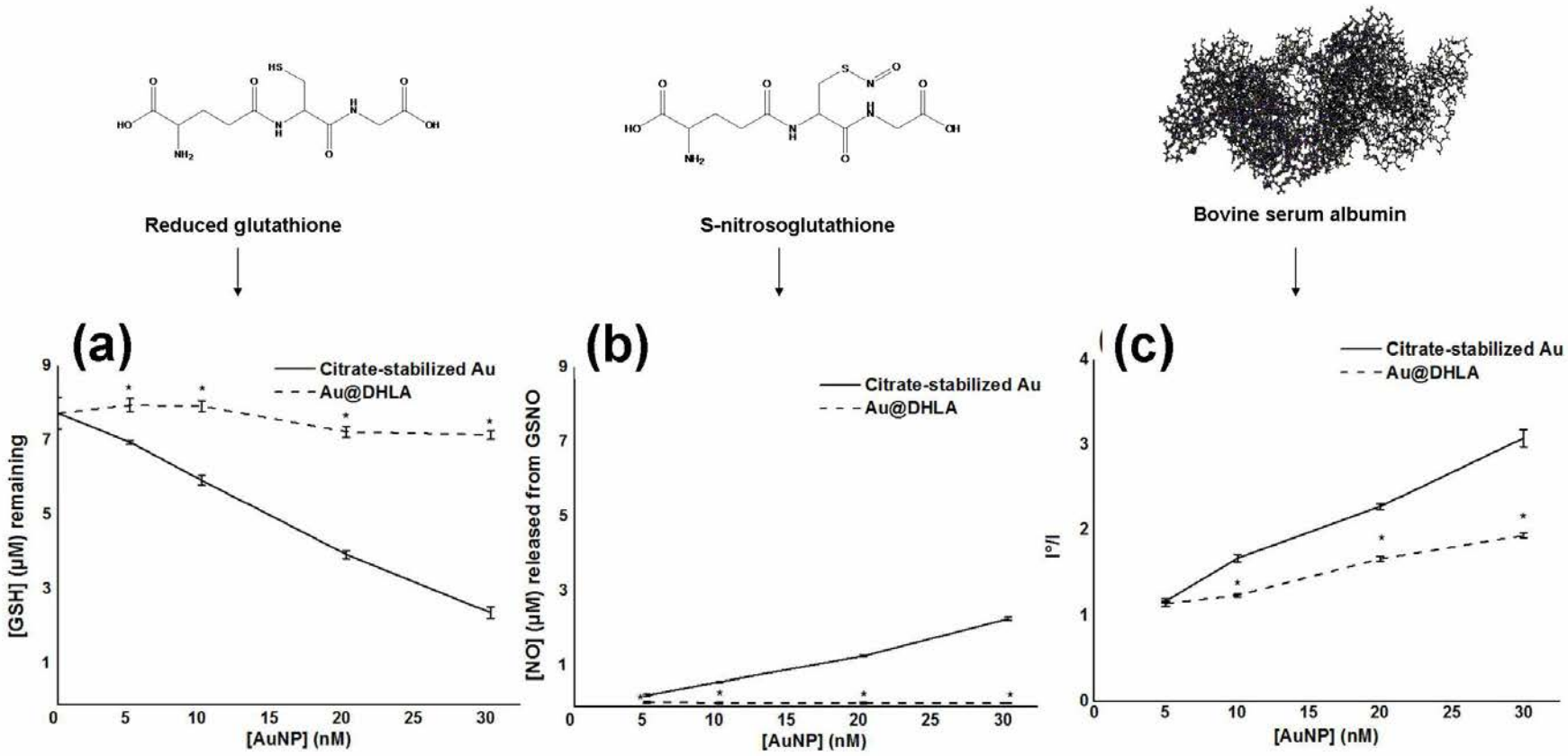

(d)

AuNP (10 nM)	Hydrodynamic size of AuNP (nm) incubation at 37°C for 1h in PBS medium	
	Without BSA	After interaction with BSA
Citrate-stabilized AuNP	1180.0	40.0
Au@DHLA NP	7.7	10.1

Figure 3

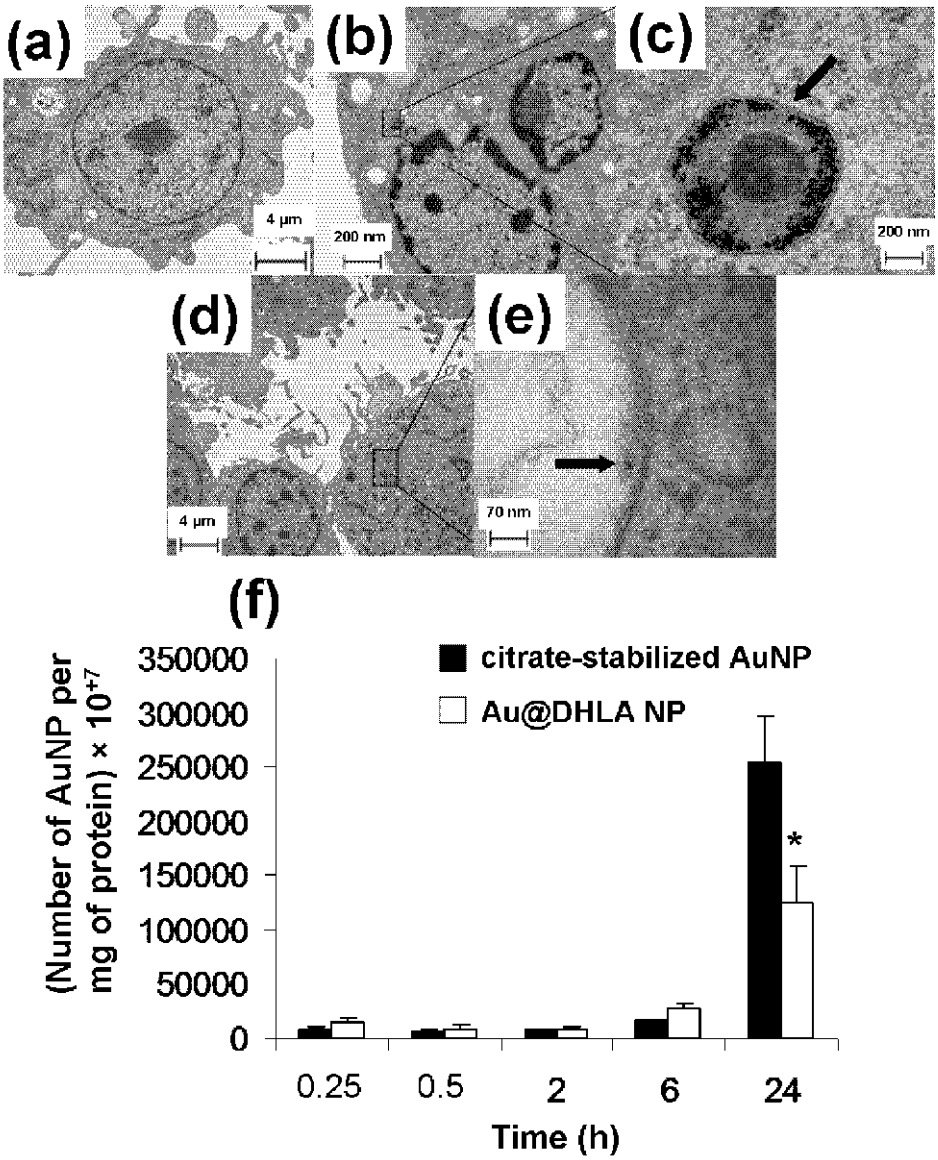
(a)
(b)
(c)
4 µm
200 nm
200 nm
(d)
(e)
4 µm
70 nm
(f)
(Number of AuNP per mg of protein) × 10+7
350000
300000
250000
200000
150000
100000
50000
0
citrate-stabilized AuNP
Au@DHLA NP
*
0.25
0.5
2
6
24
Time (h)

Figure 4

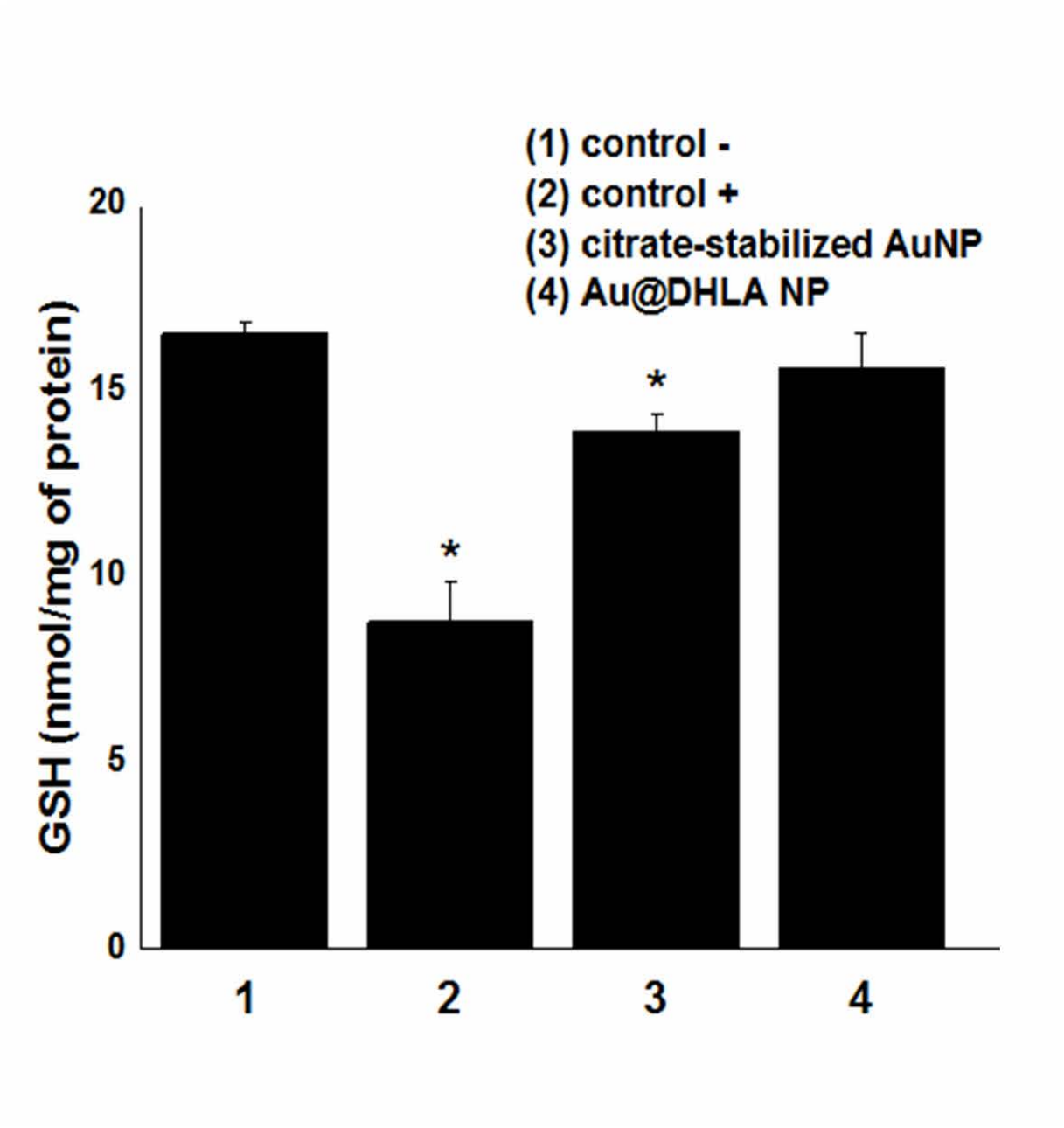
(1) control -
(2) control +
(3) citrate-stabilized AuNP
(4) Au@DHLA NP
GSH (nmol/mg of protein)
20
15
10
5
0
*
*
1
2
3
4

Figure 5

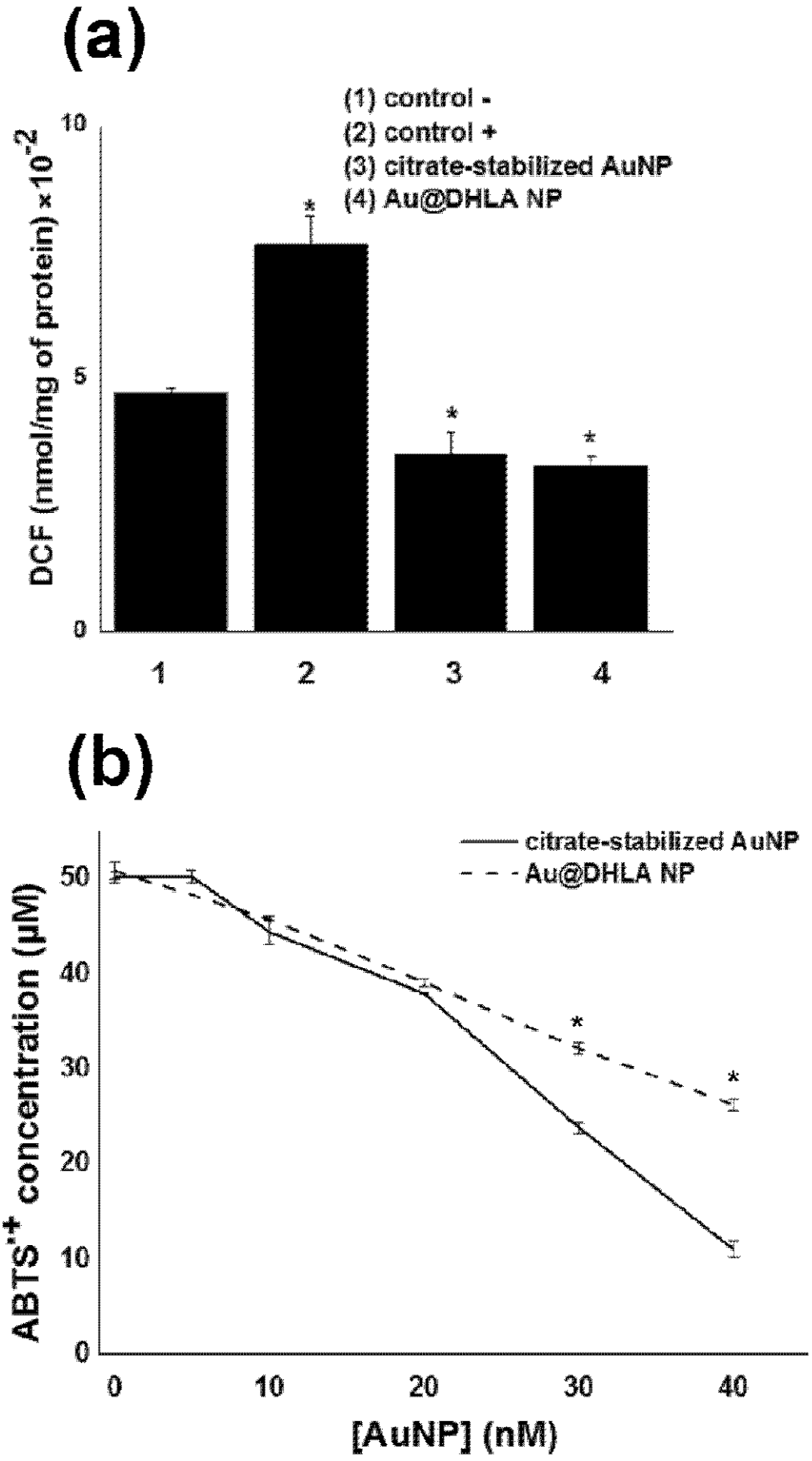
(a)
(1) control -
(2) control +
(3) citrate-stabilized AuNP
(4) Au@DHLA NP
DCF (nmol/mg of protein) × 10-2
10
5
0
1
2
3
4
*
(b)
citrate-stabilized AuNP
Au@DHLA NP
ABTS•+ concentration (μM)
50
40
30
20
10
0
0
10
20
30
40
[AuNP] (nM)

Figure 6

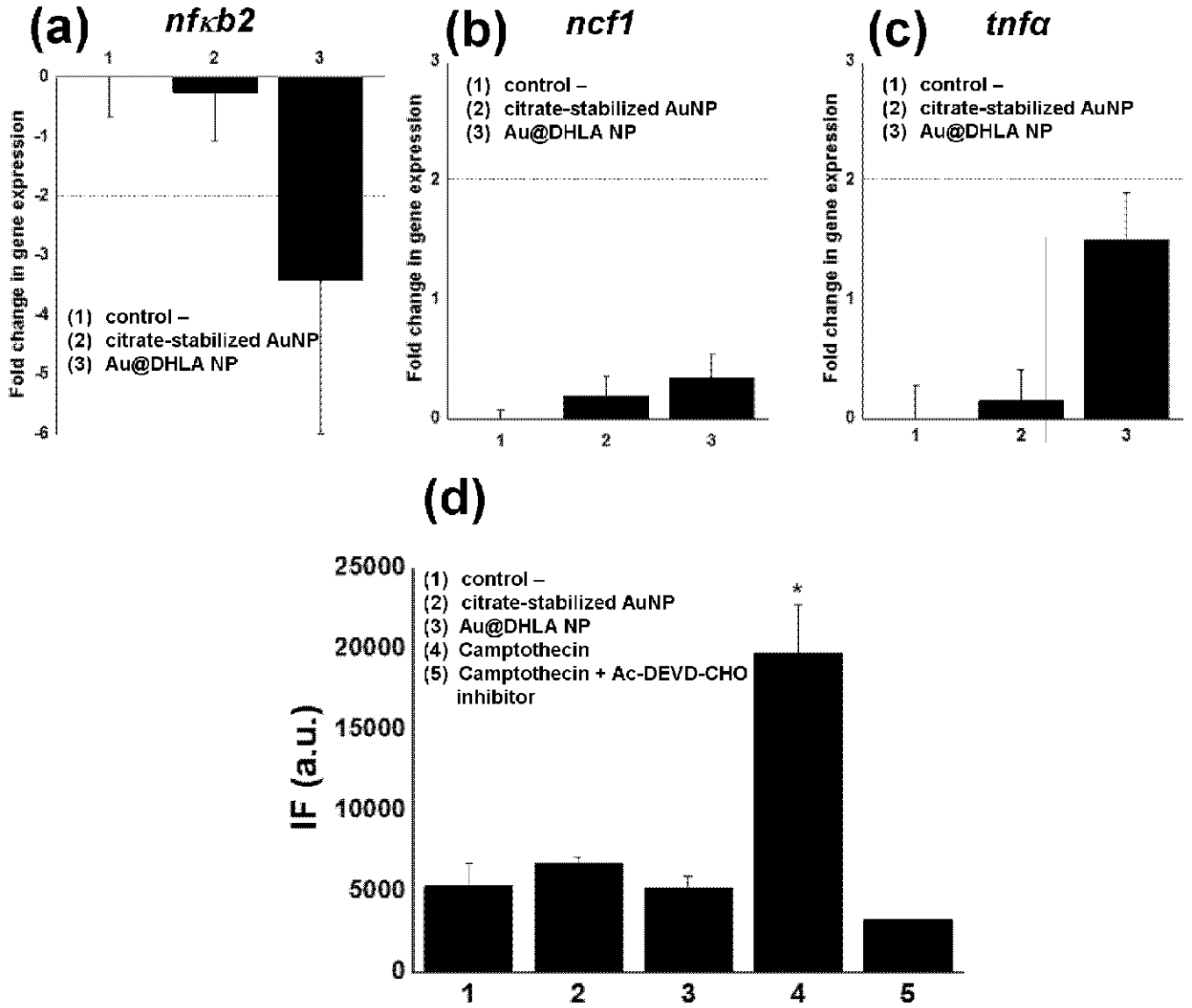
(a)
nfκb2
Fold change in gene expression
(1) control –
(2) citrate-stabilized AuNP
(3) Au@DHLA NP
(b)
ncf1
Fold change in gene expression
(1) control –
(2) citrate-stabilized AuNP
(3) Au@DHLA NP
(c)
tnfα
Fold change in gene expression
(1) control –
(2) citrate-stabilized AuNP
(3) Au@DHLA NP
(d)
IF (a.u.)
(1) control –
(2) citrate-stabilized AuNP
(3) Au@DHLA NP
(4) Camptothecin
(5) Camptothecin + Ac-DEVD-CHO inhibitor
*

International Journal of Pharmaceutics 422 (2012) 495–503

Contents lists available at SciVerse ScienceDirect

International Journal of Pharmaceutics

journal homepage: www.elsevier.com/locate/ijpharm

Pharmaceutical nanotechnology

Drug delivery by polymeric nanoparticles induces autophagy in macrophages

Eidi H.[a], Joubert O.[a], Némos C.[b,e], Grandemange S.[c], Mograbi B.[d], Foliguet B.[e], Tournebize J.[a], Maincent P.[a], Le Faou A.[a], Aboukhamis I.[f], Rihn B.H.[a,*]

[a] Faculté de Pharmacie, EA 3452 CITHEFOR, Nancy-Université, 54001 Nancy Cedex, France
[b] Human Genetics Laboratory, EA 4368, Centre Hospitalier et Universitaire de Nancy, Nancy-Université, Vandoeuvre-Lès-Nancy, Nancy, France
[c] Faculté de Sciences et Technique, EA 4421 SIGRETO, Nancy-Université, Vandoeuvre-Lès-Nancy, Nancy, France
[d] Inserm ERI-21/EA 4319, Faculté de Médecine, University of Nice Sophia-Antipolis, Nice, France
[e] Histology-Embryology-Cytogenetics Department of Faculté de Médecine, Nancy-Université, Vandoeuvre- Lès-Nancy, Nancy, France
[f] Biochemistry Department, Arab European University and Damascus University, Damascus, Syria

ARTICLE INFO

Article history:
Received 9 September 2011
Received in revised form 9 November 2011
Accepted 12 November 2011
Available online 22 November 2011

Keywords:
Nanoparticles
Drug delivery
Autophagy
Apoptosis
Microarray
Mitochondria

ABSTRACT

Drug delivery nanosystems are currently used in human therapy. In preliminary studies we have observed that Eudragit® RS nanoparticles, prepared by nanoprecipitation or double emulsion techniques, are cytotoxic for NR8383 rat macrophages. In this study, we expand our previous analysis and suggest that unloaded Eudragit® RS nanoparticles prepared by nanoprecipitation (NP/ERS) may induce important morphological and biochemical cellular modifications leading to cellular death. In NR8383 rat macrophages cell line exposed to doses varying from 15 to 100 μg/mL, NP/ERS nanoparticles are internalized inside the cells, reach the mitochondria and alter the structure of these organelles. In addition, the exposure to nanoparticles induces cellular autophagy as demonstrated by electron microscopy analysis, microchip array, qRT-PCR and Western blot assays. Although toxicity of nanoparticles has already been evidenced, it is the first time that results show clearly that the toxicity of polymeric nanovectors may be related to an activation of autophagy.

1. Introduction

Nano-drug delivery systems (NDDS) based on polymeric biomaterials have received considerable interest as drug delivery vehicles, and as nonviral gene delivery systems (Unger et al., 2007). Nanoparticles used as drug delivery vehicles are generally <500 nm in at least one dimension, and consist of different biodegradable or non biodegradable materials such as natural or synthetic polymers, lipids or metals (Hoffart et al., 2006; Suri et al., 2007). Despite their wide use, their toxicity is seldom evaluated and the studies are limited, in most cases, to the effect of loaded nanoparticles. On the contrary, the toxicity of the unloaded nanoparticles is not investigated and the mechanisms through which they might interfere with the cellular metabolism are largely unknown. Among the numerous available nanoparticles, those prepared from Eudragit® RS (ERS), a non-biodegradable positively charged copolymer, licensed for clinical use by the major health authorities of Europe, Japan and USA (Hoffart et al., 2006), are efficient NDDS. ERS nanoparticles prepared by nanoprecipitation (NP) or by double emulsion (DE) techniques containing ibuprofen (Pignatello et al., 2002), cyclosporin (Pignatello et al., 2002), indomethacin (Bhardwaj et al., 2010), melatonin (Schaffazick et al., 2008), DNA plasmid (Gargouri et al., 2009) and low molecular weight heparin (Jiao et al., 2002) (LMWH) have been obtained and suggested to be used for the treatment of different pathological conditions. A previous work from our laboratory has already shown, by using MTT and Trypan blue exclusion tests, that unloaded NP/ERS nanoparticles, at a final concentrations ranging from 25 to 400 μg/mL, have cytotoxic effects on the rat macrophage cell line NR8383 (Eidi et al., 2010). Additionally, other studies performed on ERS nanoparticles toxicity are scarce and often they are limited to cell survival (Gargouri et al., 2009; Lamprecht et al., 2006). Taking into consideration that (i) 44% of the total nanoparticles present in a formulation is empty (Eidi et al., 2010); (ii) as demonstrated in rabbits, nanoparticles reach the blood stream after oral administration (Hoffart et al., 2006) and that (iii) macrophages are among the first cells they interact with, we extended our study on the effect of

Abbreviations: CHL, chloroquine; $DCFH_2$-DA, 2′,7′-dichlorofluorescin diacetate; DE, double emulsion; DE/ERS, Eudragit® RS empty nanoparticles prepared by double emulsion technique; ERS, Eudragit® RS PO; GO, gene ontology terms; LPS, lipopolysaccharide; LMWH, low molecular weight heparin; NDA, naphthalene-2,3 dicarboxyaldehyde; NDDS, nano drug delivery systems; NP, nanoprecipitation; NP/ERS, Eudragit® RS PO empty nanoparticles prepared by nanoprecipitation technique; SWCNTs, single-walled carbon nanotubes; SDS, sodium dodecyl sulfate; SEM, scanning electron microscopy; TEM, transmission electronic microscopy.

* Corresponding author at: Faculté de Pharmacie, 5 rue Albert Lebrun, BP 80403, 54001 Nancy Cedex, France. Tel.: +33 0383 682 355; fax: +33 0383 682 301.
E-mail addresses: bertrand.rihn@pharma.uhp-nancy.fr, housam.eidi@gmail.com (B.H. Rihn).

0378-5173/$ – see front matter © 2011 Elsevier B.V. All rights reserved.
doi:10.1016/j.ijpharm.2011.11.020

NP/ERS on NR8383 rat macrophages, which evolve in fully activated macrophages (Nguea et al., 2008), with the aim to better elucidate the molecular mechanisms that may be responsible of the observed cytotoxicity and so to further address the safety issues surrounding nanoparticles use.

2. Materials and methods

2.1. Materials

Eudragit® RS PO (ERS; MW = 150,000 Da) was a gift of Evonik polymers (Darmstadt, Germany). CAS number: 33434-24-1, chemical/IUPAC name: poly(ethyl acrylate-co-methyl methacrylate-co trimethylammonioethyl methacrylate chloride) 1:2:0.1. INCI name: Acrylates/Ammonium Methacrylate Copolymer, molecular weight: 32 g/mol. Eudragit® RS PO was described in the following monographs: (i) European pharmacopoeia: Ammonio Methacrylate Copolymer, Type B; (ii) USA pharmacopoeia: Ammonio Methacrylate Copolymer, Type B – NF; (iii) Japanese pharmacopoeia: Aminoalkyl Methacrylate Copolymer RS. Pluronic® F68 [CAS number: 11104-97-5] (Saint-Quentin Fallavier, France) was used as surfactant for particle preparations. Reduced glutathione (GSH), naphthalene-2,3- dicarboxyaldehyde (NDA), 2′,7′-dichlorofluorescin diacetate ($DCFH_2$-DA) and dichlorofluorescein (DCF) were purchased from Sigma–Aldrich (France).

2.2. Methods

2.2.1. Nanoparticle preparation

Nanoparticles were prepared by nanoprecipitation as previously described (Bodmeier et al., 1991; Fessi and Puisieux, 1989). Briefly, 300 mg of polymer were dissolved in 15 mL of acetone (organic phase). The solution was poured in a glass syringe, and flowed slowly under stirring, in 40 mL of a Pluronic® F68 (0.5%, w/v) aqueous solution. The solvent was removed by rotary evaporation under vacuum at 40 °C (Heidolph, Schwabach, Germany) and the solution concentrated to 15 mL.

2.2.2. Particle size measurement

Particle sizes were estimated by photon correlation spectroscopy (PCS) using a Zetasizer™ (Malvern Instruments Worcestershire, UK). Each sample was diluted with filtrated bidistilled water until the appropriate concentration of particles was achieved to avoid multiscattering events. Using cumulative analysis software and exponential sampling method, particle size (*z*-average) and polydispersity index of equivalent hydrodynamic spheres were determined using the results of three determinations.

2.2.3. Zeta potential measurement

Particle electrophoretic mobility was determined three times for each sample by laser Doppler anemometry in a microelectrophoresis cell of Zetasizer™.

2.2.4. Scanning electron microscopy (SEM)

Briefly, nanoparticles deposited on a plastic coverslip (Thermanox, 174950, Merck Eurolab, Strasbourg, France) were dehydrated by increased ethanol concentrations (25°, 50°, 70°, 90°, and 100°) and treated with hexamethyldisilazane for 10 min at room temperature. The coverslips were coated with gold. Preparations were observed under SEM (Stereoscan 240 S/N, Léo, Rueil-Malmaison, France) at less than 20 kV.

2.2.5. Cells and cell culture

The NR8383 rat alveolar macrophage cell line was purchased from the American Type Culture Collection (CRL-2192, ATCC, Manassas, VA). Cells were grown as 50% adherent and 50% floating cells in Dulbecco's modified Eagle's medium (DMEM: GIBCO Invitrogen, Cergy Pontoise, France) supplemented with 15% fetal calf serum (FCS, Eurobio, Les Ullis, France), 200 mM L-glutamine (G7513, Sigma–Aldrich, Saint Quentin Fallavier, France) and antibiotic (A5955, Sigma–Aldrich, Saint Quentin Fallavier, France) at 37 °C under 5% CO_2. Cells were treated with nanoparticles using this culture medium in all the following experiments.

2.2.6. Transmission electron microscopy (TEM)

Briefly, NR8383 cells were treated with 15 and 25 μg/mL of NP/ERS for 2 h, then they were immediately fixed with ice-cold 3% glutaraldehyde for 3 h. Cells were then post-fixed in 1% OsO_4 for 1 h at 4 °C, progressively dehydrated by increasing concentrations of ethanol and finally treated with propylene oxide and included in resin semi-fine (1.5 μm) and ultra-fine sections (70–90 nm) were prepared with an ultra-microtome (Reichert-Yung) and examined with the electron microscope Philips CM12 (FEI Electron Optics, Eindhoven, The Netherlands).

2.2.7. Total RNA extraction

Total RNA was extracted from cells, treated with 15 and 100 μg/mL of NP/ERS for 24 h, using RNeasy Mini Kit (QIAGEN, Courtaboeuf, France) following manufacturer instructions. RNA purity and concentration were determined spectrophotometrically using a NanoDrop ND-1000 (NanoDrop Technologies, Wilmington, DE).

2.2.8. Microarray

Microarray experiments were performed following the MIAME (Minimal Information About a Microarray Experiment) criteria (Brazma et al., 2001). Briefly, RNA samples were extracted from NR8383 cells and melted at 65 °C. cDNA was then synthesized using M-MLV reverse transcriptase (RT) (EC 2.7.7.6.9, Invitrogen, Cergy Pontoise, France). The cDNA was transcripted to cRNA using T7 RNA polymerase and labeled with fluorescent Cyanine 3-CTP. The cRNA (350 ng) was amplified and labeled using One-Color Gene Amp Labeling Kit (Agilent Technologies, Massy, France) following manufacturer's instructions, then purified using RNeasy Mini Kit (QIAGEN, Courtaboeuf, France) and quantified spectrophotometrically using a NanoDrop ND-1000 (NanoDrop Technologies, Wilmington, DE). The One-Color Spike-In Kit (Agilent Technologies, Massy, France) was used to provide positive controls. Before the hybridization step, 1.65 μg of cRNA was fragmented using the Gene Expression Hybridization Kit (Agilent Technologies, Massy, France) by incubation with fragmentation buffer and 10× blocking agent for 30 min at 60 °C. Fragmented cRNA was hybridized to Agilent 4× 44 K Whole Rat Genome Microarray (Agilent Technologies, Massy, France) using hybridization chambers (Agilent Technologies, Massy, France) and hybridization oven (Agilent Technologies, Massy, France) for 20 h at 65 °C. One-minute wash was performed twice using wash solution 1 and 2, respectively (Agilent Technologies, Massy, France). Microarrays were stabilized and dried by acetonitrile (Sigma–Aldrich, Saint Quentin Fallavier, France). The slides were scanned with the Agilent Microarray Scanner (Agilent technologies, Palo Alto, CA, USA) and the scanned images were extracted using Feature Extraction Software version 9.5.3 (Agilent). Analysis was performed with Genespring GX10 (Agilent Technologies, Palo Alto, CA, USA).

2.2.9. RNA reverse transcription and quantitative RT-PCR (qRT-PCR)

Total RNA (1 μg) from control or treated cell samples were reverse-transcripted with 50 nmol of oligo (dT) using M-MLV reverse transcriptase (RT) [EC 2.7.7.4.49, Invitrogen, Cergy Pontoise, France] following manufacturer's protocol. qRT-PCR was

Table 1
Primers sequences used in qRT-PCR experiments.

Primers	Sens	Anti sens
s18	5′-CGCCGCTAGACGTAGAATTCT-3′	5′CATTCTTGGCAAATGCTTTGC-3′
nfκb2	5′-TTCGGAACTGGGCAAATGTT-3′	5′-ACACGTAGCGGAATCGAAAT-3′
opa1	5′-TCCTGTGCATTCAAGATGGA-3′	5′-GAGCTTTCATTGGGAAGAGC-3′
tnf	5′-TAGCCCACGTCGTAGCAAAC-3′	5′-TGGTATGAAATGGCAAATCG-3′
bcl2l13	5′-TGGGATGCCTTTGTGGAACTAT-3′	5′-GGTCTGCTGACCTCACTTGT-3′
casp8	5′-GGTTTCTGCCTACAGGGTTA-3′	5′-TCGTAATCGTCGATCCTTCC-3′
pdcd4	5′-GGTGTGCCCGTGTTGGCAGT-3′	5′-GGCCCACCAATCGTGGTGCT-3′
ncf1	5′-TTCACAACTACGCAGGTGAA-3′	5′-TTATCTCCTCCCCAGCCTTC-3′
atg16l1	5′-CTTGTAATTCCCGCATTGCT-3′	5′-GCCTCGTATGTCTTTGATGC-3′

performed with a Stratagene Mx3000p system and Mesa Green qPCR MasterMix Plus for SYBR® (RT-SY2X-03-WOULR, Eurogentec, Belgium). Briefly, 100 ng of reverse-transcripted RNA from each sample were mixed with appropriate concentrations of tested gene primers (Table 1) and the Mesa Green qPCR MasterMix. *MRPSI8A* (*s18*) was used as internal control gene. PCR amplifications were carried out as follows: 5 min at 95 °C; 45 cycles (15 s at 95 °C, 40 s at 60 °C and 40 s at 72 °C). A standard curve was made for each gene and the subsequent slope was used to calculate the PCR reaction efficiency ($E = 10^{(-1/\text{slope})}$). For each sample, the gene expression level was calculated from the threshold cycle (C_t), which is the number of cycles necessary for the first detection of a PCR product.

2.2.10. Western blot

Total proteins (25 μg) from NR8383 cells either exposed (25 and 100 μg/mL of NP/ERS for 4, 10, 24, 36, 48 and 72 h) or not to nanoparticles were run on SDS-polyacrylamide gels (10%) as previously described (Corcelle et al., 2006; Laemmli, 1970) and transferred onto a PVDF membrane, followed by immunoblot analysis using monoclonal antibodies directed against anti-cleaved PARP (cat #552596, BD Biosciences Pharmingen, France), anti-p65 (cat #sc7178, Santa Cruz Biotechnology, France), mouse anti-OPA1 (cat #612606, BD Transduction Laboratories, France), anti LC3-II (clone 5F10; Nanotools, France), anti-actin (cat #C-11, Santa Cruz Biotechnology, France) or anti-tubulin (Santa Cruz Biotechnology, France) at the optimized dilutions. Bands were detected using an IgG polyclonal anti-mouse antibody conjugated to peroxidase (EC 1.11.1.7; Sigma) after addition of a chemiluminescent substrate (Roche).

2.2.11. Immunofluorescence

Cells were treated with either NP/ERS (0, 25, 50 and 100 μg/mL for 4 h) or chloroquine (CHL) CAs # [58175-87-4] as a positive control of autophagy (30 μM, 4 h). Cells deposited on a glass coverslip were fixed for 15 min in 4% paraformaldehyde in PBS at 4 °C and washed in PBS. Nonspecific binding was blocked with 1% bovine serum albumin–PBS for 15 min. Anti-LC3 antibody (1/100) was applied overnight at 4 °C. After two washes with PBS, sections were incubated with FITC-conjugated anti-mouse secondary antibody for 1 h at room temperature. The preparations were examined under a confocal laser-scanning microscope (Zeiss LSM510 Meta™) fitted with a 405 and 488 krypton/argon laser for simultaneous detection of DAPI and FITC fluorescence.

2.2.12. Intracellular reduced glutathione (GSH) measurement

Reduced glutathione measurements were performed as previously described (Lewicki et al., 2006), with some modifications. Briefly, cells were dispensed (5×10^5 cells/well) into a 6-well microplate. Cells were incubated with 25 and 100 μg/mL of NP/ERS for 24 h. Then, cells were washed three times with PBS solution (pH 7.4), and 1 mL of lysis solution [0.5 M perchloric acid, 0.1 M HCl and 2 mM EDTA] was added to cells. In order to remove the precipitated protein, cell lysates were centrifuged at 10,000 × *g* at 4 °C

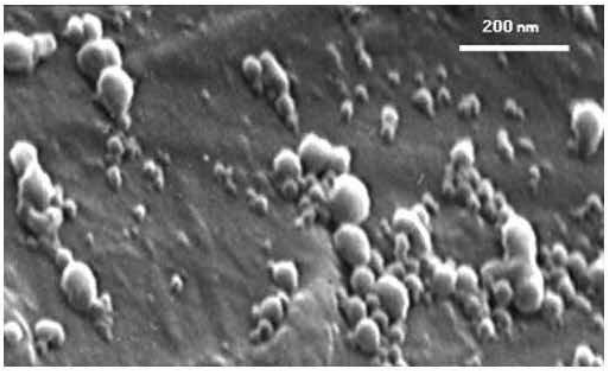

Fig. 1. SEM observation of NP/ERS nanoparticles.

for 15 min. 60 μL of supernatant, 120 μL of borate buffer (0.4 M, pH 9.2) and 20 μL of naphthalene-2,3- dicarboxyaldehyde (NDA) solution in ethanol were mixed in a 96-black well microplate and incubated in the dark at 4 °C for 25 min. Fluorescence intensity was then measured at 485-nm excitation and 528-nm emission using a microplate reader (Biotek Synergy). Results were expressed as nmol of GSH per mg of protein. Total protein quantity in cell lysate was determined by the Lowry method (Lowry et al., 1951).

2.2.13. Intracellular ROS measurement

The production of intracellular reactive oxygen species (ROS) was measured using an oxidation-sensitive fluorescent probe, 2′,7′-dichlorofluorescin diacetate ($DCFH_2$-DA) (Wang and Joseph, 1999). $DCFH_2$-DA passively enters the cell where it reacts with ROS to form a highly fluorescent compound, namely the dichlorofluorescein (DCF). Briefly, cells were dispensed (5×10^5 cells/well) into a 6-well microplate. Cells were exposed to 25 and 100 μg/mL for 24 h of NP/ERS. Lipopolysaccharide (LPS) was used as a positive control of ROS production (1 μg/mL for 24 h). Cells were washed three times with PBS solution (pH 7.4), resuspended in 1 mL of 4 μM $DCFH_2$-DA solution and incubated for 40 min at 37 °C. Cells were lysed using a lysis buffer (0.5 M Tris–HCl, 1.5 M NaCl, 3.5 mM SDS, 16 mM Triton X-100 and 1× protease inhibitor cocktail). The conversion of DCFH to the fluorescent product (DCF) was measured using a microplate reader (Biotek Synergy) with 485-nm excitation and 528-nm emission. ROS production was quantified from a DCF standard curve and results were expressed as DCF concentration (nM).

2.2.14. Statistical and data analysis

Microarray data and statistics were analyzed using GeneSpring GX10 software. Regarding qRT-PCR and array results, genes which showed more than a 2-fold or less than 0.5-fold intensity as compared to control, were considered respectively as up- or down-regulated (Lin et al., 2003). In our study, the differences between the control and the experimental group were evaluated with the one-paired *t*-test. *p*-Values ≤0.01 were considered as significant.

3. Results

3.1. Nanoparticle characterization

NP/ERS nanoparticles were positively charged (+40.6 ± 5 mV) owing to the quaternary ammonium groups of the polycationic ERS polymer. In addition, these nanoparticles had a mean nominal diameter value of 54.2 ± 6 nm and a weak polydispersity index (0.5 ± 0.04). Particle size results obtained by Zetasizer™ were comparable to those measured by SEM analysis (Fig. 1).

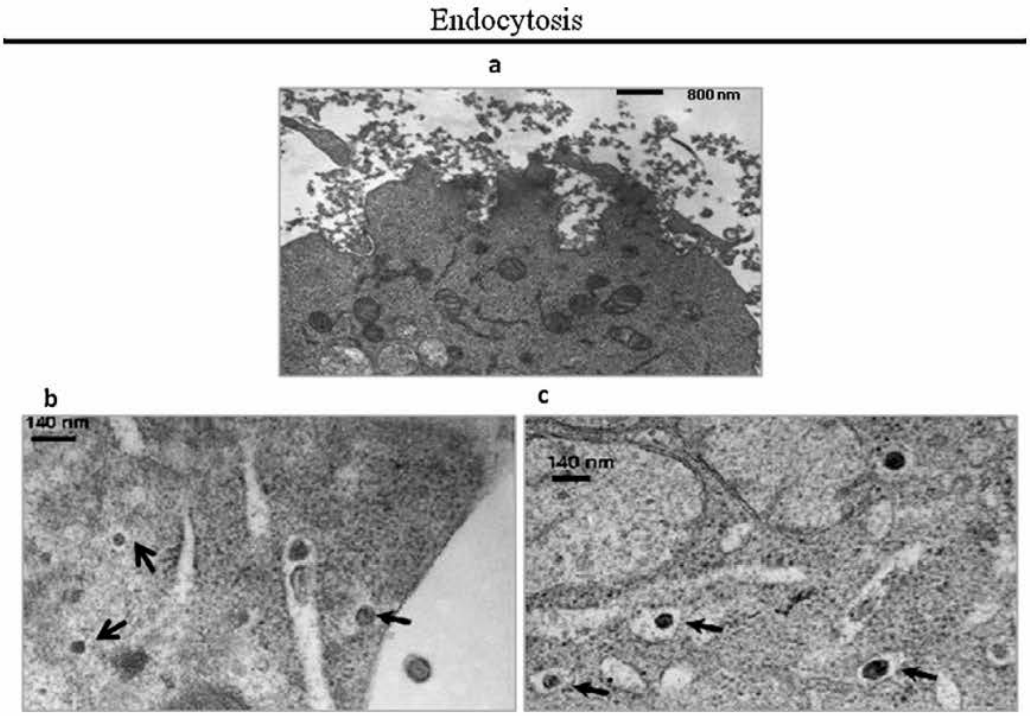

Fig. 2. Nanoparticle uptake by NR8383 macrophages. Macrophages exposed for 2 h to nanoparticles at a final concentration of 25 μg/mL (a) and 15 μg/mL (b and c). Arrows indicate internalized nanoparticles (a).

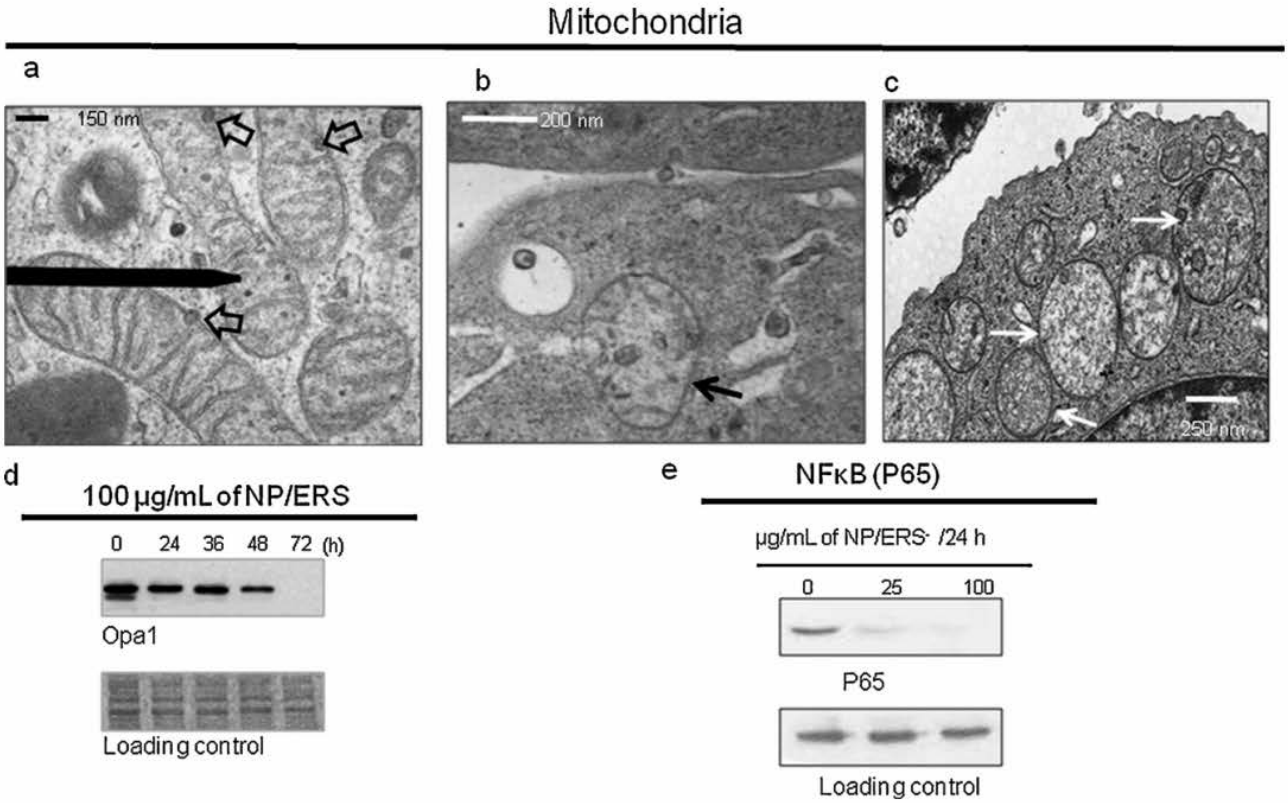

Fig. 3. Mitochondria are the intracellular target of NP/ERS nanoparticles. (a) Macrophages exposed to 15 μg/mL of nanoparticles for 1 h. Arrows indicate internalized nanoparticles into the cells and present on the border or inside the mitochondria. (b and c) Particle in an endosome and disorganization of *cristae* structure of mitochondria, cells were treated with 15 and 50 μg/mL of NP/ERS for 1 and 6 h, respectively. (d) and (e) Western blotting: (d) time-dependent down regulation of OPA1, (e) effect of nanoparticle concentration on the down regulation of NfκB (loading control is stained with Red Ponceau).

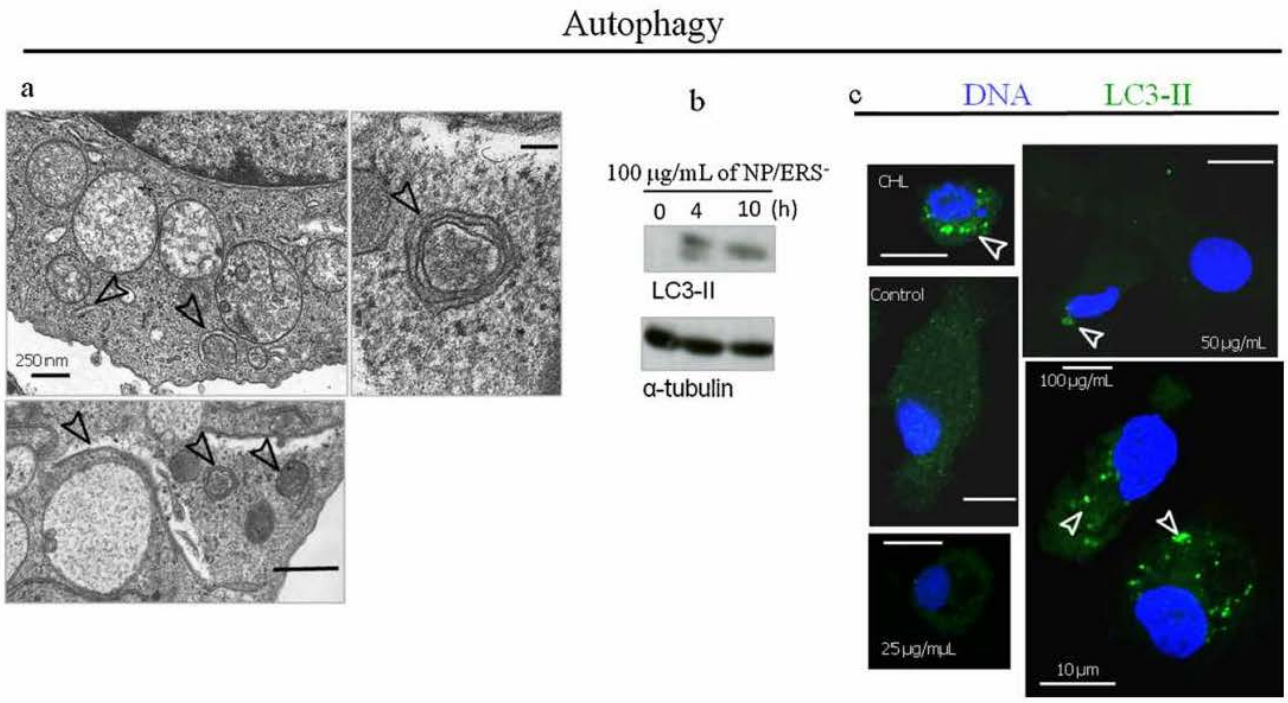

Fig. 4. Autophagy induced by NP/ERS particles. (a) Cells exposed to 50 µg/mL of nanoparticles for 6 h. Arrows indicate accumulation of double- and multi-membrane phagophores as well as lamellar autophagosomes. Note the dense aspect of mitochondria. (b) LC3-II protein levels obtained by Western blotting. No LC3-II protein was evidenced in control cells. Cells were exposed to 100 µg/mL of nanoparticles for 4 and 10 h, respectively. α-Tubulin was used as loading control. (c) In vitro accumulation of LC3-positive vesicles in NR8383 cells treated with NP/ERS observed by confocal fluorescence microscopy. Arrows indicate LC3-positive vesicles (green fluorescence). The blue fluorescence corresponds to DNA (stained with DAPI). (For interpretation of the references to color in the figure caption, the reader is referred to the web version of the article.)

3.2. TEM observations

Uptake of particles occurred in NR8383 macrophages upon incubation for 2 h with nanoparticles at a final concentration of 15 and 25 µg/mL. The particles were inside endosomes, free in the cytoplasm (Fig. 2a–c) or in contact with mitochondria. Some particles were inside those organelles, associated to their inner membrane (Fig. 3a). Alteration in the structure of mitochondria and disorganization of the *cristae* were also noted (Fig. 3b and c). When exposed to higher doses, namely 50 µg/mL for 6 h, cells displayed additional modifications characteristic of autophagy such as phagophore and autophagosome formation (Fig. 4a).

3.3. Microarray result analysis

Cells exposed to 25 µg/mL or 100 µg/mL nanoparticles had 56 and 427 transcripts significantly and differentially expressed as compared to unexposed cells. Several down or up regulated genes were associated with autophagy, G-protein signaling pathway, apoptosis and oxidative stress (Table 2). The effect was dose dependent

Table 2
Incidence of nanoparticles on gene expression as measured by microarray analysis. Only genes showing a significant up or down regulation are noted ($p \leq 0.01$).

	Approved gene symbol	Fold change in gene expression ± SD		HUGO approved gene name
		25 µg/mL	100 µg/mL	
GO[a]:0006915, apoptosis	*pdcd4*	−2.46 ± 0.08	−4.16 ± 0.09	Programmed cell death 4 (neoplastic transformation inhibitor)
	bcl2l13	–	−2.18 ± 0.05	BCL2-like 13 (apoptosis facilitator)
	bfar	–	−2.13 ± 0.04	Bifunctional apoptosis regulator
	casp8	–	−2.00 ± 0.03	Caspase 8
	rtkn	–	+2.08 ± 0.07	Rhotekin
	opa1	–	−2.23 ± 0.03	Optic atrophy 1 (autosomal dominant)
	tnfrsf5	–	+2.26 ± 0.09	Tumor necrosis factor receptor superfamily, member 5
	tnf	–	−2.53 ± 0.06	Tumor necrosis factor (*tnf* superfamily, member 2)
GO:0007165, signal transduction	*arhgap22*	–	+2.07 ± 0.8	Rho GTPase activating protein 22
	rhov	–	+2.17 ± 0.05	ras homolog gene family, member V
GO:0003824, catalytic activity	*atg16l1*	–	+2.30 ± 0.03	atg16 autophagy related 16-like 1
GO:0001664, G-protein coupled receptor binding	*apln*	–	+2.20 ± 0.09	Apelin
GO:0003700, transcription factor activity	*nfκb2*	–	−2.61 ± 0.04	Nuclear factor of kappa light polypeptide gene enhancer in B-cells 2 (p49/p100)
GO: response to oxidative stress	*gclc*	–	+2.53 ± 0.04	*Rattus norvegicus* glutamate-cysteine ligase, catalytic subunit

[a] Gene ontology terms.

Table 3
Incidence of nanoparticles on gene expression as measured by RT-qPCR ($p \leq 0.01$).

Approved gene symbol	Fold change ± SD	
	NP/ERS (25 μg/mL)	NP/ERS (100 μg/mL)
pdcd4	−1.22 ± 0.07	−2.10 ± 0.08
bcl2	−1.29 ± 0.06	−2.00 ± 0.05
casp8	−0.85 ± 0.04	−1.90 ± 0.03
opa1	−1.35 ± 0.05	−2.45 ± 0.04
tnf	−1.00 ± 0.02	−1.80 ± 0.08
nfκb2	−1.76 ± 0.07	−2.28 ± 0.05
atg16l1	+19.20 ± 0.92	+17.45 ± 0.68
ncf1	+4.78 ± 0.14	+9.82 ± 0.29

− and + indicate under- and up-expression, respectively as compared to untreated cells.

and more pronounced in 100 μg/mL treated cells. The exposure of cells to nanoparticles at a concentration of 100 μg/mL resulted in the down regulation of the *opa1* gene, of the two anti-apoptotic genes *bcl2l13* and *nfκb2* and of the bifunctional apoptosis regulator (*bfar*) as well as of the pro-apototic genes *casp8* and *pdcd4*. On the contrary, the *tnfrsf5* genes (TNF receptor superfamily member 5 and cd40), the anti-apoptotic genes [*rhov* and *arhgap22* (a rho GTPase activating protein), *rtkn* (the rho effector rhotekin) and *apln* (apelin related to G-proteins)] as well as *atg16l1 a* pro-autophagic gene encoding for a protein belonging to a large protein complex necessary for autophagy (Saitoh et al., 2008), were up regulated. The gene of the glutamate-cysteine ligase (a key gene in the glutathione homeostasis) catalytic subunit (*gclc*) was also up regulated in cells treated with 100 μg/mL NP/ERS (Table 2).

3.4. qRT-PCR

qRT-PCR confirmed the microarray data indicating a down-expression of *opa1*, *bcl2l13*, *pdcd4*, *casp8*, *tnf* and *nfκb2* in 100 μg/mL particle-treated cells (Table 3). Our results showed also a significant up regulation of *atg16l1* in cells treated with 25 and 100 μg/mL of NP/ERS (Table 3). Additionally, a dose-dependent up regulation of *ncf1* (neutrophil cytosolic factor 1), an $O_2^{\bullet -}$ generating enzyme, was evidenced (Table 3)

3.5. Western blot

Western blot showed a time- and dose-dependent decrease of OPA1 and NFκB protein content in cells exposed to 100 μg/mL NP (Fig. 3d and e). In agreement with up regulation of the autophagy *atg16l1* gene, above reported, the conversion of microtubule-associated protein 1 light chain 3 (LC3) into the LC3-II isoform, a common autophagy marker (Asanuma et al., 2003), was also detected in nanoparticle exposed cells (Fig. 4b). Additionally, no poly(ADP-ribose) polymerase (PARP) protein fragmentation was detected in the NP/ERS-treated cells whatever the nanoparticle concentration (data not shown).

3.6. Immunofluorescence assay

Treatment of NR8383 with NP/ERS at a final concentration of 25, 50 and 100 μg/mL for 4 h induced a dose-dependent accumulation of LC3-positive vesicles (Fig. 4c).

3.7. Intracellular GSH

Our data showed a significant decrease of intracellular reduced GSH (~52%) in cells treated with the higher concentration of NP/ERS, 100 μg/mL for 24 h, as compared to control (Fig. 5).

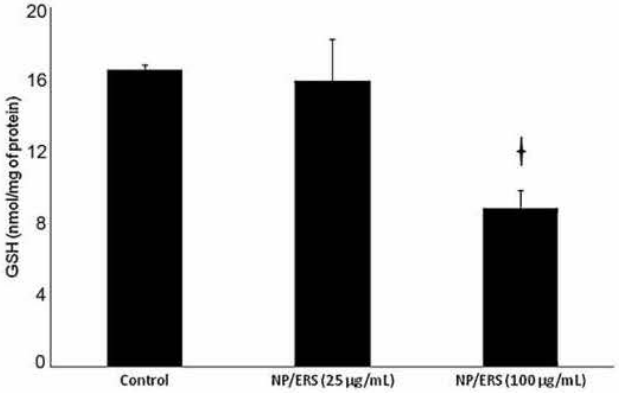

Fig. 5. The decrease of intracellular reduced GSH level in NR8383 cells exposed to 25 and 100 μg/mL of NP/ERS for 24 h. Data were expressed as nmol of GSH per mg of protein. Dagger indicates a significant difference at $p \leq 0.01$.

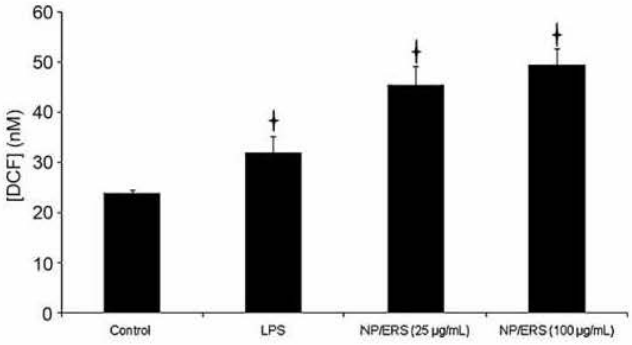

Fig. 6. Intracellular ROS level increase in NR8383 cells after a 24 h exposure to NP/ERS. LPS (1 μg/mL) is used as a ROS inducer. Dagger indicates a significant difference at $p \leq 0.01$.

3.8. ROS production

A significant increase of ROS production ratio, expressed by DCF concentration (nM), was evidenced in cells incubated with 25 (~1.9 times) and 100 μg/mL (~2.1 times) of NP/ERS for 24 h as compared to unexposed cells (Fig. 6).

4. Discussion

4.1. NP/ERS uptake by NR8383 macrophages and mitochondria targeting

It has been reported that endocytosis pathway plays a fundamental role in a wide range of cellular function; in particular it affects the functions of mitochondria (Polo and Di Fiore, 2006). Uptake of particles by endocytosis depends primarily on their size and ionic charge (Xia et al., 2006). It has been documented that cationic and small diameter nanoparticles, such as 60 nm NH_2-labeled nanospheres, are internalized into the cells and gain access to cellular organelles and may damage mitochondria. On the contrary, anionic and larger nanoparticles of 200 nm diameter do not (Xia et al., 2006, 2008). In addition, it has been reported that single-walled carbon nanotubes (SWCNTs), which are known to induce cytotoxicity, target the mitochondria (Yang et al., 2010). In line with these evidences, in our study we observed numerous NP/ERS in the vicinity of the inner mitochondria membrane. Among the genes responsible of mitochondria functions, *opa1* gene plays a major role in the maintenance of the mitochondrial network morphology and dynamics and in the regulation of the signal pathways of cellular death (Chen et al., 2003). In fact, *opa1* was reported to play this

role along with *mfn1* and *mfn2* genes, of which respective products mitofusin1 and 2, are mediators of mitochondrial fusion. In retinal ganglial cells, a down regulation of *opa1* has been reported to promote the aggregation of the mitochondrial network and to alter the structure of the mitochondrial inner membrane (Kamei et al., 2005). In particular the disorganization of the *cristae*, the release of cytochrome *c* and the induction of intrinsic apoptosis has been observed (Arnoult et al., 2005; Olichon et al., 2003). In our study, *opa1* down regulation as well as electron microscopy observations suggest that NP/ERS cytotoxicity in macrophages is triggered by their effect on mitochondria. However, it is difficult to determine whether nanoparticles induce the mitochondrial decay by altering gene expression or by a mechanical impairment, e.g. by abolishing transmembrane proton gradient.

4.2. Oxidative stress induction by ERS nanoparticles

Damage to the mitochondrial inner membrane, caused by *opa1* down expression, increases ROS production that causes further lysosomal disruption (Arnoult et al., 2005). This disruption could liberate nanoparticles enclosed in endocytic vesicles which eventually reach their target, namely the mitochondria and penetrate them triggering the autophagy process. These data suggest that crosstalk between the lysosome and mitochondria could play an important role in determining cell death type. Intracellular reactive oxygen species (ROS) production as well as oxidative stress occurs in NP/ERS-treated cells. In fact, by using qRT-PCR assays we observed the over expression of both *ncf1*, a gene encoding a subunit of NADPH oxidase (Dika Nguea et al., 2008), and of *gclc*, one of the key genes responsible for GSH homeostasis (Dickinson et al., 2004). In agreement with these data, in NP/ERS-treated cells we evidenced a significant decrease of the cellular concentration of reduced glutathione (GSH) and an increase of ROS production.

4.3. Apoptosis inhibition by NP/ERS

Treatment of NR8383 cells with NP/ERS nanoparticles does not induce apoptotic cellular death. In our previous work, we have shown the absence of apoptotic processes that was ascertained by the facts that neither the poly(ADP-ribose) polymerase (PARP) fragmentation nor the formation of DNA laddering was observed. However, histochemical assays indicate the activation of caspase 3 and caspase 7 (Eidi et al., 2010). Although many reports indicate that *tnf* expression was elevated by nanoparticle treatment (Chen et al., 2006; Minematsu et al., 2007), there are contradictory data on its expression due to the use of different experimental cell models (Niu et al., 2007). TNF receptor superfamily member 5 (*tnfrsf5*), known as a potent inhibitor of *nfκb2* gene expression in dendritic cells (Mann et al., 2002) affecting the extrinsic apoptosis pathway (Wallach et al., 1997), was up regulated in our experiment. It has been proved also that *tnf* is able to induce extrinsic apoptosis through the *casp8* activation pathway that was under expressed in our study (Bhattacharyya et al., 2010). Evidence of suppression of the cellular signaling pathway leading to extrinsic apoptosis was obtained in our study by the down regulation of proapoptotic genes, e.g. *pdcd4* (Vikhreva et al., 2010), *casp8* and *bcl2L13* (Talotta et al., 2009). Furthermore, genes involved in extrinsic apoptosis inhibition were up regulated like *rhov*, *arhgap22*, *rtkn* and *apln*. Those data are not in favor of an underlying extrinsic apoptosis process triggered by nanoparticles and we explored further the intrinsic apoptosis. In fact, a possible activation of intrinsic apoptosis is supported by microarray and qRT-PCR assays which show the down regulation of *opa1*, *nfκb2*, *bcl2*. Indeed, some reports have indicated that *nfκb2* induced *bcl2* expression and promoted cell survival (Oberdorster et al., 2005; Viatour et al., 2003). Furthermore, the bifunctional apoptosis regulator (*bfar*), an inhibitor of BAX-induced apoptosis (Zhang et al., 2000), was down-regulated in our experiment. Interestingly, our data showed that neither extrinsic nor intrinsic apoptotic cell death pathways are activated in NR/ERS-treated cells. Instead NR/ERS seem to lead the cells toward the autophagic cell death.

4.4. ERS nanoparticles induce autophagy

An inverse relationship between the activation of the genes involved in the apoptosis and those involved in the autophagy, which may corresponds to a switch from apoptosis to autophagy, has been described (Luo and Rubinsztein, 2007; Shimizu et al., 2004). In particular a decrease in the expression of the apoptotic *bcl* family genes and the activation of the autophagic *atg* family genes has been reported. In our system we observe a decreased expression of *bcl2*, an efficient autophagy inhibitor (Sasi et al., 2009) and an over expression of *atg16l1* as well as the conversion of the microtubule-associated protein 1 light chain 3 (LC3) into the LC3-II isoform, a common marker of autophagy (Asanuma et al., 2003). Moreover, we report the down regulation of proautophagic gene, namely *casp8* that was reported to induce autophagy cell death in U937 macrophages (Yu et al., 2004). Furthermore, we observed cellular alterations characteristic of autophagic cell death: phagophores, autophagosomes and "mitophagy". Such morphological modifications have been described recently in cells treated with gold nanoparticles (Li et al., 2010), soluble fullerenes (Yamawaki and Iwai, 2006), viruses (Sir and Ou, 2008), quantum dots (Seleverstov et al., 2006) and SWCNTs (Yang et al., 2010). Through autophagy, cells not only recycle intracellular components and compensate for nutrient deprivation but also they eliminate selectively damaged organelles/proteins and maintain cellular homeostasis. Non-selective autophagy degrades all organelles and long-lived proteins to provide the energy required for cell survival. By contrast, mitophagy selectively eliminates mitochondria to regulate their number as well as to remove specifically the damaged ones (Youle and Narendra, 2011). Our results demonstrate that NP/ERS-mediated cell toxicity occurs *via* organelle, notably mitochondrion, autophagy which amplifies a physiological process. In a future work, it would be interesting to study the cytotoxicity and cell morphological modifications occurring after longer exposure of macrophages with lower doses.

5. Conclusion

Nanotechnology has attracted increasing interest among almost all fields of research. Notable improvements in our knowledge about metallic nano-objects or carbon nanotubes toxicity and their influence on the expression of genes and the impairment of the oxidant/antioxidant cellular balance have been obtained. Nevertheless, data on the toxicity of drug delivery nanoparticles remain extremely scarce. To the best of our knowledge, this article is the first to report that polymeric nanoparticles designed for drug delivery, upon their enclosure into macrophages by endocytosis, are able to cross the mitochondrial membranes and enter inside these organelles. This process induces a cascade of events such as the unbalance of the oxidant/antioxidant homeostasis and the modification of the expression of genes and proteins, especially those implied in macrophages activation and autophagy. As a consequence, a mitochondrial decay through phagophore and autophagosome formation and eventually mitophagy occurs. How immune cells deal with nanoparticles is an interesting issue as this process presents some analogy with viral infections. Furthermore, the identification of the early cellular markers described and discussed in this article may serve as a conceptual scaffold for designing experiments for a better understanding of the cellular

toxicity of loaded and unloaded nanoparticles. The evaluation of cytotoxic effects in term of autophagy is a rather new concept but it should be investigated for every type of carrier to be used for drug delivery. As we have used a model of rat macrophages, human derived cell lines as well as in vivo models should be also tested to confirm these results.

Acknowledgements

The authors thank Dr. Lucia Marcocci for her help and support in reviewing the manuscript. Authors would like to acknowledge Lu Zhang, Kevin Dalleau, Bouchra Mouaraki, Christine Manencq and Ramia Safar for their kind help in microarray and PCR experiments.

References

Arnoult, D., Grodet, A., Lee, Y.J., Estaquier, J., Blackstone, C., 2005. Release of OPA1 during apoptosis participates in the rapid and complete release of cytochrome c and subsequent mitochondrial fragmentation. J. Biol. Chem. 280, 35742–35750.

Asanuma, K., Tanida, I., Shirato, I., Ueno, T., Takahara, H., Nishitani, T., Kominami, E., Tomino, Y., 2003. MAP-LC3, a promising autophagosomal marker, is processed during the differentiation and recovery of podocytes from PAN nephrosis. FASEB J. 17, 1165–1167.

Bhardwaj, P., Chaurasia, H., Chaurasia, D., Prajapati, S.K., Singh, S., 2010. Formulation and in-vitro evaluation of floating microballoons of indomethacin. Acta Pol. Pharm. 67, 291–298.

Bhattacharyya, S., Dudeja, P.K., Tobacman, J.K., 2010. Tumor necrosis factor alpha-induced inflammation is increased but apoptosis is inhibited by common food additive carrageenan. J. Biol. Chem. 285, 39511–39522.

Bodmeier, R., Chen, H., Tyle, P., Jarosz, P., 1991. Spontaneous formation of drug-containing acrylic nanoparticles. J. Microencapsul. 8, 161–170.

Brazma, A., Hingamp, P., Quackenbush, J., Sherlock, G., Spellman, P., Stoeckert, C., Aach, J., Ansorge, W., Ball, C.A., Causton, H.C., Gaasterland, T., Glenisson, P., Holstege, F.C., Kim, I.F., Markowitz, V., Matese, J.C., Parkinson, H., Robinson, A., Sarkans, U., Schulze-Kremer, S., Stewart, J., Taylor, R., Vilo, J., Vingron, M., 2001. Minimum information about a microarray experiment (MIAME)-toward standards for microarray data. Nat. Genet. 29, 365–371.

Chen, H., Detmer, S.A., Ewald, A.J., Griffin, E.E., Fraser, S.E., Chan, D.C., 2003. Mitofusins Mfn1 and Mfn2 coordinately regulate mitochondrial fusion and are essential for embryonic development. J. Cell Biol. 160, 189–200.

Chen, H.W., Su, S.F., Chien, C.T., Lin, W.H., Yu, S.L., Chou, C.C., Chen, J.J., Yang, P.C., 2006. Titanium dioxide nanoparticles induce emphysema-like lung injury in mice. FASEB J. 20, 2393–2395.

Corcelle, E., Nebout, M., Bekri, S., Gauthier, N., Hofman, P., Poujeol, P., Fenichel, P., Mograbi, B., 2006. Disruption of autophagy at the maturation step by the carcinogen lindane is associated with the sustained mitogen-activated protein kinase/extracellular signal-regulated kinase activity. Cancer Res. 66, 6861–6870.

Dickinson, D.A., Levonen, A.L., Moellering, D.R., Arnold, E.K., Zhang, H., Darley-Usmar, V.M., Forman, H.J., 2004. Human glutamate cysteine ligase gene regulation through the electrophile response element. Free Radic. Biol. Med. 37, 1152–1159.

Dika Nguea, H., de Reydellet, A., Lehuede, P., De Meringo, A., Le Faou, A., Marcocci, L., Rihn, B.H., 2008. Gene expression profile in monocyte during in vitro mineral fiber degradation. Arch. Toxicol. 82, 355–362.

Eidi, H., Joubert, O., Attik, G., Duval, R.E., Bottin, M.C., Hamouia, A., Maincent, P., Rihn, B.H., 2010. Cytotoxicity assessment of heparin nanoparticles in NR8383 macrophages. Int. J. Pharm.

Fessi, H., Puisieux, F., 1989. Nanocapsule formation by interfacial polymer deposition following solvent displacement. Int. J. Pharm. 55, 1–4.

Gargouri, M., Sapin, A., Bouli, S., Becuwe, P., Merlin, J.L., Maincent, P., 2009. Optimization of a new non-viral vector for transfection: Eudragit nanoparticles for the delivery of a DNA plasmid. Technol. Cancer Res. Treat. 8, 433–444.

Hoffart, V., Lamprecht, A., Maincent, P., Lecompte, T., Vigneron, C., Ubrich, N., 2006. Oral bioavailability of a low molecular weight heparin using a polymeric delivery system. J. Control. Release 113, 38–42.

Jiao, Y., Ubrich, N., Marchand-Arvier, M., Vigneron, C., Hoffman, M., Lecompte, T., Maincent, P., 2002. In vitro and in vivo evaluation of oral heparin-loaded polymeric nanoparticles in rabbits. Circulation 105, 230–235.

Kamei, S., Chen-Kuo-Chang, M., Cazevieille, C., Lenaers, G., Olichon, A., Belenguer, P., Roussignol, G., Renard, N., Eybalin, M., Michelin, A., Delettre, C., Brabet, P., Hamel, C.P., 2005. Expression of the Opa1 mitochondrial protein in retinal ganglion cells: its downregulation causes aggregation of the mitochondrial network. Invest. Ophthalmol. Vis. Sci. 46, 4288–4294.

Laemmli, U.K., 1970. Cleavage of structural proteins during the assembly of the head of bacteriophage T4. Nature 227, 680–685.

Lamprecht, A., Koenig, P., Ubrich, N., Maincent, P., Neumann, D., 2006. Low molecular weight heparin nanoparticles: mucoadhesion and behaviour in Caco-2 cells. Nanotechnology 17, 3673–3680.

Lewicki, K., Marchand, S., Matoub, L., Lulek, J., Coulon, J., Leroy, P., 2006. Development of a fluorescence-based microtiter plate method for the measurement of glutathione in yeast. Talanta 70, 876–882.

Li, J.J., Hartono, D., Ong, C.N., Bay, B.H., Yung, L.Y., 2010. Autophagy and oxidative stress associated with gold nanoparticles. Biomaterials 31, 5996–6003.

Lin, Z., Fillmore, G.C., Um, T.H., Elenitoba-Johnson, K.S., Lim, M.S., 2003. Comparative microarray analysis of gene expression during activation of human peripheral blood T cells and leukemic Jurkat T cells. Lab. Invest. 83, 765–776.

Lowry, O.H., Rosebrough, N.J., Farr, A.L., Randall, R.J., 1951. Protein measurement with the Folin phenol reagent. J. Biol. Chem. 193, 265–275.

Luo, S., Rubinsztein, D.C., 2007. Atg5 and Bcl-2 provide novel insights into the interplay between apoptosis and autophagy. Cell Death Differ. 14, 1247–1250.

Mann, J., Oakley, F., Johnson, P.W., Mann, D.A., 2002. CD40 induces interleukin-6 gene transcription in dendritic cells: regulation by TRAF2, AP-1, NF-kappa B, and CBF1. J. Biol. Chem. 277, 17125–17138.

Minematsu, H., Shin, M.J., Celil Aydemir, A.B., Seo, S.W., Kim, D.W., Blaine, T.A., Macian, F., Yang, J., Young-In Lee, F., 2007. Orthopedic implant particle-induced tumor necrosis factor-alpha production in macrophage-monocyte lineage cells is mediated by nuclear factor of activated T cells. Ann. N. Y. Acad. Sci. 1117, 143–150.

Nguea, H.D., de Reydellet, A., Le Faou, A., Zaiou, M., Rihn, B., 2008. Macrophage culture as a suitable paradigm for evaluation of synthetic vitreous fibers. Crit. Rev. Toxicol. 38, 675–695.

Niu, J., Azfer, A., Rogers, L.M., Wang, X., Kolattukudy, P.E., 2007. Cardioprotective effects of cerium oxide nanoparticles in a transgenic murine model of cardiomyopathy. Cardiovasc. Res. 73, 549–559.

Oberdorster, G., Maynard, A., Donaldson, K., Castranova, V., Fitzpatrick, J., Ausman, K., Carter, J., Karn, B., Kreyling, W., Lai, D., Olin, S., Monteiro-Riviere, N., Warheit, D., Yang, H., 2005. Principles for characterizing the potential human health effects from exposure to nanomaterials: elements of a screening strategy. Part Fibre Toxicol. 2, 8.

Olichon, A., Baricault, L., Gas, N., Guillou, E., Valette, A., Belenguer, P., Lenaers, G., 2003. Loss of OPA1 perturbates the mitochondrial inner membrane structure and integrity, leading to cytochrome c release and apoptosis. J. Biol. Chem. 278, 7743–7746.

Pignatello, R., Bucolo, C., Ferrara, P., Maltese, A., Puleo, A., Puglisi, G., 2002. Eudragit RS100 nanosuspensions for the ophthalmic controlled delivery of ibuprofen. Eur. J. Pharm. Sci. 16, 53–61.

Polo, S., Di Fiore, P.P., 2006. Endocytosis conducts the cell signaling orchestra. Cell 124, 897–900.

Saitoh, T., Fujita, N., Jang, M.H., Uematsu, S., Yang, B.G., Satoh, T., Omori, H., Noda, T., Yamamoto, N., Komatsu, M., Tanaka, K., Kawai, T., Tsujimura, T., Takeuchi, O., Yoshimori, T., Akira, S., 2008. Loss of the autophagy protein Atg16L1 enhances endotoxin-induced IL-1beta production. Nature 456, 264–268.

Sasi, N., Hwang, M., Jaboin, J., Csiki, I., Lu, B., 2009. Regulated cell death pathways: new twists in modulation of BCL2 family function. Mol. Cancer Ther. 8, 1421–1429.

Schaffazick, S.R., Siqueira, I.R., Badejo, A.S., Jornada, D.S., Pohlmann, A.R., Netto, C.A., Guterres, S.S., 2008. Incorporation in polymeric nanocapsules improves the antioxidant effect of melatonin against lipid peroxidation in mice brain and liver. Eur. J. Pharm. Biopharm. 69, 64–71.

Seleverstov, O., Zabirnyk, O., Zscharnack, M., Bulavina, L., Nowicki, M., Heinrich, J.M., Yezhelyev, M., Emmrich, F., O'Regan, R., Bader, A., 2006. Quantum dots for human mesenchymal stem cells labeling. A size-dependent autophagy activation. Nano Lett. 6, 2826–2832.

Shimizu, S., Kanaseki, T., Mizushima, N., Mizuta, T., Arakawa-Kobayashi, S., Thompson, C.B., Tsujimoto, Y., 2004. Role of Bcl-2 family proteins in a non-apoptotic programmed cell death dependent on autophagy genes. Nat. Cell Biol. 6, 1221–1228.

Sir, D., Ou, J.H., 2008. Autophagy in viral replication and pathogenesis. Mol. Cells 29, 1–7.

Suri, S.S., Fenniri, H., Singh, B., 2007. Nanotechnology-based drug delivery systems. J. Occup. Med. Toxicol. 2, 16.

Talotta, F., Cimmino, A., Matarazzo, M.R., Casalino, L., De Vita, G., D'Esposito, M., Di Lauro, R., Verde, P., 2009. An autoregulatory loop mediated by miR-21 and PDCD4 controls the AP-1 activity in RAS transformation. Oncogene 28, 73–84.

Unger, F., Wittmar, M., Kissel, T., 2007. Branched polyesters based on poly[vinyl-3-(dialkylamino)alkylcarbamate-co-vinyl acetate-co-vinyl alcohol]-graftpoly(D,L-lactide-co-glycolide): effects of polymer structure on cytotoxicity. Biomaterials 28, 1610–1619.

Viatour, P., Bentires-Alj, M., Chariot, A., Deregowski, V., de Leval, L., Merville, M.P., Bours, V., 2003. NF- kappa B2/p100 induces Bcl-2 expression. Leukemia 17, 1349–1356.

Vikhreva, P.N., Shepelev, M.V., Korobko, E.V., Korobko, I.V., 2010. Pdcd4 tumor suppressor: properties, functions, and their application to oncology. Mol. Gen. Mikrobiol. Virusol., 3–11.

Wallach, D., Boldin, M., Varfolomeev, E., Beyaert, R., Vandenabeele, P., Fiers, W., 1997. Cell death induction by receptors of the TNF family: towards a molecular understanding. FEBS Lett. 410, 96–106.

Wang, H., Joseph, J.A., 1999. Quantifying cellular oxidative stress by dichlorofluorescein assay using microplate reader. Free Radic. Biol. Med. 27, 612–616.

Xia, T., Kovochich, M., Brant, J., Hotze, M., Sempf, J., Oberley, T., Sioutas, C., Yeh, J.I., Wiesner, M.R., Nel, A.E., 2006. Comparison of the abilities of ambient and manufactured nanoparticles to induce cellular toxicity according to an oxidative stress paradigm. Nano Lett. 6, 1794–1807.

Xia, T., Kovochich, M., Liong, M., Zink, J.I., Nel, A.E., 2008. Cationic polystyrene nanosphere toxicity depends on cell-specific endocytic and mitochondrial injury pathways. ACS Nano 2, 85–96.

Yamawaki, H., Iwai, N., 2006. Cytotoxicity of water-soluble fullerene in vascular endothelial cells. Am. J. Physiol. Cell Physiol. 290, C1495–C1502.
Yang, Z., Zhang, Y., Yang, Y., Sun, L., Han, D., Li, H., Wang, C., 2010. Pharmacological and toxicological target organelles and safe use of single-walled carbon nanotubes as drug carriers in treating Alzheimer disease. Nanomedicine 6, 427–441.
Youle, R.J., Narendra, D.P., 2011. Mechanisms of mitophagy. Nat. Rev. Mol. Cell Biol. 12, 9–14.
Yu, L., Alva, A., Su, H., Dutt, P., Freundt, E., Welsh, S., Baehrecke, E.H., Lenardo, M.J., 2004. Regulation of an ATG7-beclin 1 program of autophagic cell death by caspase-8. Science 304, 1500–1502.
Zhang, H., Xu, Q., Krajewski, S., Krajewska, M., Xie, Z., Fuess, S., Kitada, S., Pawlowski, K., Godzik, A., Reed, J.C., 2000. BAR: an apoptosis regulator at the intersection of caspases and Bcl-2 family proteins. Proc. Natl. Acad. Sci. U.S.A. 97, 2597–2602.

Chapitre IV.

Discussion générale, conclusion et perspectives

Dans ce dernier chapitre, nous discuterons successivement du choix du système nanoparticulaire, de la difficulté pour caractériser les NP d'or rencontrée dans les laboratoires de recherche, de la stratégie adoptée pour les stabiliser dans des conditions physiologiques, et de leurs effets biologiques sur une lignée cellulaire immunitaire ; nous terminerons cette discussion par une réflexion sur le rapport bénéfices/risques lié à l'utilisation potentielle de ces NP en thérapeutique.

IV.1 Choix des nanoparticules

L'objectif de cette étude consiste en l'élaboration d'une plateforme nanoparticulaire stable et de taille la plus petite possible pour faciliter la diffusion dans les fluides biologiques et au travers des barrières physiologiques (nasale, intestinale, membrane cellulaire,...). De plus, cette plateforme doit être capable de véhiculer un agent thérapeutique pour traiter diverses pathologies telles que les maladies cardiovasculaires et le cancer. Afin d'assurer ces attentes et ce rôle de plateforme thérapeutique, les NP doivent répondre à un certain nombre de critères : i) présenter une taille inférieure à 100 nm; ii) être non cytotoxiques et biocompatibles; iii) être stables (pas d'agrégation) au contact des fluides corporels; iv) être « furtives » vis-à-vis du système des phagocytes mononucléés (SPM) pour prolonger leur temps de circulation dans le sang; v) être non immunogéniques, etc...

Parmi les différents types de NP utilisées pour le transport des médicaments, notre choix s'est porté sur les NP d'or. En effet, les NP d'or connaisent un grand essor en particulier dans le domaine de la santé en tant que vecteur de petites molécules, de protéines, de peptides et d'acides nucléiques pour le traitement de pathologies diverses. Par exemple, les NP d'or ont été utilisées en tant que véhicule pour améliorer la perméabilité de principes actifs (tels que l'insuline, le méthotrexate, le paclitaxel, la streptomycine et la kanamycine) à travers les barrières physiologiques (Joshi *et al.*, 2006, Chen *et al.*, 2007, Gibson *et al.*, 2007, Ghosh *et al.*, 2008, Burygin *et al.*, 2009). De plus, les NP d'or ont été proposées comme véhicule pour transporter le TNF-α vers les cellules cancéreuses. Des essais cliniques en phase I ont montré que des doses élevées de TNF-α, administrées par voie intraveineuse à 30 patients portant différentes tumeurs en stade avancé, n'entrainaient pas d'effets secondaires et présentaient une action ciblée lorsque le TNF-α était greffé sur des NP d'or (Libutti *et al.*, 2010). Récemment, un essai clinique de phase I a été approuvé par l'agence de réglementation suisse pour évaluer le potentiel des NP d'or en tant que véhicule pour l'administration par voie orale de l'insuline chez l'Homme (Alan, 2011).

La dimension nanométrique des NP d'or (souvent autour de 5 nm, inférieure à 20 nm) facilite leur passage à travers des barrières physiologiques, mais surtout évite aux NP d'or d'être éliminées rapidement par les systèmes de défense de l'organisme, ce qui permet d'augmenter leur temps de résidence dans le sang. Cette dimension représente donc un avantage pour leur fonction de vecteur. Néanmoins, des efforts doivent être menés, notamment sur la fonctionnalisation de surface de la NP, pour répondre aussi aux critères de stabilité et de biocompatibilité. La réactivité de la surface métallique des NP d'or vis-à-vis de molécules présentes dans le corps doit être réduite par des agents stabilisants. Il est indispensable que les NP d'or (cœur métallique et agent stabilisant) ne présentent aucun danger pour le patient. De plus, les NP d'or doivent pouvoir venir se concentrer dans l'organe ou le tissu cible (par exemple la tumeur) et non pas s'accumuler dans les organes purificateurs comme le foie et les reins.

Pour répondre à ces critères, les objectifs de notre étude étaient les suivants :

- la synthèse de NP d'or (d'une taille de l'ordre de 5 nm) et l'optimisation de la densité de leur couverture afin d'augmenter leur stabilité ainsi que de réduire leur réactivité de surface non spécifique vis-à-vis de molécules présentes dans l'organisme;
- la présence à la surface extrême des NP de groupements organiques fonctionnels libres en nombre suffisant pour permettre le greffage ultérieur de molécules d'intérêt pharmacologique;
- le développement et l'optimisation de méthodes de routine pour mieux caractériser ces entités d'un point de vue physico-chimique;
- l'évaluation des effets biologiques des NP d'or et l'influence de la fonctionnalisation de surface sur leur « capture » par les macrophages.

Nous discuterons dans la suite de ce chapitre de la démarche expérimentale retenue pour atteindre les objectifs précités.

IV.2 Choix de la méthode de synthèse

Parmi les différentes méthodes de synthèse des NP d'or, deux d'entre elles ont plus particulièrement attiré notre attention au début de cette recherche.

La première consiste à réduire un sel d'or ($HAuCl_4$) à l'aide de $NaBH_4$, en présence de citrate de sodium. Cette voie, proposée en 1999 par Brown, conduit directement à la synthèse de NP d'or, de l'ordre de 5 nm de diamètre, stabilisées par les ions citrate qui génèrent des répulsions électrostatiques à la surface des NP.

La seconde méthode proposée dans cette étude correspond à la synthèse de NP d'or fonctionnalisées par l'acide dihydrolipoïque (NP Au@DHLA). Pour ce faire, nous nous sommes appuyés sur les travaux menés précédemment par l'équipe de Roux *et al.* sur la synthèse de NP Au@DHLA en milieu organique. Contrairement à Roux *et al.*, nous avons choisi de synthétiser les NP Au@DHLA en phase aqueuse. En effet, l'utilisation de l'eau comme solvant est plus adéquat pour des applications ultérieures dans le domaine de la santé. Nous avons utilisé une synthèse en deux étapes : premièrement, la synthèse de NP d'or stabilisées par les ions citrate (par la méthode de Brown *et al.*, 1999), puis leur modification chimique de surface par le DHLA dans l'eau. Quatre concentrations différentes de DHLA, toutes en excès par rapport à la concentration en Au présent en surface (*i.e.* ×28, ×56, ×140 et ×222) ont été utilisées lors de la 2ème étape de synthèse, pour évaluer l'impact de la densité de couverture sur la stabilité et la réactivité des NP.

Le DHLA a été choisi comme agent stabilisant car c'est un composé non toxique et biocompatible. Ce ligand possède un groupement polaire chargé négativement à pH supérieur à 4,85, entraînant une répulsion entre les NP d'or de même charge et une chaîne latérale lipophile créant un effet stérique. De plus, le DHLA se lie fortement à la surface des NP d'or de manière covalente, assurant une faible réactivité chimique des NP d'or (Roux *et al.*, 2005).

Une suite possible à notre étude serait de greffer à la surface des NP Au@DHLA des principes actifs à visée antioxydante tels que le glutathion ou d'autres thiols. Par nitrosation des groupements thiols, il serait aussi envisageable de transformer ces nanoobjets en donneurs de $^{\bullet}NO$.

Il s'en suivrait une caractérisation approfondie des nouvelles NP obtenues et une évaluation de leur potentiel thérapeutique en utilisant des modèles *in vitro* et *in vivo* établis pour tester l'activité anti-oxydante ou donneur de $^{\bullet}NO$. Pour ce faire, nous envisagerions d'activer les groupements carboxylique présents à la surface extrême des NP Au@DHLA par le mélange *N*-hydroxysuccinimide/*N*-éthyl-*N'*-(3-diméthylaminopropyl)carbodiimide) (NHS/EDC), avant réaction avec les groupements amine des molécules pharmacologiquement actives pour former une liaison covalente de type amide (figure 9). L'acétylation du groupement thiol du GSH pour

empêcher son interaction avec la surface métallique de l'or durant l'étape de fonctionnalisation s'avérera nécessaire.

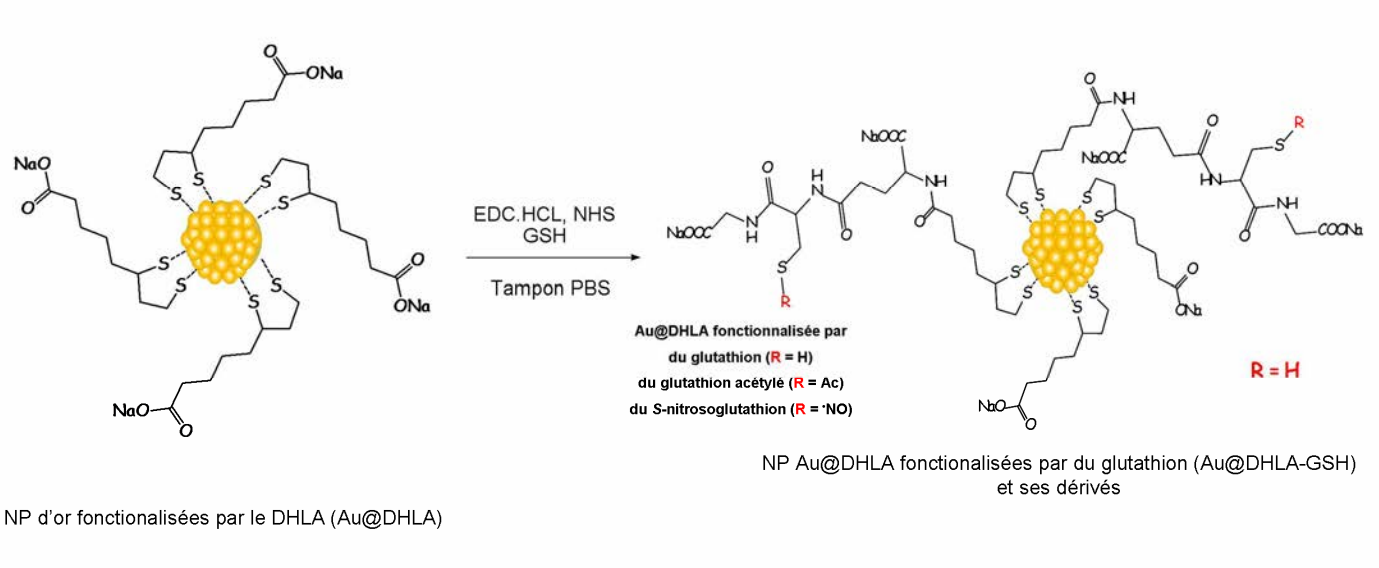

Figure 9. Fonctionnalisation de la surface des NP d'or stabilisées par le DHLA par des molécules actives à visée antioxydante.

IV.3 Caractérisation physico-chimique des nanoparticules d'or : les difficultés rencontrées

La caractérisation approfondie des propriétés physico-chimiques – taille, morphologie, concentration, état de surface, etc... – des NP est primordiale pour valider le mode de synthèse, mieux prévoir les effets biologiques et les applications à venir. Cependant, la caractérisation complète des NP d'or reste un exercice extrêmement complexe, qui tend à freiner la recherche dans ce domaine.

Dans cette étude, la caractérisation physico-chimique des NP d'or stabilisées par les ions citrate et NP Au@DHLA a été réalisée avec des méthodes classiquement décrites dans la littérature (tableau 2, Chapitre 1). En effet, nous avons évalué la taille et l'homogénéité de taille des NP d'or, par différentes méthodes tel que la TEM, ou des techniques de spectroscopie d'absorption et de diffusion de la lumière. Nous avons aussi évalué l'état de surface (présence et densité du ligand), par XPS et ICP-OES.

Les NP d'or stabilisées par les ions citrate ont un diamètre hydrodynamique de l'ordre de 5 - 6 nm, avec une distribution relativement homogène en accord avec la littérature (Brown *et al.*,

1999). De plus, la bande plasmon de ces NP se situe à 517 nm confirmant le faible diamètre et la faible polydispersité observée en TEM et DLS. Afin de prouver la fonctionnalisation de surface par le DHLA, nous avons évalué les propriétés de taille et de surface. La fonctionnalisation des NP d'or par le DHLA a provoqué un déplacement bathochromique de λ_{max}, ce qui prouve l'échange de ligand. Par DLS, nous avons observé l'apparition d'une couronne hydrodynamique suite au greffage de DHLA. Par XPS, nous avons confirmé le greffage du DHLA sur les NP d'or. Par ICP-OES (dosage du S) et par spectrophotocolorimétrie (dosage de l'or), nous avons observé que le rapport [S]/[Au] augmente en fonction du rapport [DHLA]/[Au] (×28, ×56, ×140, ×222) utilisé, confirmant que les NP sont différemment recouvertes en DHLA, à l'exception des NP Au@DHLA$_{140}$ et Au@DHLA$_{222}$.

Cependant, les méthodes de mesure fiables, peu coûteuses et standardisées pour mesurer la taille et la forme des NP ainsi que leur état de surface font actuellement défaut. La plupart du temps, les laboratoires de recherche (comme le nôtre) doivent sous-traiter leurs analyses par un laboratoire doté des équipements adéquats.

Pour que les NP d'or soient utilisées dans des applications biomédicales, une détermination précise de leur concentration en or est primordiale afin de déterminer la concentration nanoparticulaire de ces entités. A l'heure actuelle, des techniques coûteuses et complexes (telles que l'ICP-MS et l'ICP-OES) sont les outils les plus utilisés pour mesurer la teneur en or dans les NP (Allabashi *et al.*, 2009, Scheffer *et al.*, 2008, Yu et Andriola, 2010). Dans cette thèse, nous avons développé et validé une méthode de dosage spectrophotocolorimétrique qui permet de calculer la concentration et l'absorbance molaires des NP d'or et qui peut être utilisée en routine (Tournebize *et al.*, 2011). Le dosage spectrophotocolorimétrique de l'or mériterait d'être amélioré en matière de limite de quantification tout simplement en effectuant une lecture finale par spectrofluorimétrie (Marinenko et May, 1968). Le principal intérêt serait de réduire la taille de l'échantillon prélevé sur chaque lot de NP. En outre, le dosage du contenu en élément soufre des NP synthétisées à l'aide d'un ligand de type thiol nécessiterait également de disposer d'une technique analytique simple, par exemple une technique de minéralisation du soufre organique en ions sulfate suivie d'un dosage des ions sulfate par spectrophotométrie ou par chromatographie ionique. Nous avons débuté quelques essais dans ce sens mais ceux-ci n'ont pu aboutir à un développement méthodologique complet.

IV.4. Stabilité et réactivité des nanoparticules d'or

Afin d'assurer leur rôle de « vecteurs de molécules actives », les NP d'or doivent être stables dans un milieu physiologique, et présenter une surface non réactive aux molécules présentes dans

l'organisme. Notre hypothèse de travail a été la suivante : les NP d'or sont d'autant plus stables et non réactives vis-à-vis des biomolécules qu'elles sont fortement stabilisées et plus couvertes par le ligand greffé (Sperling et Parak, 2010, Biswas *et al.*, 2012).

Pour tester cette hypothèse, nous avons étudié le rôle de deux paramètres sur la stabilité et la réactivité des NP d'or :

- le type d'agent stabilisant, en utilisant les NP d'or stabilisées par les ions citrate (interaction de faible énergie avec le cœur métallique) et les NP Au@DHLA (interaction de forte énergie);
- la densité de couverture, en variant le rapport [DHLA]/[Au] (×28, ×56, ×140 et ×222).

IV.4.1 Étude de la stabilité des nanoparticules d'or par différentes stratégies

Premièrement, trois tests de stabilité ont été menés pour évaluer si les NP d'or résistent à l'agrégation, et de ce fait présentent une stabilité dans un milieu physiologique.

Le premier test a porté sur l'emploi d'une solution saline tampon pH 7,4 (PBS), contre laquelle les NP d'or ont été dialysées pendant 48 h à 23°C et conservées à 4°C tout le long de l'étude (50 j). Cette étude réalisée dans un milieu électrolytique comme le PBS (pH = 7,4, force ionique 150 mM) permet également d'évaluer l'affinité de la liaison du ligand à la surface métallique. Ce test a permis de mettre en évidence la nécessité d'une forte interaction entre l'agent stabilisant et la surface métallique pour éviter leur agrégation dans un milieu physiologique. En effet, les NP d'or stabilisées par les ions citrate se sont avérées fortement sensibles à ce milieu salin et elles précipitent complètement dans les 24 h qui suivent leur dialyse. De plus, la stabilité des NP Au@DHLA dépend de leur densité de couverture. Les NP Au@DHLA$_{140}$ et Au@DHLA$_{222}$ sont stables (pas de modification du rayon hydrodynamique et du λ_{max}) pendant toute la durée de l'étude. En revanche, les NP d'or moins couvertes par le DHLA (×28 et ×56) sont devenues progressivement instables au cours du temps (augmentation du rayon hydrodynamique et déplacement bathochromique de λ_{max}), indiquant l'existence probable d'une forte agrégation.

Ensuite, la stabilité des NP d'or a été évaluée par la modification de la force ionique de la solution par ajout d'un sel neutre (NaCl 1M) et par l'ajout d'un dithiol (DTT) pouvant déplacer de façon compétitive le ligand initialement greffé, le DHLA.

La modification de la force ionique de la solution par l'ajout d'un sel à forte concentration est une méthode souvent employée pour la prédiction de la stabilité des NP (Roux *et al.*, 2005, Zhang *et al.*, 2007). Nous avons remarqué que les NP d'or stabilisées par de faibles interactions avec

l'agent stabilisant sont plus sensibles à la présence de sels dans la solution que les NP d'or avec une plus forte interaction. Les NP d'or stabilisées par les ions citrate et les NP Au@DHLA (×28 et ×56) étaient fortement déstabilisées avec une concentration en NaCl de 1 M, alors que les NP d'or plus couvertes par le DHLA (×140 et ×222) se sont avérées plus stables.

Une autre méthode employée pour évaluer la stabilité des NP d'or a consisté à ajouter un ligand du type dithiol (DTT) à la solution contenant les NP stabilisées par les ions citrate et les NP Au@DHLA. Le ligand (citrate ou DHLA) est échangeable s'il se lie faiblement à la surface métallique. Comme prévu, les ions citrate présents à la surface des NP d'or peuvent être facilement échangés en solution par le DTT. En revanche, toutes les NP stabilisées par le DHLA conduisent à un taux d'échange de ligand très faible en raison de la forte interaction entre le DHLA et la surface métallique.

Les résultats obtenus par ces trois tests de stabilité ont démontré que les NP d'or stabilisées par les ions citrate ne sont pas adaptées pour une application biomédicale. En effet, les ions citrate sont adsorbés à la surface métallique par des liaisons hydrogène non stables en milieu physiologique. En revanche, les NP Au@DHLA, en raison de ses deux groupements thiol s'ancrant de façon covalente à la surface métallique, offrent une meilleure stabilité à la NP d'or pour des applications biologiques futures. De plus, la densité de couverture est un paramètre crucial pour améliorer la stabilité des NP d'or en solution physiologique. Une densité élevée est idéale pour obtenir une meilleure stabilité colloïdale.

Une perspective à nos travaux serait d'utiliser d'autres ligands polythiols d'origine naturelle donc « *a priori* » biocompatibles pour faciliter l'ancrage à la surface des NP et leur stabilité dans le temps. Nous pensons par exemple aux phytochélatines qui sont des polymères dérivés du glutathion ($(\gamma\text{-glucys})_n\text{-gly}$; n = 2 à 6) biosynthétisés par les plantes en réponse à des stress métalliques (Béraud *et al.*, 2007, Heikal *et al.*, 2011) et qui pourraient parfaitement convenir pour ce type d'opération. A notre connaissance, cette application n'a pas encore été envisagée dans la littérature.

IV.4.2 Réactivité des nanoparticules d'or avec des biomolécules

Comprendre les interactions entre les molécules de l'organisme et les NP est d'une grande importance pour prédire le comportement des NP d'or dans le corps humain.

Les NP d'or ont des propriétés de surface particulières telles qu'une activité catalytique élevée, ce qui favorise leur réactivité avec des molécules bioactives. Dans cette thèse, nous avons choisi trois molécules impliquées dans l'homéostasie redox cellulaire (l'albumine, le GSH et le GSNO) et deux radicaux libres ($DPPH^{\bullet}$ et $ABTS^{\bullet+}$) pour évaluer si le type de ligand utilisé (citrate

ou DHLA) et la densité de couverture (×28, ×56, ×140, ×222) jouent un rôle dans l'affinité entre ces composés et les NP d'or.

Nous avons observé que les NP d'or stabilisées par les ions citrate sont plus réactives vis-à-vis des molécules régulatrices de l'homéostasie redox que les NP Au@DHLA. En effet, les NP Au@DHLA ne réagissent pas avec le GSH et GSNO, et elles présentent une réactivité moindre voire nulle vis-à-vis la BSA en comparaison avec les NP d'or stabilisées par les ions citrate.

Nous avons également remarqué que l'interaction entre les NP d'or et la BSA dépend de la densité de couverture des NP d'or. En effet, les résultats obtenus montrent que lorsque les NP d'or sont moins couvertes par le DHLA, il y a une forte interaction de la BSA avec les NP. En revanche, la densité de couverture n'influence pas la réactivité vis-à-vis le GSH et GSNO. Ces résultats sont dus à la forte interaction entre le DHLA et la surface métallique ce qui réduit la réactivité de surface de ces entités.

De façon générale, un radical libre est très réactif et il réagit rapidement avec des molécules environnantes. Ainsi, nous avons étudié la bioréactivité des NP d'or à l'aide de deux modèles de radicaux libres, *i.e.* $DPPH^{\bullet}$ et $ABTS^{\bullet+}$.

Le $DPPH^{\bullet}$ est un radical stable de couleur violette intense dont le maximum d'absorption se situe à 515 nm, de ce fait interférant avec le suivi de la réaction des NP d'or (bande plasmon à 517 nm). Ainsi, une nouvelle méthode a été développée durant cette thèse pour limiter l'interférence liée aux propriétés optiques des NP d'or, par l'utilisation d'une technique de CLHP. Elle a permis de prouver le transfert d'un atome d'hydrogène entre le $DPPH^{\bullet}$ et les NP d'or stabilisées par les ions citrate (Boudier *et al.*, 2012). Néanmoins, la réaction avec le $DPPH^{\bullet}$ ne peut se dérouler que dans un milieu organique, et un autre radical, *i.e.* $ABTS^{\bullet+}$, réagissant en solution aqueuse et présentant un maximum d'absorption nettement plus élevé que celui des NP d'or, a été utilisé dans un deuxième temps.

En raison de leur surface plus accessible, les NP d'or stabilisées par des faibles interactions avec le ligand sont capables d'interagir plus fortement avec l'$ABTS^{\bullet+}$. De plus, la densité de couverture contrôle l'interaction de l'$ABTS^{\bullet+}$ avec la surface métallique. En effet, les NP plus recouvertes par le DHLA ont présenté une plus faible réactivité avec le radical.

A l'aide de ces tests de bioréactivité, nous avons démontré que la fonctionnalisation chimique de surface *via* un composé dithiol ainsi que la densité de couverture permettent de diminuer la réactivité de surface des NP d'or, ce qui est très important pour des applications biologiques ultérieures.

Pour compléter nos études, le pouvoir réducteur des NP d'or mériterait aussi d'être étudié de façon plus approfondie par des techniques électrochimiques, telles que la voltammétrie cyclique, afin de mieux connaître le comportement redox de ces NP d'or. Cette étude pourrait nous donner des réponses très intéressantes à propos de la variation du potentiel redox des NP d'or en fonction du ligand de surface et de sa densité, et éventuellment en permettant de relier le potentiel des NP à leur réactivité vis-à-vis de biomolécules (Guo et Wang, 2007).

IV.5 La reconnaissance des nanoparticules d'or par des macrophages et les effets biologiques

Une fois achevée l'optimisation de la synthèse de NP d'or stables et faiblement réactives vis-à-vis de molécules présentes dans le corps, celles-ci ont été évaluées *in vitro* dans une lignée cellulaire de macrophages. En effet, la possibilité d'utiliser des NP d'or en tant que vecteur de médicament, nécessite une très faible toxicité ainsi qu'une faible reconnaissance par le SPM.

De nombreuses questions se posent sur l'impact toxicologique des NP d'or. Ces craintes sont justifiées car à ce jour, nos connaissances sur la toxicité des NP d'or sont limitées (manque de recul et résultats contradictoires des dernières études). Les NP d'or stabilisées par les ions citrate et les NP Au@DHLA$_{222}$ ont été sélectionnées pour évaluer l'impact du ligand de surface sur l'interaction avec des cellules. Pour ce faire, nous avons tout d'abord effectué une étude de la toxicité aiguë des NP sur un modèle cellulaire, ensuite nous avons étudié l'internalisation des NP d'or et la réponse précoce des cellules à une exposition à des doses non toxiques de NP d'or.

La toxicité des NP est souvent associée à leur internalisation par les cellules phagocytaires telles que les neutrophiles, les monocytes, les macrophages et les cellules dendritiques. Ces cellules sont utilisées comme des modèles expérimentaux en raison de leur capacité à phagocyter les NP, reconnues comme un élément du « non soi », leur réponse sécrétoire de cytokines, leur activation des cascades de signalisation et leur capacité à produire des ROS. Les cellules phagocytaires primaires représentées par les monocytes du sang périphérique, les macrophages péritonéaux, alvéolaires ou les monocytes issus de la moelle osseuse. Les cellules immortalisées secondaires (capacité de division non limitée) possédant un phénotype phagocytaire comprennent les lignées cellulaires RAW264.7, J774.1, IC-21, THP-1, Jurkat, NR8383, etc... (Jones et Grainger, 2009).

Parmi ces différents types cellulaires, nous avons choisi les macrophages alvéolaires de la lignée NR8383 car ces cellules phagocytent généralement les objets étrangers *in vitro* et sont connues pour produire des cytokines en répondant à l'internalisation des NP. De plus, la grande majorité des données toxicologiques vient des études *in vitro* sur des macrophages. En raison de

leur capacité à franchir les barrières physiologiques et leur activité phagocytaire, les macrophages jouent un rôle crucial dans la biopersistance des particules étrangères et dans leur effet inflammatoire.

Premièrement, nous avons réalisé quelques expériences afin de savoir si les NP d'or possèdent une toxicité aiguë. Pour ce faire, nous avons réalisé deux tests (test MTT et Bleu Trypan) utilisés classiquement pour tester la toxicité des produits chimiques. Néanmoins, à des fortes concentrations en NP, l'évaluation de la cytotoxicité s'est heurtée à des difficultés techniques dues à des interférences spectrales entre le formazan produit lors du test MTT et les NP d'or (comme décrit dans l'article 1). En utilisant le test Bleu Trypan, nous avons pu étudier la mortalité cellulaire à des fortes concentrations en NP.

En effet, nous avons trouvé une IC50 égale à 66 nM sur une culture de macrophages NR8383 exposée aux NP d'or pendant 24 h à 37 °C, et ce quel que soit le type d'agent stabilisant (citrate ou DHLA).

Après administration intraveineuse, les NP sont opsonisées, c'est-à-dire recouvertes de protéines, ce qui favorise leur reconnaissance précoce par les macrophages (Aggarwal *et al.,* 2009). Pour prolonger le temps de résidence des NP d'or dans la circulation sanguine, il faut donc réduire les interactions avec les protéines plasmatiques qui rendent ces vecteurs « furtives », c'est-à-dire invisibles pour le système immunitaire. Au cours de nos travaux de thèse, nous avons évalué la furtivité des NP d'or *in vitro* par le biais de deux tests : i) l'interaction avec l'albumine (test BSA décrit précédement) et ii) l'interaction avec des cellules. Notre hypothèse a été la suivante : le ligand de surface influence l'interaction des NP d'or avec les protéines, ce qui rend ces entités plus facilement reconnaissables par les macrophages. Contrairement aux NP d'or stabilisées par des ions citrate, les NP Au@DHLA ont une réactivité très faible voire nulle vis-à-vis de la BSA ce qui a engendré une internalisation par des macrophages plus faible. Ainsi, les NP Au@DHLA étant moins «opsonisées» par des protéines telles que l'albumine et moins reconnues par les cellules du SPM (démonstration *in vitro*), elles devraient s'avérer plus furtives *in vivo*. Seule une étude *in vivo* sur animal entier ayant pour but de déterminer la demi-vie plasmatique des NP donnera un verdict réel sur leur réelle furtivité.

Une dernière perspective de notre étude serait de greffer à la surface des NP Au@DHLA des polymères hydrophiles (comme le PEG, des poloxamères, des poloxamines etc...) capables de diminuer encore plus la reconnaissance des NP d'or par les macrophages et d'augmenter leur durée de vie dans la circulation.

Lorsque les NP sont phagocytées par une cellule, elles peuvent interagir avec la membrane plasmique et les organites cellulaires, tels que les mitochondries (source de $O_2^{\bullet -}$, de H_2O_2 et de

Ca^{2+}) et le réticulum endoplasmique (source de Ca^{2+}) favorisant la production de ROS et RNS. Les NP d'or, en raison de leur réactivité de surface élevée, peuvent également interagir directement avec les antioxydants présents dans la cellule (tel que le GSH), affectant le potentiel redox de la cellule et provoquant la production de ROS et RNS. Ces perturbations peuvent activer des voies de signalisation (par exemple le NF-κB et des MAP kinases) impliquées dans l'activation des gènes de l'inflammation (libération des médiateurs de l'inflammation), de l'apoptose et de la réponse immunitaire.

Un déséquilibre entre la production excessive de ROS et RNS et/ou une diminution du taux d'antioxydants entraîne un stress oxydant provoquent des dommages importants et irréversibles dans les cellules (Forman et Torres, 2001). De multiples structures cellulaires telles que les protéines, les lipides, les glucides et l'ADN, subissent des attaques oxydantes de la part de ces radicaux, provoquant des altérations et des dysfonctionnements cellulaires. A terme, cela peut provoquer la mort cellulaire par nécrose ou apoptose. L'intensité de ces effets dépend de plusieurs paramètres comme la dose et les caractéristiques physico-chimiques des NP (tels que les propriétés de surface).

Des résultats récents dans la littérature ont étudié la toxicité aiguë des NP d'or sur des cellules et ils suggèrent l'implication du stress oxydant (Li *et al.*, 2010, Jia *et al.*, 2011, Gao *et al.*, 2011, Zhao *et al.*, 2011). Cependant, les doses en NP d'or utilisées pendant ces études sont loin d'être celles qui seront utilisées en thérapeutique. Pour répondre à ce manque de la littérature, nous avons évalué l'effet de l'exposition des macrophages à une faible concentration en NP d'or, *i.e.* 10 nM, car à cette concentration les NP d'or sont peu toxiques (80 % de cellules viables) et cette concentration est plus représentative de la dose maximale qui serait ultérieurement utilisée en thérapeutique. A faible concentration, sans pour autant affecter la viabilité cellulaire, les NP d'or peuvent modifier le fonctionnement cellulaire en modifiant certaines molécules impliquées dans l'homéostasie redox ainsi que certaines voies de signalisation, la régulation de facteurs de transcriptions et l'expression de certains gènes. Ces marqueurs apportent une réponse fiable pour identifier précocement la toxicité potentielle d'un composé (même à des doses non toxiques) et ils ont été utilisés dans cette étude pour évaluer la réponse précoce des macrophages vis-à-vis des NP d'or.

Ensuite, nous avons évalué l'interaction entre les NP d'or et les macrophages, en considérant plus particulièrement l'effet du ligand de surface des NP d'or sur leur impact dans l'homéostasie redox. En effet, les NP d'or stabilisées par les ions citrate diminuent de 20% le niveau intracellulaire en GSH sans relation apparente avec la formation de ROS. Au contraire, une diminution de la production en ROS avec les cellules exposées aux deux types de NP d'or testés a été observée.

Comme évoqué précédemment, les NP d'or stabilisées par les ions citrate et les NP Au@DHLA sont capables de piéger des radicaux libres (tels que l'$ABTS^{\bullet+}$) et cela pourrait expliquer la diminution du contenu cellulaire en ROS.

Dans cette étude, la production des ROS a été mesurée par l'emploi de la sonde H_2DCF-DA. Cette dernière est peu sélective car oxydée par quasi tous les types de ROS. L'utilisation d'autres sondes plus spécifiques telles que le dihydroéthidium (spécifique de l'anion superoxyde) et la sonde dihydrorhodamine 123 (spécifique du peroxyde d'hydrogène et du peroxynitrite produits par la mitochondrie) aurait pu être envisagée afin d'affiner nos résultats.

En outre, l'utilisation d'autres biomarqueurs pour évaluer le statut du stress oxydant tels que la mesure de l'actvité d'enzymes antioxydantes (la superoxyde dismutase, la glutathion peroxydase, etc...) pourrait être considérée pour compléter notre étude. Enfin, notre étude manque d'une vérification de la présence ou de l'absence d'effets délétères du stress oxydant vis-à-vis des constituants cellulaires, en particulier par la mesure des dommages de la membrane plasmique *via* le dosage du biomarqueur de la peroxydation lipidique : le malondialdéhyde.

Pour affiner ces résultats, nous avons déterminé la capacité des NP d'or à modifier la régulation d'un facteur de transcription et l'expression de gènes impliquées dans l'homéostasie redox. Les NP d'or ne semblent pas indure l'activation des mRNA associées à la réponse inflammatoire (*tnfα*) et au stress oxydant (*ncf1*).

De façon intéressante, nous avons observé que les macrophages exposés aux NP Au@DHLA présentent une sous-régulation du facteur de transcription *nfκb2*. Les complexes organométalliques à base d'or (par exemple, l'aurothiomalate de sodium), utilisés dans le traitement de fond de l'arthrite rhumatoïde, sont capables de bloquer l'activation des facteurs de transcription, tels que *ap-1* et *nfκb*, conduisent à l'expression des gènes pro-inflammatoires liés à la production de RNS et ROS (Jeon *et al.*, 2000). Un mécanisme similaire peut être appliqué aux NP Au@DHLA, c'est-à-dire une sous régulation du facteur de transcription *nfκb2* conduisant à une diminution de la production des ROS. De plus, les NP Au@DHLA pourraient réagir directement avec les ROS comme cela a été confirmé par les études avec l'$ABTS^{\bullet+}$.

La mesure de l'expression de gènes impliqués dans l'homéostasie cellulaire fournit des informations très intéressantes sur l'activité antioxidante de la cellule et sur la réponse inflammatoire. Cependant, beaucoup plus d'informations sont acquises sur l'expression de protéines. Ainsi, une des perspectives de cette thèse serait d'évaluer l'expression de protéines de *nfκb2*, de *ncf1* et de *tnf-α*.

Il manque aussi l'étude d'autres facteur de transcription. Par exemple, l'impact des NP d'or sur la régulation des facteurs de transcription érythroïde (tels que le *nrf1*, *nrf2* et *nfr3*) mériterait

d'être évalué. En effet, ces derniers jouent un rôle très important dans l'expression de multiples gènes de défense.

Les NP Au@DHLA se sont révélées avoir un fort potentiel en tant que vecteur de médicament car elles sont synthétisées par une méthode de synthèse sans résidu de solvant organique, elles sont stables dans des conditions physiologique (à pH = 7.4 et à une force ionique de 150 mM), elles ne sont pas réactives vis-à-vis des molécules redox présentes dans le corps, elles sont faiblement reconnues par les macrophages et elles ne modifient pas l'homéostasie redox de ces cellules. Cependant, au vue d'une utilisation à long terme (traitement chronique), deux questions se posent : comment les NP d'or peuvent-elle être éliminées de l'organisme ? Une accumulation de NP d'or dans certains organes pourrait-elle engendrer des effets nocifs à court et/ou long terme ?

Ainsi, avant d'utiliser des NP d'or pour un traitement donné, il est primordial de connaître leur biodistribution au sein de l'organisme, et notamment de savoir quels organes accumulent les NP et quelle est l'évolution de cette accumulation au cours du temps.

De nombreuses publications sont apparues dans la littérature pour répondre à ces questions (De Jong *et al.*, 2008, Cho *et al.*, 2009, Sadauskas *et al.*, 2009, Balasubramanian *et al.*, 2010b, Arnida et al., 2011, Zhang *et al.*, 2012, etc…). Cependant, la plupart de ces travaux sont limités à l'étude de la biodistribution des NP d'or stabilisées par les ions citrate et fonctionnalisées par le PEG après administration par voie intraveineuse dans des rats et des souris ; dans certain cas, l'impact de cette accumulation a été évalué (tableau 8).

Les NP d'or stabilisées par les ions citrate sont rapidement éliminées de la circulation systémique par le SPM. En effet, le foie et la rate possèdent des quantités importantes de macrophages pouvant phagocyter les NP représentant ainsi des importants sites d'accumulation/élimination des NP d'or (Khlebtsov et Dykman, 2010). Sadauskas *et al.* (2009) ont observé que l'administration par voie intraveineuse de NP d'or stabilisées par les ions citrate entraîne leur accumulation dans le foie jusqu'à la fin de l'étude (6 mois). La faible élimination peut être due à la grande taille (consécutive à l'agrégation dans un milieu physiologique), ce qui empêche une élimination par voie rénale. Certaines études ont démontré que la fonctionnalisation de la surface des NP d'or par des polymères tels que le PEG et des peptides conférant un caractère hydrophile aux NP, ce qui les rend « invisibles » au SPM et de ce fait prolonge leur demi-vie plasmatique (Cho *et al.*, 2009, Zhang *et al.*, 2009 Arnida *et al.*, 2011).

Néanmoins, quel que soit le type d'agent stabilisant, la taille, la forme et la dose utilisée, le foie et la rate sont les organes préférentiels pour l'accumulation des NP d'or à long terme (Zhang *et al.*, 2009, Balasubramanian *et al.*, 2010b). Ceci suggère, que la stabilité des NP dans un milieu

complexe tel que le sang est un facteur primordial pour l'excrétion des NP d'or par les reins et par le système hépatobiliaire (Zhang *et al.*, 2009).

Tableau 8. Etude de la biodistribution et des effets toxiques des nanoparticules d'or dans des modèles animaux

Propriétés physico-chimique des NP d'or			**Etude *in vivo***				**Résultats**				
			Modèle animal	**Paramètres d'exposition**			**Biodistribution**			**Toxicité (méthodes)**	**Références**
Agent stabilisant	**Taille (nm)**	**ζ (mV)**		**Voie**	**Dose**	**Temps**	**Organes, tissus (% de la dose injectée)***	**Cellules**	**$t_{1/2}$ (h)**		
PEG-SH	13	*ND*	Souris	IV	0.85, 4.26 $\mu g.g^{-1}$	5, 30 min, 4, 24 h, 7 j	Foie (39 – 45 %) Rate (12 – 20 %)	Macrophages spléniques Cellules de Kupffer	30	Foie – Apoptose, inflammation (coupe histologique)	Cho *et al.*, 2009
BSA	8	*ND*	Souris	IP	7550 $mg.kg^{-1}$	24 h, 28 j	Urine (5 %)	*ND*	*ND*	BSA plus toxique (coupes histologiques ; analyses hématologique et biochimique)	Zhang *et al.*, 2012
GSH	2	*ND*					Urine (94 %)				
Citrate	20	*ND*	Rat	IV	0,01 – 0,015 $\mu g.g^{-1}$	1, 7 j, 1, 2 mois	Foie (72 ng/g tissus) Reins (5 ng/g tissus) Fèces et urines	*ND*	*ND*	*ND*	Balasubramanian *et al.*, 2010b
Citrate	10, 50, 100, 250	*ND*	Rat	IV	0,3 – 0,5 $\mu g.\ g^{-1}$	24 h	Foie (20 - 46 %) Rate (1 – 2 %)	*ND*	*ND*	*ND*	De Jong *et al.*, 2008
Citrate	40	*ND*	Souris		1.5 $\mu g.g^{-1}$	24 h, 1, 3,6 mois	Foie (20 %)	*ND*	*ND*	*ND*	Sadauskas *et al.*, 2009

Tableau 8. *Suite*

Propriétés physico-chimique des NP d'or			Etude *in vivo*				Résultats				
			Modèle animal	Paramètres d'exposition			Biodistribution			Toxicité (méthodes)	Références
Agent stabilisant	Taille (nm)	ζ (mV)		Voie	Dose	Temps	Organes, tissus (% de la dose injectée)*	Cellules	$t_{1/2}$ (h)		
PEG-TA	20 40 80	- 8 - 8 - 9	Souris	IV	1×10^{11}	10 min, 2, 24 et 48 h	Foie (30 %/g de tissus) Rate (15 %/g de tissus) *ND* Foie (53 %/g de tissus) Rate (63 % /g de tissus)	*ND*	22 10 16	*ND*	Zhang *et al.*, 2009
Citrate	22	-45	Rats	IV	0.6 – 1 mg Au. kg^{-1}	0.5, 2, 6 et 24 h	Foie (58 %)	*ND*	*ND*	*ND*	Moraes *et al.*, 2012
MUA	33	-37					Foie (59 %)				
CALNN	34	-47					Foie (86 %)				
CALND	35	-44					Foie (77 %)				
CALNS	35	-40					Foie (74 %)				
PEG	50	- 27	Souris	IV	60 µg	30 min, 2, 6, 24 h et 7 j	Foie (10 %) Rate (20 %)	*ND*	*ND*	*ND*	Arnida *et al.*, 2011
PEG	10 × 45	+ 1			40 µg						

* Pourcentage (%) déterminé dans le dernier temps testé; IV : intraveineuse; IP : intrapéritonéale; *ND* : non déterminé ; MUA : acide 11-mercaptoundécanoïque; CALND : Cys-Ala-Leu-Asn-Asp; CALNN : Cys-Ala-Leu-Asn-Asn; CALNS : Cys-Ala-Leu-Asn-Ser.

Références bibliographiques

Aam, B.B., Fonnum, F. Carbon black particles increase reactive oxygen species formation in rat alveolar macrophages in vitro. Arch Toxicol. 2007; 81: 441-446.

Abad, J.M., Mertens, S.F., Pita, M., Fernandez, V.M., Schiffrin, D.J. Functionalization of thioctic acid-capped gold nanoparticles for specific immobilization of histidine-tagged proteins. J Am Chem Soc. 2005; 127: 5689-5694.

Abd El-Baky, H.H., El-Baz, F., El-Baroty, G.S. Enhancement of antioxidant production in Spirulina platensis under oxidative stress. Int J Food Sci Technol. 2009; 44: 1688–1695.

Ackerson, C.J., Jadzinsky, P.D., Sexton, J.Z., Bushnell, D.A., Kornberg, R.D. Synthesis and bioconjugation of 2 and 3 nm-diameter gold nanoparticles. Bioconjugate Chem. 2010; 21: 214-218.

Aggarwal, P., Hall, J.B., McLeland, C.B., Dobrovolskaia, M.A., McNeil, S.E. Nanoparticle interaction with plasma proteins as it relates to particle biodistribution, biocompatibility and therapeutic efficacy. Adv Drug Deliv Rev. 2009; 61: 428–437.

Ahamed, M., Akhtar, J.M., Siddiqui, M.A., Ahamad, J., Musarrat, J., Al-Khedhairy, A.A., Alsalhi, M.S., Alrokayan, S.A. Oxidative stress mediated apoptosis induced by nickel ferrite nanoparticles in cultured A549 cells. Toxicology. 2011; 283: 101-108.

Allabashi, R., Stach, W., de la Escosura-Muñiz, A., Liste-Calleja, L., Merkoçi, A. ICP-MS: a powerful technique for quantitative determination of gold nanoparticles without previous dissolving. J Nanoparticle Res. 2009; 11: 2003-2011.

Al-Sa'Doni, H., Ferro, A. *S*-Nitrosothiols: a class of nitric oxide-donor drugs. Clin Sci. 2000; 98: 507-520.

Alan. Trial of Insulin-Coated Gold Nanoparticles Approved. In: Science Business; 2011. http://sciencebusiness.technewslit.com/?p=6957

Aldeek, F., Mustin, C., Balan, L., Roques-Carmes, T., Fontaine-Aupart, M.-P., Schneider, R. Surface-engineered quantum dots for the labelling of hydrophobic microdomains in bacterial biofilms. Biomaterials. 2011; 32: 5459-5470.

Alexandridis, P., Tsianou, M. Block copolymer-directed metal nanoparticle morphogenesis and organization. Eur Polym J. 2011; 47: 569-583.

Alivisatos, P. The use of nanocrystals in biological detection. Nat Biotechnol. 2004; 22: 47-52.

Allen, R.G., Tresini, M. Oxidative stress and gene regulation. Free Radic Biol Med. 2000; 28: 463-499.

Alkilany, A.M., Murphy, C.J. Gold Nanoparticles with a polymerizable surfactant bilayer: synthesis, polymerization, and stability evaluation. Langmuir. 2009; 25: 13874-13879.

Alkilany, A.M., Murphy, C.J. Toxicity and cellular uptake of gold nanoparticles: what we have learned so far? J Nanopart Res. 2010; 12: 2313-2333.

Arnida, M.A., Ghandehari, H. Cellular uptake and toxicity of gold nanoparticles in prostate cancer cells: a comparative study of rods and spheres. J Appl Toxicol. 2010; 30: 212-217.

Arnida, Janat-Amsbury, M.M., Ray, A., Peterson, C.M., Ghandehari, H. Geometry and surface characteristics of gold nanoparticles influence their biodistribution and uptake by macrophages. Eur J Pharm Biopharm. 2011; 77: 417-423.

Arnoult, D., Grodet, A., Lee, Y.J., Estaquier, J., Blackstone, C. Release of OPA1 during apoptosis participates in the rapid and complete release of cytochrome c and subsequent mitochondrial fragmentation. J Biol Chem. 2005; 280: 35742–35750.

Arora, S., Jain, J., Rajwade, J.M., Paknikar, K.M. Cellular responses induced by silver nanoparticles: In vitro studies. Toxicol Lett. 2008; 179: 93-100.

Asanuma, K., Tanida, I., Shirato, I., Ueno, T., Takahara, H., Nishitani, T., Kominami, E., Tomino, Y. MAP-LC3, a promising autophagosomal marker, is processed during the differentiation and recovery of podocytes from PAN nephrosis. FASEB J. 2003; 17: 1165–1167.

Astruc, D., Daniel, M.C., Ruiz, J. Dendrimers and gold nanoparticles as exo-receptors sensing biologically important anions. Chem Commun. 2004; 23: 2637-2649.

Auffan, M., Achouak, W., Rose, J., Roncato, M.A., Chaneac, C., Waite, D.T., Masion, A., Woicik, J.C., Wiesner, M.R., Bottero, J.Y. Relation between the redox state of iron-based nanoparticles and their cytotoxicity toward Escherichia coli. Environ Sci Technol. 2008; 42: 6730-6735.

Auffan, M., Rose, J., Wiesner, M.R., Bottero, J.-Y. Chemical stability of metallic nanoparticles: A parameter controlling their potential cellular toxicity in vitro. Environ Pollut. 2009; 157: 1127-1133.

Baciu, C., Gauld, J.W. An assessment of theoretical methods for the calculation of accurate structures and S-N bond dissociation energies of S-nitrosothiols (RSNOs). J Phys Chem A. 2003; 107: 9946-9952.

Baciocchi, E., Calcagni, A., Lanzalunga, O. A kinetic study of the reaction of N,N-dimethylanilines with 2,2-diphenyl-1-picrylhydrazyl radical: A concerted proton-electron transfer? J Org Chem. 2008; 73: 4110-4115.

Baek, Y.-S., Haas, S., Hackstein, H., Bein, G., Hernandez-Santana, M., Lehrach, H., Sauer, S., Seitz, H. Identification of novel transcriptional regulators involved in macrophage differentiation and activation in U937 cells. BMC Immunol. 2009; 10: 18.

Balasubramanian, S.K., Yang, L., Yung, L.-Y.L., Ong, C.-N., Ong, W.-Y., Yu, L.E. Characterization, purification, and stability of gold nanoparticles. Biomaterials. 2010a; 31: 9023-9030.

Balasubramanian, S.K., Jittiwat, J., Manikandan, J., Ong, C.-N., Yu, L.E., Ong, W.-Y. Biodistribution of gold nanoparticles and gene expression changes in the liver and spleen after intravenous administration in rats. Biomaterials. 2010b; 31: 2034-2042.

Baptista, P., Pereira, E., Eaton, P., Doria, G., Miranda, A., Gomes, I., Quaresma, P., Franco, R. Gold nanoparticles for the development of clinical diagnosis methods. Anal Bioanal Chem. 2008; 391: 943-950.

Bartasiute, A., Westerink, B.H.C., Verpoorte, E., Niederländer, H.A.G. Improving the *in vivo* predictability of an on-line HPLC stable free radical decoloration assay for antioxidant activity in methanol-buffer medium. Free Radic Biol Med. 2007; 42: 413-423.

Bartneck, M., Keul, H.A., Singh, S., Czaja, K., Bornemann, J., Bockstaller, M., Moeller, M., Zwadlo-Klarwasser, G., Groll, J. Rapid uptake of gold nanorods by primary human blood phagocytes and immunomodulatory effects of surface chemistry. ACS Nano. 2010; 4: 3073-3086.

Belyanskaya, L., Manser, P., Spohn, P., Bruinink, A., Wick, P. The reliability and limits of the MTT reduction assay for carbon nanotubes-cell interaction. Carbon. 2007; 45: 2643–2648.

Bastús, N.G., Sánchez-Tilló, E., Pujals, S., Farrera, C., Kogan, M.J., Giralt, E., Celada, A., Lloberas, J., Puntes, V. Peptides conjugated to gold nanoparticles induce macrophage activation. Mol Immunol. 2009a; 46: 743-748.

Bastús, N.G., Sánchez-Tilló, E., Pujals, S., Farrera, C., Lopez, C., Giralt, E., Celada, A., Lloberas, J., Puntes, V. Homogeneous conjugation of peptides onto gold nanoparticles enhances macrophage response. ACS Nano. 2009b; 3: 1335-1344.

Belloni, J., Mostafavi, M., Remita, H., Marignier, J.-L., Delcourt, M.-O. Radiation-induced synthesis of mono- and multi-metallic clusters and nanocolloids. New J Chem. 1998; 22: 1239-1255.

Benzie, I.F.F., Strain, J.J. The ferric reducing ability of plasma (FRAP) as a measure of "antioxidant power": The FRAP assay. Anal Biochem. 1996; 239: 70-76.

Béraud, E., Cotelle, S., Leroy, P., Férard, J.-F. Genotoxic effects and induction of phytochelatins in the presence of cadmium in *Vicia faba* roots. Mutat Res Genet Toxicol Environ Mutagen. 2007; 633: 112-116.

Biswas, M., Dinda, E., Rashid, Md. H., Mandal, T.K. Correlation between catalytic activity and surface ligands of monolayer protected gold nanoparticles. J Colloid Interf Sci. 2012; 368: 77-85.

Bhardwaj, P., Chaurasia, H., Chaurasia, D., Prajapati, S.K., Singh, S., 2010. Formulation and in-vitro evaluation of floating microballoons of indomethacin. Acta Pol Pharm. 2010; 67: 291–298.

Bhattacharya, K., Davoren, M., Boertz, J., Schins, R.P.F., Hoffmann, E., Dopp, E. Titanium dioxide nanoparticles induce oxidative stress and DNA-adduct formation but not DNA-breakage in human lung cells. Part Fibre Toxicol. 2009; 6: 1-11.

Bhattacharya, S., Dudeja, P.K., Tobacman, J.K. Tumor necrosis factor alpha-induced inflammation is increased but apoptosis is inhibited by common food additive carrageenan. J Biol Chem. 2010; 285: 39511–39522.

Biswas, M., Dinda, E., Rashid, M.H., Mandal, T.K. Correlation between catalytic activity and surface ligands of monolayer protected gold nanoparticles. J Colloid Interf Sci. 2012; 368: 77-85.

Blois, M.S. Antioxidant determinations by the use of a stable free radical. Nature. 1958; 181: 1199-1200.

Bodmeier, R., Chen, H., Tyle, P., Jarosz, P. Spontaneous formation of drug-containing acrylic nanoparticles. J Microencapsul. 1991; 8: 161–170.

Bogliotti, N., Oberleitner, B., Di-Cicco, A., Schmidt, F., Florent, J.C., Semetey, V. J. Optimizing the formation of biocompatible gold nanorods for cancer research: Functionalization, stabilization and purification. Colloid Interf Sci. 2011; 357; 75-81.

Bohren, C.F., Huffman, D.R., editors. Adsorption and scattering of light by small particles. NY, USA: Wiley; 1983.

Boisselier, E., Astruc, D. Gold nanoparticles in nanomedicine: preparations, imaging, diagnostics, therapies and toxicity. Chem Soc Rev. 2009; 38: 1759-1782.

Bond, G.C., Sermon, P.A., Webb, G., Buchanan, D.A., Wells, P.B. Hydrogenation over supported gold catalysts. J Chem Soc., Chem Commun. 1973; 444b-445.

Bond, G.C., Thompson, D.T. Status of catalysis by gold following an AURICAT Workshop. Appl Catal A-Gen. 2006; 302: 1-4.

Boudier, A., Castagnos, P., Soussan, E., Beaune, G., Belkhelfa, H., Ménager, C., Cabuil, V., Haddioui, L., Roques, C., Rico-Lattes, I., Blanzat, M. Polyvalent catanionic vesicles: exploring the drug delivery mechanisms. Int J Pharmaceut. 2011; 403: 230-236.

Boudier, A., Tournebize, J., Bartosz, G., El Hani, S., Bengueddour, R., Sapin-Minet, A., Leroy, P. High-performance liquid chromatographic method to evaluate the hydrogen atom transfer during reaction between 1,1-diphenyl-2-picryl-hydrazyl radical and antioxidants. Anal Chim Acta. 2012; 711: 97-106.

Brandenberger, C., Rothen-Rutishauser, B., Mühlfeld, C., Schmid, O., Ferron, G.A., Maier, K.L., Gehr, P., Lenz, A.G. Effects and uptake of gold nanoparticles deposited at the air-liquid interface of a human epithelial airway model. Toxicol Appl Pharmacol. 2010; 242: 56-65.

Brand-Williams, W., Cuvelier, M. E., Berset, C. Use of a free radical method to evaluate antioxidant activity. Food Sci Technol. 1995; 28: 25–30.

Brazma, A., Hingamp, P., Quackenbush, J., Sherlock, G., Spellman, P., Stoeckert, C., Aach, J., Ansorge, W., Ball, C.A., Causton, H.C., Gaasterland, T., Glenisson, P., Holstege, F.C., Kim, I.F., Markowitz, V., Matese, J.C., Parkinson, H., Robinson, A., Sarkans, U., Schulze-Kremer, S., Stewart, J., Taylor, R., Vilo, J., Vingron, M. Minimum information about a microarray experiment (MIAME)-toward standards for microarray data. Nat Genet. 2001; 29: 365–371.

Brewer, S. H., Glomm, W. R., Johnson, M. C., Knag, M. K., Franzen, S. Probing BSA binding to citrate-coated gold nanoparticles and surfaces. Langmuir. 2005; 21: 9303-9307.

Brown, K.R., Walter, D.G., Natan, M.J. Seeding of colloidal Au nanoparticle solutions. 2. improved control of particle size and shape. Chem Mater. 2000; 12: 306-313.

Brown, D.M., Dickson, C., Duncan, P., Al-Attili, F., Stone, V. Interaction between nanoparticles and cytokine proteins: impact on protein and particle functionality. Nanotechnology. 2010; 21: 2155104-215113.

Brust, M., Walker, M., Bethell, D., Schiffrin, D.J., Whyman, R. Synthesis of thiol-derivatized gold nanoparticles in a 2-phase liquid-liquid system. J Chem Soc, Chem Commun. 1994: 801-802.

Buettner, G.R. The pecking order of free-radicals and antioxidants - lipid-peroxidation, alpha-tocopherol, and ascorbate. Arch Biochem Biophys. 1993; 300: 535-543.

Burygin, G.L., Khlebtsov, B.N., Shantrokha, A.N., Dykman, L.A., Bogatyrev, V.A., Khlebtsov, N.G. On the enhanced antibacterial activity of antibiotics mixed with gold nanoparticles. Nanoscale Res Lett. 2009; 4: 794–801.

Cadenas, E., Merényi, G., Lind, J. Pulse radiolysis study on the reactivity of Trolox C phenoxyl radical with superoxide anion. FEBS Lett. 1989; 253: 235-238.

Candiano, G., Petretto, A., Bruschi, M., Santucci, L., Dimuccio, V., Prunotto, M., Gusmano, R., Urbani, A., Ghiggeri, G.M. The oxido-redox potential of albumin methodological approach and relevance to human diseases. J Proteomics. 2009; 73: 188-195.

Cano, A., Alcaraz, O., Arnao, M.B. Free radical-scavenging activity of indolic compounds in aqueous and ethanolic media. Anal Bioanal Chem. 2003; 376: 33-37.

Carlson, C., Hussain, S.M., Schrand, A.M., Braydich-Stolle, L.K., Hess, K.L., Jones, R.L., Schlager, J.J. Unique cellular interaction of silver nanoparticles: size-dependent generation of reactive oxygen species. J Phys Chem B. 2008; 112: 13608-13619.

Casey, A., Herzog, E., Davoren, M., Lyng, F.M., Byrne, H.J., Chambers, G. Chambers spectroscopic analysis confirms the interactions between single walled carbon nanotubes and various dyes commonly used to assess cytotoxicity. Carbon. 2007; 45: 1425–1432.

Chai, F., Wang, C., Wang, T., Li, L., Su, Z. Colorimetric detection of Pb2+ using glutathione functionalized gold nanoparticles. ACS Appl Mater Inter. 2010; 2: 1466-1470.

Chakraborty, S., Joshi, P., Shanker, V., Ansari, Z.A., Singh, S. P., Chakrabarti, P. Contrasting effect of gold nanoparticles and nanorods with different surface modifications on the structure and activity of bovine serum albumin. Langmuir. 2011; 27: 7722-7731.

Chandrasekar, D., Madhusudhana, K., Ramakrishna, S., Diwan, P.V. Determination of DPPH free radical scavenging activity by reversed-phase HPLC: a sensitive screening method for polyherbal formulations. J Pharm Biomed Anal. 2006; 40: 460-464.

Chapel, J.P., Berret, J.F. Versatile electrostatic assembly of nanoparticles and polyelectrolytes: Coating, clustering and layer-by-layer processes. Curr Opin Colloid In. 2012; 17: 97-105.

Chen, H., Detmer, S.A., Ewald, A.J., Griffin, E.E., Fraser, S.E., Chan, D.C. Mitofusins Mfn1 and Mfn2 coordinately regulate mitochondrial fusion and are essential for embryonic development. J Cell Biol. 2003; 160: 189–200.

Chen, H.W., Su, S.F., Chien, C.T., Lin, W.H., Yu, S.L., Chou, C.C., Chen, J.J., Yang, P.C. Titanium dioxide nanoparticles induce emphysema-like lung injury in mice. FASEB J. 2006; 20: 2393–2395.

Chen, S., Kimura, K. Synthesis and characterization of carboxylate-modified gold nanoparticle powders dispersible in water. Langmuir. 1999; 15: 1075-1082.

Chen, X.Y., Li, J.R., Jiang, L., Chen, X.Y., Li, J.R. Two-dimensional arrangement of octadecylamine-functionalized gold nanoparticles using the LB technique. Nanotechnology. 2000; 11: 108-111.

Chithrani, B.D., Chan, W.C. Elucidating the mechanism of cellular uptake and removal of protein-coated gold nanoparticles of different sizes and shapes. Nano Lett. 2007; 7: 1542-1550.

Chithrani, B.D., Ghazani, A.A., Chan, W.C.W. Determining the size and shape dependence of gold nanoparticle uptake into mammalian cells. Nano Lett. 2006; 6: 662-668.

Chen, Y.-H., Tsai, C.-Y., Huang, P.-Y., Chang, M.-Y., Cheng, P.-C., Chou, C.-H., Chen, D.-H., Wang, C.-R., Shiau, A.-L., Wu, C.-L. Methotrexate conjugated to gold nanoparticles inhibits tumor growth in a syngeneic lungtumor model. Mol Pharm. 2007; 4: 713–722.

Cho, W.-S., Cho, M., Jeong, J., Choi, M., Cho, H.-Y., Han, B. S., Kim, S. H., Kim, H. O., Lim, Y. T., Chung, B.H., Jeong, J. Acute toxicity and pharmacokinetics of 13 nm-sized PEG-coated gold nanoparticles. Toxicol Appl Pharmacol. 2009; 236: 16–24.

Chompoosor, A., Han, G., Rotello, V.M. Charge dependence of ligand release and monolayer stability of gold nanoparticles by biogenic thiols. Bioconjugate Chem. 2008; 19: 1342-1345.

Chorny, M., Hood, E., Levy, R.J., Muzykantov, V.R. Endothelial delivery of antioxidant enzymes loaded into non-polymeric magnetic nanoparticles. J Control Release. 2010; 146: 144-151.

Connor, E., Mwamuka, J., Gole, A., Murphy, C., Wyatt, M. Gold nanoparticles are taken up by human cells but do not cause acute cytotoxicity. Small. 2005; 1: 325 - 327.

Corcelle, E., Nebout, M., Bekri, S., Gauthier, N., Hofman, P., Poujeol, P., Fenichel, P., Mograbi, B. Disruption of autophagy at the maturation step by the carcinogen lindane is associated with the sustained mitogen-activated protein kinase/extracellular signal-regulated kinase activity. Cancer Res. 2006; 66: 6861–6870.

Corma, A., Garcia, H. Supported gold nanoparticles as catalysts for organic reactions. Chem Soc Rev. 2008; 37: 2096-2126.

Cook, J.A., Kim, S.Y., Teague, D., Krishna, M.C., Pacelli, R., Mitchell, J.B., Vodovotz, Y., Nims, R.W., Christodoulou, D., Miles, A.M., Grisham, M.B., Wink, D.A. Convenient colorimetric and fluorometric assays for *S*-nitrosothiols. Anal Biochem. 1996; 238: 150-158.

Dadras, S., Jafarkhani, P., Torkamany, M.J., Sabbaghzadeh, J. Effects of ultrasound radiation on the synthesis of laser ablated gold nanoparticles. J Phys D Appl Phys. 2009; 42.

Daniel, M.C., Astruc, D. Gold nanoparticles: assembly, supramolecular chemistry, quantum-size-related properties, and applications toward biology, catalysis, and nanotechnology. Chem Rev. 2004; 104: 293-346.

De, M., Ghosh, P.S., Rotello, V.M. Applications of nanoparticles in biology. Adv Mater. 2008; 20: 4225-4241.

De Jong, W.H., Hagens, W.I., Krystek, P., Burger, M.C., Sips, A.J., Geertsma, R.E. Particle size-dependent organ distribution of gold nanoparticles after intravenous administration. Biomaterials. 2008; 29: 1912–1921.

De Paoli Lacerda, S.H., Park, J.J., Meuse, C., Pristinski, D., Becker, M.L., Karim, A., Douglas, J.F. Interaction of gold nanoparticles with common human blood proteins. ACSNano. 2010; 4: 365-379.

Deng, Z., Mortimer, G., Schiller, T., Musumeci, A., Martin, D., Minchin, R.F. Differential plasma protein binding to metal oxide nanoparticle. Nanotechnology. 2009; 20: 455101-455110.

Derjaguin, B.; Landau, L. Theory of the stability of strongly charged lyophobic sols and of the adhesion of strongly charged particles in solutions of electrolytes. Acta Physicochim URSS. 1941; 14: 633-662.

Dhawan, A., Sharma, V. Toxicity assessment of nanomaterials: methods and challenges. Anal Bioanal Chem. 2010; 398: 589-605.

Dickinson, D.A., Levonen, A.L., Moellering, D.R., Arnold, E.K., Zhang, H., Darley-Usmar, V.M., Forman, H.J. Human glutamate cysteine ligase gene regulation through the electrophile response element. Free Radic Biol Med. 2004; 37: 1152–1159.

Dika Nguea, H., de Reydellet, A., Lehuede, P., De Meringo, A., Le Faou, A., Marcocci, L., Rihn, B.H. Gene expression profile in monocyte during in vitro mineral fiber degradation. Arch Toxicol. 2008; 82: 355–362.

Dreaden, E.C., Alkilany, A.M., Huang, X., Murphy, C.J., El-Sayed, M.A. The golden age: gold nanoparticles for biomedicine. Chem Soc Rev. 2012; 41: 2740-2779.

Doak, S.H., Griffiths, S.M., Manshian, B., Singh, N., Williams, P.M., Brown, A.P., Jenkins, G.J.S. Confounding experimental considerations in nanogenotoxicology. Mutagenesis. 2009; 24: 285-293.

Dugan, L.L., Turetsky, D.M., Du, C., Lobner, D., Wheeler, M., Almli, C.R., Shen, C.K.F., Luh, T.Y., Choi, D.W., Lin, T.S. Carboxyfullerenes as neuroprotective agents. Proc Natl Acad Sci USA. 1997; 94: 9434-9439.

Duncan, B., Kim, C., Rotello, V.M. Gold nanoparticules platforms as drug and biomacromolecule delivery systems. J Control Release. 2010; 148: 122-127.

Eidi, H., Joubert, O., Attik, G., Duval, R.E., Bottin, M.C., Hamouia, A., Maincent, P., Rihn, B.H. Cytotoxicity assessment of heparin nanoparticles in NR8383 macrophages. Int J Pharmaceut. 2010; 396: 156-165.

Eidi, H., Joubert, O., Némos, C., Grandemange, S., Mograbi, B., Foliguet, B., Tournebize, J., Maincent, P., Le Faou, A., Aboukhamis, I., Rihn, B.H. Drug delivery by polymeric nanoparticles induced autophagy in macrophages. Int J Pharmaceut. 2012; 422: 495-503.

El-Sayed, I.H., Huang, X.H., El-Sayed, M.A. Surface plasmon resonance scattering and absorption of anti-EGFR antibody conjugated gold nanoparticles in cancer diagnostics: applications in oral cancer. Nano Lett. 2005; 5: 829-834.

El-Sayed, M.A. Some interesting properties of metals confined in time and nanometer space of different shapes. Acc Chem Res. 2001; 34: 257-264.

El-Shahawi, M.S., Bashammakh, A.S., Bahaffi, S.O. Chemical speciation and recovery of gold(I, III) from wastewater and silver by liquid-liquid extraction with the ion-pair reagent amiloride mono hydrochloride and AAS determination. Talanta. 2007; 72: 1494-1499.

Endo, T., Fukunaga, T., Yoshimura, T., Esumi, K. Scavenging DPPH radicals catalyzed by binary noble metal-dendrimer nanocomposites. J Colloid Interface Sci. 2006; 302: 516-521.

Era, S., Kazuo, K., Imai, H., Nakamura, K., Hayashi, T., Sogami, M. Age-related change in redox state of human serum albumin. Biochim Biophys Acta Protein Struct Mol Enzymol. 1995; 1247: 12-16.

Esumi, K., Takei, N., Yoshimura, T. Antioxidant-potentiality of gold-chitosan nanocomposites. Colloid Surface B. 2003; 32: 117-123.

Esumi, K., Houdatsu, H., Yoshimura, T. Antioxidant action by gold-PAMAM dendrimer nanocomposites. Langmuir. 2004; 20: 2536-2538.

European commission. 2012. http://ec.europa.eu/health/nanotechnology/policy/index_en.htm

Fan, C., Jiang, L. Preparation of hydrophobic nanometer gold particles and their optical absorption in chloroform. Langmuir. 1997; 13: 3059-3062.

Fang, R., Jing, H., Chai, Z., Zhao, G, Stoll, S., Ren, F, Liu, F., Leng, X. Design and characterization of protein-quercetin bioactive nanoparticles. J Nanobiotechnology. 2011; 9: 1-14.

Faraday, M. Experimental relations of gold (and other metals) to light. Philos Trans R Soc. 1857; 147: 145.

Felidj, N., Aubard, J., Levi, G., Krenn, J.R., Hohenau, A., Schider, G., Leitner, A., Aussenegg, F.R. Optimized surface-enhanced Raman scattering on gold nanoparticle arrays. Appl Phys Lett. 2003; 82: 3095-3097.

Fenoglio, I., Tomatis, M., Lison, D., Muller, J., Fonseca, A., Nagy, J.B., Fubini, B. Reactivity of carbon nanotubes: Free radical generation or scavenging activity? Free Rad Biol Med. 2006; 40: 1227-1233.

Fessi, H., Puisieux, F. Nanocapsule formation by interfacial polymer deposition following solvent displacement. Int J Pharm. 1989; 55: 1–4.

Forman, J.H., Torres, M. Redox signaling in macrophages. Mol Aspects Med. 2001; 22: 189-216.

Foti, M.C., Daquino, C., Mackie, I.D., DiLabio, G.A., Ingold, K.U. Reaction of phenols with the 2,2-diphenyl-1-picrylhydrazyl radical. Kinetics and DFT calculations applied to determine ArO-H bond dissociation enthalpies and reaction mechanism. J Org Chem. 2008; 73: 9270-9282.

Frens, G. Controlled nucleation for the regulation of the particle size in monodisperse gold suspensions. Nature. 1973; 241: 20-22.

Fukui, K.-I., Namai, Y., Iwasawa, Y. Imaging of surface oxygen atoms and their defect structures on CeO_2 (111) by noncontact atomic force microscopy. Appl Surf Sci. 2002; 188: 252-256.

Gao, W., Xu, K., Ji, L., Tang, B. Effect of gold nanoparticles on glutathione depletion-induced hydrogen peroxide generation and apoptosis in HL7702 cells. Toxicol Lett. 2011; 205: 86-95.

Garcia, B., Salome, M., Lemelle, L., Bridot, J.L., Gillet, P., Perriat, P., Roux, S., Tillement, O. Sulfur K-edge XANES study of dihydrolipoic acid capped gold nanoparticles: dihydrolipoic acid is bound by both sulfur ends. Chem Commun. 2005: 369-371.

Garg, N., Mohanty, A., Lazarus, N., Schultz, L., Rozzi, T.R., Santhanam, S., Weiss, L., Snyder, J.L., Fedder, G.K., Jin, R.C. Robust gold nanoparticles stabilized by trithiol for application in chemiresistive sensors. Nanotechnology. 2010; 21: 405501

Gargouri, M., Sapin, A., Bouali, S., Becuwe, P., Merlin, J.L., Maincent, P. Optimization of a new non-viral vector for transfection: Eudragit nanoparticles for the delivery of a DNA Plasmid. Technol Cancer Res T. 2009; 8: 433-443.

Gibson, J.D., Khanal, B.P., Zubarev, E.R. Paclitaxel-functionalized gold nanoparticles. J Am Chem Soc. 2007; 129: 11653–11661.

Ghosh, P., Han, G., De, M., Kim, C.K., Rotello, V.M. Gold nanoparticles in delivery applications. Adv Drug Deliv Rev. 2008; 60: 1307-1315.

Goldschmidt, S., Renn, K. Amine oxidation IV. Diphenyl-trinitrophenylhydrazyl. Chem Ber. 1922; 55: 628-643

Gofberg, I., Mandler, D. Preparation and comparison between different thiol-protected Au nanoparticles. J Nanopart Res. 2010; 12: 1807-1811.

Goodman, C.M., McCusker, C.D., Yilmaz, T., Rotello, V.M. Toxicity of gold nanoparticles functionalized with cationic and anionic side chains. Bioconjugate Chem. 2004; 15: 897-900.

Goraca, A., Huk-Kolega, H., Piechota, A., Kleniewska, P., Ciejka, E., Skibska, B. Lipoic acid - biological activity and therapeutic potential. Pharm Reports. 2011; 63: 849-858.

Griffin, F., Fitzmaurice, D. Preparation and thermally promoted ripening of water-soluble gold nanoparticles stabilized by weakly physisorbed ligands. Langmuir. 2007; 23: 10262-10271.

Grzelczak, M., Perez-Juste, J., Mulvaney, P., Liz-Marzan, L.M. Shape control in gold nanoparticle synthesis. Chem Soc Rev. 2008; 37: 1783-1791.

Guo, S.J., Wang, E.K. Synthesis and electrochemical applications of gold nanoparticles. Anal Chim Acta. 2007; 598: 181-192.

Gupta, A.K., Gupta, M. Synthesis and surface engineering of iron oxide nanoparticles for biomedical applications. Biomaterials. 2005; 26: 3995-4021.

Haes, A.J., Hall, W.P., Chang, L., Klein, W.L., Van Duyne, R.P. A localized surface plasmon resonance biosensor: First steps toward an assay for Alzheimer's disease. Nano Lett. 2004; 4: 1029-1034.

Hainfeld, J.F., Slatkin, D.N., Focella, T.M., Smilowitz, H.M. Gold nanoparticles: a new X-ray contrast agent. Br J Radiol. 2006; 79: 248–253.

Han, X.L., Gelein, R., Corson, N., Wade-Mercer, P., Jiang, J., Biswas, P., Finkelstein, J.N., Elder, A., Oberdörster, G. Validation of an LDH assay for assessing nanoparticle toxicity. Toxicology. 2011; 287: 99-104.

Haruta, M., Kobayashi, T., Sano, H., Yamada, N. Novel gold catalysts for the oxidation of carbon-monoxide at a temperature far below 0°C. Chem Lett. 1987: 405-408.

Hauck, T.S., Ghazani, A.A., Chan, W.C.W. Assessing the effect of surface chemistry on gold nanorod uptake, toxicity, and gene expression in mammalian cells. Small. 2008; 4: 153-159.

He, D., Jones, A.M., Garg, S., Pham, A.N., Waite, T.D. Silver nanoparticle−reactive oxygen species interactions: Application of a charging−discharging model. J Phys Chem C. 2011; 115: 5461-5468.

Heckert, E.G., Seal, S., Self, W.T. Fenton-like reaction catalyzed by the rare earth inner transition metal cerium. Environ Sci Technol. 2008; 42: 5014-5019.

Heikal, L., Aaronson, P.I., Ferro, A. *S*-nitrosophytochelatins: Investigation of the bioactivity of an oligopeptide nitric oxide delivery system. Biomacromolecules. 2011; 6: 2013-2113.

Hikosaka, K., Kim, J., Kajita, M., Kanayama, A., Miyamoto, Y. Platinum nanoparticles have an activity similar to mitochondrial NADH:ubiquinone oxidoreductase. Colloids Surf B. 2008; 66: 195-200.

Hiramatsu, H., Osterloh, F.E. A simple large-scale synthesis of nearly monodisperse gold and silver nanoparticles with adjustable sizes and with exchangeable surfactants. Chem Mater. 2004; 16: 2509-2511.

Hirsch, C., Kaiser, J.-P., Wessling, F., Fischer, K., Roesslein, M., Wick, P., Krug, H.F. A novel comprehensive evaluation platform to assess nanoparticle toxicity in vitro. J Phys Conf Ser. 2011; 304: 012053.

Hoffart, V., Lamprecht, A., Maincent, P., Lecompte, T., Vigneron, C., Ubrich, N. Oral bioavailability of a low molecular weight heparin using a polymeric delivery system. J Control Release. 2006; 113: 38–42.

Horie, M., Nishio, K., Kato, H., Fujita, K., Endoh, S., Nakamura, A., Miyauchi, A., Kinugasa, S., Yamamoto, K., Niki, E., Yoshida, Y., Hagihara, Y., Iwahashi, H. Cellular responses induced by cerium oxide nanoparticles: induction of intracellular calcium level and oxidative stress on culture cells. J Biochem. 2011; 150: 461-471.

Hoskins, C., Wang, L., Cheng, W., Cuschieri, A. Dilemmas in the reliable estimation of the in-vitro cell viability in magnetic nanoparticle engineering: which tests and what protocols? Nanoscale Res Lett. 2012; 7: 1-12.

Hu, D., Han, H., Zhou, R., Dong, F., Bei, W., Jia, F., Chen, H. Gold(III) enhanced chemiluminescence immunoassay for detection of antibody against ApxIV of Actinobacillus pleuropneumoniae. Analyst. 2008; 133: 768-773.

Huang, X., El-Sayed, I.H., Yi, X., El-Sayed, M.A. Gold nanoparticles: catalyst for the oxidation of NADH to NAD(+). J Photochem Photobiol B. 2005; 81: 76-83.

Huang, X., Jain, P.K., El-Sayed, I.H., El-Sayed, M.A. Plasmonic photothermal therapy (PPTT) using gold nanoparticles. Lasers Med Sci. 2008; 23: 217-228.

Huang, X.H., Jain, P.K., El-Sayed, I.H., El-Sayed, M.A. Gold nanoparticles: interesting optical properties and recent applications in cancer diagnostic and therapy. Nanomedicine. 2007; 2: 681-693.

Hussain, I., Graham, S., Wang, Z.X., Tan, B., Sherrington, D.C., Rannard, S.P., Cooper, A.I., Brust, M. Size-controlled synthesis of near-monodisperse gold nanoparticles in the 1-4 nm range using polymeric stabilizers. J Am Chem Soc. 2005a; 127: 16398-16399.

Hussain, S., Thomassen, L.C.J., Ferecatu, I., Borot, M.-C., Andreau, K., Martens, J.A., Fleury, J., Baeza-Squiban, A., Marano, F., Boland, S. Research Carbon black and titanium dioxide nanoparticles elicit distinct apoptotic pathways in bronchial epithelial cells. Part Fibre Toxicol. 2010; 7: 1-17.

Hussain, S.M., Hess, K.L., Gearhart, J.M., Geiss, K.T., Schlager, J.J. In vitro toxicity of nanoparticles in BRL 3A rat liver cells. Toxicol In Vitro. 2005b; 19: 975-983. b ou a ?

Hutter, E., Boridy, S., Labrecque, S., Lalancette-Hébert, M., Kriz, J., Winnik, F.M., Maysinger, D. Microglial response to gold nanoparticles. ACS Nano. 2010; 4: 2595-2606.

Ionita, P. Is DPPH stable free radical a good scavenger for oxygen active species? Chem Pap. 2005; 59: 11-16.

Ionita, P., Spafiu, F., Ghica, C. Dual behavior of gold nanoparticles, as generators and scavengers for free radicals. J Mater Sci. 2008; 43: 6571-6574.

Irache, J.M., Esparza, I., Gamazo, C., Agüeros, M., Espuelas, S. Nanomedicine: Novel approaches in human and veterinary therapeutics. Vet Parasitol. 2011; 180: 47-71.

ISO14502-1: Determination of substances characteristic of green and black tea - Part 1: Content of total polyphenols in tea - Colorimetric method using Folin-Ciocalteu reagent, 2005.

Isono, R., Yoshimura, T., Esumi, K. Preparation of Au/TiO_2 nanocomposites and their catalytic activity for DPPH radical scavenging reaction. J Colloid Interf Sci. 2005; 288: 177-183.

Jacob, C., Winyard , P.G. Redox Signaling and Regulation in Biology and Medicine. Weinheim: Wiley-VCH Verlag GmbH & Co. KGaA, 2009: 433–464.

Jain, P.K., Huang, X., El-Sayed, I.H., El-Sayed, M.A. Review of some interesting surface plasmon resonance-enhanced properties of noble metal nanoparticles and their applications to biosystems. Plasmonics. 2007; 2: 107-118.

Jain, P.K., Lee, K.S., El-Sayed, I.H., El-Sayed, M.A. Calculated absorption and scattering properties of gold nanoparticles of different size, shape, and composition: applications in biological imaging and biomedicine. J Phys Chem B. 2006; 110: 7238-7248.

Jana, N.R., Gearheart, L., Murphy, C.J. Seeding growth for size control of 5-40 nm diameter gold nanoparticles. Langmuir. 2001; 17: 6782-6786.

Jana, N.R., Peng, X. Single-phase and gram-scale routes toward nearly monodisperse Au and other noble metal nanocrystals. J Am Chem Soc. 2003; 125: 14280-14281.

Jans, H., Huo, Q. Gold nanoparticle-enabled biological and chemical detection and analysis. Chem Soc Rev. 2012; 41: 2849-2866.

Jans, H., Stakenborg, T., Jans, K., Van De Broek, B., Peeters, S., Bonroy, K., Lagae, L., Borghs, G., Maes, G. Increased stability of mercapto alkane functionalized Au nanoparticles towards DNA sensing. Nanotechnology. 2010; 21: 285608-285616.

Jansen, M. The chemistry of gold as an anion. Chem Soc Rev. 2008; 37: 1824-1835.

Jeon, K.-I., Jeong, J.-Y., Jue, D.-M. Thiol-reactive metal compounds inhibit NF-κB activation by blocking IκB kinase. J Immunol. 2000; 164: 5981-5989.

Jia, H.Y., Han, X., Li, Z.W., Tian, Q., Miao, X.X., Du, L.B., Liu, Y. Gold nanoparticles-based catalysis for detection of S-nitrosothiols in blood serum. Talanta. 2011; 85: 1871-1875.

Jia, H.Y., Liu, Y., Zhang, X.J., Han, L., Du, L.B., Tian, Q., Xu, Y.C. Potential oxidative stress of gold nanoparticles by induced-NO releasing in serum. J Am Chem Soc. 2009; 131: 40-41.

Jiao, Y., Ubrich, N., Marchand-Arvier, M., Vigneron, C., Hoffman, M., Lecompte, T., Maincent, P. In vitro and in vivo evaluation of oral heparin-loaded polymeric nanoparticles in rabbits. Circulation. 2002; 105: 230–235.

Jin, F. Spectroscopic investigated to the interaction of human serum albumin with fluorescence carbon nanoparticles. Mater Sci Forum. 2011; 694: 396-398.

Jones, C.F., Grainger, D.W. In vitro assessments of nanomaterial cytotoxicity. Adv Drug Deliv Rev. 2009; 61: 438-456.

Joshi, H.M., Bhumkar, D.R., Joshi, K., Pokharkar, V., Sastry, M. Gold nanoparticles as carriers for efficient transmucosal insulin delivery. Langmuir. 2006; 22: 300-305.

Joshi, P., Chakraborty, S., Dey, S., Shanker, V., Ansari, Z.A., Singh, S.P., Chakrabarti, P. Binding of chloroquine-conjugated gold nanoparticles with bovine serum albumin. J Colloid Interface Sci. 2011; 355: 402-409.

Kajita, M., Hikosaka, K., Iitsuka, M., Kanayama, A., Toshima, N., Miyamoto, Y. Platinum nanoparticle is a useful scavenger of superoxide anion and hydrogen peroxide. Free Radic Res. 2007; 41: 615-626.

Kamei, S., Chen-Kuo-Chang, M., Cazevieille, C., Lenaers, G., Olichon, A., Belenguer, P., Roussignol, G., Renard, N., Eybalin, M., Michelin, A., Delettre, C., Brabet, P., Hamel, C.P. Expression of the Opa1 mitochondrial protein in retinal ganglion cells: its downregulation causes aggregation of the mitochondrial network. Invest Ophthalmol Vis Sci. 2005; 46: 4288–4294.

Karakoti, A., Singh, S., Dowding, J.M., Seal, S., Self, W.T. Redox-active radical scavenging nanomaterials. Chem Soc Rev. 2010; 39: 4422-4432.

Kelly, K.L., Coronado, E., Zhao, L.L., Schatz, G.C. The optical properties of metal nanoparticles: the influence of size, shape, and dielectric environment. J Phys Chem B. 2003; 107: 668-677.

Khan, J.A., Pillai, B., Das, T.K., Singh, Y., Maiti, S. Molecular effects of uptake of gold nanoparticles in HeLa cells. Chem Biochem. 2007; 8: 1237-1240.

Khlebtsov, N., Dykmann, L. Biodistribution and toxicity of engineered gold nanoparticles: a review of *in vitro* and *in vivo* studies. Chem Soc Rev. 2011; 40: 1647-1671.

Kim, C.-K., Ghosh, P., Rotello, V.M. Multimodal drug delivery using gold nanoparticles. Nanoscale. 2009; 1: 61-67.

Kim, E.J., Yeum, J.H., Ghim, H.D., Lee, S.G., Lee, G.H., Lee, H.J., Han, S.I., Choi, J.H. Ultrasmall polyethyleneimine-gold nanoparticles with high stability. Polym-Korea. 2011; 35: 161-165.

Kim, J.-Y., Lee, J.-S. Synthesis and thermally reversible assembly of DNA-gold nanoparticles cluster conjugates. Nano Lett. 2009; 9: 4564-4569.

Kim, T., Lee, C.H., Joo, S.W., Lee, K. Kinetics of gold nanoparticles aggregation: experiments and modelling. J Colloid Interface Sci. 2008; 318: 238-243.

Kim, T., Lee, K., Gong, M.S., Joo, S.W. Control of gold nanoparticle aggregates by manipulation of interparticle interaction. Langmuir. 2005; 21: 9524-9528.

Kimling, J., Maier, M., Okenve, B., Kotaidis, V., Ballot, H., Plech, A. Turkevich method for gold nanoparticle synthesis revisited. J Phys Chem B. 2006; 110: 15700-15707.

Kocbach, A., Totlandsdal, A.I., Låg, M., Refsnes, M., Schwarze, P.E. Differential binding of cytokines to environmentally relevant particles: A possible source for misinterpretation of in vitro results? Toxicol Lett. 2008; 176: 131-137.

Kosar, M., Dorman, H.J.D., Bachmayer, O., Baser, K.H.C., Hiltunen, R. An improved on-line HPLC-DPPH$^{\bullet}$ method for the screening of the radical scavenging compounds in water extracts of Lamiaceae plants. Chem Nat Compd. 2003; 39: 161-166.

Konwarh, R., Gogoi, B., Philip, R., Laskar, M.A., Karak, N. Biomimetic preparation of polymer-supported free radical scavenging, cytocompatible and antimicrobial “green” silver nanoparticles using aqueous extract of Citrus sinensis peel. Colloid Surface B. 2011; 84: 338-345.

Kreibig, U., Vollmer, M. Optical properties of metal clusters. Berlin, Germany: Springer, 1995.

Kroll, A., Dierker, C., Rommel, C., Hahn, D., Wohlleben, W., Schulze-Isfort, C., Gobbert, C., Voetz, M., Hardinghaus, F., Schnekenburger, J. Cytotoxicity screening of 23 engineered nanomaterials using a test matrix of ten cell lines and three different assays. Part Fibre Toxicol. 2011; 8: 9-23.

Kroll, A., Pillukat, M.H., Hahn, D., Schnekenburger, J. Current in vitro methods in nanoparticle risk assessment: Limitations and challenges. Eur J Pharm Biopharm. 2009; 72: 370-377.

Kroll, A., Pillukat, M., Hahn, D., Schnekenburger, J. Interference of engineered nanoparticles with in vitro toxicity assays. Arch Toxicol. 2012: 1-14.

Krpetic, Z., Porta, F., Caneva, E., Dal Santo, V., Scari, G. Phagocytosis of biocompatible gold nanoparticles. Langmuir. 2010; 26: 14799-14805.

Laemmli, U.K. Cleavage of structural proteins during the assembly of the head of bacteriophage T4. Nature. 1970; 227: 680–685.

Lamprecht, A., Koenig, P., Ubrich, N., Maincent, P., Neumann, D. Low molecular weight heparin nanoparticles: mucoadhesion and behaviour in Caco-2 cells. Nanotechnology. 2006; 17: 3673–3680.

Lee, H., Lee, K., Kim, I.-K., Park, T.G. Fluorescent gold nanoprobe sensitive to intracellular reactive oxygen species. Adv Funct Mater. 2009; 19: 1884-1890.

Lee, H., Lee, K., Kim, I.-K., Park, T.G. Bodipy-functionalized gold nanoparticles as a selective fluoro-chromogenic chemosensor for imaging Cu^{2+} in living cells. Analyst. 2010; 135: 728: 2022-2027.

Lee, H., Lee, K., Kim, I.K., Park, T.G. Synthesis, characterization, and in vivo diagnostic applications of hyaluronic acid immobilized gold nanoprobes. Biomaterials. 2008; 29: 4709-4718.

Lee, M.S., Kim, Y.J. Signaling pathways downstream of pattern-recognition receptors and their cross talk. Annu Rev Biochem. 2007; 76: 447-480.

Lee, H.-M., Shin, D.-M., Song, H.-M., Yuk, J.-M., Lee, Z.-W., Lee, S.-H., Hwang, S.M., Kim, J.-M., Lee, C.-S., Jo, E.-K. Nanoparticles up-regulate tumor necrosis factor-α and CXCL8 via reactive oxygen species and mitogen-activated protein kinase activation. Toxicol Appl Pharmacol. 2009; 238: 160-169.

Leff, D.V., Brandt, L., Heath, J.R. Synthesis and characterization of hydrophobic, organically-soluble gold nanocrystals functionalized with primary amines. Langmuir. 1996; 12: 4723-4730.

Lemire, C., Meyer, R., Shaikhutdinov, S., Freund, H.-J. Do quantum size effects control CO adsorption on gold nanoparticles? Angew Chem Int Edit. 2004; 43: 118-121.

Leroy, P., Sapin-Minet, A., Pitarch, A., Boudier, A., Tournebize, J., Schneider, R. Interactions between gold nanoparticles and macrophages: Activation or inhibition? Letter to the Editor, Nitric Oxide-Biol Chem. 2011; 25: 54-56.

Lewinski, N., Colvin, V., Drezedk, R. Cytotoxicity of nanoparticles. Small. 2008; 4: 26–49.

Lewicki, K., Marchand, S., Matoub, L., Lulek, J., Coulon, J., Leroy, P. Development of a fluorescence-based microtiter plate method for the measurement of glutathione in yeast. Talanta. 2006; 70: 876–882.

Lewis, D.J., Day, T.M., MacPherson, J.V., Pikramenou, Z. Luminescent nanobeads: attachment of surface reactive Eu(III) complexes to gold nanoparticles. Chem Comm. 2006; 13: 1433-1435.

Li, J.J., Hartono, D., Ong, C.N., Bay, B.H., Yung, L.Y. Autophagy and oxidative stress associated with gold nanoparticles. Biomaterials. 2010; 31: 5996–6003.

Li, J.J., Lo, S.L., Ng, C.T., Gurung, R.L., Hartono, D., Hande, M.P., Ong, C.N., Bay, B.H., Yung, L.Y.L. Genomic instability of gold nanoparticle treated human lung fibroblast cells. Biomaterials. 2011; 32: 5515-5523.

Li, L., Li, B. Sensitive and selective detection of cysteine using gold nanoparticles as colorimetric probes. Analyst. 2009; 134: 1361-1365.

Li, X.-M., Jong, M.R.d., Inoue, K., Shinkai, S., Huskens, J., Reinhoudt, D.N. Formation of gold colloids using thioether derivatives as stabilizing ligands. J Mater Chem. 2001; 11: 1919-1923.

Li, Z., Jin, R., Mirkin, C.A., Letsinger, R.L. Multiple thiol-anchor capped DNA-gold nanoparticle conjugates. Nucleic Acids Res. 2002; 30: 1558-1562.

Libutti, S.K., Paciotti, G.F., Byrnes, A.A., Alexander, H.R., Gannon, W.E., Walker, M., Seidel, G.D., Yuldasheva, N., Tamarkin, L. Phase I and pharmacokinetic studies of CYT-6091, a novel PEGylated colloidal gold-rhTNF nanomedicine. Clin Cancer Res. 2010; 16: 6139-6149.

Lien, E.J., Ren, S.J., Bui, H.Y.H., Wang, R.B. Quantitative structure-activity relationship analysis of phenolic antioxidants. Free Radic Biol Med. 1999; 26: 285-294.

Lin, C.-A.J., Yang, T.-Y., Lee, C.-H., Huang, S.H., Sperling, R.A., Zanella, M., Li, J.K., Shen, J.-L., Wang, H.-H., Yeh, H.-I., Parak, W.J., Chang, W.H. Synthesis, characterization, and bioconjugation of fluorescent gold nanoclusters toward biological labeling applications. ACS Nano. 2009; 3: 395-401.

Lin, J.H., Chang, C.W., Tseng, W.L. Fluorescent sensing of homocysteine in urine: using fluorosurfactant-capped gold nanoparticles and o-Phthaldialdehyde. Analyst. 2010; 135: 104-110.

Lin, Z., Fillmore, G.C., Um, T.H., Elenitoba-Johnson, K.S., Lim, M.S. Comparative microarray analysis of gene expression during activation of human peripheral blood T cells and leukemic Jurkat T cells. Lab Invest. 2003; 83: 765–776.

Link, S., El-Sayed, M.A. Optical properties and ultrafast dynamics of metallic nanocrystals. Ann Rev Phys Chem. 2003; 54: 331-366.

Link, S., El-Sayed, M.A. Spectral properties and relaxation dynamics of surface plasmon electronic oscillations in gold and silver nanodots and nanorods. J Phys Chem B. 1999; 103: 8410-8426.

Liu, J., Ong, W., Román, E., Lynn, M.J., Kaifer, A.E. Cyclodextrin-modified gold nanospheres. Langmuir. 2000; 16: 3000-3002.

Liu, S.J., Han, Y.C., Qiao, R.R., Zeng, J.F., Jia, Q.J., Wang, Y.L., Gao, M.Y. Investigations on the interactions between plasma proteins and magnetic iron oxide nanoparticles with different surface modifications. J Phys Chem C. 2010; 114: 21270-21276.

Liu, X., Atwater, M., Wang, J., Huo, Q. Extinction coefficient of gold nanoparticles with different sizes and different capping ligands. Colloids Surf B. 2007; 58: 3-7.

Liu, X., Sun, J.A. Endothelial cells dysfunction induced by silica nanoparticles through oxidative stress via JNK/P53 and NF-kappa B pathways. Biomaterials. 2010; 31: 8198-8209.

Liu, Y., Chen, Z., Wang, J. Systematic evaluation of biocompatibility of magnetic magnetic Fe_3O_4 nanoparticles with six different mammalian cell lines. J Nanopart Res. 2011; 13: 199-212.

Llevot, A., Astruc, D. Applications of vectorized gold nanoparticles to the diagnosis and therapy of cancer. Chem Soc Rev. 2012; 41: 242-257.

Loo, C., Lowery, A., Halas, N., West, J., Drezek, R. Immunotargeted nanoshells for integrated cancer imaging and therapy. Nano Lett. 2005; 5: 709-711.

Love, J.C., Estroff, L.A., Kriebel, J.K., Nuzzo, R.G., Whitesides, G.M. Self-assembled monolayers of thiolates on metals as a form of nanotechnology. Chem Rev. 2005; 105: 1103-1169.

Loo, C., Lowery, A., Halas, N., West, J., Drezek, R. Immunotargeted nanoshells for integrated cancer imaging and therapy. Nano Lett. 2005; 5: 709-711.

Lowry, O.H., Rosebrough, N.J., Farr, A.L., Randall, R.J. Protein measurement with the Folin phenol reagent. J Biol Chem. 1951; 193: 265–275.

Lubitz, I., Kotlyar, A. G4-DNA-Coated gold nanoparticles: synthesis and assembly. Bioconjugate Chem. 2011; 22: 2043-2047.

Luo, S., Rubinsztein, D.C. Atg5 and bcl-2 provide novel insights into the interplay between apoptosis and autophagy. Cell Death Differ. 2007; 14: 1247–1250.

Ma, J.S., Kim, W.J., Kim, J.J., Kim, T.J., Ye, S.K., Song, M.D., Kang, H., Kim, D.W., Moon, W.K., Lee, K.H. Gold nanoparticles attenuate LPS-induced NO production through the inhibition of NF-κB and IFN-β/STAT1 pathways in RAW264.7 cells. Nitric Oxide-Biol Chem. 2010; 23: 214-219.

Ma, X., Wu, Y., Jin, S., Tian, Y., Zhang, X., Zhao, Y., Yu, L., Liang, X.-J. Gold Nanoparticles induce autophagosome accumulation through size-dependent nanoparticle uptake and lysosome impairment. ACS Nano. 2011; 5: 8629-8639.

Macnulty, B.J., Wollard, L.D. The use of rhodamine B in analytical chemistry: The determination of small quantities of gold. Anal Chim Acta. 1955; 13: 154-158.

Magdolenova, Z., Bilanicova, D., Pojana, G., Fjellsbo, L.M., Hudecova, A., Hasplova, K., Marcomini, A., Dusinska, M. Impact of agglomeration and different dispersions of titanium dioxide nanoparticles on the human related in vitro cytotoxicity and genotoxicity. J Environ Monit. 2012; 14: 455-464.

Mann, J., Oakley, F., Johnson, P.W., Mann, D.A. CD40 induces interleukin-6 gene transcription in dendritic cells: regulation by TRAF2, AP-1, NF-kappa B, and CBF1. J Biol Chem. 2002; 277: 17125–17138.

Marano, F., Hussain, S., Rodrigues-Lima, F., Baeza-Squiban, A., Boland, S. Nanoparticles: molecular targets and cell signalling. Arch Toxicol. 2011; 85: 733-741.

Marinenko, J., May, I. Fluorometric determination of gold in rocks with rhodamine B. US Geological Survey.1968; 7: 1137-1139.

Mattoussi, H., Mauro, J.M., Goldman, E.R., Anderson, G.P., Sundar, V.C., Mikulec, F.V., Bawendi, M.G. Self-assembly of CdSe-ZnS quantum dot bioconjugates using an engineered recombinant protein. J Am Chem Soc. 2000; 122: 12142-12150.

Mie, G. Beiträge zur optik trüber medien, speziell kolloidaler metallösungen. Ann Phys. 1908; 25: 377-445

Mei, B.C., Oh, E., Susumu, K., Farrell, D., Mountziaris, T.J., Mattoussi, H. Effects of ligand coordination number and surface curvature on the stability of gold nanoparticles in aqueous solutions. Langmuir. 2009; 25: 10604-10611.

Minematsu, H., Shin, M.J., Celil Aydemir, A.B., Seo, S.W., Kim, D.W., Blaine, T.A., Macian, F., Yang, J., Young-In Lee, F. Orthopedic implant particle-induced tumor necrosis factor-alpha production in macrophage-monocyte lineage cells is mediated by nuclear factor of activated T cells. Ann N Y Acad Sci. 2007; 1117: 143–150.

Moini, H., Packer, L., Saris, N.E.L. Antioxidant and prooxidant activities of α-lipoic acid and dihydrolipoic acid. Toxicol Appl Pharm. 2002; 182: 84-90.

Möller, M., Denicola, A. Study of protein-ligand binding by fluorescence. Biochem Mol Biol Educ. 2002; 30: 175–178.

Moon, J.K., Shibamoto, T. Antioxidant assays for plant and food components. J Agric Food Chem. 2009; 57: 1655-1666.

Monteiro-Riviere, N.A., Inman, A.O. Challenges for assessing carbon nanomaterial toxicity to the skin. Carbon. 2006; 44: 1070-1078.

Monteiro-Riviere, N.A., Inman, A.O., Zhang, L.W. Limitations and relative utility of screening assays to assess engineered nanoparticle toxicity in a human cell line. Toxicol Appl Pharmacol. 2009; 234: 222-235.

Mucic, R.C., Storhoff, J.J., Mirkin, C.A., Letsinger, R.L. DNA-directed synthesis of binary nanoparticle network materials. J Am Chem Soc. 1998; 120: 12674-12675.

Murphy, C.J., Gole, A.M., Stone, J.W., Sisco, P.N., Alkilany, A.M., Goldsmith, E.C., Baxter, S.C. Gold nanoparticles in biology: beyond toxicity to cellular imaging. Acc Chem Res. 2008; 41: 1721-1730.

Murphy, C.J., San, T.K., Gole, A.M., Orendorff, C.J., Gao, J.X., Gou, L., Hunyadi, S.E., Li, T. Anisotropic metal nanoparticles: Synthesis, assembly, and optical applications. J Phys Chem B. 2005; 109: 13857-13870.

Musialik, M., Litwinienko, G. Scavenging of DPPH center dot radicals by vitamin E is accelerated by its partial ionization: The role of sequential proton loss electron transfer. Org Lett. 2005; 7: 4951-4954.

Muthu, M.S., Rawat, M.K., Mishra, A., Singh, S. PLGA nanoparticle formulations of risperidone: preparation and neuropharmacological evaluation. Nanomed Nanotech Biol Med. 2009; 5: 323-333.

Murphy, C.J., Gole, A.M., Stone, J.W., Sisco, P.N., Alkilany, A.M., Goldsmith, E.C., Baxter, S.C. Gold nanoparticles in biology: beyond toxicity to cellular imaging. Acc Chem Res. 2008; 41: 1721-1730.

Nativo, P., Prior, I.A., Brust, M. Uptake and intracellular fate of surface-modified gold nanoparticles. ACS Nano. 2008; 2: 1639-1644.

Nanowerk. Nanotechnology databases from Nanowerk. 2012. http://www.nanowerk.com/

Nel, A.E., Madler, L., Velegol, D., Xia, T., Hoek, E.M.V., Somasundaran, P., Klaessig, F., Castranova, V., Thompson, M. Understanding biophysicochemical interactions at the nano-bio interface. Nat Mater. 2009; 8: 543-557.

Nguyen, D.T., Kim, D.-J., Kim, K.-S. Controlled synthesis and biomolecular probe application of gold nanoparticles. Micron. 2011; 42: 207-227.

Nguea, H.D., de Reydellet, A., Le Faou, A., Zaiou, M., Rihn, B. Macrophage culture as a suitable paradigm for evaluation of synthetic vitreous fibers. Crit Rev Toxicol. 2008; 38: 675–695.

Nie, Z., Liu, K.J., Zhong, C.J., Wang, L.F., Yang, Y., Tian, Q., Liu, Y. Enhanced radical scavenging activity by antioxidant-functionalized gold nanoparticles: a novel inspiration for development of new artificial antioxidants. Free Radic Biol Med. 2007; 43: 1243-1254.

Niederländer, H.A., van Beek, T.A., Bartasiute, A., Koleva, I.I. Antioxidant activity assays on-line with liquid chromatography. J Chromatogr A. 2008; 1210: 121-134.

Niidome, T., Nakashima, K., Takahashi, H., Niidome, Y. Preparation of primary amine-modified gold nanoparticles and their transfection ability into cultivated cells. Chem Commun. 2004: 1978-1979.

Niu, J., Azfer, A., Rogers, L.M., Wang, X., Kolattukudy, P.E. Cardioprotective effects of cerium oxide nanoparticles in a transgenic murine model of cardiomyopathy. Cardiovasc Res. 2007; 73: 549–559.

Noipa, T., Srijaranai, S., Tuntulani, T., Ngeontae, W. New approach for evaluation of the antioxidant capacity based on scavenging DPPH free radical in micelle systems. Food Res Int. 2011; 44: 798-806.

Note, C., Koetz, J., Kosmella, S., Tiersch, B. Hydrophobically modified polyelectrolytes used as reducing and stabilizing agent for the formation of gold nanoparticles. Colloid Polym Sci. 2005; 283: 1334-1342.

Nuengchamnong, N., Ingkaninan, K. On-line HPLC-MS-DPPH assay for the analysis of phenolic antioxidant compounds in fruit wine: Antidesma thwaitesianum Muell. Food Chem. 2010; 118: 147-152.

Oberdorster, G., Maynard, A., Donaldson, K., Castranova, V., Fitzpatrick, J., Ausman, K., Carter, J., Karn, B., Kreyling, W., Lai, D., Olin, S., Monteiro-Riviere, N., Warheit, D., Yang, H. Principles for characterizing the potential human health effects from exposure to nanomaterials: elements of a screening strategy. Part Fibre Toxicol. 2005; 2: 8.

Olichon, A., Baricault, L., Gas, N., Guillou, E., Valette, A., Belenguer, P., Lenaers, G. Loss of OPA1 perturbates the mitochondrial inner membrane structure and integrity, leading to cytochrome c release and apoptosis. J Biol Chem. 2003; 278: 7743–7746.

Oh, E., Susumu, K., Goswami, R., Mattoussi, H. One phase synthesis of water-soluble gold nanoparticles with control over size and surface functionalities. Langmuir. 2010; 26: 7604-7613.

Oostingh, G., Casals, E., Italiani, P., Colognato, R., Stritzinger, R., Ponti, J., Pfaller, T., Kohl, Y., Ooms, D., Favilli, F., Leppens, H., Lucchesi, D., Rossi, F., Nelissen, I., Thielecke, H., Puntes, V., Duschl, A., Boraschi, D. Problems and challenges in the development and validation of human cell-based assays to determine nanoparticle-induced immunomodulatory effects. Part Fibre Toxicol. 2011; 8: 1-21.

Owens III, D.E., Peppas, N.A. Opsonization, biodistribution, and pharma-cokinetics of polymeric nanoparticles. Int J Pharmaceut. 2006; 307: 93-102.

Paciotti, G.F., Kingston, D.G.I., Tamarkin, L.. Colloidal gold nanoparticles: a novel nanoparticle platform for developing multifunctional tumor-targeted drug delivery vectors Drug Dev Res. 2006; 67: 47-54.

Paciotti, G.F., Myer, L., Weinreich, D., Goia, D., Pavel, N., McLaughlin, R.E., Tamarkin, L. Colloidal gold: a novel nanoparticle vector for tumor directed drug delivery. Drug Deliv. 2004; 11: 169-183.

Pal, A. Photochemical dissolution of gold nanoparticles by bromine containing trihalomethanes (THMs) in an aqueous triton X-100 medium and its analytical application. J Photochem Photobiol Chem. 2001; 142: 59-65.

Pan, Y., Neuss, S., Leifert, A., Fischler, M., Wen, F., Simon, U., Schmid, G., Brandau, W., Jahnen-Dechent, W. Size-dependent cytotoxicity of gold nanoparticles. Small. 2007; 3: 1941-1949.

Pan, Y., Leifert, A., Ruau, D., Neuss, S., Bornemann, J., Schmid, G., Wolfgang, B., Ulrich, S., Willi, J.-D. Gold nanoparticles of diameter 1.4 nm trigger necrosis by oxidative stress and mitochondrial damage. Small. 2009; 5: 2067–2076.

Papavassiliou, G.C. Optical properties of small inorganic and organic metal particles. Prog Solid State Chem. 1979; 12: 185-271.

Park, E.J., Park, K. Oxidative stress and pro-inflammatory responses induced by silica nanoparticles in vivo and in vitro. Toxicol Lett. 2009; 184: 18-25.

Park, J., Lim, D.H., Lim, H.J., Kwon, T., Choi, J.S., Jeong, S., Choi, I.H., Cheon, J. Size dependent macrophage responses and toxicological effects of Ag nanoparticles. Chem Commun. 2011; 47: 4382-4384.

Paszko, E., Ehrhardt, C., Senge, M.O., Kelleher, D.P., Reynolds, J.V. Nanodrug applications in photodynamic therapy. Photodiagn Photodyn. 2011; 8: 14-29.

Patra, H.K., Banerjee, S., Chaudhuri, U., Lahiri, P., Dasgupta, A.K. Cell selective response to gold nanoparticles. Nanomed Nanotech Biol Med. 2007; 3: 111-119.

Pellegrino, T., Sperling, R.A., Alivisatos, A.P., Parak, W.J. Gel electrophoresis of gold-DNA nanoconjugates. J Biomed Biotechnol. 2007; 2007: 26796-26805.

Peng, C., Wang, H., Guo, R., Shen, M.W., Cao, X.Y., Zhang, G.X., Shi, X.Y. Acetylation of dendrimer-entrapped gold nanoparticles: Synthesis, stability, and X-ray attenuation property. J Appl Polym Sci. 2011: 119; 1673-1682.

Perez-Juste, J., Pastoriza-Santos, I., Liz-Marzan, L.M., Mulvaney, P. Gold nanorods: Synthesis, characterization and applications. Coordin Chem Rev. 2005; 249: 1870-1901.

Peterle, T., Leifert, A., Timper, J., Sologubenko, A., Simon, U., Mayor, M. Multidentate thioether ligands coating gold nanoparticles. Chem Commun. 2008; 29: 3438-3440.

Pfaller, T., Puntes, V., Casals, E., Duschl, A., Oostingh, G.J. In vitro investigation of immunomodulatory effects caused by engineered inorganic nanoparticles - the impact of experimental design and cell choice. Nanotoxicology. 2010; 4: 138-138.

Pignatello, R., Bucolo, C., Ferrara, P., Maltese, A., Puleo, A., Puglisi, G. Eudragit RS100 nanosuspensions for the ophthalmic controlled delivery of ibuprofen. Eur J Pharm Sci. 2002; 16: 53–61.

Pissuwan, D., Valenzuela, S.M., Cortie, M.B. Therapeutic possibilities of plasmonically heated gold nanoparticles. Trends Biotechnol. 2006; 24: 62-67.

Pissuwan, D., Niidome, T., Cortie, M.B. The forthcoming applications of gold nanoparticles in drug and gene delivery systems. J Control Release. 2011; 149: 65-71.

Polo, S., Di Fiore, P.P. Endocytosis conducts the cell signaling orchestra. Cell. 2006; 124: 897–900.

Porter, L.A., Jr., Ji, D., Westcott, S.L., Graupe, M., Czernuszewicz, R.S., Halas, N.J., Lee, T.R. Gold and silver nanoparticles functionalized by the adsorption of dialkyl disulfides. Langmuir. 1998; 14: 7378-7386.

Prabha, S., Zhou, W.Z., Panyam, J., Labhasetwar, V. Size-dependency of nanoparticle mediated gene transfection: studies with fractionated nanoparticles. Int J Pharm. 2002; 244: 105-115.

Pramanik, S., Banerjee, P., Sarkar, A., Bhattacharya, S.C. Size-dependent interaction of gold nanoparticles with transport protein. J Lumin. 2008; 128: 1969-1974.

Prior, R.L., Wu, X.L., Schaich, K. Standardized methods for the determination of antioxidant capacity and phenolics in foods and dietary supplements. J Agric Food Chem. 2005; 53: 4290-4302.

Pulskamp, K., Diabate, S., Krug, H.F. Carbon nanotubes show no sign of acute toxicity but induce intracellular reactive oxygen species in dependence on contaminants. Toxicol Lett. 2007; 168: 58 – 74.

Qiao, F.Y, Liu, J., Li, F.R., Kong, X.L., Zhang, H.L., Zhou, H.X. Antibody and DNA dual-labeled gold nanoparticles: Stability and reactivity. Appl Surf Sci. 2008; 254: 2941-2946.

Quentmeier, H., Drexler, H.G., Fleckenstein, D., Zaborski, M., Armstrong, A., Sims, J.E., Lyman, S.D. Cloning of human thymic stromal lymphopoietin (tslp) and signaling mechanisms leading to proliferation. Leukemia. 2001; 15: 1286-1292.

Rao, C.N.R., Kulkarni, G.U., Thomas, P.J., Edwards, P.P. Metal nanoparticles and their assemblies. Chem Soc Rev. 2000; 29: 27-37.

Rao, C.N.R., Mèuller, A., Cheetham, A.K., editors. The chemistry of nanomaterials: Synthesis, properties and applications in 2 volumes. Allemagne: Weinheim: Wiley-VCH; 2004.

Re, R., Pellegrini, N., Proteggente, A., Pannala, A., Yang, M., Rice-Evans, C. Antioxidant activity applying an improved ABTS radical cation decolorization assay. Free Radic Bio Med. 1999; 26: 1231-1237.

Rosi, N.L., Mirkin, C.A. Nanostructures in biodiagnostics. Chem Rev. 2005; 105: 1547-1562.

Rosi, N.L., Giljohann, D.A., Thaxton, C.S., Lytton-Jean, A.K., Han, M.S., Mirkin, C.A. Oligonucleotide-modified gold nanoparticles for intracellular gene regulation. Science. 2006; 312: 1027-1030.

Roux, S., Garcia, B., Bridot, J.-L., Salomé, M., Marquette, C., Lemelle, L., Gillet, P., Blum, L., Perriat, P., Tillement, O. Synthesis, characterization of dihydrolipoic acid capped gold nanoparticles, and functionalization by the electroluminescent luminol. Langmuir. 2005; 21: 2526-2536.

Saitoh, T., Fujita, N., Jang, M.H., Uematsu, S., Yang, B.G., Satoh, T., Omori, H., Noda, T., Yamamoto, N., Komatsu, M., Tanaka, K., Kawai, T., Tsujimura, T., Takeuchi, O., Yoshimori, T., Akira, S. Loss of the autophagy protein atg16L1 enhances endotoxin-induced IL-1beta production. Nature. 2008; 456: 264–268.

Sakai, T., Alexandridis, P. Single-step synthesis and stabilization of metal nanoparticles in aqueous pluronic block copolymer solutions at ambient temperature. Langmuir. 2004; 20: 8426-8430.

Sakamoto, M., Tachikawa, T., Fujitsuka, M., Majima, T. Photochemical reactivity of gold clusters: Dependence on size and spin multiplicity. Langmuir. 2009; 25: 13888-13893.

Sakura, T., Takahashi, T., Kataoka, K., Nagasaki, Y. One-pot preparation of mono-dispersed and physiologically stabilized gold colloid. Colloid Polym Sci. 2005; 284: 97.

Sadauskas, E., Danscher, G., Stoltenberg, M., Vogel, U., Larsen, A., Wallin, H. Protacted elimination of gold nanoparticles from mouse liver. Nanomed Nanotech Biol Med. 2009; 5: 162-169.

Sanz, A., Barja, G., Pamplona, R., Leeuwenbugh, C. in: C. Jacob, P.G. Winyard (WILEY-VCH Verlag GmbH & Co. KGaA) Redox signaling and regulation in biology and medicine Weinheim. 2009; 433-464.

Sasi, N., Hwang, M., Jaboin, J., Csiki, I., Lu, B. Regulated cell death pathways: new twists in modulation of BCL2 family function. Mol Cancer Ther. 2009; 8: 1421–1429.

Schaffazick, S.R., Siqueira, I.R., Badejo, A.S., Jornada, D.S., Pohlmann, A.R., Netto, C.A., Guterres, S.S. Incorporation in polymeric nanocapsules improves the antioxidant effect of melatonin against lipid peroxidation in mice brain and liver. Eur J Pharm Biopharm. 2008; 69: 64–71.

Scheffer, A., Engelhard, C., Sperling, M., Buscher, W. ICP-MS as a new tool for the determination of gold nanoparticles in bioanalytical applications. Anal Bioanal Chem. 2008; 390: 249-252.

Schmidbaur, H., Schier, A. Aurophilic interactions as a subject of current research: an up-date. Chem Soc Rev. 2012; 41: 370-412.

Schulze, C., Schaefer, U.F., Ruge, C.A., Wohlleben, W., Lehr, C.-M. Interaction of metal oxide nanoparticles with lung surfactant protein A. Eur J Pharm Biopharm. 2011; 77: 376-383.

Seleverstov, O., Zabirnyk, O., Zscharnack, M., Bulavina, L., Nowicki, M., Heinrich, J.M., Yezhelyev, M., Emmrich, F., O'Regan, R., Bader, A. Quantum dots for human mesenchymal stem cells labeling. A size-dependent autophagy activation. Nano Lett. 2006; 6: 2826–2832.

Selvakannan, P.R., Mandal, S., Phadtare, S., Pasricha, R., Sastry, M. Capping of gold nanoparticles by the amino acid lysine renders them water-dispersible. Langmuir. 2003; 19: 3545-3549.

Sen, C.K. Redox signaling and the emerging therapeutic potential of thiol antioxidants. Biochem Pharmacol. 1998; 55: 1747-1758.

Sharma, O.P., Bhat, T.K. DPPH antioxidant assay revisited. Food Chem. 2009; 113: 1202-1205.

Shimizu, S., Kanaseki, T., Mizushima, N., Mizuta, T., Arakawa-Kobayashi, S., Thompson, C.B., Tsujimoto, Y. Role of Bcl-2 family proteins in a non-apoptotic programmed cell death dependent on autophagy genes. Nat Cell Biol. 2004; 6: 1221–1228.

Shukla, R., Bansal, V., Chaudhary, M., Basu, A., Bhonde, R.R., Sastry, M. Biocompatibility of gold nanoparticles and their endocytotic fate inside the cellular compartment: A microscopic overview. Langmuir. 2005; 23: 10644-10654.

Sies, H. Glutathione and its role in cellular functions. Free Radical Bio Med. 1999; 27: 916-921.

Sir, D., Ou, J.H. Autophagy in viral replication and pathogenesis. Mol Cells. 2008; 29: 1–7.

Skrabalak, S.E., Chen, J.Y., Sun, Y.G., Lu, X.M., Au, L., Cobley, C.M., Xia, Y.N. Gold nanocages: synthesis, properties, and applications. Accounts Chem Res. 2008; 41: 1587-1595.

Skorodumova, N.V., Simak, S.I., Lundqvist, B.I., Abrikosov, I.A., Johansson, B. Quantum origin of the oxygen storage capability of ceria. Phys Rev Lett. 2002; 89: 1-4.

Slocik, J.M., Stone, M.O., Naik, R.R. Synthesis of gold nanoparticles using multifunctional peptides. Small. 2005; 1: 1048-1052.

Sobhan, M.A., Withford, M.J., Goldys, E.M. Enhanced stability of gold colloids produced by femtosecond laser synthesis in aqueous solution of CTAB. Langmuir. 2010; 26: 3156-3159.

Soenen, S.J., Rivera-Gil, P., Montenegro, J.-M., Parak, W.J., Smedt, S.C.D. Cellular toxicity of inorganic nanoparticles: Common aspects and guidelines for improved nanotoxicity evaluation. Nanotoday. 2011; 6: 446-465.

Sokolov, K., Follen, M., Aaron, J., Pavlova, I., Malpica, A., Lotan, R., Richards-Kortum, R. Real-time vital optical imaging of precancer using anti-epidermal growth factor receptor antibodies conjugated to gold nanoparticles. Cancer Res. 2003; 63: 1999-2004.

Song, M.M., Song, W.J., Bi, H., Wang, J., Wu, W.L., Sun, J., Yu, M. Cytotoxicity and cellular uptake of iron nanowires. Biomaterials. 2010; 31: 1509 – 1517

Sperling, R.A., Rivera Gil, P., Zhang, F., Zanella, M., Parak, W.J. Biological applications of gold nanoparticles. Chem Soc Rev. 2008; 37: 1896-1908.
Sperling, R.A., Parak, W.J. Surface modification, functionalization and bioconjugation of colloidal inorganic nanoparticles. Philos Trans A. 2010; 368: 1333-1383.

Stobiecka, M., Coopersmith, K., Hepel, M. Resonance elastic light scattering (RELS) spectroscopy of fast non-Langmuirian ligand-exchange in glutathione-induced gold nanoparticle assembly. J Colloid Interface Sci. 2010; 350: 168-177.

Stewart, M.H., Susumu, K., Mei, B.C., Medintz, I.L., Delehanty, J.B., Blanco-Canosa, J.B., Dawson, P.E., Mattoussi, H. Multidentate poly(ethylene glycol) ligands provide colloidal stability to semiconductor and metallic nanocrystals in extreme conditions. J Am Chem Soc. 2010; 132: 9804-9813.

Su, K.H., Wei, Q.H., Zhang, X., Mock, J.J., Smith, D.R., Schultz, S. Interparticle coupling effects on plasmon resonances of nanogold particles. Nano Lett. 2003; 3: 1087-1090.
Suja, K.P., Jayalekshmy, A., Arumughan, C. Free radical scavenging behavior of antioxidant compounds of sesame (sesamum indicum L.) in DPPH(*) system. J Agric Food Chem. 2004; 52: 912-915.

Sudeep, P.K., Joseph, S.T.S., Thomas, K.G. Selective detection of cysteine and glutathione using gold nanorods. J Am Chem Soc. 2005; 127: 6516-6517.

Summa, D., Spiga, O., Bernini, A., Venditti, V., Priora, R., Frosali, S., Margaritis, A., Giuseppe, D.D., Niccolai, N., Simplicio, P.D. Protein–thiol substitution or protein dethiolation by thiol/disulfide exchange reactions: the albumin model. Proteins. 2007; 69: 369-378.

Suri, S.S., Fenniri, H., Singh, B. Nanotechnology-based drug delivery systems. J Occup Med Toxicol. 2007; 2: 16.

Takahashi, H., Niidome, Y., Niidome, T., Kaneko, K., Kawasaki, H., Yamada, S. Modification of gold nanorods using phosphatidylcholine to reduce cytotoxicity. Langmuir. 2005; 22: 2-5.

Talotta, F., Cimmino, A., Matarazzo, M.R., Casalino, L., De Vita, G., D'Esposito, M., Di Lauro, R., Verde, P. An autoregulatory loop mediated by miR-21 and PDCD4 controls the AP-1 activity in RAS transformation. Oncogene. 2009; 28: 73–84.

Tatarchuk, V.V., Sergievskaya, A.P., Druzhinina, I.A., Zaikovsky, V.I. Kinetics and mechanism of the growth of gold nanoparticles by reduction of tetrachloroauric acid by hydrazine in Triton N-42 reverse micelles. J Nanopart Res. 2011; 13: 4997-5007.

Teow, Y., Asharani, P.V., Hande, M.P., Valiyaveettil, S. Health impact and safety of engineered nanomaterials. Chem Commun. 2011; 47: 7025-7038.

Templeton, A.C., Wuelfing, W.P., Murray, R.W. Monolayer-protected cluster molecules. Acc Chem Res. 2000; 33: 27-36.

Thaipong, K., Boonprakob, U., Crosby, K., Cisneros-Zevallos, L., Byrne, D.H. Comparison of ABTS, DPPH, FRAP, and ORAC assays for estimating antioxidant activity from guava fruit extracts. J Food Compos Anal. 2006; 19: 669-675.

Thaxton, C.S., Hill, H.D., Georganopoulou, D.G., Stoeva, S.I., Mirkin, C.A. A bio-bar-code assay based upon dithiothreitol-induced oligonucleotide release. Anal Chem. 2005; 77: 8174-8178.

Tiano, L., Armeni, T., Venditti, E., Barucca, G., Mincarelli, L., Damiani, E. Modified TiO(2) particles differentially affect human skin fibroblasts exposed to UVA light. Free Radic Biol Med. 2010; 49: 408-415.

Tirzitis, G., Bartosz, G. Determination of antiradical and antioxidant activity: basic principles and new insights. Acta Biochim Pol. 2010; 57: 139-142.

Tournebize, J., Sapin-Minet, A., Schneider, R., Boudier, A., Maincent, P., Leroy, P. Simple spectrophotocolorimetric method for quantitative determination of gold in nanoparticles. Talanta. 2011; 83: 1780–1783.

Trouillas, P., Marsal, P., Svobodova, A., Vostalova, J., Gazak, R., Hrbac, J., Sedmera, P., Kren, V., Lazzaroni, R., Duroux, J.L., Walterova, D. Mechanism of the antioxidant action of silybin and 2,3-dehydrosilybin flavonolignans: A joint experimental and theoretical study. J Phy Chem A. 2008; 112: 1054-1063.

Turkevich, J., Stevenson, P.C., Hillier, J. A study of the nucleation and growth processes in the synthesis of colloidal gold. Discuss Faraday Soc. 1951; 11: 55-75.

Tzhayik, O., Sawant, P., Efrima, S., Kovalev, E., Klug, J.T. Xanthate capping of silver, copper, and gold colloids. Langmuir. 2002; 18: 3364-3369.

Ukeda, H., Adachi, Y., Sawamura, M. Flow injection analysis of DPPH radical based on electron spin resonance. Talanta. 2002; 58: 1279-1283.

Unfried, K., Albrecht, C., Klotz, L.O., Von Mikecz, A., Grether-Beck, S., Schins, R.P.F. Cellular responses to nanoparticles: target structures and mechanisms. Nanotoxicology. 2007; 1: 52-71.

Unger, F., Wittmar, M., Kissel, T. Branched polyesters based on poly[vinyl-3-(dialkylamino)alkylcarbamate-co-vinyl acetate-co-vinyl alcohol]-graftpoly(d,l-lactide-co-glycolide): effects of polymer structure on cytotoxicity. Biomaterials. 2007; 28: 1610–1619.

Valodkar, M., Jadeja, R.N., Thounaojam, M.C., Devkar, R.V., Thakore, S. Biocompatible synthesis of peptide capped copper nanoparticles and their biological effect on tumor cells. Mater Chem Phys. 2011; 128: 83-89.

Valodkar, M., Rathore, P.S., Jadeja, R.N., Thounaojam, M., Devkar, R.V., Thakore, S. Cytotoxicity evaluation and antimicrobial studies of starch capped water soluble copper nanoparticles. J Hazard Mater. 2011; 201-202: 244-249.

van Meersbergen, M.T., Lorenzen, L., Van Deventer, J.S.J. The electrochemical dissolution of gold in bromine medium. Miner Eng. 1993; 6: 1067-1079.

Vance, A.L., Willey, T.M., Nelson, A.J., van Buuren, T., Bostedt, C., Terminello, L.J., Fox, G.A., Engelhard, M., Bear, D. XAS and XPS characterization of monolayers derived from a dithiol and structurally related disulfide-containing polyamides. Langmuir. 2002; 18: 8123-8128.

Vargas, M.C., Giannozzi, P., Selloni, A., Scoles, G. Coverage-dependent adsorption of CH_3S and $(CH_3S)_2$ on Au(111). J Phys Chem B. 2001; 105: 9509-9513.

Veranth, J.M., Kaser, E.G., Veranth, M.M., Koch, M., Yost, G.S. Cytokine responses of human lung cells (BEAS-2B) treated with micron-sized and nanoparticles of metal oxides compared to soil dusts. Part Fibre Toxicol. 2007; 4: 1-18.

Verwey, E.J.W., Overbeek, J.Th.G. Theory of the stability of lyophobic colloids. Elsevier, Amsterdam, 1948.

Viatour, P., Bentires-Alj, M., Chariot, A., Deregowski, V., de Leval, L., Merville, M.P., Bours, V. NF- kappaB2/p100 induces Bcl-2 expression. Leukemia. 2003; 17: 1349–1356.

Viirlaid, S., Mahlapuu, R., Kilk, K., Kuznetsov, A., Soomets, U., Jarv, J. Mechanism and stoichiometry of 2,2-diphenyl-1-picrylhydrazyl radical scavenging by glutathione and its novel alpha-glutamyl derivative. Bioorg Chem. 2009; 37: 126-132.

Vikhreva, P.N., Shepelev, M.V., Korobko, E.V., Korobko, I.V. Pdcd4 tumor suppressor: properties, functions, and their application to oncology. Mol Gen Mikrobiol Virusol. 2010; 3–11.

Wallach, D., Boldin, M., Varfolomeev, E., Beyaert, R., Vandenabeele, P., Fiers, W. Cell death induction by receptors of the TNF family: towards a molecular understanding. FEBS Lett. 1997; 410: 96–106.

Wang, H., Joseph, J.A. Quantifying cellular oxidative stress by dichlorofluorescein assay using microplate reader. Free Radic Biol Med. 1999; 27: 612–616.

Warsi, M.F., Adams, R.W., Duckett, S.B., Chechik, V. Gd-functionalised Au nanoparticles as targeted contrast agents in MRI: relaxivity enhancement by polyelectrolyte coating. Chem. Commun. 2010; 46: 451-453.

Watanabe, A., Kajita, M., Kim, J., Kanayama, A., Takahashi, K., Mashino, T., Miyamoto, Y. In vitro free radical scavenging activity of platinum nanoparticles. Nanotechnology. 2009; 20: 1-9.

Wilhelmi, V., Fischer, U., van Berlo, D., Schulze-Osthoff, K., Schins, R.P.F., Albrecht, C. Evaluation of apoptosis induced by nanoparticles and fine particles in RAW 264.7 macrophages: Facts and artefacts. Toxicol In Vitro. 2012; 26: 323-334.

Woods, C.G., Burns, A.M., Bradford, B.U., Ross, P.K., Kosyk, O., Swenberg, J.A., Cunningham, M.L., Rusyn, I. WY-14,643–induced cell proliferation and oxidative stress in mouse liver are independent of NADPH oxidase. Toxicol Sci. 2007; 98: 366-374.

Worle-Knirsch, J.M., Pulskamp, K., Krug, H.F. Oops they did it again! Carbon nanotubes hoax scientists in viability assays. Nano Lett. 2006; 6: 1261-1268.

Wuelfing, W.P., Gross, S.M., Miles, D.T., Murray, R.W. Nanometer gold clusters protected by surface-bound monolayers of thiolated poly(ethylene glycol) polymer electrolyte. J Am Chem Soc. 1998; 120: 12696-12697.

Xia, T., Kovochich, M., Brant, J., Hotze, M., Sempf, J., Oberley, T., Sioutas, C., Yeh, J.I., Wiesner, M.R., Nel, A.E. Comparison of the abilities of ambient and manufactured nanoparticles to induce cellular toxicity according to an oxidative stress paradigm. Nano Lett. 2006; 6: 1794–1807.

Xia, T., Kovochich, M., Liong, M., Zink, J.I., Nel, A.E. Cationic polystyrene nanosphere toxicity depends on cell-specific endocytic and mitochondrial injury pathways. ACS Nano. 2008; 2: 85–96.
Xu, S., Yuan, H., Xu, A., Wang, J., Wu, L. Rapid synthesis of stable and functional conjugates of DNA/gold nanoparticles mediated by Tween 80. Langmuir. 2011; 27: 13629-13634.

Yakimovich, N.O., Ezhevskii, A.A., Guseinov, D.V., Smirnova, L.A., Gracheva, T.A., Klychkov, K.S. Antioxidant properties of gold nanoparticles studied by ESR spectroscopy. Russ Chem B+. 2008; 57: 520-523.

Yamawaki, H., Iwai, N. Cytotoxicity of water-soluble fullerene in vascular endothelial cells. Am J Physiol Cell Physiol. 2006; 290: C1495–C1502.

Yamaguchi, T., Takamura, H., Matoba, T., Terao, J. HPLC method for evaluation of the free radical-scavenging activity of foods by using 1,1-diphenyl-2-picrylhydrazyl. Biosci Biotechnol Biochem. 1998; 62: 1201-1204.

Yamakoshi, Y., Umezawa, N., Ryu, A., Arakane, K., Miyata, N., Goda, Y., Masumizu, T., Nagano, T. Active oxygen species generated from photoexcited fullerene (C60) as potential medicines: $O_2^{-\bullet}$ versus $^1O_2$. J Am Chem Soc. 2003; 125: 12803-12809.

Yang, Z., Zhang, Y., Yang, Y., Sun, L., Han, D., Li, H., Wang, C. Pharmacological and toxicological target organelles and safe use of single-walled carbon nano-tubes as drug carriers in treating Alzheimer disease. Nanomedicine. 2010; 6: 427–441.

Yonezawa, T., Yasui, K., Kimizuka, N. Controlled formation of smaller gold nanoparticles by the use of four-chained disulfide stabilizer. Langmuir. 2001; 17: 271–273.

Yordanov, N.D., Christova, A.G. Quantitative spectrophotometric and EPR-determination of 1,1-diphenyl-2-picryl-hydrazyl (DPPH). Fresenius J Anal Chem. 1997; 358: 610-613.

Youk, J.H., Park, M.-K., Locklin, J., Advincula, R., Yang, J., Mays, J. Preparation of aggregation stable gold nanoparticles using star-block copolymers. Langmuir. 2002; 18: 2455-2458.

Youle, R.J., Narendra, D.P. Mechanisms of mitophagy. Nat Rev Mol Cell Biol. 2011; 12: 9–14.

Yu, L., Andriola, A. Quantitative gold nanoparticle analysis methods: A review. Talanta. 2010; 82: 869-875.

Yu, L., Alva, A., Su, H., Dutt, P., Freundt, E., Welsh, S., Baehrecke, E.H., Lenardo, M.J. Regulation of an ATG7-beclin 1 program of autophagic cell death by caspase-8. Science. 2004; 304: 1500–1502.

Zhang, F., Skoda, M.W.A., Jacobs, R.M.J., Zorn, S., Martin, R.A., Martin, C.M., Clark, G.F., Goerigk, G., Schreiber, F. Gold nanoparticles decorated with oligo(ethylene glycol) thiols: protein resistance and colloidal stability. J Phys Chem A. 2007; 111: 12229–12237.

Zhang, G., Yang, Z., Lu, W., Zhang, R., Huang, Q., Tian, M., Li, L., Liang, D., Li, C. Influence of anchoring ligands and particle size on the colloidal stability and *in vivo* biodistribution of polyethylene glycol-coated gold nanoparticles in tumor-xenografted mice. Biomaterials. 2009; 30: 1928-1936.

Zhang, H., Xu, Q., Krajewski, S., Krajewska, M., Xie, Z., Fuess, S., Kitada, S., Pawlowski, K., Godzik, A., Reed, J.C. BAR: an apoptosis regulator at the intersection of caspases and Bcl-2 family proteins. Proc Natl Acad Sci U.S.A. 2000; 97: 2597–2602.

Zhang, G.D., Yang, Z., Lu, W., Zhang, R., Huang, Q., Tian, M., Li, L., Liang, D., Li, C. Influence of anchoring ligands and particle size on the colloidal stability and *in vivo* biodistribution of polyethylene glycol-coated gold nanoparticles in tumor-xenografted mice. Biomaterials. 2009; 30: 1928-1936.

Zhang, S.Z., Kou, X.S., Yang, Z., Shi, Q.H., Stucky, G.D., Sun, L.D., Wang, J.F., Yan, C.H. Nanonecklaces assembled from gold rods, spheres, and bipyramids. Chem Commun. 2007: 1816-1818.

Zhao, Y., Gu, X., Ma, H., He, X., Liu, M., Ding, Y. Association of glutathione level and cytotoxicity of gold nanoparticles in lung cancer cells. J Phys Chem C. 2011; 115: 12797-12802.

Zhang, Y., Huang, R., Zhu, X., Wang, L., Wu, C. Synthesis, properties, and optical applications of noble metal nanoparticle-biomolecule conjugates. Chinese Sci Bull. 2012; 57: 238-246.

Zhang, Y., Shi, S., Wang, Y., Huang, K. Target-guided isolation and purification of antioxidants from Selaginella sinensis by offline coupling of DPPH-HPLC and HSCCC experiments. J Chrom B. 2011; 879: 191-196.

Zhang, Z., Berg, A., Levanon, H., Fessenden, R.W., Meisel, D. On the interactions of free radicals with gold nanoparticles. J Am Chem Soc. 2003; 125: 7959-7963.

Zhang, Z.W., Jia, J., Lai, Y.Q., Ma, Y.Y., Weng, J., Sun, L.P. Conjugating folic acid to gold nanoparticles through glutathione for targeting and detecting cancer cells. Bioorg Med Chem. 2010; 18: 5528-5534.

Zhao, W., Lam, J.C.F., Chiuman, W., Brook, M.A., Li, Y. Enzymatic cleavage of nucleic acids on gold nanoparticles: a generic platform for facile colorimetric biosensors. Small. 2008; 4: 810–816.

Zhao, Y., Gu, X., Ma, H., He, X., Liu, M., Ding, Y. Association of glutathione level and cytotoxicity of gold Nanoparticles in lung cancer cells. J Phys Chem C. 2011; 115: 12797-12802.

Zheng, J., Huang, W., Chen, S., Niu, Z., Li, Z. New oscillatory phenomena during gold electrodissolution in sulfuric acid containing Br- or in concentrated HCl. Electrochem Commun. 2006a; 8: 600-604. a ou nada ?

Zheng, J., Stevenson, M.S., Hikida, R.S., Patten, P.G.V. Influence of pH on dendrimer-protected nanoparticles. J Phys Chem B. 2002; 106: 1252-1255.

Zheng, P., Jiang, X., Zhang, X., Zhang, W., Shi, L. Formation of gold@polymer core-shell particles and gold particle clusters on a template of thermoresponsive and pH-responsive coordination triblock copolymer. Langmuir. 2006b; 22: 9393-9396.

Zhou, J.F., Ralston, J., Sedev, R., Beattie, D.A. Functionalized gold nanoparticles: Synthesis, structure and colloid stability. J Colloid Interface Sci. 2009; 331: 251-262.

Zhu, T., Vasilev, K., Kreiter, M., Mittler, S., Knoll, W. Surface modification of citrate-reduced colloidal gold nanoparticles with 2-mercaptosuccinic acid. Langmuir. 2003; 19: 9518-9525.

Zhuang, Q., Scholz, F., Pragst, F. The voltammetric behaviour of solid 2,2-diphenyl-1-picrylhydrazyl (DPPH) microparticles. Electrochem Commun. 1999; 1: 406-410.

Résumé

Synthèse de nanoparticules d'or fonctionnalisées par l'acide dihydrolipoïque : caractérisation, étude de stabilité et impact sur l'homéostasie redox cellulaire

L'objectif de notre travail consiste en la conception de nanoparticules d'or (NP d'or) monodisperses, stables en conditions physiologiques, et dotées d'une forte potentialité pour des applications biomédicales ; puis en l'évaluation de l'effet des propriétés de surface de NP d'or sur leur internalisation et leur toxicité dans une lignée cellulaire (macrophages alvéolaires de rat NR8383). Nous avons synthétisé des NP d'or soit stabilisées par les ions citrate soit fonctionnalisées par un dithiol, l'acide dihydrolipoïque (DHLA) (NP Au@DHLA). Nous avons montré que la densité de couverture est un paramètre crucial pour améliorer la stabilité colloïdale des NP d'or dans des conditions physiologiques. Nous avons caractérisé complètement les NP d'or d'un point de vue physico-chimique, en particulier en développant une méthode de dosage spectrophotocolorimétrique de l'or. Nous avons aussi étudié les effets biologiques des NP d'or. Tout d'abord, en absence de cellules, nous avons évalué le rôle de la fonctionnalisation de surface des NP d'or sur l'interaction entre celles-ci et des biomarqueurs de l'homéostasie redox cellulaire tels que le glutathion réduit (GSH), le *S*-nitrosoglutathion (GSNO), et l'albumine de serum bovin (BSA). Enfin, nous avons évalué l'influence de la fonctionnalisation de surface des NP d'or sur leur internalisation ainsi que sur leur impact dans l'homéostasie redox des macrophages en mesurant les espèces réactives de l'oxygène (ROS), le GSH, et l'expression des mRNA associées à la réponse inflammatoire (*tnf*), au stress oxydant (*ncf1*) et à l'apoptose (*nfκb2*). Nos résultats révèlent que la fonctionnalisation de surface de NP d'or affecte la réactivité avec des biomolécules (les NP d'or stabilisées par les ions citrate interagissant avec toutes les molécules testées), l'internalisation par les cellules (les NP d'or stabilisées par les ions citrate sont deux fois plus internalisées) et l'état redox cellulaire (les NP d'or stabilisées par les ions citrate diminuent de 20% le niveau intracellulaire de GSH) sans relation apparente avec la formation de ROS. En outre, les NP d'or ne semblent pas induire une réponse inflammatoire, un stress oxydant et l'apoptose, paramètres essentiels pour préserver l'intégrité de la cellule et de l'organisme, et envisager l'utilisation de ces NP comme plateforme pharmaceutique.

Mots clés : nanoparticules d'or, acide dihydrolipoïque, stabilité, cytotoxicité, état redox cellulaire, vecteurs de médicaments.

Abstract

Synthesis of gold nanoparticles functionalized with dihydrolipoic acid: characterization, stability studies and impact on cellular redox homeostasis

The aim of our work was to produce highly monodisperse and stable gold nanoparticles (AuNP) with potential for biomedical applications, and to evaluate the effect of AuNP surface properties on their uptake and cytotoxicity in a cultured cell line (rat-alveolar macrophages-NR8383). We synthesized AuNP either stabilized with citrate (citrate-stabilized AuNP) or capped with a dithiol, *i.e.* dihydrolipoic acid (Au@DHLA NP). The present study shows that the surface packing density is a crucial parameter to enhance the colloidal stability of AuNP in physiological conditions. We fully characterized the considered AuNP from a physico-chemical point of view. Indeed, we optimized a spectrocolorimetric and a HPLC method to evaluate the properties of AuNP. We studied the biological effects of AuNP. First, we evaluated, under cell-free conditions, how AuNP coating could influence redox status of their environment by developing different *in vitro* assays based on AuNP reactivity with reduced glutathione (GSH), S-nitrosoglutathione (GSNO), bovine serum albumin (BSA). At last, the effect of AuNP coating on macrophage internalization, and modifications of redox biomarkers such as reactive oxygen species (ROS), $^{\bullet}$NO-production, GSH, mRNA expression related to inflammatory response (*tnfα*), oxidative stress (*ncf1*) and apoptosis (*nfκb2*), were evaluated.
Our results reveal that AuNP coating affects their reactivity with biomolecules (citrate interact with all molecules), the cellular uptake (citrate-stabilized AuNP are two times more effective) and redox status (citrate-stabilized AuNP decrease the intracellular GSH level by *ca* 20%) with no apparent relationship with ROS formation. Furthermore, both AuNP appear not to induce inflammatory response, oxidative stress and apoptosis, parameters of main importance to preserve cellular integrity and body safety, and to assure pharmaceutical platform function.

Key words : gold nanoparticles, dihydrolipoic acid, stability, cytotoxicity, cell redox status, drug delivery.